The immune-evasive potential of MYC in pancreatic ductal adenocarcinoma

Das immunevasive Potential von MYC im Pankreaskarzinom

Doctoral Thesis

for a doctoral degree at the Graduate School of Life Sciences

Julius-Maximilians-Universität Würzburg,

Section Biomedicine

Submitted by

Bastian Krenz

from Rimpar

Würzburg, 2022

Members of the thesis committee:

Chairperson:	Prof. Dr. Alexander Buchberger
Primary supervisor:	Prof. Dr. Martin Eilers
Secondary supervisor:	Prof. Dr. Georg Gasteiger
Third supervisor:	Prof. Dr. Dean Felsher

Submitted on:

Date of Public Defense:

Date of Receipt of Certificate:

Each exists for but a short time,
and in that time explore but a
small part of the whole universe.

Stephan Hawking

Substantial part of this thesis was published in the following article:

B. Krenz*, A. Gebhardt-Wolf*, C. P. Ade, A. Gaballa, F. Roehrig, E. Vendelova, A. Baluapuri, U. Eilers, P. Gallant, L. D'Artista, A. Wiegering, G. Gasteiger, M. T. Rosenfeldt, S. Bauer, L. Zender, E. Wolf, M. Eilers (2021): MYC- and MIZ1-Dependent Vesicular Transport of Double-Strand RNA Controls Immune Evasion in Pancreatic Ductal Adenocarcinoma.
Cancer Research, DOI: 10.1158/0008-5472.CAN-21-1677

*authors contributed equally

Content

Summary

Pancreatic ductal adenocarcinoma (PDAC) is predominantly driven by mutations in KRAS and TP53. However, PDAC tumors display deregulated levels of MYC and are a paradigm example for MYC-driven and -addicted tumors. For many years MYC was described as a transcription factor that regulates a pleiotropic number of genes to drive proliferation. Recent work sheds a different light on MYC biology. First, changes in gene expression that come along with the activation of MYC are mild and MYC seems to act more as a factor that reduces stress and increases resilience towards challenges during transcription. Second, MYC is a strong driver of immune evasion in different entities. In this study we depleted MYC in murine PDAC cells and revealed the immune dependent regression of tumors in an orthotope transplant model, as well as the activation of the innate immune system using global expression analysis, immunoblotting and fCLIP.

These experiments revealed that endogenous double-stranded RNA is binding as a viral mimicry to Toll-like receptor 3, causing activation of TBK1 and downstream activation of a proimmunogenic transcription program. The regression of tumors upon depletion of MYC is dependent on this pathway since the knockout of TBK1 prevents regression of tumors after depletion of MYC.

We can summarize this study in three main findings: First, the dominant and most important function of MYC in tumors is not to drive proliferation but to promote immune evasion and prevent immune-dependent regression of tumors. Second, cells monitor defects or delay in splicing and RNA processing and activate the immune system to clear cells that face problems with co-transcriptional processing. Third, MYC suppresses the activation of the cell-intrinsic innate immune system and shields highly proliferating cells from the recognition by the immune system.

To translate this into a therapeutically approach, we replaced the shRNA mediated depletion of MYC by treatment with cardiac glycosides. Upon treatment with cardiac glycosides tumor cells reduce uptake of nutrients, causing a downregulation of MYC translation, inhibition of proliferation, glycolysis and lactate secretion. Lactate is a major reason for immune evasion in solid tumors since it dampens, amongst others, cytotoxic T cells and promotes regulatory T cells.
Treatment of mice with cardiac glycosides causes a complete and immune-dependent remission of PDAC tumors *in vivo*, pointing out that cardiac glycosides have strong proimmunogenic, anti-cancer effects. More detailed analyses will be needed to dissect the full mechanism how cardiac glycosides act on MYC translation and immune evasion in PDAC tumors.

Zusammenfassung

Pankreaskarzinome entwickeln sich in den meisten Fällen durch die Mutation von KRAS und TP53. Nichtsdestotrotz weisen Pankreaskarzinome sehr hohe, deregulierte Level des MYC Proteins auf und sind exemplarisch für Tumore, deren Wachstum abhängig von MYC ist. Für lange Zeit wurde MYC als Transkriptionsfaktor beschrieben, der vor allem Gene aktiviert, die für die Proliferation von Zellen notwendig sind. Die jüngste Forschung wirft jedoch ein anderes Bild auf die Biologie von MYC. Zum einen sind die transkriptionellen Veränderung nach Aktivierung von MYC mild und vieles deutet darauf hin, dass die Funktion von MYC zum einen in der Reduktion von transkriptionellem Stress liegt. Zum anderen verhindert MYC die Erkennung von Tumorzellen durch das Immunsystem. In dieser Studie wurde MYC in murinen Pankreaskarzinomzellen depletiert und die immunabhängige Regression der Tumore in einem orthotopen Transplantationsmodel untersucht. Die Aktivierung der zell-intrinsischen Immunantwort wurde mittels globaler Expressionsanalyse, Immunoblots und fCLIP Experimenten untersucht.

Diese Experimente haben gezeigt, dass endogene doppel-strängige RNAs als virales Mimikry an Toll-like Rezeptor 3 binden, worauf TBK1 phosphoryliert und ein pro-immunogenes Transkriptionsprogram aktiviert wird. Die Deletion von TBK1 konnte beweisen werden, dass die Regression der Tumore von diesem Signalweg abhängig ist.

Die Ergebnisse der Studie lassen sich in drei zentrale Erkenntnisse zusammenfassen: Erstens ist die prä-dominante Funktion von MYC in Tumoren *in vivo* nicht die Proliferation der Zellen zu fördern, sondern zu verhindern, dass der Tumor vom Immunsystem erkannt und bekämpft wird. Zweitens überwachen Zellen das richtige Prozessieren von RNA und aktivieren bei Bedarf das Immunsystem um defekte Zellen zu entfernen. Drittens unterdrückt MYC die Aktivierung dieses zell-intrinsischen Signalweges und schirmt den Tumor dadurch vom Immunsystem ab.

Um diese Ergebnisse in einen translationalen Ansatz zu überführen, haben wir die shRNA vermittelte Depletion von MYC durch die Behandlung mit Herzglykosiden ersetzt, die die Aufnahme von Nährstoffen reduzieren, Proliferation einschränken, die Translation des MYC Proteins stoppen und Glykolyse und Laktatsekretion herunterfahren. Laktat hat starke immunsuppressive Eigenschaften in soliden Tumoren, da es zytotoxische T Zellen erschöpft und regulatorische T Zellen aktiviert.
Die Behandlung von Mäusen mit Herzglykosiden führte in Abhängigkeit vom Immunsystem zur kompletten Remission der Tumore, auch wenn noch weitere Forschung notwendig ist, um die exakten Zusammenhänge besser zu verstehen.

1 Introduction

MYC and its family members MYCN and MYCL are oncogenes that are overexpressed, amplified, activated or deregulated in multiple cancer entities and are controlling all hallmarks of cancer biology by integrating growth promoting and proproliferative signals into transcription (Gabay *et al.*, 2014). Consequently, understanding the function and biology of this transcription factor, that binds to the core promoter of all actively transcribed genes (Baluapuri *et al.*, 2020), is of key interest for both, extending our knowledge on MYC's regulation of transcription by RNA polymerase II (RNAPII) as well as for translational research. Pancreatic ductal adenocarcinoma (PDAC) is a paradigm example of an entity that is dependent on MYC expression and has a devastatingly poor prognosis, further reinforcing the need for better understanding the role of MYC in initiation and maintenance of these tumors.

1.1 The transcription factor MYC

1.1.1 The family of MYC proteins and their network

MYC proteins, which include MYCL, MYCN and MYC (historically named c-MYC), belong to the helix-loop-helix/leucin zipper transcription factor family. MYC and its paralogs MYCL and MYCN are all implicated in a variety of human neoplasia. Depending on the entity, genomic amplification or translocation as well as overexpression are observed in tumors and the ability of MYC to transform cells and tissues has been described in several experimental settings (Dang, 2012; Land *et al.*, 1983; Leder *et al.*, 1986). MYCN was originally found to be dramatically amplified in a panel of neuroblastoma cell lines and its strong capacity to transform cells in culture has been demonstrated using rat embryo fibroblasts (Kohl *et al.*, 1983; Yancopoulos *et al.*, 1985). It is a driver of cancers originating in neural or neuroendocrine tissue (Rickman *et al.*, 2018). In contrast, deregulation of MYC is pervasive in human cancer. It is long known that MYC is translocated in Burkitt's lymphoma and multiple myeloma (Mikulasova *et al.*, 2017; Schmitz *et al.*, 2014). Very often it is strongly transcriptionally upregulated by oncogenic activation of one or more of the pathways including Wnt-APC, Notch and MAP kinases (Dang, 2012). Therefore, medulloblastoma, colorectal cancer, breast cancer, lung cancer, melanoma and pancreatic cancer are only very few paradigm examples for tumors with deregulated levels of MYC and accordingly oncogenic addiction (Brägelmann *et al.*, 2017; Hessmann *et al.*, 2016; Roussel and Robinson, 2013; Schaub *et al.*, 2018; Topper *et al.*, 2017).

MYC is highly expressed in proliferating or dividing cells and it has a critical role during development, as shown by the embryonal death of MYC-deficient mice (Zimmerman *et al.*, 1986). MYCN can substitute this function of MYC in the embryonic development of the mouse, pointing out that they have at least partially redundant function (Malynn *et al.*, 2000). Moreover, MYC does not only play a pivotal

role in growth, proliferation and tumorigenesis, but is also one of four genes that can induce pluripotency in fibroblasts (Takahashi and Yamanaka, 2006).

MYC proteins are predominantly found in the nucleus of cells and a significant proportion of MYC is bound to chromatin together with a partner protein termed MAX. While *in vitro* the MYC/MAX heterodimer binds to a well-defined DNA sequence called E-box (CACGTG), the binding behavior of the MYC/MAX heterodimer in culture is less strict and depends on the MYC protein level. With increasing concentrations of MYC protein in the cell, MYC binding invades all active core promoters (Lorenzin *et al.*, 2016). Besides the interaction with MYC, MAX can form homodimers and heterodimers with MXD proteins and together they form a network of transcription factors that interact with each other *via* the helix-loop-helix/leucine zipper (Conacci-Sorrell *et al.*, 2014). While the interaction of MYC and MAX is essential for MYC-mediated proliferation and growth in eukaryotic cells (Blackwood and Eisenman, 1991; Gallant *et al.*, 1996), MXD proteins (i.e., MNT or MGA1) seem to counteract and outbalance these effects by promoting suppression of growth (Hurlin *et al.*, 2003; Mathsyaraja *et al.*, 2019). The important role of this network in taming the function of MYC is underlined by the observation that these MYC antagonists are frequently mutated in cancer (Schaub *et al.*, 2018).

Another partner protein of MYC is the zinc finger protein MIZ1, which also interacts with the carboxy-terminus of MYC. The MYC/MIZ1 heterodimer represses transcriptional activation by binding to the core promoters of genes (Walz *et al.*, 2014). While there is little evidence that MYC and MIZ1 are interacting at physiological levels of MYC in untransformed cells, the association of MYC and MIZ1 becomes detectable at supraphysiological levels of the MYC protein (Wiese *et al.*, 2013). MIZ1 on its own transcriptionally activates genes involved in autophagy by directly binding to a non-palindromic sequence at the core promoter of these genes (Wolf *et al.*, 2013). The MIZ1 POZ domain is essential for MIZ1 tetramerization and chromatin recruitment, as a POZ domain deletion hinders MIZ1 binding to chromatin (Kosan *et al.*, 2010; Stead *et al.*, 2007). In contrast, the MYC/MIZ1 complex transcriptionally represses the cell-cycle inhibitors p15INK4b and p21CIP1 and thereby the response to TGF-β *in vitro* and *in vivo* (Gebhardt *et al.*, 2006; Seoane *et al.*, 2002). Moreover, MIZ1 promotes the expression of the antiapoptotic BCL-2 gene and MYC and MIZ1 cooperate to repress integrins to enable cells to exit the stem cell compartment (Saba *et al.*, 2011; Waikel *et al.*, 2001). A mutation in MYC at amino acid 394, replacing a valine with an asparagine (MYC^{V394D}, MYCVD), prevents MYC binding to MIZ1 without disrupting the interface that interacts with MAX (Herold *et al.*, 2002). While systemic deletion of MIZ1 or deletion of the POZ domain is embryonic lethal (Adhikary *et al.*, 2003; Kosan *et al.*, 2010), mice with a systemic knock-in of MYC^{V394D} are viable (Wiese *et al.*, 2013). Importantly, there is clear evidence that the MYC/MIZ1 interaction is crucial for the development and maintenance of tumors *in vivo*. Similar to the depletion of one allele of MYC, depletion of the POZ domain of one allele of MIZ1 significantly retarded the development and progression of pancreatic cancer in $KRas^{G12D}$ and $Tp53^{R172H}$ driven mouse models (Walz *et al.*, 2014). In addition, a mouse hemizygous for $Myc^{V394D/-}$ shows a significant increase in overall survival in a model of APC-driven colorectal carcinogenesis compared to mice with

two or one allele of wild-type MYC (Wiese *et al.*, 2013). Mechanistically, the destruction of MYC/MIZ1 interaction is associated with chromatin invasion by the repressive H3K9me3 mark. This event, probably dependent on the lack of repression by CDK inhibitors, suggests the reason for the reduced transforming potential (van Riggelen *et al.*, 2010).

1.1.2 The structure and interactome of MYC

MYC is a highly unstructured protein and the homology among the three paralogs is limited. However, MYC proteins share amino acid stretches with a high conservation, called MYC boxes (MB). These MYC boxes are numbered from 0 to IV and each of the MYC boxes provides the binding interface for partner proteins. MB 0 and MB I provide the interface for the interaction with Aurora A, that stabilizes and antagonizes E3-ligase dependent turnover of MYC and MYCN (Dauch *et al.*, 2016; Otto *et al.*, 2009; Richards *et al.*, 2016). The stability of MYC proteins is regulated by a highly conserved phospho-degron (T58, S62, S64, S67) in MB I. Phosphorylation of S62 by CDKs causes a subsequent phosphorylation of T58 by GSK3, overall resulting in the recruitment of SCF^{FBXW7} and SCF^{FBXL3} (Welcker *et al.*, 2004). This ubiquitination event and thus, the stability and half-life of MYC proteins is counteracted by the de-ubiquitinating enzyme USP28 (Popov *et al.*, 2007a; Popov *et al.*, 2007b). Furthermore, MB I binds TFIIF, a general transcription factor that is part of the RNAPII preinitiation complex (Kalkat *et al.*, 2018). MB II enables MYC binding to proteins that remodel or modify chromatin, namely TRRAP and P400. Acetylation of the chromatin via the TRRAP-Nu4A-axis increases the accessibility of the chromatin together with the helicase P400 to promote transcription. Mutant TRRAP or deletion of MB II prevent MYC-mediated transformation, indicating that major oncogenic potential of MYC is mediated by its interaction with TRRAP (McMahon *et al.*, 1998; Zhang *et al.*, 2014a). MB IIIb binds WDR5 to mediate trimethylation of H3K4, a marker for active promoters, and increase the occupancy of MYC at the promoter. This ability is crucial to induce stem cells pluripotency (Thomas *et al.*, 2015). MB IV is essential for the binding of host cell factor 1 (HCF1) through its tetrapeptide HCF-binding motif. Point mutations of MYC that disrupt this interaction show a reduced potential to drive tumorigenesis in mice (Thomas *et al.*, 2016). HCF1 links MYC to the regulation of ribosome biogenesis and mitochondrial gene expression, two functions that are hard-wired in MYC biology (Popay *et al.*, 2021). The C-terminal region of the MYC protein contains the helix-loop-helix/leucin zipper. The leucine zipper provides the DNA binding domain and binds MAX and MIZ1 to activate or repress transcription.

1.1.3 Regulation of MYC

MYC transcription, translation and protein stability are tightly controlled to prevent uncontrolled growth and transformation. Transcription of the MYC gene is regulated by a wide range of growth-promoting signaling pathways, including WNT, Notch, JAK-STAT, MAPK and Hedgehog. This is counteracted by TGF-beta signaling that suppresses the transcription of MYC (Dang, 2012; Kress *et al.*, 2015). The translation of MYC mRNA is controlled on several levels, e.g. by mTORC1-S6K1, MAPK-HNRPK and MAPK-FOXO3A, but also by the presence of glutamine and nucleotides (Csibi *et al.*, 2014; Dejure *et*

al., 2017; Notari *et al.*, 2006). The stability of MYC protein increases with the activation of the PI3K-AKT and RAS-MAPK pathway (Sears *et al.*, 1999; Sears *et al.*, 2000; Vaseva *et al.*, 2018).
As described in ***section 1.1.2***, MYC stability is regulated via MB I through the balance between the activities of SCF^{FBW7} and USP28 (Popov *et al.*, 2007a; Schulein-Volk *et al.*, 2014). Additionally, MYC and MYCN protein stability is regulated by the interaction with Aurora A, albeit the association with MYC is weaker than with MYCN (Dauch *et al.*, 2016; Otto *et al.*, 2009).

1.1.4 Transcriptional regulation by MYC

A central debate in MYC biology is whether there is a crucial MYC-driven transcription program that mediates the transformative potential of MYC. Four central assumptions underlie this discussion: First, MYC is overexpressed in a large variety of cancers and can induce neoplastic growth (Small *et al.*, 1987). Second, MYC can induce the expression of specific genes in reporter assays (Greasley *et al.*, 2000; Kretzner *et al.*, 1992). Third, MYC is strongly associated with chromatin, especially at the core promoters of genes that are actively transcribed by RNAPII (Walz *et al.*, 2014). Fourth, MYC induction promotes the upregulation of a broad range of biological processes, most of them linked to protein biosynthesis, metabolism, transcription factors and cell cycle (Eilers and Eisenman, 2008).

Many early publications on the role of MYC in transcription favor a **gene-specific regulatory model** by showing the regulation of specific genes using RQ-PCR or reporter assays ***(Figure 1A)***. This is in line with MYC being highly associated with the promoter of some genes. In this view, MYC binds to a specific group of genes to activate or repress them to promote proliferation, growth and transformation. However, two aspects of MYC biology do not fit in a model based on MYC binding and regulation of a distinct set of target genes: First, ChIP-Rx sequencing data show that MYC is bound to the promoter of all genes actively transcribed by RNAPII. Second, changes in global expression profiles are subtle and only a few MYC bound genes are regulated more than twofold (Baluapuri *et al.*, 2020; Herold *et al.*, 2019; Walz *et al.*, 2014). Consequently, there are more genes bound by MYC at the core promoter than genes significantly regulated by changes in MYC protein levels. These experiments suggest that there is no correlation between genes bound by MYC and genes regulated by MYC.

Strikingly, two seminal works which used B cells as a model system suggested a different view on MYC's biology, named the **global amplifier model**. B cell stimulation resulted in increased global binding of MYC to the core promoter and increased global transcription of all MYC-bound genes (Lin *et al.*, 2012; Nie *et al.*, 2012) ***(Figure 1B)***. Increasing amount of mRNA upon MYC induction could be measured in human Burkitt's lymphoma cells. Total amount of RNA in these cells follows the increase in MYC levels. Importantly, some studies claim that global changes in gene expression or total amount of mRNA have been previously overlooked because of data normalization or the lack of spike-normalized sequencing (Lovén *et al.*, 2012). This model is supported by the high sensitivity of MYC driven cancers towards the inhibition of CDK7 or CDK9, both being essential for transcription via RNAPII (Chipumuro *et al.*, 2014;

Huang *et al.*, 2014). Albeit MYC globally increases transcription elongation rates measured using 4sU-DRB-sequencing to detect nascent RNA synthesis (Baluapuri *et al.*, 2019), total RNA content of cells did not change in other biological systems (Walz *et al.*, 2014). This indicates that these observations may highly depend on the conditions and especially the biological system that is used.

The third concept is based on the observation that an increase in MYC protein also causes an increase in MYC-bound promoters, resulting in changes in the global expression profile. This **gene-specific affinity model** categorizes the promoters of genes according to their ability to recruit MYC, i.e., "MYC affinity" (Lorenzin *et al.*, 2016). Consequently, MYC does not switch the transcription of genes on and off, but it gradually changes the global transcription profile, also considering the different state of cells with increasing levels of MYC protein, namely, resting, not proliferating cells, proliferating cells and transformed cancer cells (Lorenzin *et al.*, 2016) ***(Figure 1C)***.

None of the three discussed models can explain the discrepancy between global chromatin occupancy at core promoters and only mild regulation of transcription. These two aspects can be explained by an emerging **transcription-stress-resilience model** in which MYC does not control transcription rate or special gene sets, but acts at the core promoter of genes to increase processivity of RNAPII and also to promote resilience towards transcriptional stress, such as torsional stress (Das *et al.*, 2022; Herold *et al.*, 2008), R-loop formation (Herold *et al.*, 2019), coordination of transcription and replication (Roeschert *et al.*, 2021; Solvie *et al.*, 2022), double-strand breaks at promoters (Endres *et al.*, 2021) and stalling polymerase (Papadopoulos *et al.*, 2022). This model is in line with recently published interactomes of MYC and MYCN, which showed that MYC and MYCN are able to bind to an extensive variety of proteins with distinct functions, including not only transcription and elongation factors, but also chromatin remodelers, RNA processing enzymes, histone acetyltransferases, chromatin topology affecting proteins and many more (Baluapuri *et al.*, 2019; Baluapuri *et al.*, 2020; Büchel *et al.*, 2017; Kalkat *et al.*, 2018) ***(Figure 1D)***. MYC and MYCN induce productive elongation of RNAPII (Rahl *et al.*, 2010) and MYC mediates the transfer of the elongation complex DSIF (containing SPT4 and SPT5) onto RNAPII to induce productive elongation, processivity and directionality (Baluapuri *et al.*, 2019). Collectively, MYC primes RNAPII for productive elongation on multiple levels and there is an increasing number of factors that are recruited by MYC or MYCN to increase stress resilience at the promoter. For example, MYC recruits the PAF1 complex to the promoter to both, ensure productive elongation (Jaenicke *et al.*, 2016) and secondly, to repair double-strand breaks (Endres *et al.*, 2021). Moreover, MYCN-driven neuroblastoma relies on high BRCA1 levels to recruit de-capping factors to prevent formation of promoter-proximal R-loops formed by non-productive RNAPII (Herold *et al.*, 2019). In MYC driven cells these R-loops can also be resolved by the PAF1 complex. This shows that MYC and MYCN can both solve very similar challenges of the RNAPII by recruiting different partner proteins (Shivji *et al.*, 2018). A further example of this is represented by the S phase-related MYC/MYCN functions. In the S phase, DNA and RNA polymerases are both associated with chromatin. To avoid collisions between

the two polymerases, origins of replication and genes are precisely located and orientated on the chromatin (Lin and Pasero, 2017; Merrikh, 2017; Petryk *et al.*, 2016). Nevertheless, both processes need to be well coordinated, since conflicts between transcription and replication pose a threat to genomic stability of cells (Hamperl *et al.*, 2017; Macheret and Halazonetis, 2018).

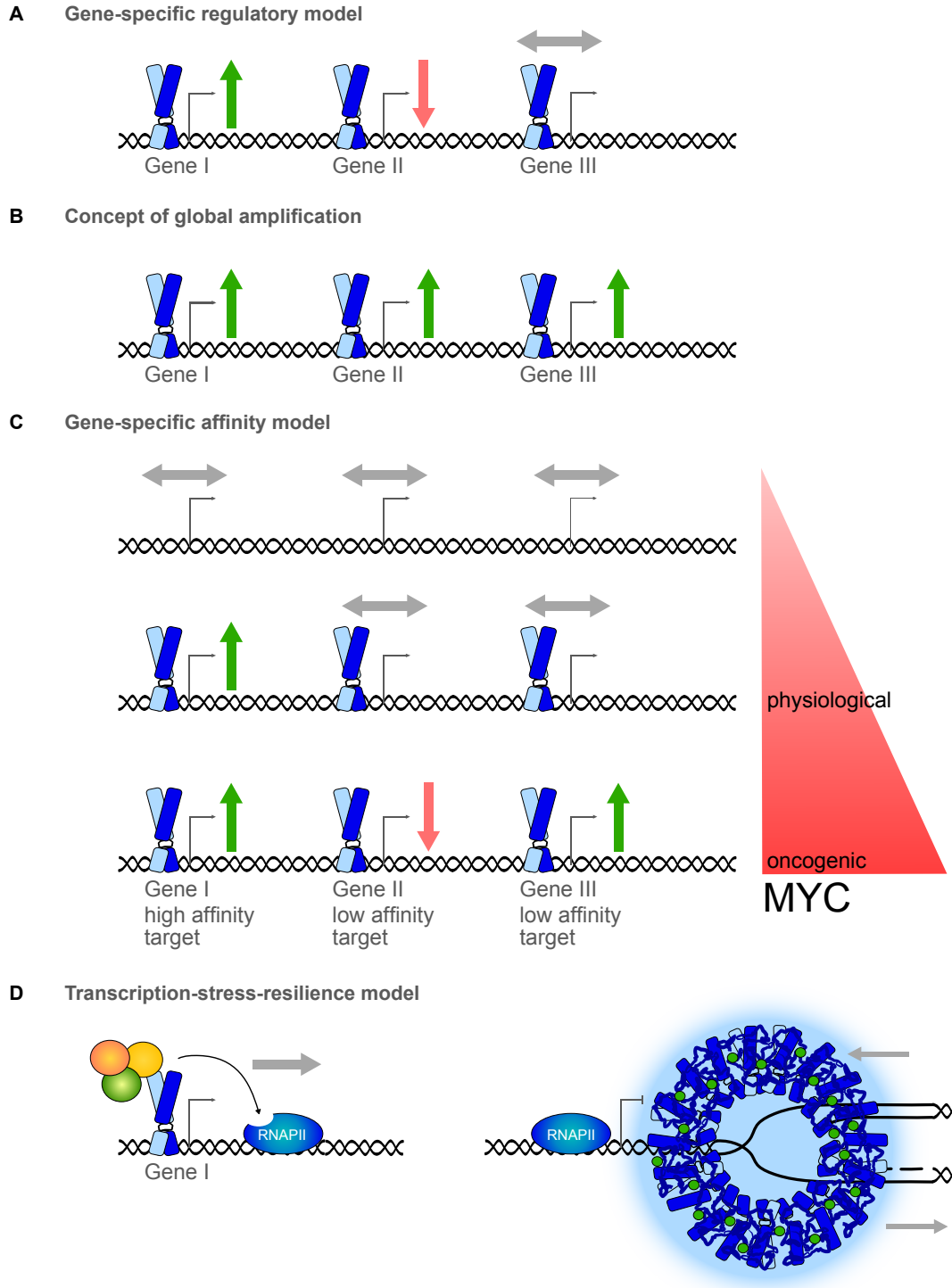

Figure 1: Mechanisms of MYC-dependent transcription. *A: gene-specific regulatory model B: concept of global amplification C: gene-specific affinity model D: transcription-stress-resilience model. Model (A-C) was adapted from Baluapuri et al., 2020.*

Aurora A, a kinase that stabilizes MYCN by counteracting SCF^{FBW7}, binds MYCN in S phase and thereby competes with proteins that promote pause release and elongation to prevent transcription-replication conflicts (Roeschert *et al.*, 2021). Comparable phenotypes have been observed with MIZ1, which was shown to interact with the checkpoint that controls transition to S phase (Herold *et al.*, 2002).
Recent work showed that MYC can multimerize and re-localize to new binding sites when cells have to face transcriptional and/or replicational stress to protect stalled replication forks. This pathway is promoted by HUWE1, already implicated in transcription-associated DNA repair at core promoters (Endres *et al.*, 2021). MYC multimers prevent antisense transcription and stabilize FANCD2 on the chromatin. Moreover, MYC multimers sequester SPT5 from the RNAPII and thereby repress the transcription of genes under stress-conditions ***(Figure 1D)*** (Solvie *et al.*, 2022).
In summary, there are supportive data for all four models in terms of MYC biology. However, new methods such as ChIP-Rx, CUT&RUN sequencing and spiked-normalized analysis of nascent RNA are shifting the view on MYC proteins from an oncogenic transcription factor, which drives specific gene to promote tumorigenesis, to a protein-hub or "resilience booster" that enables rapidly proliferating cells to deal with the resulting challenges at promoters or during elongation when the RNAPII faces the DNA polymerase during replication.

1.1.5 Mechanisms of repression by MYC

The repression of gene expression by the MYC proteins is in part covered by the **gene-specific regulatory model**, with MYC and MIZ1, which cooperatively bind to the core promoter of specific genes (Kress *et al.*, 2015). Several inhibitors of the cell cycle and integrins are repressed by MYC and MIZ1 (Gebhardt *et al.*, 2006; Seoane *et al.*, 2001). The MYC/MIZ1 heterodimer is critical in the tumorigenesis of hepatocellular carcinoma (HCC) in mice and represses distinct sets of genes including metabolic processes, cell-cell contacts, and, most importantly, a panel of gene sets involved in inflammation and immune activation (Kress *et al.*, 2016). The cooperative binding of MYC and MIZ1 to some distinct genes has been described in detail (Wiese *et al.*, 2013). However, many more genes that are transcriptionally repressed by MYC proteins are neither bound by MYC nor MIZ1 on the chromatin.

MYC promotes processive elongation via a hand-over mechanism of SPT5 and depletion of MYC results in unprocessive, abortive transcription (Baluapuri *et al.*, 2019). Oncogenic levels of MYC protein not only facilitate the rapid transfer of STP5 to drive transcription, but also cause sequestration of non-functional MYC-SPT5 complexes that result in repression of genes that have no or only mild MYC binding. Oncogenic levels of MYC cause a gain-of-function to squelch SPT5 from the promoter of distinct gene sets, such as TGF-beta and NF-κB target genes (Baluapuri *et al.*, 2019; Baluapuri *et al.*, 2020). This is in line with the observation that genes that are activated by oncogenic levels of MYC protein show the most increase of MYC binding to the core promoter ('MYC share') compared to low levels of MYC, while repressed genes do not show a pronounced increase in MYC occupancy. 'MYC share'

genes include all pathways that are hard-wired to MYC biology: nucleotide metabolism, cell growth and division, biosynthesis and DNA replication (de Pretis *et al.*, 2017; Tesi *et al.*, 2019).

Induction of various kinds of stress in tumor cells causes multimerization of MYC and sequestration of SPT5 from the polymerase to repress the transcription. Squelching/sequestration and the 'MYC share' concept account more for the **transcription-stress-resilience *(Figure 1D)*** model where MYC proteins recruit factors to facilitate proper transcription and processive elongation ***(Figure 2)***. This is supported by the fact that MYCN repressed genes display the same rate of pause-release from the promoter, but they lack processive elongation (Herold *et al.*, 2019).

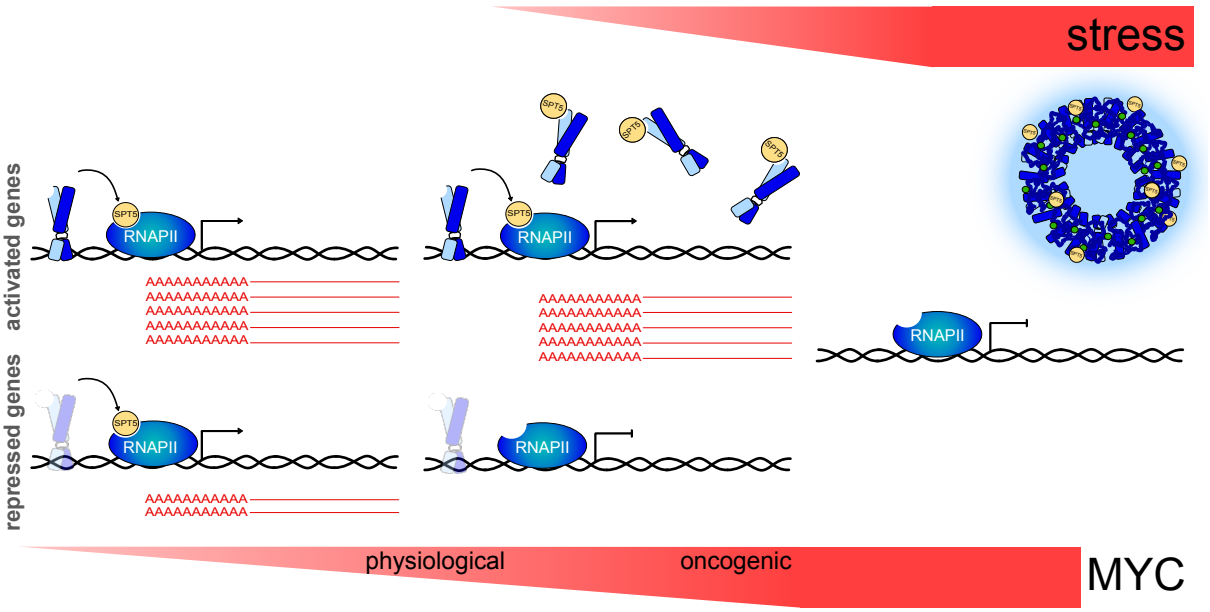

Figure 2: MYC squelches SPT5 from the RNAPII. *Oncogenic levels of MYC sequester SPT5 and cause transcriptional repression of genes with no or only mild binding of MYC protein to the core promoter. Under stress conditions MYC multimerizes and sequesters SPT5 to prevent transcription and resulting damage to the integrity of the cell. Model was adapted from Baluapuri et al., 2020.*

Broad analysis with different experimental systems *in vivo* and in culture revealed that there is a substantial number of genes involved in inflammation, inflammatory response, interferon signaling and cytokines, which are downregulated by MYC. Some of these genes are repressed by MYC or MYC and MIZ1, but in many cases the binding of MYC is not conserved across different entities or is strongly dependent on the cellular context (Casey *et al.*, 2016; Kortlever *et al.*, 2017; Muthalagu *et al.*, 2020; Sodir *et al.*, 2020; Topper *et al.*, 2017; Zimmerli *et al.*, 2022). These observations point out that the hard-wired function of MYC to repress proimmunogenic genes is working via a different mechanism.

1.2 PDAC – Pancreatic ductal adenocarcinoma

1.2.1 Origin and development of PDAC

Pancreatic ductal adenocarcinoma (PDAC) is a devastating, malignant disease originating from acinar and/or ductal cells in the pancreas with a five-year survival rate of only 5% (Rahib *et al.*, 2014). PDAC is a paradigm example for a MYC-dependent tumor, due to the nearly universal mutation in KRAS which drives MYC upregulation (Hessmann *et al.*, 2016; Morris *et al.*, 2010; Vaseva *et al.*, 2018). Beyond KRAS, TP53, CDKN2A and alterations in the TGF-β signaling are the most common genetic alterations found in patients (Bailey *et al.*, 2016; Mueller *et al.*, 2018) ***(Figure 3)***.

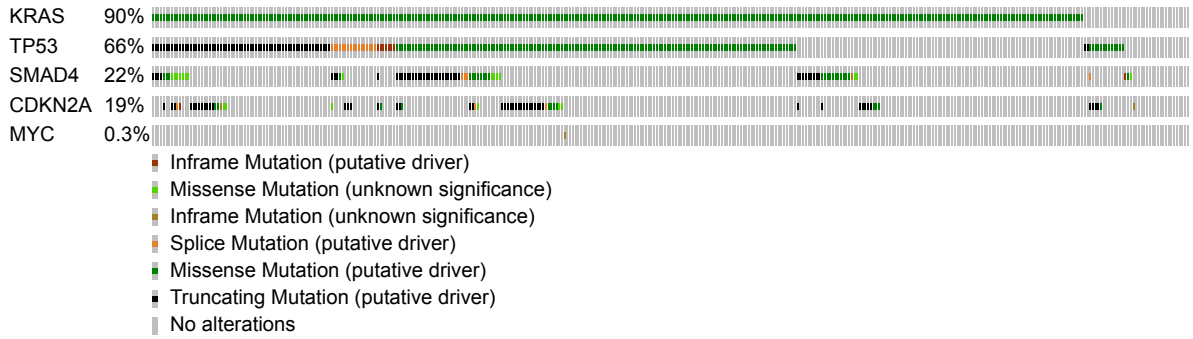

Figure 3: Genetic alterations of tumor drivers and tumor suppressors in pancreatic ductal adenocarcinoma *(Bailey et al., 2016).*

The pancreas is composed of cells from three different origins: exocrine (acinar), epithelial (ductal) and endocrine origin. Acinar cells are responsible for homeostasis and regeneration since the pancreas does not have a defined stem cell compartment (Puri *et al.*, 2015).

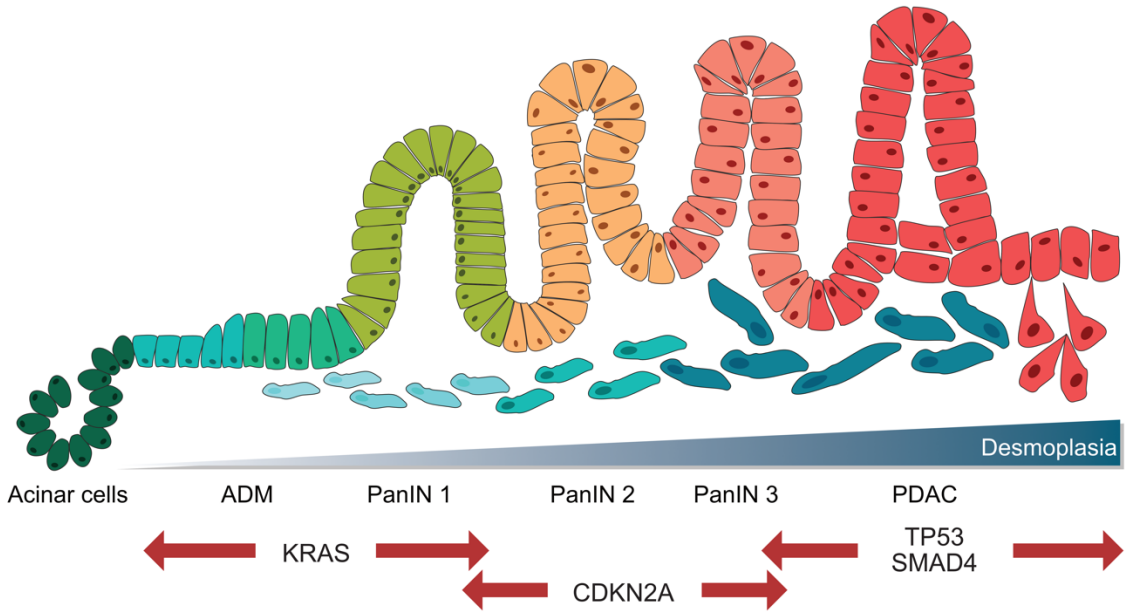

Figure 4: Development of pancreatic ductal adenocarcinoma. *Model was adapted from Orth et al., 2019.*

The cell-type of which PDAC origins is still debated, despite most people in the field agreeing on a concept in which acinar cells, the most plastic cell type in the pancreas, undergo acinar-to-ductal metaplasia (ADM). In detail, ADM is associated with the gain of an epithelial (ductal-like) phenotype as a consequence of stress, inflammation or injuries (Friedlander *et al.*, 2009; Kopp *et al.*, 2012). Mutations in KRAS are one of the very early alterations in the development of pancreatic cancer causing the transformation towards pancreatic intra-epithelial neoplasias (PanIN). PanIN lesions are the initial steps before tumor progress through the stepwise accumulation of additional mutations, especially the loss of tumor suppressor genes to a PDAC (Orth *et al.*, 2019) ***(Figure 4)***.

1.2.2 Treatment of PDAC

In general, the outcome and overall survival of PDAC patients are poor for two reasons: First and foremost, due to the late onset of symptoms, only 10-20% of patients are diagnosed with a PDAC that is still resectable. The vast majority of patients has already advanced and non-resectable tumors with distant metastasis at the time of diagnosis (Gillen *et al.*, 2010). Second, PDAC tumors reveal an immunosuppressive enviroment, are highly desmoplastic and have a low number of neo-antigens, making the tumor difficult to access for immunotherapies (Dougan, 2017). Patients with non-resectable tumors receive systemic chemotherapy with nucleoside analogues (5-fluorouracil, gemcitabine) or mitotic inhibitors (paclitaxel). Radiotherapy is rarely used since most PDAC patients present with an already advanced disease and local therapies are less useful. Moreover, PDAC are very resistant to radiotherapy (Hall and Goodman, 2019). Still, radiotherapy can be used as neo-adjuvant strategy to improve outcome of resections or to make the tumor resectable (Roeder, 2016). To address the high radioresistance, radiotherapy is combined with sensitizing agents like gemcitabine or other nucleoside analogues (Mukherjee *et al.*, 2013).

Immunotherapy using checkpoint inhibition – a game-changer in several diseases like melanoma or lung cancer – was effectively only in a small subgroup of patients with microsatellite instability (Brahmer *et al.*, 2012; Orth *et al.*, 2019). Allogenic transplant of T cells with chimeric antigen receptors (CAR-T cells), which specifically recognize and eliminate cells that express a certain protein on the surface, have shown promising results in leukemia (Sheykhhasan *et al.*, 2022). However, solid tumors are difficult to target with CAR-T cells due to the immunosuppressive microenvironment which antagonize CAR-T cell invasion to the tumor area. Nevertheless, targeting the microenvironment to prime the tumor for CAR-T cell recognition showed first promising results and gave rise to hope that this technique can be used for solid tumors in the future (Akce *et al.*, 2018; Liu *et al.*, 2021; Srivastava *et al.*, 2021).

1.2.3 Mouse models to study MYC in PDAC

In vivo studies investigating the role of MYC in PDAC have been performed with two main strategies. First, transformation of the pancreas can be induced by activating the MYC protein e.g. with MYC-ER chimeras that can be initiated with tamoxifen or by inducing ectopic expression of MYC with a tissue specific Cre-recombinase (Felsher and Bishop, 1999; Muthalagu *et al.*, 2020; Sodir *et al.*, 2020).

On the other hand, MYC can be studied in the context of a genetic engineered mouse model (GEMM) with mutations in KRas and Tp53, which better reflect mutations and pathology of human patients. There is a overwhelming amount of different GEMM that model the pathophysiological role of mutations and oncogene activations in pancreas. For example, the activation of $KRas^{G12D}$ alone induced formation of PDAC over time, while mutations in tumor suppressors alone (Cdkn2a, Smad4, Tp53) were not sufficient to cause either PanIN lesions or pancreatic cancer to develop (Westphalen and Olive, 2012). In recent years the KPC (KRas, Tp53, Cre-Recombinase) GEMM has become the gold standard for investigating the development and progression of pancreatic ductal adenocarcinoma (Hessmann *et al.*, 2016) ***(Figure 5)***. In the KPC model, tissue specific activation of the Cre-recombinase induces concomitant expression of $Tp53^{R172H}$ and $KRas^{G12D}$ mutants from their endogenous locus (Hingorani *et al.*, 2005).

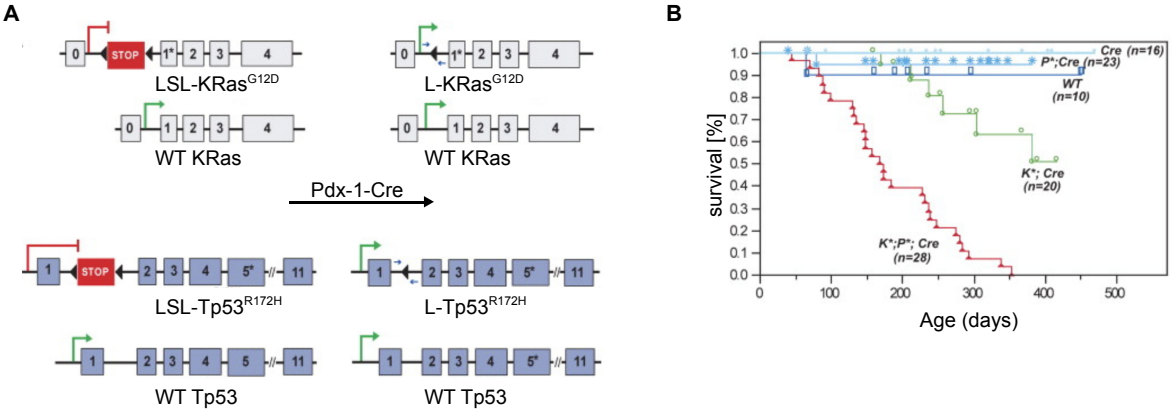

Figure 5: Mouse model for PDAC driven by mutations in KRas and Tp53*. A: Scheme shows conditional activation of mutated KRas and Tp53 in pancreata of mice. B: Survival of mice with activation of different alleles. Figure adopted from Hingorani et al., 2005.*

In the KPC mouse model the Cre recombinase is in most cases controlled by the Pdx-promoter, but there are also Cre-recombinases that are controlled by the Sox9- or Ptf1a-promoter, all leading to early transformation of the pancreas. Ptf1a is exclusively expressed in acinar cells in the adult mice, while Pdx is restricted to islet cells (Hingorani *et al.*, 2003). Sox9 is expressed in ductal cells and centroacinar cells (CAC) (Shroff *et al.*, 2014). Comparison between Sox9-CreER and Ptf1a-CreER showed that Sox9 can be used to distinguish between recombination in the ductal or acinar compartment. Formation of PanIN lesions was reduced in Sox9-Cre driven transformation compared to Ptf1a-Cre driven transformation (Kopp *et al.*, 2012). The Tuveson laboratory established PDAC tumors by using Pdx- or Ptf1a-Cre and LSL-$KRas^{G12D}$, both leading to the development of PanIN lesions (Westphalen and Olive, 2012). Activation of the driver mutation in KRas and the tumor suppressor Tp53 cause very fast onset of pancreatic ductal adenocarcinoma. The combination of both accelerates the development of a metastatic PDAC in mice compared to $KRas^{G12D}$ activation alone (Hingorani *et al.*, 2003; Hingorani *et al.*, 2005). Tumors from the KPC mouse model display loss of heterozygosity (LOH) at the *Tp53* locus and also genetic instability that allows further accumulations of mutations (Hingorani *et al.*, 2005).
Comparison between Sox9- and Ptf1a-Cre, $KRas^{G12D}$ and $Trp53^{f/f}$ mice revealed significant difference in the activation of interferon (IFN) related genes and dsRNA-sensors (Espinet *et al.*, 2021). Moreover,

different mutations in Tp53, as well as $Tp53^{0/0}$ (complete deletion of Tp53), elicit a very different immunogenic response in the cells when compared to wildtype murine Tp53 (Ghosh *et al.*, 2021). This points out that there are multiple layers that influence PDAC development and maintenance, and that there are different evolutionary pressures for the tumor resulting in diverse evolutionary routes.

Besides its strong capacity in recapitulating the mutational pattern, pathology and progression of human PDAC patients, two bottelnecks challenge the work with the KPC GEMM: First, the tumors arise spontaneously and it may take some time for them to develop and progress to PDAC. Second, integrating genetic modifications in the tumor cells to study the influence of oncogenes and tumor suppressors is not only time-consuming but also presupposes crossing of mouse strains. The latter problem could be overcome by genetic manipulation of mouse-derived KPC allografts, which can then later be orthotopically re-transplanted to investigate the consequences of manipulation on tumor engraftment and maintenance in an immune-competent mouse. Orthotopic transplantation into the pancreata of syngeneic mice phenocopies histology, desmoplasmia, stromal response and exclusion of T cells (Li *et al.*, 2019a; Pham *et al.*, 2021). These methods provide a comparably easy and fast protocol to, firstly, genetically modify murine PDAC cells using for instance lentiviral infection or CRISPR-Cas9 technology, and, secondly, investigating cellular consequences of these modifications in culture and *in vivo*.

1.3 Immunity in cancer

1.3.1 The immune system: Two lines of defense

Evolutionarily the immune system developed as a complex network consisiting of highly specific cells, chemicals and signaling pathways that collaborate to protect the integrity of a single cell as well as a complex organism ***(Figure 6)***. In a simplified view on this highly complex system, the immune system consists of "two lines of defense", the innate and the adaptive immune system. While the innate system responds fast, non-specifically and independently of antigens to the invasion of the cell and the organism, the adaptive system relies on the recognition of specific antigens and can memorize antigens. Thus, it learns to respond fast and precisely to fight pathogens quickly and efficiently (Marshall *et al.*, 2018).

The **innate immune system** acts as the first line barrier to prevent and defend against infections. This includes barrier surfaces (such as skin and mucosa), but also specialized myeloid and lymphoid cells that recognize and fight infections. The immune system is a tightly controlled, balanced and versatile interplay of several cell types, physical barriers and signaling molecules to efficiently fight pathogenes, but also to prevent overactivation and systemic inflammation, which is harmful to the individual (Janeway, 2005).

Cellular pattern recognition receptors (PRR) sense these pathogens and infections, activate intracellular pathways and induce the secretion of specific factors to communicate with the microenvironment as well as innate immune cells and adaptive immune cells (Brubaker *et al.*, 2015).

Innate immune cells can arise from the myeloid or lymphoid lineage. Common myeloid progenitor cells give rise to, amongst others, neutrophils, macrophages, dendritic cells, while natural killer (NK) cells differentiate from lymphoide progenitors ***(Figure 6)***.

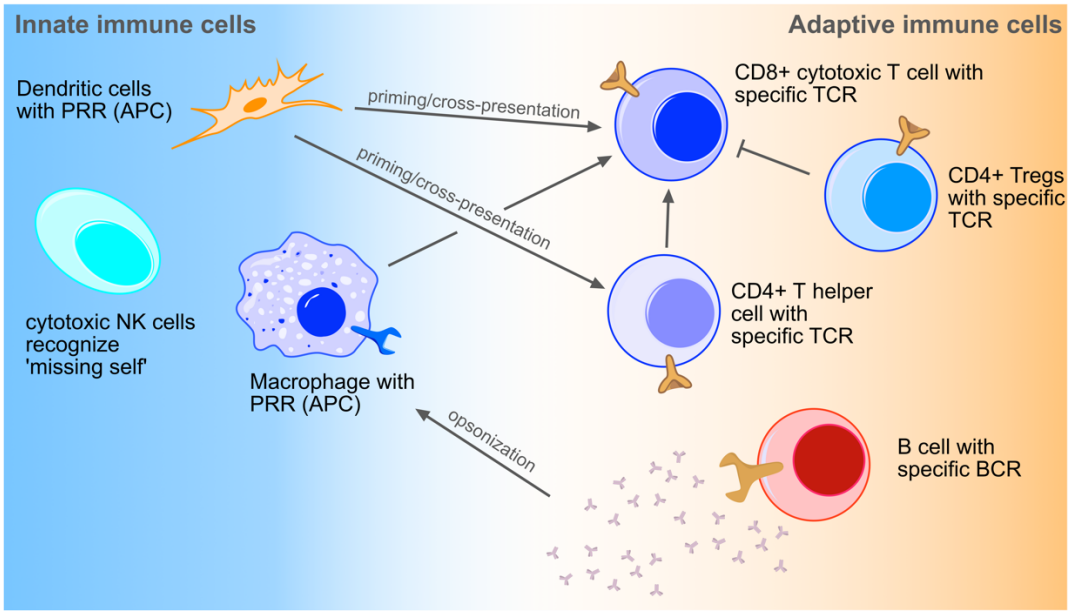

Figure 6: Simplified view on the innate and adaptive immune system and their crosstalk. *The innate and adaptive immune system communicate to form a memory for antigens and to modulate the immune response.*

NK cells are effector lymphocytes that can target pathogens or tumor cells, therefore limiting their expansion. The cell surface presentation of MHC class I molecules inhibits NK cell function, while stress-induced MHC class I-deficient cells are cleared by NK cells ("missing self") (Kärre *et al.*, 1986). This stress can range from viral infection to neoplastic transformation, that can trigger stress in the endoplasmtic reticulum limiting peptide processing (Granados *et al.*, 2009). However, there are several mechanisms how tumor cells prevent the eradication via NK cells. In the tumor microenvironment (TME) NK-activating surface-ligands for the NKG2D receptor are downregulated by their release in exosomes or by metalloproteinase-mediated cleavage (Chitadze *et al.*, 2013a; Chitadze *et al.*, 2013b; Paczulla *et al.*, 2019; Raulet *et al.*, 2013). The presentation of peptide-loaded HLA-E acts as a ligand for the CD94-NKG2A complex, that inhibits NK function (Braud *et al.*, 1998). Also the release of transforming growth factor-β (TGF-β) by tumor cells can reduce NK cell proliferation and cytotoxicity (Viel *et al.*, 2016).

Macrophages can remove and recycle dead cells, tissue debris or pathogens by phagocytosis and thereby play an essential role in homeostasis of organs (Mosser *et al.*, 2021). They are also highly sensitive for pathogen-associated molecular patterns (PAMPs), and damage-associated molecular patterns (DAMPs). Therefore, they show a high expression of specific receptors, which are described in more detail in ***section 1.3.2***.
Engagement of these receptors causes major changes in the expression profile of macrophages, from an M0 to an activated M1 phenotype with the potential to destroy tumor cells (Su *et al.*, 2016). M1 macrophages are phagocytes and can remove infected or transformed cells. Pathogens or cells are labelled via opsonization with antibodies secreted by plasma cells. The Fc receptor on macrophages recognizes these antibodies and eliminates the labelled pathogen or cell. Importantly, tumor cells are able to establish an immunosuppressive transcriptional program that can convert macrophages to the M2 phenotype. M2 macrophages are defined as tumor-associated macrophages (TAM) and contribute to tumor progression by providing an immunosuppressive microenvironment (Lin *et al.*, 2019).
Dendritic cells (DC) are antigen-presenting cells that are needed to establish an antigen-specific immunity, but also to ensure self-tolerance. DCs are sensing patterns of pathogens and damage with different receptors to integrate environmental signals (Schlitzer *et al.*, 2015). They link the innate immune system to the adaptive immune system by priming cytotoxic T cells or activating T helper cells by processing and cross-presentation of tumor-associated antigens. The presence of dendritic cells is a marker for good prognosis and expression of IL-12, a product of DCs, correlates with a good response to chemotherapy (Böttcher *et al.*, 2018; Broz *et al.*, 2014; Diao *et al.*, 2018; Ruffell *et al.*, 2014). Knockout mice lacking DCs have no capacity to recruit cytotoxic T cells to tumors (Spranger *et al.*, 2017).

The **adaptive immune system**, also called **acquired immunity**, can recognize specific "non-self" antigens ***(Figure 6)***. It memorizes specific antigens and therefore after a first infection has the capacity to respond fast and specific to known pathogens (Marshall *et al.*, 2018). This memory develops via

interaction with the innate immune system, e.g. dendritic cells. Two types of immune cells drive this specific immune response: T cells and B cells.

T cells originate in the bone marrow and mature in the thymus. Each T cell expresses a single, specific T cell receptor (TCR) that can recognize one specific antigen. They highly specific express CD3 on their surface. Once a T cell is stimulated by binding to an MHC class I presented peptide, the T cells can rapidly proliferate and expand to elicit a very fast and highly specific response (Marshall *et al.*, 2018). To achieve this specificity and tightly control activation, several subpopulations contribute to the adaptive immune response of T cells. CD8-positive cytotoxic T cells (effector T cells) secrete perforines and granzymes to induce programmed cell in target cells and eliminate infected cells (Salti *et al.*, 2011). CD4-positive T helper cells contribute by activation of effector T cells (and also B cells) by secreting IFN-γ, but also by dampening regulatory T cells (Tregs). Regulatory T cells have the capability to quench the activation of cytotoxic effector cells (Bold and Ernst, 2012; Castro *et al.*, 2018; Janeway, 1999).

Theoretically, T cells per se have a great ability to eliminate tumor cells, but tumors developed several mechanisms to evade the cytotoxic effect of T cells. First, many tumors (40-90%) downregulate the surface presentation of MHC class I proteins and thereby limit the presentation of antigens (or neoantigens) on the surface (Cornel *et al.*, 2020). Second, T cells need two stimuli to get fully activated. The binding of the TCR to an antigen in the absence of inflammation or co-stimulation leaves the T cell in a hyporesponsive state called “anergy”, pointing out that indeed also tumor cells need to release certain proinflammatory signals. Moreover, T cells in the tumor microenvironment are often in a dysfunctional state called “exhaustion” or can be inactive due to the release of immunesuppressive cytokines. This state describes T cells with very poor effector function and expression of inhibitory receptors like PD-1 (Wherry, 2011).

There are several mechanisms described how T cells are getting in an exhausted state in the TME. Due to their aberrant metabolism, cancer cells release lactate to the TME (de la Cruz-López *et al.*, 2019). On the on hand, lactate suppresses the proliferation of the effector T cells and, on the other hand serves as a carbon source for regulatory T cells, further dampening the activity of cytotoxic T cells against cancer cells (de la Cruz-López *et al.*, 2019; Multhoff and Vaupel, 2021; Quinn *et al.*, 2020). In addition, especially SMAD4 mutated tumors secrete TGF-β, which prevents the activation of the immune system (Batlle and Massagué, 2019).

Moreover, T cells have a specific TCR that recognizes a specific antigens, but sequencing of patient samples uncovered that not all patients have tumor-reactive T cells in the TME at all. This underlines the importance of the crosstalk between the innate and the adaptive immune system to generate a highly-specific immune response against tumors. This crosstalk can be perturbed in the tumor microenviroment, preventing a adaptive immune response (Spranger *et al.*, 2015; Spranger *et al.*, 2017).

B cells mature in the bone marrow and are the majore source of humoral immunity. Like T cells, B cells have a specific receptor (BCR, B cell receptor) that can recognize a specific antigen. If a B cell gets activate it transdifferentiates into plasma cells, memory B cells or follicular B cells that than produce and

secrete antibodies. These antibodies opsonize specific antigens and thereby mediate the recognition via the Fc receptor of phagocytes to eleminate the pathogens or an infected cells (Janeway, 1999). This again emphazies that the innate and adaptive immune systems not only talk to each other, but also condition each other, especially through cross-presentation of peptides to establish the antigen-specific immune response.

1.3.2 Intracellular innate immune system

As described, the innate immune system is a complex network of receptors, physical barriers and cells that monitor the presence of pathogens. More precisely the innate immune system recognizes “patterns” indicating the presence of pathogens, such as double-stranded RNA or DNA in the cytoplasm, uncapped RNA, CpG-rich DNA, unmethylated RNA, lipopolysaccharides and various kinds of lipids which are pathogenic (by)products. This is very similar to PAMPs and DAMPs, which arise in cells as a consequence of cell death, DNA damage, transcriptional or replicational stress. In order to surveil whether there is an infection or a damage, both, PAMPs and DAMPs, engage a versatile network of PRRs (Amarante-Mendes *et al.*, 2018). They are predominantly located in the cytoplasm or are associated with compartments like endosomal membranes or the plasma membrane of the cell (Medzhitov and Janeway, 1997) ***(Figure 7)***.

There are five major classes of PRRs: The family of Toll-like receptors (TLR), the retinoic acid-inducible gene I-like receptor (RLR), the nucleotide oligomerization domain (NOD)-like receptors (NLR), the C-type lectin receptors (CLRs) and absent in melanoma-2 (AIM2)-like receptors (ALRs) (Li and Wu, 2021). Engagement of these receptors activates downstream signaling to stimulate proinflammatory programs, increase for instance autophagy to clear infectious agents, induce cell death to eliminate infected cells, or activate immune cells to attack infected cells (Bortoluci and Medzhitov, 2010; Delgado and Deretic, 2009; Medzhitov *et al.*, 1997).

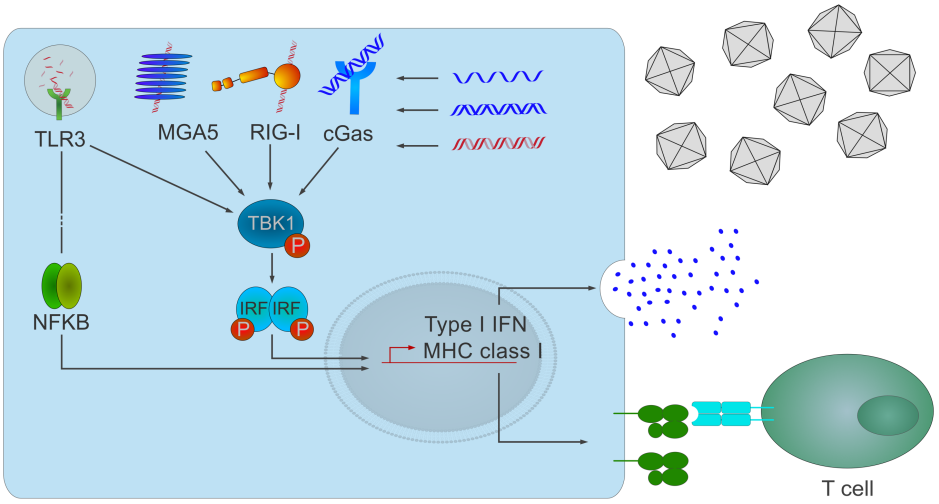

Figure 7: Pattern recognition receptors monitor infections and pathogens in the cell and its environment. *PRRs can sense foreign nucleic acids and activate the innate immune system. This causes upregulation of antigen presentation and secretion of type I interferons.*

There is a long list of PAMPs and DAMPs, but this introduction focuses on the description of PRRs that recognize various types of RNA and DNA which appear as DAMPs in normal cells and cancer cells. PRRs have been discovered first as part of the first line of defense against for instance viral or bacterial infection. The pathogen-derived RNA and DNA presents special patterns that can be recognized by PRRs: Some PRRs recognize double-stranded RNA in the cytoplasm, endosomes or in the cell periphery (TLR3, TLR10, RIG-I, MDA5, LGP2), others recognize single-stranded RNA (TLR7, TLR8, TLR13), double-stranded DNA in the cytoplasm (ALRs, cGAS) or single-stranded DNA in the cytoplasm (TLR9) (Kumar, 2021; Pohar *et al.*, 2017). However, there is increasing evidence that also endogenous RNAs and DNAs significantly engage these receptors and communicate with the immune system, especially in the context of tumorigenic growth or autoimmune diseases.

Endogenous immunogenic RNA and DNA can originate from two subcellular compartments. First, RNA and DNA from mitochondria is highly immunogenic. The circular mitochondrial chromosome is transcribed from two promoters, resulting in long, polycistronic transcripts. Even though mitochondrial transcription is tuned to process RNA co-transcriptionally, double-stranded RNA can still escape from this bidirectional transcription process (Linder and Hornung, 2018). Loss of mitochondrial integrity due to stress or damage can result in mitochondrial leakage and RNA accumulation in the cytoplasm. Also, mitochondrial DNA (mtDNA) was shown to trigger TLR9, inflammasome (NLRP3), AIM2 and cGAS (West and Shadel, 2017).

Second, also nuclear genomic DNA or transcripts can activate the innate immune system. Single-stranded or double-stranded DNA fragments originating from DNA damage or DNA-RNA hybrids (R-loops) are engaging PRRs (cGAS, AIM2) as soon as they are shedding out of the nucleus (Weinreb *et al.*, 2021; Wolf *et al.*, 2016). Also, micronuclei are recruiting cGAS and activate the cGAS-Sting axis (Decout *et al.*, 2021; Mackenzie *et al.*, 2017). Another DAMP that originates from the nucleus is double-stranded RNA. The predominant source of nuclear dsRNA are repetitive elements interspersed throughout the genome. These repetitive elements make up to 50-75% of the human genome (de Koning *et al.*, 2011; Liehr, 2021).

One family of repetitive elements are Alu elements (in humans) and B1 and B2 elements (in mice), that belong to the short-interspersed elements (SINE) which are located throughout the whole genome. These SINE elements have a size of 150-300 bp (Deininger, 2011; Krayev *et al.*, 1982). A single Alu (or B1/B2) element cannot be recognized by most PRR as it cannot form a duplex structure longer than 40 bp (Athanasiadis *et al.*, 2004). Two Alu (or B1/B2) elements oriented as inverted repeats (IR) can instead internally hybridize in a single RNA strand and form a duplex structure (Ahmad *et al.*, 2018).

Considering this high immunogenic potential of endogenous dsRNA, the cell has developed several mechanisms to prevent undesirable systemic activation of the immune system. First, mtDNA, mtRNA and nuclear DNA are protected in a subcellular compartment that is not invaded by PRRs. Second, there are several mechanisms to degrade these RNA and DNA species once they are leaking out of their intended compartment. For instance, AGO1x and DICER1 prevent accumulation of dsRNA in the cytoplasm, while the TREX1 exonuclease degrades ssDNA and ADAR1 edits dsRNA by changing

adenosines to inosines in the duplex structure (Ghosh *et al.*, 2020; Kaneko *et al.*, 2011; Yang *et al.*, 2007). Modification by ADAR1 helps to prevent recognition by PRR that can now distinguish between foreign and self-RNA (Ahmad *et al.*, 2018; Liddicoat *et al.*, 2015). Third, multiple strategies allow PRR to discriminate between self and foreign RNA. RIG-I monitors the 5'-end of RNA for the lack of eukaryotic posttranscriptional modifications (e.g. 5'-cap) (Rehwinkel and Gack, 2020). MDA5 does not recognize duplexes edited by ADAR1, and TLR3 is located in endosomes and at the plasma membrane, preventing immediate engagement by dsRNA that is shedding out of the nucleus (Ahmad *et al.*, 2018; Matsumoto *et al.*, 2014).

Once engaged, PRRs activate a signaling cascade that promotes antiviral, proinflammatory and pro-immunogenic pathways. Both RIG-I and MDA5 oligomerize and activate MAVS that is implicated to induce the autophosphorylation of TBK1. TLR3, anchored in the endosomal membrane, recruits TRAF3/TRIF/TAK1 to activate the canonical NF-κB signaling and can in parallel also induce the autophosphorylation of TBK1 (Li and Wu, 2021). Engagement of cGAS with dsDNA causes production of cGAMP that activates STING and downstream TBK1.

TBK1 is mainly described to activate IRF3 and IRF7 (both implicated in type I interferon response), but also promotes autophagy and vesicular transport by e.g. phosphorylating SQSTM, optineurin or Rab proteins that control endosomal maturation (Alonso-Curbelo *et al.*, 2014; Heo *et al.*, 2018; Honda *et al.*, 2006; Outlioua *et al.*, 2018; Richter *et al.*, 2016; Ritter *et al.*, 2020; Schlütermann *et al.*, 2021; Wandinger-Ness and Zerial, 2014).

Mutations in all these pathways are causing severe autoimmune disorders like Aicardi-Goutières syndrome (AGS) or systemic lupus erythematosus (SLE). However, their role in cancer is vastly emerging, and several publications over the last decade clearly linked immunity of cancer cells to engagement of PRRs with endogenous DAMPs.

Long dsRNAs originating from mitochondria are highly immunogenic, engage MDA5 and activate downstream type I interferon signaling (Dhir *et al.*, 2018). Ghosh and colleagues showed that a gain-of-function mutation in AGO1 is needed to degrade dsRNA, prevent type I IFN signaling as well as apoptosis, and support proliferation of breast cancer tissue (Ghosh *et al.*, 2020). These findings open up potential novel avenues in cancer therapy through the restoration of the visibility of cancer cells to the immune system. For instance, inhibition of DDX3X, together with ADAR1, stabilizes dsRNA and promotes anti-tumor immune response (Choi *et al.*, 2021). Also targeting splicing and thereby increasing the intron-retention and amount of dsRNA provides a promising strategy (Bowling *et al.*, 2021; Wu *et al.*, 2018). Very similar approaches that utilize the cGAS-STING axis are also promising mediators to restore immune surveillance and induce tumor regression (Decout *et al.*, 2021; Hoong *et al.*, 2020; Morel *et al.*, 2021). Moreover, the use of DAMP-mimetics to activate the innate immune system is currently under investigation (Asthana *et al.*, 2020; Qu *et al.*, 2013). For example, poly (I:C), a synthetic TLR3 ligand, is used as an adjuvant to promote effects of CAR-T cells (Di *et al.*, 2019).

On the other hand, cancer cells developed a variety of mechanisms to escape these responses. For example, the loci containing the interferon genes that are essential for immune response are in some cases completely deleted, especially in tumors with alterations of the *CDKN2A* locus (Barriga *et al.*, 2022; Delaunay *et al.*, 2020; Grard *et al.*, 2021; Mora *et al.*, 2004). Furthermore, mutated Tp53 interferes with the activation of the innate immune system in a broad variety of entities by preventing a STING-dependent activation of TBK1 (Ghosh *et al.*, 2021). There is evidence in the literature that MYC biology, immune escape and innate immunity are converging, suggesting a protruding role of MYC proteins in promoting the escape of the tumor from the (innate) immune system (Bowling *et al.*, 2021; Lee *et al.*, 2022b; Muthalagu *et al.*, 2020; Topper *et al.*, 2017; Wu *et al.*, 2021; Zimmerli *et al.*, 2022).

1.3.3 MYC-driven immune evasion

Over the past decade, two key observations in the field became more and more important: First, tumors develop and progress in the presence of the immune system. Which mechanism drives the immune evasion and prevents immune surveillance is still being debated. Second, deregulated expression of MYC promotes immune evasion in several entities. Most notably, the model of MYC-mediated suppression of the immune response in cancer cells has been developed in the laboratories of Dean Felsher and Gerard Evan. Today, an increasing number of publications underline that the immune evasive capacity of the MYC protein family is hard-wired in MYC biology.

The innate and adaptive immune system as well as their interplay are critical to achieve a long-lasting regression of tumors. In a T cell lymphoblastic leukemia (T-ALL) model, CD4-positive T cells are critical to reduce minimal-residual-diseases and to achieve long-term survival after inactivation of the MYC oncogene. In this model, CD4-positive T cells reshape the microenvironment by switching off angiogenesis and preventing tumor recurrence (Rakhra *et al.*, 2010). In non-small cell lung cancer, both KRAS and MYC are needed to prevent natural killer cells from eradication of tumor cells. In detail, MYC and KRAS modulate the TME via the induction of specific chemokines that recruit tumor-associated macrophages and promote exclusion of innate and adaptive effector immune cells (Casacuberta-Serra and Soucek, 2018; Kortlever *et al.*, 2017). Casey and colleagues provide insight into the role of MYC in binding and regulating specific genes to promote immune evasion. PD-L1 and CD47, which are major mediators of immune evasion, are bound by MYC in T-ALL cells to promote expression and suppress immune surveillance. MYC inactivation induces a tumor regression which is reverted by the ectopic expression of PD-L1 or CD47, pointing out that the major oncogenic function of MYC *in vivo* is likely its potential to make tumors invisible for the immune system (Casey *et al.*, 2017; Casey *et al.*, 2016).

Sodir and colleagues used an inducible MYC chimera and the mutated $KRas^{G12D}$ to investigate the role of MYC in maintaining the integrity of pancreatic ductal adenocarcinoma. In this model KRas mutations drive the development of PanIN lesions, as also seen in patients. Additional activation of the MYC oncogene promotes the progression towards an adenocarcinoma. MYC prevents the influx of T cell, B cells and NK cells into the tumor mass and ablation of B cells also dampens NK cell influx (Sodir *et*

al., 2020). The consequences of MYC activation and inactivation in early and advanced stages of cancer have been described in different entities (Kortlever *et al.*, 2017; Sodir *et al.*, 2020).

Similarly, Muthalagu and colleagues used a tamoxifen-inducible MYC-ER chimera to induce PDAC in a mouse model (Muthalagu *et al.*, 2020). As already shown in a KPC mouse model that evolves evolutionarily with a mutational pattern that mimics human patients, MYC and MIZ1 are both haplo-insufficient during PDAC development (Walz *et al.*, 2014). In Muthalagu *et al.* they provide a model in which MYC and MIZ1 cooperatively bind to the promoter of interferon-regulatory factors (IRFs) and STAT proteins to suppress type I interferon signaling that activate the immune system (Muthalagu *et al.*, 2020). There are similar observations in non-small-cell lung cancer, where targeting epigenetic modifications reduced MYC transcription and activated type I interferon signaling and downstream secretion of T cell-activating chemokines (Topper *et al.*, 2017).

Unlike in human patients, in most of these mouse models MYC is acutely induced using tamoxifen and a MYC-ER chimera. On the one hand, this allows monitoring of the acute and immediate effects of the oncogene induction or inactivation. On the other side, tumors have supraphysiological levels of MYC and mutations do not reflect the pathology and mutation pattern in human patients, which is a major limitation of this model.

While the role of MYC in immune evasion of cancers is now widely accepted, key mechanistic details remain unsolved: Which mechanisms and signals drive the activation of immune regulatory pathways? How does MYC promote the immune evasion in highly proliferating tissue?

Answering these questions is scientifically intriguing, but also of paramount importance from a translational point of view. As the development of immune-oncology, antibody therapy and immune checkpoint inhibitors proceeds at stunning rates, a promising strategy will be the use of these therapeutic approaches to target the majority of cancers, where MYC and its paralogues are overexpressed, amplified, stabilized or deregulated.

1.4 Targeting MYC

The sections above suggest that targeting MYC as an anti-cancer therapy is a promising endeavor. Still, some features of the MYC protein make it difficult to develop efficient therapeutic strategies: First, MYC proteins are unstructured without any targetable enzymatic activity. Secondly, targeting a transcription factor that is essential for a broad range of proliferating tissues can cause severe side effects. Therefore, the discrimination between MYC oncogenic function and MYC role in healthy proliferating cells is essential for a translational approach. The conceptional work done with the overexpression of Omomyc in a $KRas^{G12D}$-driven lung cancer has proved that there is a window to systematically interfere with the function of MYC without causing severe side effects for the mice (Soucek *et al.*, 2008; Soucek *et al.*, 2013).

So far, there are five potential strategies to target MYC. First, MYC mRNA can be reduced by decreasing transcription with G4 stabilizers (e.g., JQ1) or by using antisense RNA (Mertz *et al.*, 2011; Rangan *et al.*, 2001; Wolf and Eilers, 2020). Secondly, the translation of MYC proteins can be blocked, e.g. with rapamycin, silvestrol or cymarin (Wall *et al.*, 2008; Wiegering *et al.*, 2015). Third, MYC protein stability can be reduced by targeting USP28, a deubiquitylating enzyme that counteracts the activity of SFC^{FBW7}, or USP11 (Diefenbacher *et al.*, 2015; Diefenbacher *et al.*, 2014; Herold *et al.*, 2019; Schulein-Volk *et al.*, 2014). Fourth, there are – in addition to Omomyc – drugs that destabilize MYC at chromatin (e.g. 10058-F4) or stabilize MAX homodimers that counteract the assembly of MYC/MAX heterodimers (Yin *et al.*, 2003). Finally, PROTACS (proteolysis-targeting chimeras) have been a rapidly growing field for several years with still much potential. PROTACs recruit E3 ligases to the protein of interest (i.e., MYC), inducing its ubiquitination and degradation by the proteasome (Burslem and Crews, 2020; Sakamoto *et al.*, 2001).

All these approaches are so far in early experimental stages or in very early clinical trials. Further research about MYC and its interaction partners have recently shed light on the potential Achilles heels of MYC-driven cancer cells, namely AURKA and ATR in MYCN driven neuroblastoma (Roeschert *et al.*, 2021), NUAK1 in MYC-driven colon cancer, which also offers a potential strategy via the reduction of co-transcriptional splicing (Cossa *et al.*, 2020; Liu *et al.*, 2012) or exosome-depletion in neuroblastoma (Papadopoulos *et al.*, 2022). A better understanding and validation of these interactions *in vivo* are necessary to provide further concepts that can be used for therapy.

The translation of MYC is regulated on the one hand by the IRES site in the 5'-UTR of the MYC mRNA and on the other hand by the binding of several microRNAs to the 3'-UTR, all coupled to different types of stress responses (Dejure *et al.*, 2017; Wiegering *et al.*, 2015).

The literature increasingly shows that cardiac glycosides (CG) are potent drugs for lowering MYC protein levels. Most studies focus on the decrease of MYC protein and its consequences in cell culture and *in vivo*. While some studies claim that the MYC decrease is mediated via the inhibition of IRES-mediated translation of MYC (Didiot *et al.*, 2013; Wiegering *et al.*, 2015), others only confirm that treatment with cardiac glycosides reduces MYC protein levels (Du *et al.*, 2021; Steinberger *et al.*, 2019) or is interfering

with the uncontrolled growth of cancer cells in culture and *in vivo* (Lan *et al.*, 2018; Schneider *et al.*, 2018; Shen *et al.*, 2020).

Cardiac glycosides act as inhibitors of the sodium-potassium pump (Na+/K+ pump). The sodium-potassium pump transports sodium ions out of the cell and potassium ions in the cells under the hydrolysis of ATP to maintain the membrane potential, that is also used by a number of crucial physiological processes (Pirahanchi *et al.*, 2022). For example, the import of a number of amino acids, nucleosides and calcium ions is dependent on the sodium gradient (Bhutia and Ganapathy, 2016; Gray *et al.*, 2004; Ottolia *et al.*, 2013). The mechanism by which treatment of cancer cells with cardiac glycosides causes downregulation of MYC protein levels is still unknown or at least controversial in the literature and further investigation is needed.

1.5 Aim of the thesis

There are three aspects that are hard-wired in MYC biology and make it a promising target for tumor therapy: First, MYC is activated, amplified, overexpressed and/or deregulated in nearly every single tumor. Second, MYC is binding to the core promoter of virtually all actively transcribed genes and the field is still discussing the extent and contribution of MYC to transcription and its link to tumorigenesis. Third, elevated levels of MYC protein prevent the recognition and clearance of the tumor by the immune system.

Thus, this study aims, on the one hand, to understand how and why MYC promotes an immune suppressive program that allows uncontrolled proliferation without surveillance by the immune system and on the other hand, how this knowledge can be transferred to a more translational setting in order to restore and increase the immune surveillance in MYC-dependent pancreatic cancer.

2 Results & Interpretation

2.1 MYC is critical for the growth of PDAC cells and PDAC tumors

2.1.1 MYC drives proliferation in culture

In order to investigate the role of MYC in pancreatic cancer we made use of cells from the KPC GEMM, a cell system that precisely reflects the two major driver mutations KRas and Tp53 in pancreatic cancer. Those mutations – observed in human patients – drive the transformation of the pancreas towards a highly aggressive pancreatic ductal adenocarcinoma. This model closely reflects not only the mutational pattern but also the pathophysiological features of this disease. Additionally, the KPC mouse model at least partially reflects the evolutionary development of PanIN lesions to an invasive and aggressive PDAC, changes in the tumor microenvironment and host-tumor interaction (Hingorani *et al.*, 2005). Therefore, it is a well-suited model to study pancreatic cancer, either in the GEMM, in cells isolated from the tumors, or in a syngeneic transplant system.

To better understand the immune evasive phenotype driven by high expression of the MYC oncogene, two different doxycycline-regulated systems were established to control levels of MYC protein in KPC cells derived from a murine PDAC model (Ptf1a-Cre, $KRas^{G12D/+}$, $Tp53^{R172H/+}$).
First, we lentivirally infected naïve KPC cells (constitutively expressing luciferase) with two different plasmids expressing distinct doxycycline-inducible shRNAs targeting *Myc* (hereafter: “shMyc”). From this cell pool, a single-cell-clone with a strong and stable reduction of MYC protein upon treatment with doxycycline (Dox) was established ***(Figure 8A)***. In parallel, a second system was designed to ectopically doxycycline-induce a human MYC-transgene (using a TET-on system, hereafter “MYC TET-ON”) in KPC cells with a knockout of endogenous MYC. To generate this KPC cell line, two guide RNAs binding in intron 1 and intron 2 of the endogenous MYC locus were transfected to cause a CRISPR/Cas9-mediated cut, leading to a premature stop codon after few amino acids ***(Figure 8B)***.
Immunoblot analysis revealed a strong reduction of MYC protein level in both systems. Similarly, doxycycline was effective in inducing ectopic expression of MYC, as the immunoblot showed super-physiological levels of MYC protein compared to wild-type cells.

First, the phenotype of MYC depletion in KPC cells was characterized. The proliferation of cells was measured by performing a cumulative growth curve. Reduction of MYC protein levels led to a strong decrease in cell number in both cellular systems. However, the proliferation directly correlates to the amount of MYC protein in the cells: Ectopic expression of MYC caused by far the shortest doubling time, followed by KPC cells with unaffected levels of MYC protein. Switching off MYC in TET-ON cells markedly reduced proliferation of the PDAC cells. Depletion of MYC using shRNAs was the most

effective approach to increase doubling time, leading to an apparent proliferation arrest in KPC cells ***(Figure 8C)***.

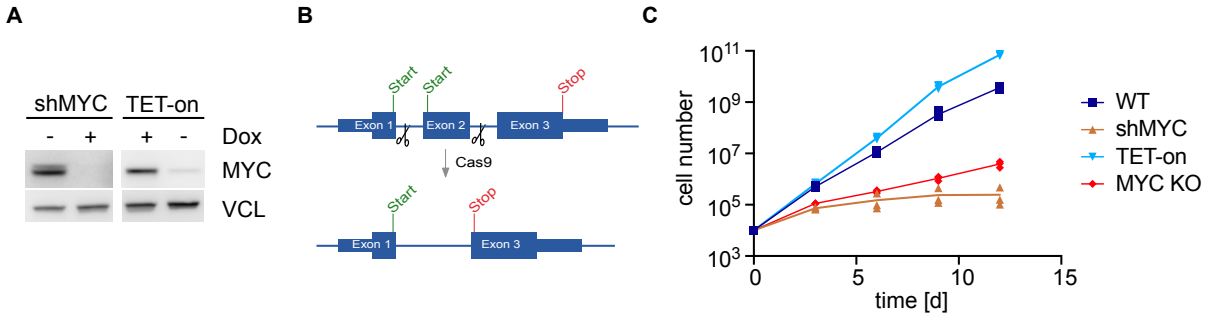

Figure 8: Targeting MYC in KPC cells decreases proliferation in culture. *A: Immunoblot of KPC cells expressing inducible shRNAs targeting MYC ("shMYC") and KPC cells bearing deleted endogenous MYC expressing an inducible MYC transgene ("MYC TET-on"). Where indicated 1 µg/mL doxycycline was added (n=5; in all subsequent figures n indicates the number of biological independent replicates). B: Schematics of CRISPR/Cas9 mediated deletion of endogenous Myc by removing exon 2. C: Cumulative growth curve of KPC cells with either inducible shRNA mediated depletion or deletion of MYC (n=3).*

To better characterize the proliferation phenotype, the thymidine analogue BrdU was added to KPC cells and BrdU incorporation was measured by immunofluorescence. The experiment showed a reduction of BrdU incorporation upon depletion of MYC, indicating that less cells progress into or through S phase ***(Figure 9A)***. Immunofluorescence also revealed a flattened morphology that is often associated with senescent cells ***(Figure 9B)***.

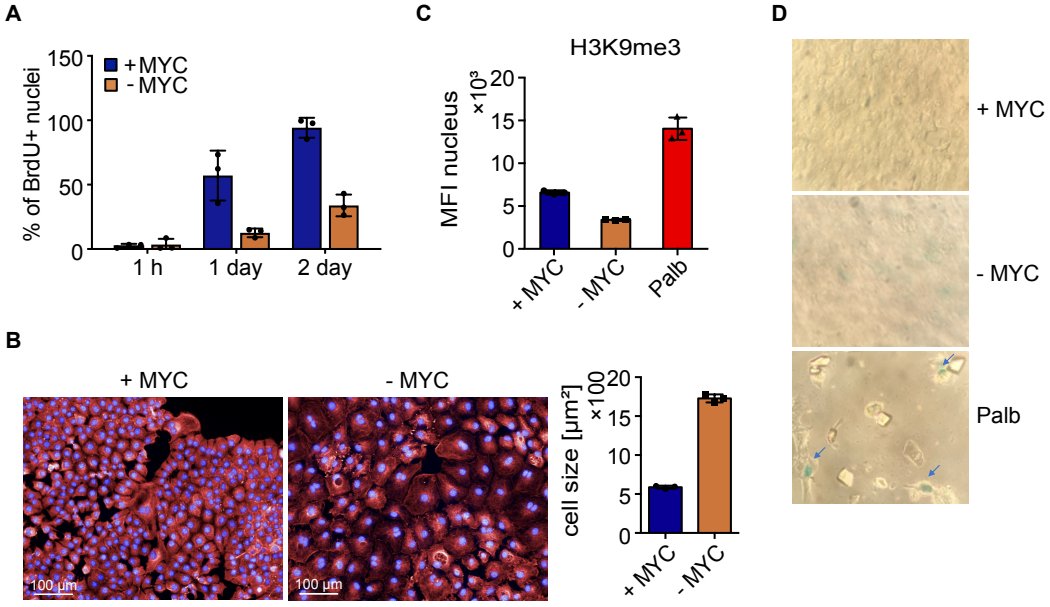

Figure 9: MYC drives proliferation of murine PDAC cells*. A: Quantification of BrdU incorporation in KPC cells upon depletion of MYC. Results are presented as individual values ±SD (standard deviation). B: Immuno-fluorescence of tubulin in KPC cells (red) with and without depletion of endogenous MYC. The cytoplasmic staining was used to measure the average cell size. Results are presented as individual values ±SD. C: Quantification of immunofluorescence against H3K9me3 in the nucleus in cells with depletion of endogenous MYC or treatment with CDK4 inhibitor palbociclib (10 µM). Results are presented as individual values ±SD. D: ß-galactosidase-assay in KPC cells with depletion of MYC. 10 µM Palbociclib was used as positive control.*

To investigate whether cells undergo senescence upon depletion of MYC we stained for H3K9me3, a common marker of senescence (Haferkamp *et al.*, 2013). Depletion of MYC caused downregulation of H3K9me3, while palbociclib (Palb), a CDK4 inhibitor (positive control for senescence), shows upregulation of H3K9me3 in the nucleus of treated cells ***(Figure 9C)***. Moreover, a β-Galactosidase assay did not show an increase in senescence after depletion of MYC ***(Figure 9D)***, pointing out that cells do not undergo senescence upon depletion of MYC.

To investigate the consequences of MYC depletion on the cell cycle progression, a PI-FACS was performed. Duration of G1 and G2/M phase was only mildly increased upon depletion of MYC while duration of S phase was increased from about 4 h to about 12 h ***(Figure 10A)***. Cells were treated for one hour with BrdU, subsequently stained with anti-BrdU-FITC and propidium iodide (PI), and finally analyzed using flow cytometry. Measurement of the BrdU incorporation showed that after 48 h of MYC depletion, cells accumulate at the beginning of S phase, as indicated by a marked shift in cell population at 2n, but fewer cells are in the remainder of S phase, as indicated by a sharp decrease in FITC signal (BrdU incorporation) ***(Figure 10B)***.

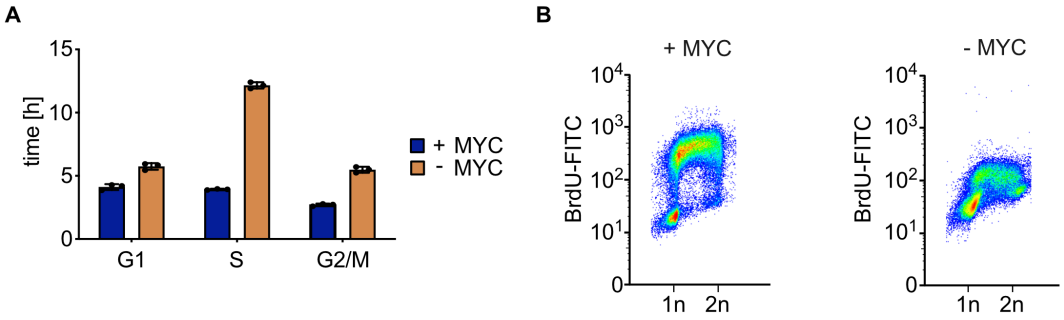

Figure 10: Depletion of MYC changes cell cycle profile. *A: Average duration of the cell cycle calculated from the doubling time and analysis of the cell cycle profile in KPC cells with or without depletion of MYC. Where indicated, MYC was depleted by addition of 1 µg/mL doxycycline. Results are presented as individual values ±SD. B: Flow-cytometry analysis of BrdU-incorporation KPC cells upon co-staining with propidium iodide (PI). MYC depletion was induced by doxycycline for 48 h (1 µg/mL).*

This observation indicates a role of MYC in mediating the progression through S phase. MYC has been shown to play a role in DNA damage repair in S phase (Endres *et al.*, 2021) and its family member MYCN is well described to play a role in transcription-replication coordination (Papadopoulos *et al.*, 2022; Roeschert *et al.*, 2021). Moreover, cells accumulate at the transition point between G1 and S phase, likely because depletion of MYC causes downregulation of genes that are essential to induce and progress in S phase (Leone *et al.*, 2001) or because they face an obstacle or stress early in the S phase that cannot be solved without MYC (Papadopoulos *et al.*, 2022; Solvie *et al.*, 2022).

2.1.2 Depletion of MYC changes expression profile of cells

To assess the effects on gene expression upon MYC depletion, RNA sequencing experiments with two different experimental approaches were carried out. First, cells were grown in 2D culture and MYC was depleted for 48 h using doxycycline-inducible shRNAs. Second, 50,000 KPC cells were orthotopically

transplanted into the pancreata of syngeneic male C57BL/6J mice. Tumors engrafted for 7 days and mice were fed with doxycycline containing food or normal food for 48 h.

RNA was extracted from cells as well as tumor tissue and a genome-wide mRNA expression analysis was performed using Illumina sequencing. Gene set enrichment analyses (GSEA) revealed that MYC-dependent changes in expression profiles are similar, both, *in vivo* and in culture. Depletion of MYC causes downregulation of all gene sets directly associated with MYC (i.e., "MYC_TARGETS_V1" and "MYC_TARGETS_V2") and all gene sets linked to cell cycle progression and proliferation ***(Figure 11A)***. A GO enrichment analysis performed for the hallmark gene sets "MYC_TARGETS_V1" and "MYC_TARGETS_V2" showed that both gene sets mainly contain genes that are linked to the canonical function of MYC, including ribosome biogenesis, translation of mRNA, and processing of mRNA ***(Figure 11B)***. Interestingly, in both experimental systems, depletion of MYC also caused a robust activation of canonical NF-κB signaling, inflammatory response, epithelial to mesenchymal transition (EMT) and TGF-β signaling ***(Figure 11A)***. The IL6/JAK/STAT3 hallmark gene set is probably induced because IL6 is a target of NF-κB (Liu *et al.*, 2017).

A

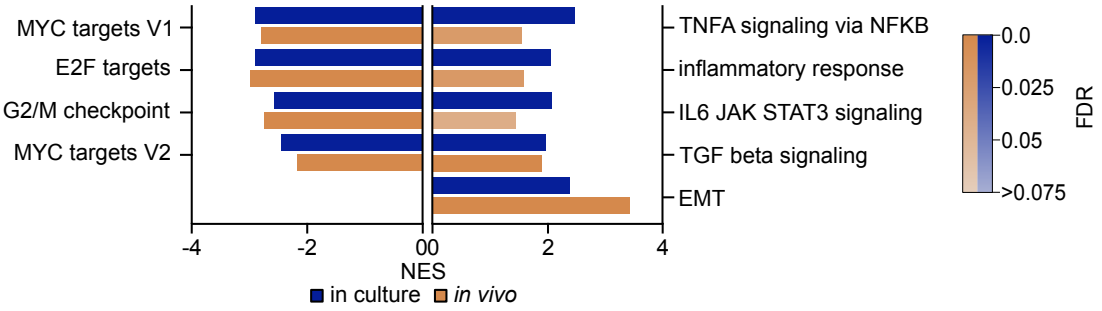

B

GO-terms	no of genes	q-value	hallmark of origin
RNA splicing	26	3.3e-16	MYC targets V1
mRNA processing	28	1.4e-15	MYC targets V1
translation	25	1.5e-10	MYC targets V1
rRNA processing	12	8.3e-12	MYC targets V2
ribosome biogenesis	9	1.5e-8	MYC targets V2

Figure 11: Changes in the global expression profile after depletion of MYC. *A: Gene set enrichment analysis of global RNA expression profile of KPC cells expressing doxycycline-inducible shRNAs to target MYC in cells from culture (n=3) and RNA derived from orthotopically transplanted KPC cells (n=5) after 48 h of doxycycline induced depletion of MYC (1 µg/mL). On the left side MYC activated hallmark gene sets are plotted, on the right side MYC repressed hallmark gene sets are plotted. NES: normalized enrichment score, FDR: false discovery rate. B: GO Term analysis of gene set MYC targets V1 and MYC targets V2.*

Strikingly, several studies indicated type I IFN signaling as a target of MYC mediated gene repression (Muthalagu *et al.*, 2020; Topper *et al.*, 2017; Zimmerli *et al.*, 2022). However, we cannot observe a consistent upregulation of IFN-α or IFN-γ target genes in KPC cells after depletion of MYC. This discrepancy could stem from the different tumor tissues analyzed (i.e., lung, breast) that probably display activity of different pathways compared to pancreatic cancer.

2.1.3 MYC-repressed genes are counter-selected against MYC binding

MYC has been shown to bind to all core promoters of actively transcribed genes (Herold *et al.*, 2019; Walz *et al.*, 2014). To understand how this translates into changes in the expression profile we analyzed chromatin-immunoprecipitation (ChIP) sequencing data of KPC cells previously generated by our lab (Walz *et al.*, 2014). We investigated MYC binding to the core promoter of up- and downregulated genes. Hallmark gene sets that are hard-wired to MYC biology (e.g., "MYC_TARGETS_V1" and "MYC_TARGETS_V2") show a strong binding of MYC to the core promoter ***(Figure 12)***.

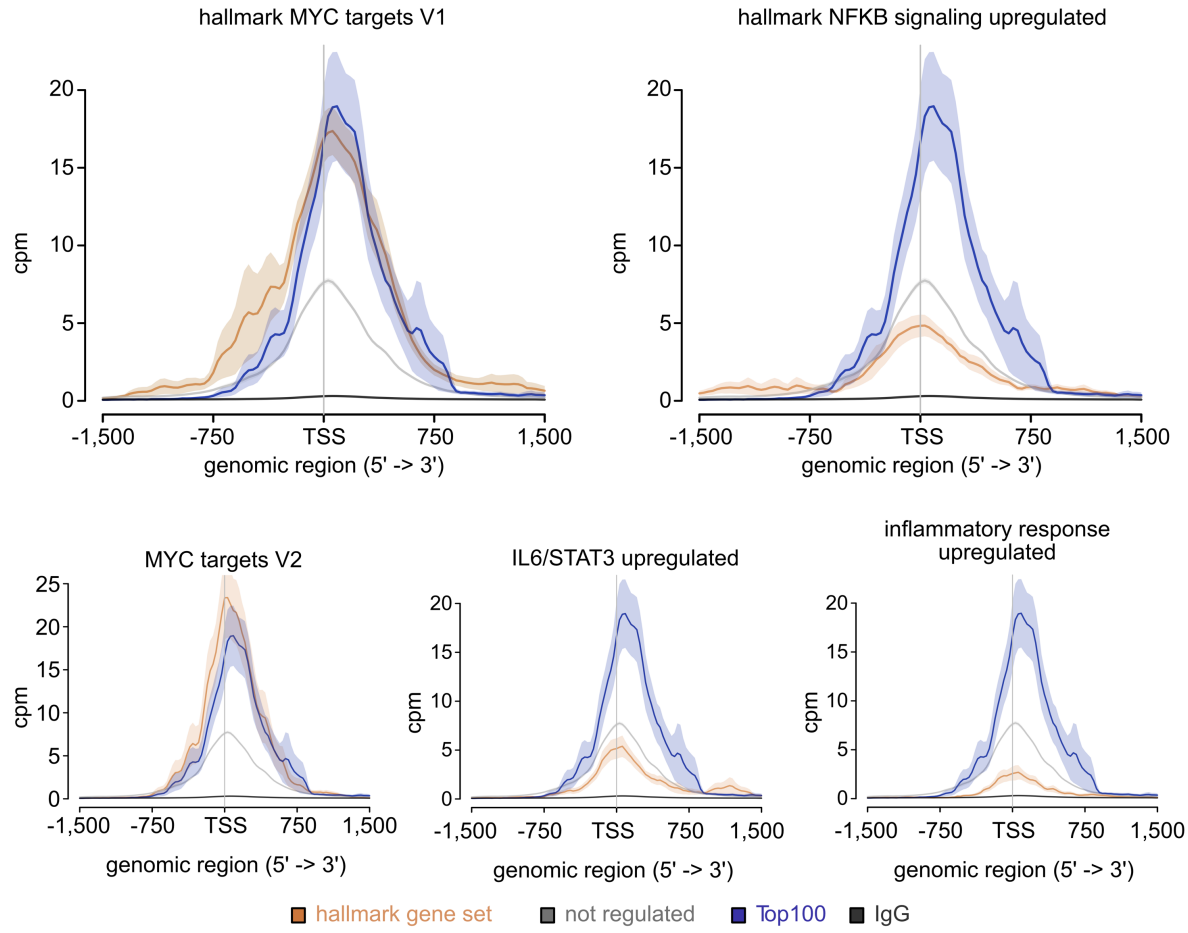

Figure 12: Metagene analysis of ChIP sequencing experiments in KPC cells showing binding of MYC at the TSS in different gene sets. *Counts per million (cpm) are plotted. Top100 indicates the 100 strongest MYC activated genes from RNA sequencing experiments. Not regulated includes 100 highly expressed genes that do not change expression with the depletion of MYC. The shadow shows the SEM (standard error of mean).*

Interestingly, this pattern is very similar to the one defined when assessing the binding of the hundred by MYC most upregulated genes ("Top100", blue). Not regulated genes (grey) still show a significant binding of MYC to the core promoter. Analysis of MYC and MIZ1 promoter binding to genes belonging to the hallmark gene sets "TNFA_SIGNALING_VIA_NFKB", "INFLAMMATORY_RESPONSE" and "IL6_JAK_ STAT3_SIGNALING", which are all repressed by MYC, showed a moderate binding, generally weaker than the one of not regulated genes ***(Figure 12)***. Similarly, MIZ1 was also not binding to the core promoter of the analyzed MYC-repressed gene sets ***(Figure 13)***.

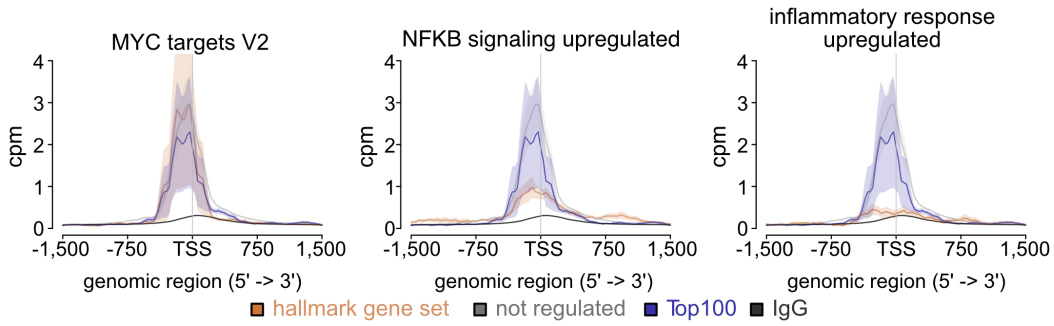

Figure 13: Metagene analysis of ChIP sequencing experiments in KPC cells showing binding of MIZ1 at the TSS in different gene sets. *Counts per million (cpm) are plotted. Top100 indicates the 100 strongest MYC activated genes from RNA sequencing experiments. Not regulated includes 100 highly expressed genes that do not change expression with the depletion of MYC. The shadow shows the SEM.*

It has been shown that oncogenic levels of MYC are causing an exhaustion of the available SPT5-pool in the cell by recruiting SPT5 either to MYC activated genes or by binding them independent of chromatin association. In parallel, low or no binding of MYC at the core promoter has been associated with poor SPT5-binding in the gene body and consequently repression of gene expression, specifically elongation ***(Figure 2)*** (Baluapuri *et al.*, 2019). We used the list of genes upregulated after depletion of MYC, that were already used in ***Figure 12***, to determine the binding of MYC. The squelching ratio was calculated from changes in SPT5-ChIP-Rx to genes U2OS cells and indicates the increase in SPT5 binding in genomic regions after activation of MYC (Baluapuri *et al.*, 2019).

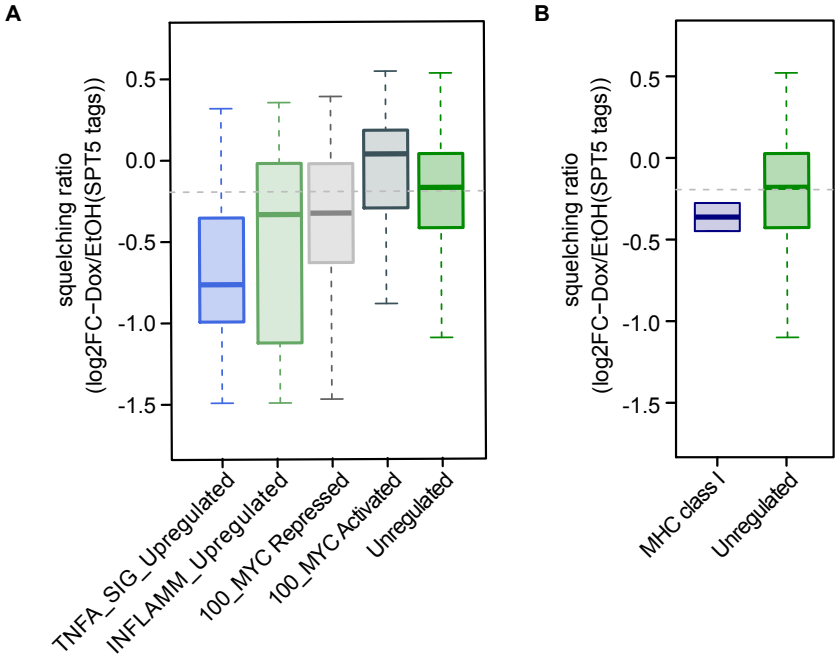

Figure 14: Squelching ratio for MYC repressed genes. *A: Squelching ratio calculated from ChIP-Rx published in (Baluapuri et al., 2019) for unregulated, Top100 activated and Top100 repressed genes. Squelching ratio of MYC-repressed genes of the hallmark.*

The Top100 activated genes show an increase in SPT5-Tags after activation of MYC. MYC-repressed hallmark gene sets like “TNFA-SIGNALING_VIA_NFKB” and “INFLAMMATORY_RESPONSE” display a reduction in SPT5 binding after MYC activation ***(Figure 14)***.

One major target of NF-κB-signaling are MHC class I genes, that have been already implicated to be repressed by MYC (Bernards *et al.*, 1986; Versteeg *et al.*, 1988). We calculated the squelching ratio of these genes and again found a reduction in SPT5-binding to these genes upon MYC activation.

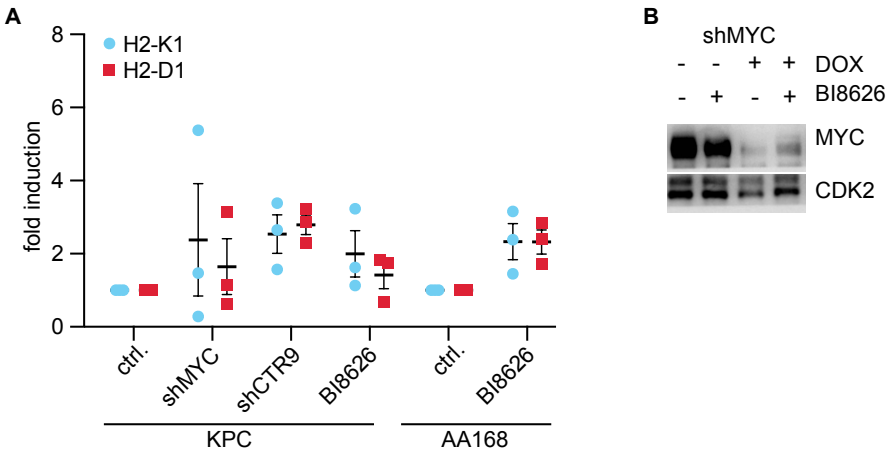

Figure 15: Inhibition of HUWE1 causes upregulation of MHC class I genes. *A: RT-PCR of H2-K1 and H2-D1 after depletion of MYC, CTR9 and inhibition of HUWE1 using 10 μM BI-8626. Data is presented as individual values and mean ± SEM (n=3) B: Immunoblot of MYC after depletion of MYC and treatment with BI-8626 for 24 h.*

Recent work supports this hypothesis showing that at oncogenic levels MYC multimerizes and relocates (with SPT5) from its cognate binding site to suppress transcription. These multimers are dependent on the ubiquitination by HUWE1, so treatment with BI-8626, a selective HUWE1 inhibitor induces the upregulation of MYC-repressed genes like the MHC class I genes H2-K1 and H2-D1 ***(Figure 15)***, that display squelching of SPT5 with oncogenic levels of MYC ***(Figure 14)***. This at least allows the hypothesis that MYC or MYC multimers promote immune evasion by squelching/ sequestration of SPT5 from the promoter of proimmunogenic genes.

Muthalagu *et al.* also studied MYC and MIZ1 mediated immune evasion in pancreatic cancer and found that MYC depletion induced the transcription of some of these genes which are bound by MYC and MIZ1 (e.g. IRF3) (Muthalagu *et al.*, 2020). In contrast, we do not observe significant binding of MYC or MIZ1 to the core promoter of these genes (Walz *et al.*, 2014). Anyhow, increased activation of especially IRFs and STATs is not implicative for increased transcription of their target genes, since they require activation by a signaling cascade to translocate. It has described already in several publications that MYC proteins are binding to the core promoter of all genes that are transcribed by RNA polymerase II. Activated genes distinguish especially in a processive elongation and not in pause release from repressed genes (Herold *et al.*, 2019; Walz *et al.*, 2014). This supports a model where oncogenic levels of MYC are squelching crucial elongation factors from a subset of genes, leading to a repression of the transcription of a proimmunogenic signature (Baluapuri *et al.*, 2019; Baluapuri *et al.*, 2020; Solvie *et al.*, 2022).

2.1.4 MYC depletion causes tumor regression in syngeneic mice

Considering the identified MYC-dependent transcriptional phenotype, we investigated the effect of MYC depletion on the *in vivo* growth of PDAC tumors. To this end, luciferase-expressing KPC cells with inducible shRNAs targeting MYC were transplanted into the pancreata of syngeneic male mice. After seven days of tumor engraftment MYC was depleted by feeding the mice with doxycycline-containing food. To study the growth of the tumors, luciferase signal was measured using the *in vivo* bio-luminescence imaging system (IVIS). Induction of a non-targeting control shRNA had no effect on the growth of tumors and the overall survival of the mice ***(Figure 16A)***.

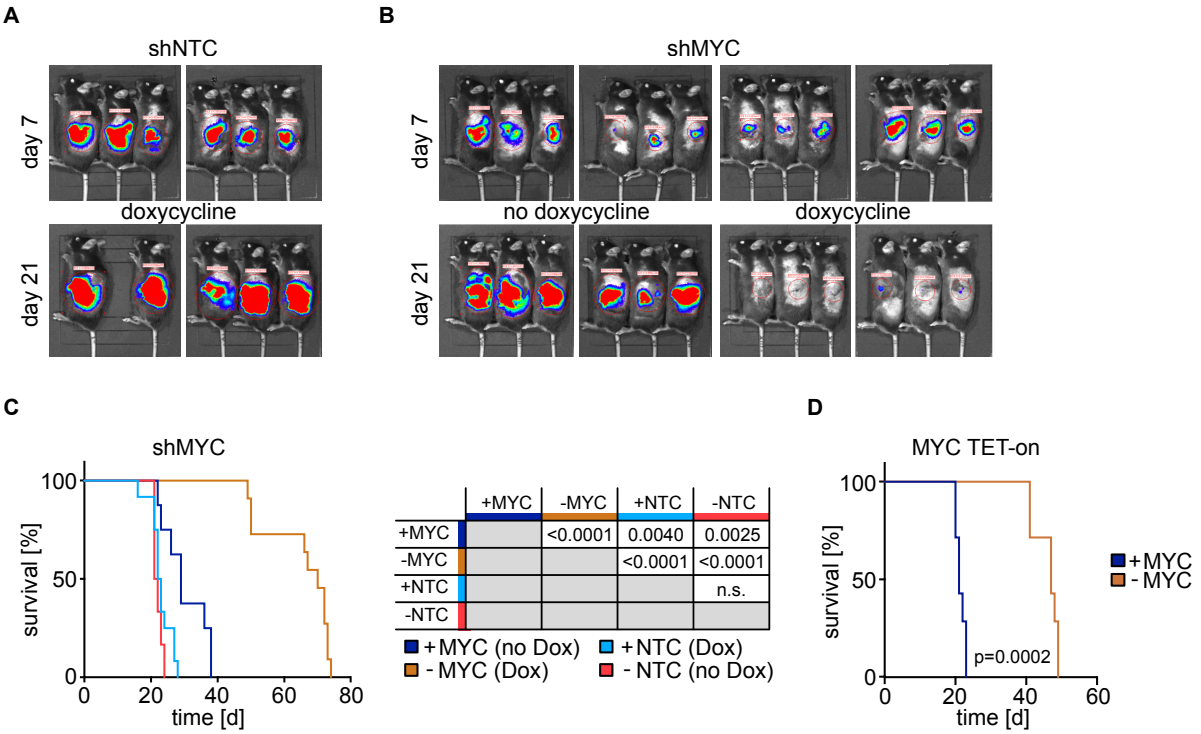

Figure 16: MYC depletion induces regression of tumors in a syngeneic orthotopic transplant model. *A: Luciferase measurement of KPC-cell-derived tumors expressing non-targeting-control (NTC) shRNA with the addition of doxycycline. KPC cells were orthotopically transplanted into C57BL/6J mice. B: Luciferase measurement of KPC-cell-derived tumors expressing doxycycline-inducible shRNAs targeting MYC. C: Left, Kaplan-Meier plot of mice that were orthotopically transplanted with KPC cells carrying either an inducible NTC shRNA or an shRNA targeting MYC. Where indicated, mice were treated with doxycycline-containing food. Right: P values between indicated cohorts were calculated using Mantel-Cox test. D: Luciferase measurement of KPC-cell-derived tumors in syngeneic C57BL/6J mice expressing a doxycycline-inducible MYC transgene. P value was calculated using Mantel-Cox test. The mouse experiment was conducted by Anneli Gebhardt-Wolf.*

However, proliferation was markedly reduced compared to cells in culture. Depletion of MYC using shRNA led not only to a strong reduction in growth of the tumors (i.e., comparable to the proliferation slowdown observed in culture) ***(Figure 16B)***, but also to a regression of tumors from day 7 to day 21. This translated in an increase in overall survival of the mice from 29 to 70 days for the tumors with shRNA mediated depletion of MYC and 21 days to 47 days with the "MYC TET-ON" cells ***(Figure 16C, D)***. Despite the regression of tumors and significant increase in overall survival after MYC depletion or deletion, tumors recur and mice with high tumor burden were sacrificed.

Immunohistochemistry of tumor tissue at early time points (2 or 4 days after treatment start) did not reveal significant differences in infiltration with T, B, NK cells or macrophages after depletion of MYC (data not shown (Krenz *et al.*, 2021)). Cibersort analyses indicates that dendritic cells are infiltrating the tumor tissue ***(Figure 17)***.

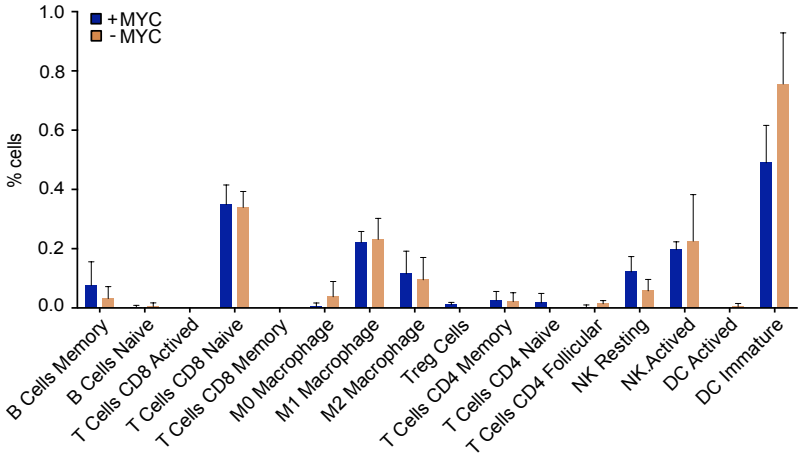

Figure 17: Cibersort analysis of tumors at day 4 after treatment start.

2.2 MYC drives immune evasion in PDAC

2.2.1 Tumor regression is dependent on T cells

Considering the transcriptomic analysis, we next assessed the contribution of the immune system in MYC-dependent tumor growth. To this end we used several immune compromised mouse models. In detail, three different mouse systems were used to determine whether the immune system is involved in the tumor regression and to identify the type of immune cells responsible for the tumor regression. We used mouse models bearing the deletion of specific subsets of immune cells: T cells (expressing CD3, CD4 or CD8), B cells and NK cells, which were described as the major effectors of tumor regression in a lung cancer model (Kortlever *et al.*, 2017).

First, KPC cells were transplanted into the pancreata of NRG mice. Due to their deficiency in RAG1 and IL2RG, as well as the NOD background (non-obese diabetic mouse), these mice lack functional T, B and NK cells and are therefore the most immunocompromised mouse strain used in this study.

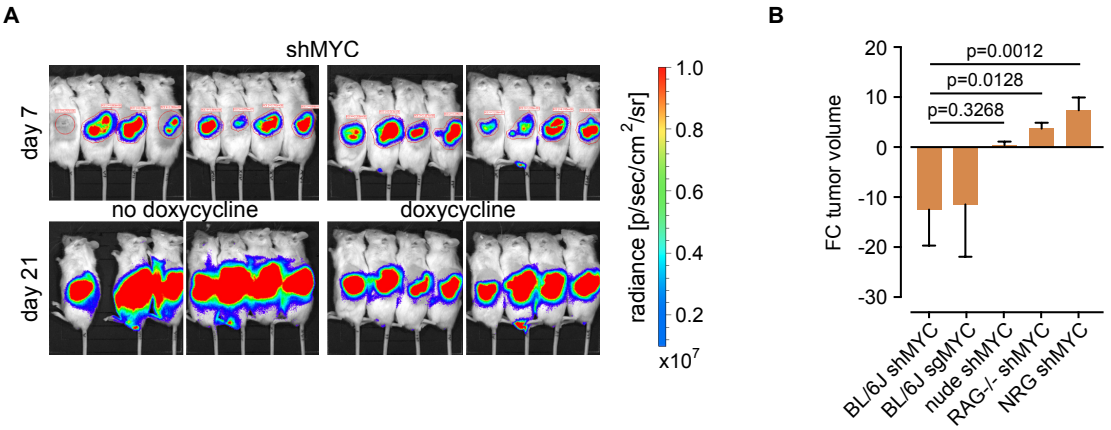

Figure 18: Tumor regression upon MYC depletion requires the immune system. *A: Luciferase measurement of KPC-cell-derived tumors expressing doxycycline-inducible shRNAs targeting MYC. KPC cells were orthotopically transplanted into NRG mice. B: Changes of tumor volume upon depletion or deletion of MYC from day 7 to day 21 after orthotopic transplantation. KPC cells were orthotopically transplanted into C57BL/6J, nude, Rag1$^{-/-}$ or NRG mice. The mouse experiment was conducted by Anneli Gebhardt-Wolf.*

Tumors efficiently engrafted in NRG mice and showed a doubling time similar to tumors in the syngeneic C57BL/6J mice ***(Figure 19A)***. In contrast, the depletion of MYC did not induce regression of tumors, but mildly reduced proliferation ***(Figure 18A)***. The same experiment was reproduced in RAG1$^{-/-}$ mice lacking T and B cells, as well as in nude mice lacking mature T cells. A reduction of tumor load upon depletion of MYC was not observed in either of the three mouse strains ***(Figure 18B)***.

We compared the doubling time of cells in culture with cells transplanted in C57BL/6J and NRG mice. First, the doubling time of cells in culture is shorter than the doubling time of transplanted tumor cells. The reduction of tumor growth in NRG mice is only mild, while MYC depletion strongly decreases the proliferation of cells in 2D culture ***(Figure 19A)***.

Comparing gene expression of cell culture and transplanted tumors showed that on the one hand growth, replication and mitosis are downregulated *in vivo* when compared to cells in culture. On the

other hand, *in vivo*, GO terms that reflect the interaction of the tumor with the microenvironment (e.g., antigen processing and presentation, regulation of cytokine production) were upregulated ***(Figure 19B)***. Crucially, the strong discrepancy between dependence of cancer cells on MYC in culture and *in vivo* suggests that in many cases the proproliferative function of MYC is overestimated and the role of MYC in preventing immune-dependent regression of tumors by establishing an immune evasive environment is its predominant oncogenic function in this model.

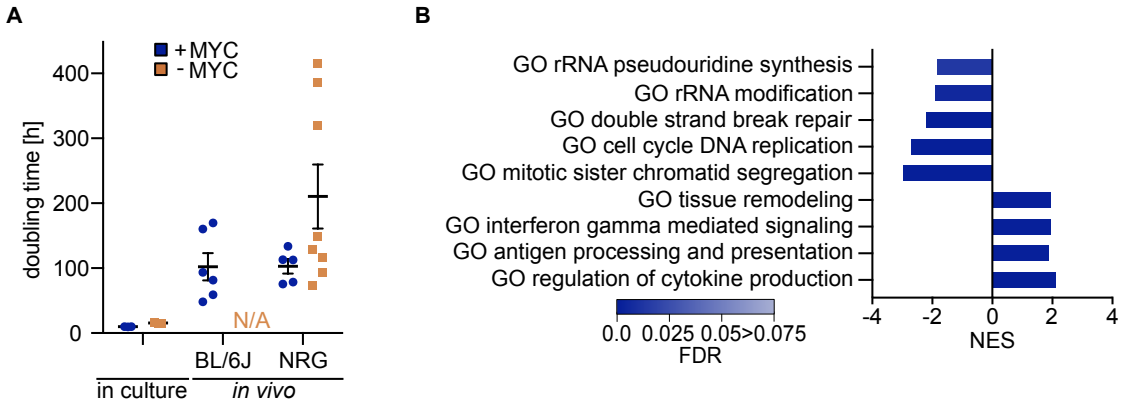

Figure 19: Growth of tumor cells is slower in vivo compared to cells in culture. *A: Calculated doubling time of KPC cells in culture (n=3) and orthotopically transplanted tumors in C57BL/6J (n=6) and NRG mice (n=5 for +MYC, n=8 for -MYC) with and without doxycycline-induced depletion of MYC. Results are presented as individual values ±SEM. B: GO term analysis of differentially expressed genes of cells in culture and tumors, both after 48 h of doxycycline-induced MYC depletion.*

Taken together, these results suggest three main implications. First, tumor regression is dependent on a functional immune system. Second, B and NK cells are needed to achieve a strong restriction of tumor growth. Third, T cells are the major driver of regression, since no reduction in tumor load was observed in mice lacking T cells.

Transplanted tumors in all conditions recur at one point, even though we observe a regression of tumors after depletion of MYC. To understand which mechanism underlies this observation, we compared the RNA expression in tumors in C57BL/6J mice at the endpoint of the experiment and after only two days of treatment. The global expression profiles of tumors at the endpoint of the experiment suggested two explanations for the recurrence of the tumors in the MYC depleted situation. First, the expression of MYC and its transcription profile on mRNA-level is partially restored. Hallmark gene sets associated with growth and proliferation are upregulated, while hallmark gene sets associated with immunity and immune response are downregulated ***(Figure 20A)***. It is likely that this happens due to silencing of the promoter of the integrated plasmid in order to restore the levels of MYC and restore proliferation and immune evasion *in vivo*. This hypothesis is supported by the fact that we observe silencing of the promoter after about two weeks of doxycycline treatment in culture.

Second, MYC is part of a transcription network that balances metabolism, proliferation and transformation. MAX preferentially forms heterodimers with proteins of the MYC family to promote transcription of genes with an E-box or cooperates with MXD/MNT/MGA proteins to repress transcription

of those genes (Carroll *et al.*, 2018; Conacci-Sorrell *et al.*, 2014). We observed specifically a reduced expression of the repressive protein MNT leading to restored proliferation and tumor growth explaining the tumor recurrence ***(Figure 20B)***.

A

up in EP tumors (- MYC) vs early tumors (- MYC)

Hallmarks	NES	FDR
MYC targets V1	3.05	0.000
E2F targets	2.45	0.000
DNA Repair	2.00	0.001
G2M checkpoint	1.69	0.006
MYC targets V2	1.15	0.211
Unfold protein resp	2.09	0.002
Protein secretion	1.58	0.010

down in EP tumors (- MYC) vs early tumors (- MYC)

Hallmarks	NES	FDR
EMT	-2.63	0.000
IL6 JAK STAT3 sig	-2.17	0.000
Inflammatory response	-2.17	0.000
Allograft rejection	-2.05	0.000
Interferon gamma resp	-1.84	0.001
Il2 STAT5 sig	-1.71	0.003
TNFA sig via NFKB	-1.60	0.010
HEDGEHOG sig	-1.53	0.019

B

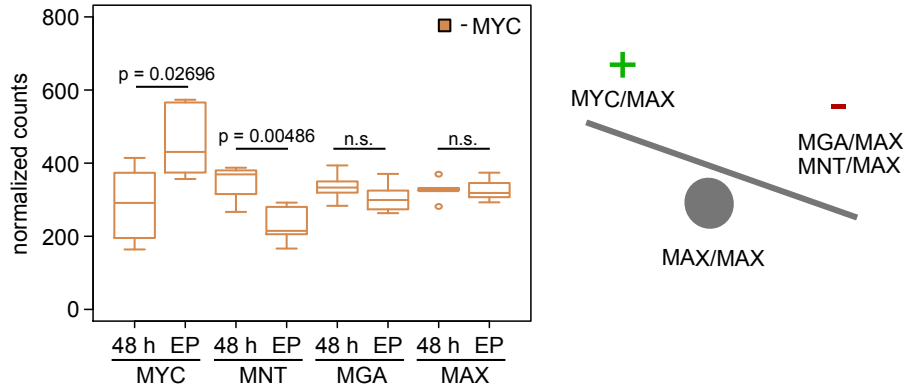

Figure 20: Tumor cells restore MYC function over time. *A: Gene set enrichment analysis comparing endpoint tumors and early tumors, upon doxycycline-induced knockdown of MYC. B, left: Box plot showing the expression of RNA of the MAX network. P value was calculated using 2-tailed, unpaired t test. B, right: MAX can bind MYC to promote transcription or bind MNT or MGA to downregulate transcription.*

2.2.2 MYC suppresses TBK1 activation to promote immune evasion

With the aim of investigating the molecular determinants of the MYC-dependent immune evasive phenotype, we analyzed a number of kinases that are known to regulate NF-κB signaling and are also involved in the innate immune response of cells that makes a cell visible to the host immune system.

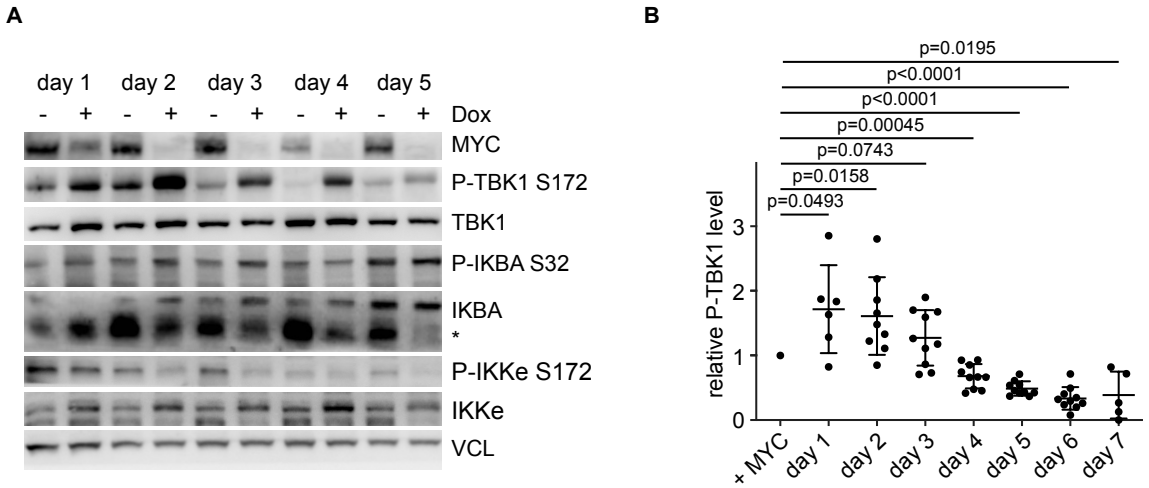

Figure 21: Depletion of MYC induces activation of TBK1. *A: Immunoblot of the indicated proteins MYC, TBK1, P-TBK1, IKBA, P-IKBA, IKKe, P-IKKe and VCL in KPC cells expressing doxycycline-inducible shRNAs targeting MYC. Doxycycline was added for the indicated time. B: Quantification of TBK1 phosphorylation at S172. Results are presented as individual values ±SD.*

TBK1 and its analogue IKKε, which are auto-phosphorylated upon activation, are both expressed in murine PDAC cells. Immunoblotting of the phosphorylated isoforms revealed that while IKKε phosphorylation is decreasing upon MYC depletion, TBK1 phosphorylation is robustly increased upon MYC depletion already within 24 h ***(Figure 21A, B)***. TBK1 activation peaks on day 2 and 3 and is mirrored by an increased phosphorylation of IKBA, indicating an activation of the NF-κB pathway ***(Figure 21A)***.

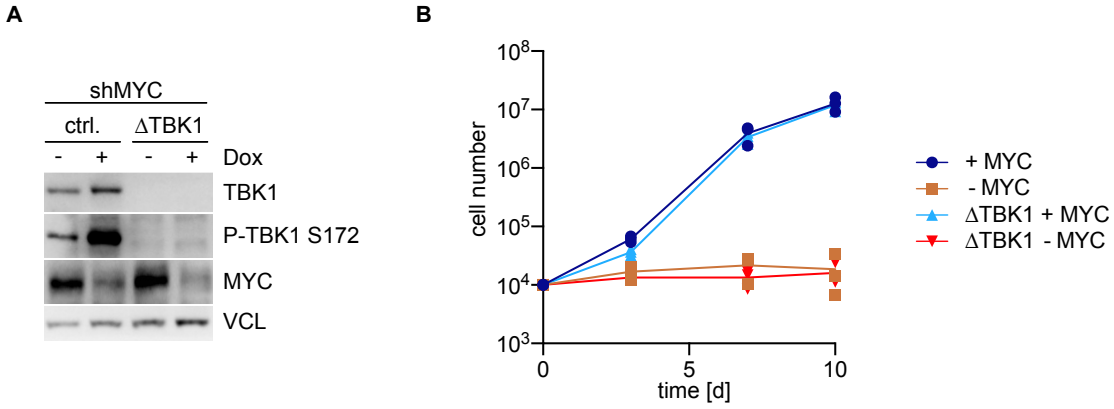

Figure 22: CRISPR/Cas9 mediated knockout of TBK1 does not impact growth of KPC cells in culture. *A: Control cells were transfected with empty vector, ΔTBK1 cells were transfected with vector expressing Cas9 and a sgRNA targeting Tbk1. Immunoblot for TBK1, P-TBK1, MYC and Vinculin in KPC cells with doxycycline-inducible shRNAs. B: Cumulative growth curve of KPC cells with doxycycline mediated depletion of MYC in cells with WT TBK1 or knockout of TBK1. Results are presented as individual values (n=3).*

To investigate the role of TBK1 in MYC-dependent immune escape, TBK1 was deleted using CRISPR/Cas9 in “shMYC KPC” ***(Figure 22A)***. Deletion of TBK1 did not have any effects on the morphology or the proliferation capacity of KPC cells in culture. Comparably, MYC depletion reduced growth in culture in both cell lines ***(Figure 22B)***. To assess the impact of a TBK1 deletion in the tumor, cells were orthotopically transplanted into syngeneic C57BL/6J mice. As described above, depletion of MYC in tumors with WT TBK1 resulted in a reduction of proliferation and regression of tumors ***(Figure 23A, left)***. Instead, TBK1-deleted tumors with high MYC expression grew comparably fast, but did not regress upon depletion of MYC ***(Figure 23A, right)***.

This is also reflected in the reduced overall survival in TBK1-deficient tumors compared to TBK1 wildtype tumors in the absence of MYC ***(Figure 23B)***.

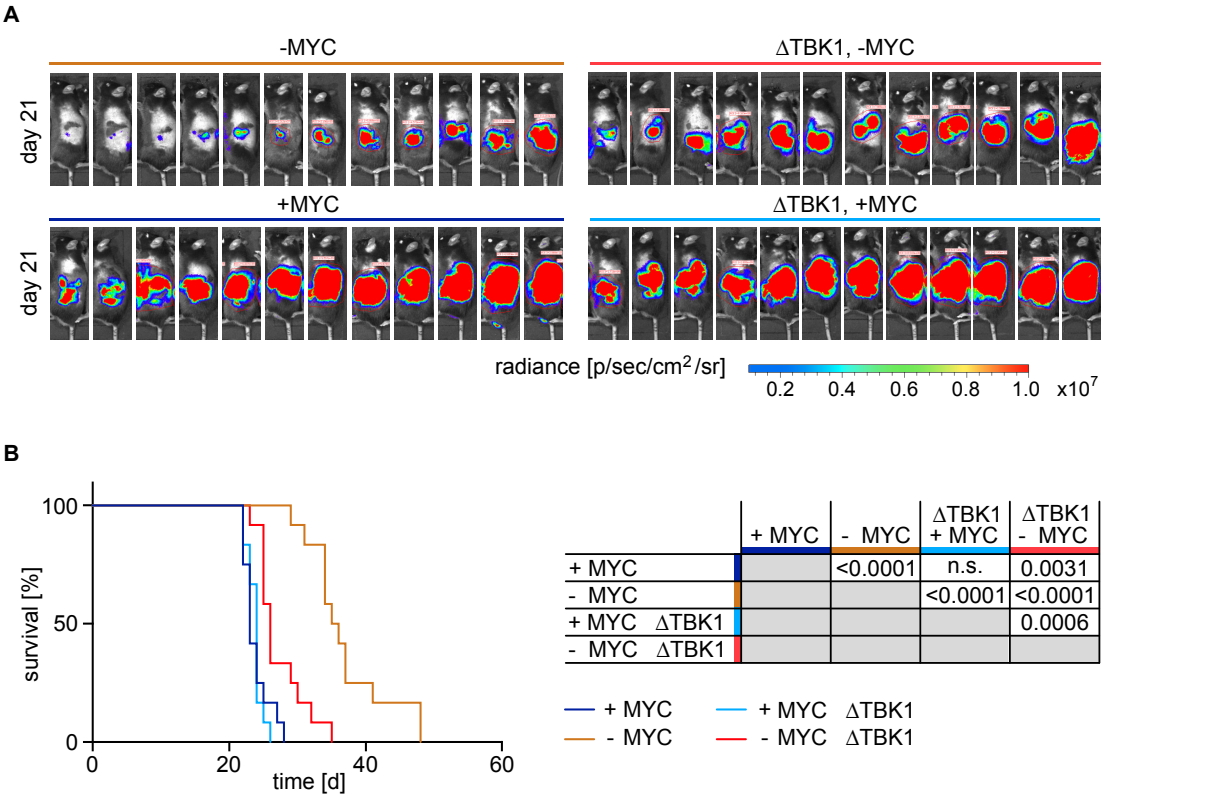

Figure 23: TBK1 mediates regression upon depletion of MYC. *A: Luciferase measurement of KPC-cell-derived tumors expressing shRNAs targeting MYC with the addition of doxycycline at day 21 post transplantation. ΔTBK1, CRISPR/Cas9-mediated TBK1 deletion. KPC cells were orthotopically transplanted into C57BL/6J mice. B: Left: Kaplan-Meier plot of mice that were orthotopically transplanted with KPC cells carrying a doxycycline-inducible shRNA targeting MYC. Where indicated, mice were treated with doxycycline containing food from day 7 onwards. Right: P values were calculated with the Mantel-Cox test. The mouse experiment was conducted by Anneli Gebhardt-Wolf.*

A side-by-side comparison of tumor growth in all used experimental models suggested that the impaired growth of tumors from TBK1-deficient KPC cells phenocopies the growth behavior upon transplantation into RAG1-deficient mice ***(Figure 24)***.

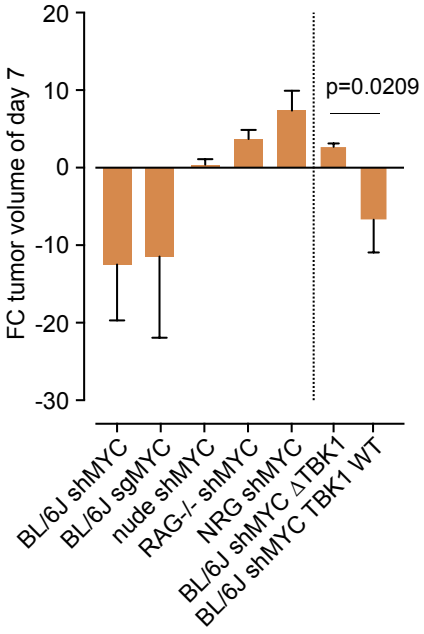

Figure 24: Comparison of tumor growth throughout different experimental models. *Change of tumor volume upon deletion or deletion of MYC from day 7 to day 21 after orthotopic transplantation. Bar graph showing the growth of KPC cells orthotopically transplanted into C57BL/6J, nude, Rag1-/- or NRG mice (as shown in 8B) compared to KPC cells with or without deletion of TBK1. P value was calculated using Kruskal-Wallis-test. Result are presented as mean ±SEM.*

2.2.3 Tumor regression is not mediated by IRF3

Die canonical target of TBK1 is IRF3. IRF3 dimerizes upon activation and shuttles to the nucleus to activate type I interferon signaling. Interestingly, MYC depletion has been connected to PAMPs accumulation and type I interferon response, although the molecular details were not investigated (Swaminathan *et al.*, 2020; Topper *et al.*, 2017). Type I interferons are signaling molecules that recruit immune cells (and especially also cytotoxic T lymphocytes) to fight infections or also proliferating tumor cells (Lu *et al.*, 2019).

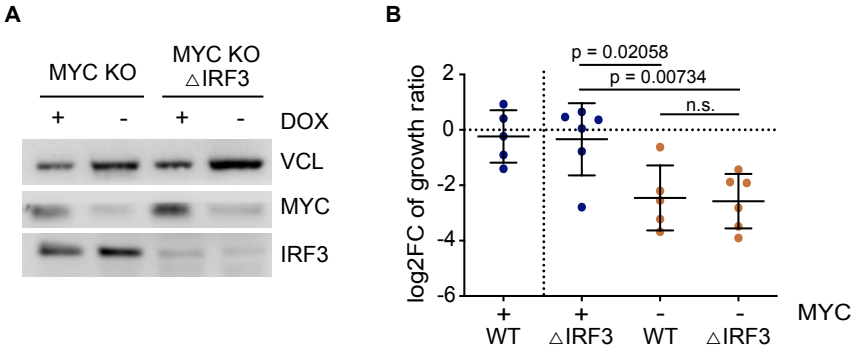

Figure 25: Knockout of IRF3 does not impact tumor growth. *A: Immunoblot of MYC, IRF3 and Vinculin from "MYC TET-on" KPC cells with CRISPR/Cas9 mediated knockout of IRF3. B: Fold change in the tumor growth ratio in syngeneic C57BL/6J mice, orthotopically transplanted with KPC cells with and without knockout of IRF3. P values were calculated using 2-tailed unpaired t test. The mouse experiment was conducted by Anneli Gebhardt-Wolf.*

We generated a knockout of IRF3 in “MYC TET-on” KPC cells ***(Figure 25A)***. These cells were transplanted into the pancreata of C57BL/6J mice, tumors engrafted for seven days and MYC was depleted using doxycycline for 14 days. Deletion of IRF3 did not have any effect on the growth ratio of tumors *in vivo*, independently of MYC levels ***(Figure 25B)***. This indicates that, besides the critical role of TBK1 in the tumor regression, its canonical downstream target IRF3 is not mediating the immune recognition. In this context, it has been recently shown that mutant TP53 in mouse KPC cells shuts down the activation of IRF3 by forming a repressive complex with TBK1 and STING (Ghosh *et al.*, 2021). This explains our observation that IRF3 is not activated upon TBK1 phosphorylation.

2.3 DAMPs drive a proimmunogenic program

2.3.1 dsRNA accumulates in the cytoplasm in a MYC-dependent manner

Our studies have shown that an important oncogenic function of MYC *in vivo* is to suppress the activation of TBK1 and consequently the activation of the immune system. TBK1 is described to be a central hub of innate immune signaling in cells. In detail, PRRs (including RIG-I, MDA5, TLR3 and cGAS) can monitor unusual DNA or RNA conformations in the cytoplasm (i.e., typically associated with the presence of pathogens or DNA damage) and activate TBK1.

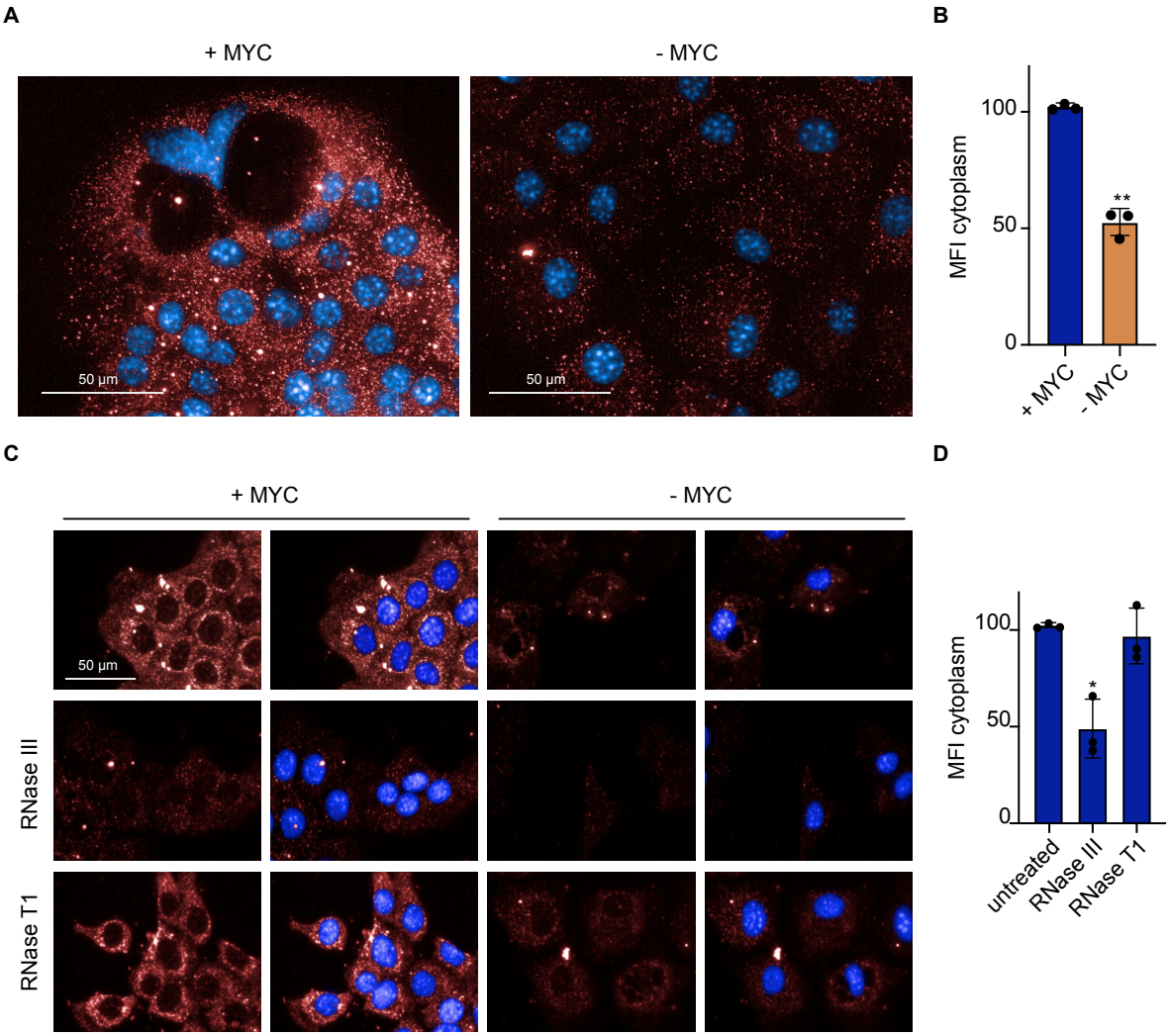

Figure 26: Murine PDAC cells accumulate dsRNA in the cytoplasm. *A: Immunofluorescence for dsRNA (red) in KPC cells with and without shRNA mediated depletion of MYC. Nuclei were stained using Hoechst. B: Quantification of cytoplasmic staining for dsRNA. P value was calculated using 2-tailed t test (n=3). C: Immunofluorescence of dsRNA in KPC cells (red) with or without shRNA mediated depletion of MYC. Where indicated, fixed cells where treated with different RNases. D: Quantification of cytoplasmic staining of KPC cells with unperturbed levels of MYC. Fixed cells were treated with specific RNases. P value was calculated using 2-tailed t test (n=3).*

To investigate the role of DAMPs and PRRs, we first assessed the presence of dsRNA using the monoclonal α-dsRNA J2 antibody. Immunofluorescence showed that dsRNA accumulates in the

cytoplasm of KPC cells in a MYC dependent manner ***(Figure 26A, B)***. Depletion of MYC resulted in a about 50% downregulation of cytoplasmic staining ***(Figure 26B)***.

The specificity of the dsRNA staining could be confirmed using different RNases. RNase III, which specifically degrades dsRNA, significantly reduced the cytoplasmic staining. Conversely, RNase T1, that specifically degrades ssRNA, did not impact the signal in the cytoplasm ***(Figure 26C, D)***.

We depleted MYC in our "MYC TET-on" KPC cells. Restoring the function of MYC in these cells also increased staining for dsRNA in a time-dependent manner ***(Figure 27A)***. MYC is described to be a regulator of transcription. Interestingly, pre-incubation of cells with specific inhibitors targeting transcription via RNA Polymerase II decreased the signal for dsRNA in the cytoplasm, comparable to what was observed when MYC was depleted ***(Figure 27B)***.

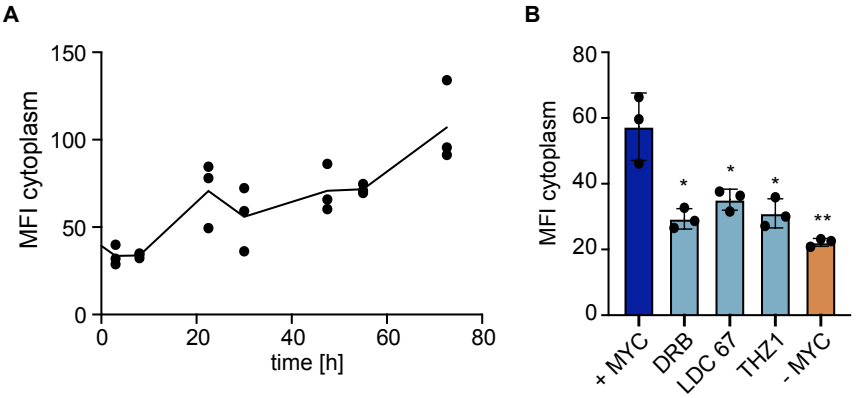

Figure 27: dsRNA accumulates in a MYC and RNAPII-dependent manner. *A: Quantification of immune-fluorescence for dsRNA in KPC cells. MYC transgene was induced in KPC cells with deletion of endogenous MYC. Data is shown as individual values. B: Quantification of immunofluorescence for dsRNA (J2) in KPC cells treated with doxycycline or indicated CDK inhibitors. Data is shown as individual values and mean ±SD. P value was calculated using 2-tailed t test.*

A second potential trigger of TBK1 activation is DNA in the cytoplasm which has been shown to accumulate in cancer cell (Coquel *et al.*, 2018; Emam *et al.*, 2022). ssDNA, coming from DNA damage, can also be recognized by PRRs and activate innate immune signaling. Immunofluorescence for ssDNA revealed a distinct staining in the cytoplasm but not in the nucleus. The specificity of the signal was confirmed by treatment with Nuclease S1, that only degrades ssDNA. MYC depletion slightly decreased the signal. However, the change in signal was less pronounced compared to the changes in dsRNA ***(Figure 28A)***.

Finally, we investigated the involvement of dsDNA by assessing the activation of the cGAS-STING axis, which is the best described pathway to recognize cytoplasmic dsDNA. Generally, cGAS can be activated due to formation of cGAS-positive micronuclei or by the recognition of dsDNA fragments in the cytoplasm. No formation of micronuclei was observed in KPC cells. To rule out a contribution of cGAS-STING axis to the phosphorylation of TBK1, cells were treated with C-178, a highly specific inhibitor for murine STING (Haag *et al.*, 2018). Inhibition of cells with C-178 did not alter the phosphorylation of TBK1 upon depletion of MYC ***(Figure 28B)***.

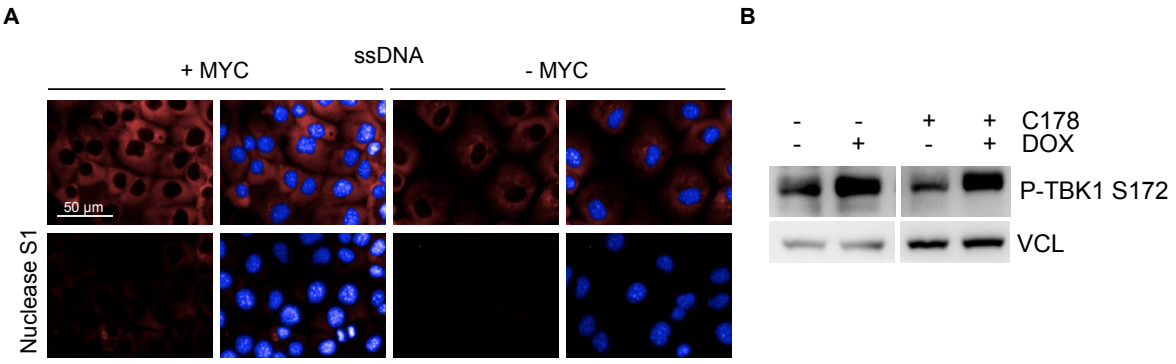

Figure 28: DNA-derived DAMPs do not affect TBK1 phosphorylation. *A: Immunofluorescence for ssDNA (red) in KPC cells with and without deletion of MYC. Nuclei were stained using Hoechst. Where indicated, fixed cells were treated with Nuclease S1. B: Immunoblot for P-TBK1 and Vinculin in KPC cells with and without depletion of MYC. Where indicated, cells were treated for 48 h with the STING-inhibitor C-178 and doxycycline.*

Taken together, KPC cells display remarkably high levels of dsRNA in the cytoplasm that are dependent on MYC and RNAPII mediated transcription, while the amount of ssDNA did not significantly change upon depletion of MYC. Since TBK1 activation did not change using a specific STING inhibitor, we could rule out an involvement of the cGAS-STING axis (Haag *et al.*, 2018; Lee *et al.*, 2022b).

2.3.2 Nuclear dsRNA originates from inverted repetitive elements

To investigate the source, composition and regulation of dsRNA, it was extracted from KPC cells. For this purpose, murine KPC cells were spiked-in with human U2OS cells, lysed and dsRNA was precipitated with the α-dsRNA antibody (J2) and prepared for sequencing. IgG and RNase III treated cells were used as control.

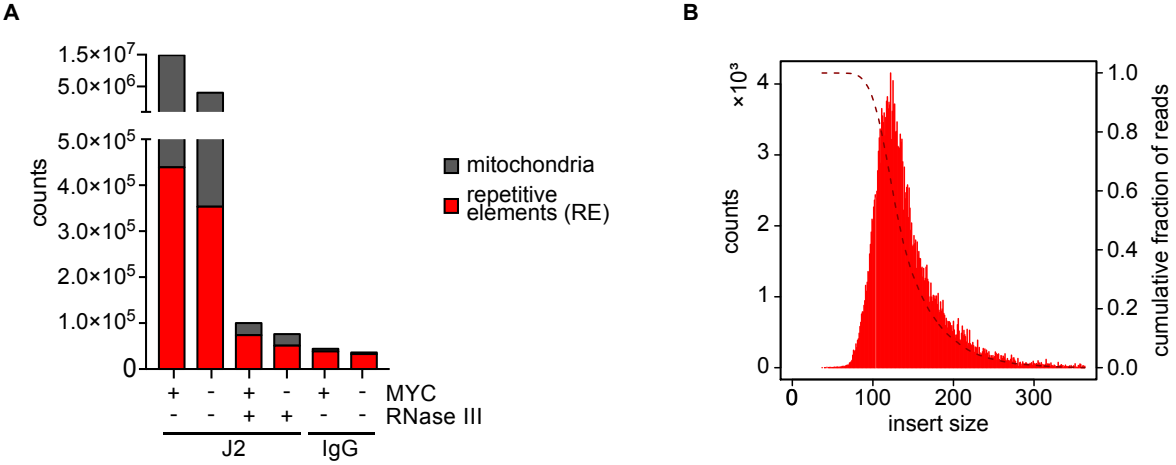

Figure 29: dsRNA in mammalian cells originates from mitochondria and repetitive elements. *A: Spike-normalized sequencing of dsRNA immunoprecipitates and their annotation to the mitochondrial chromosome and repetitive elements (nuclear origin). B: Distribution of length of reads originating from the nucleus. Dashed line marks the cumulative distribution.*

Analysis of these samples showed two findings, which confirmed the quality of the experiment: First, precipitation with the J2 antibody was specific, since a clear enrichment was visible in the

J2-immunoprecipitation compared to the IgG-immunoprecipitation. Second, RNase III reduced the reads that derived from J2-immunoprecipitation.

In general, we found two major sources of dsRNA. Most of dsRNA originates from the mitochondria likely due to bidirectional transcription, as previously described in the literature (Dhir *et al.*, 2018). About 2% of the dsRNA originates from the nuclear genome. Nuclear reads were annotated to repetitive elements which have been shown to be a source of dsRNA (Ahmad *et al.*, 2018) ***(Figure 29A)***. The size of reads which originated from the nucleus were determined and we observe a distribution from about 80 to 300 bp with a peak at 120 bp, the average size of B2 and B1 elements ***(Figure 29B)***. These are the major source of dsRNA from the nuclear genome in KPC cells.

We closer analyzed the localization and orientation of dsRNA-peaks in KPC cells. Browser tracks from the mitochondrial genome reveal a very similar pattern to what has been previously described in HeLa cells (Dhir *et al.*, 2018). The signal for dsRNA is distributed throughout the whole mitochondrial chromosome ***(Figure 30)***.

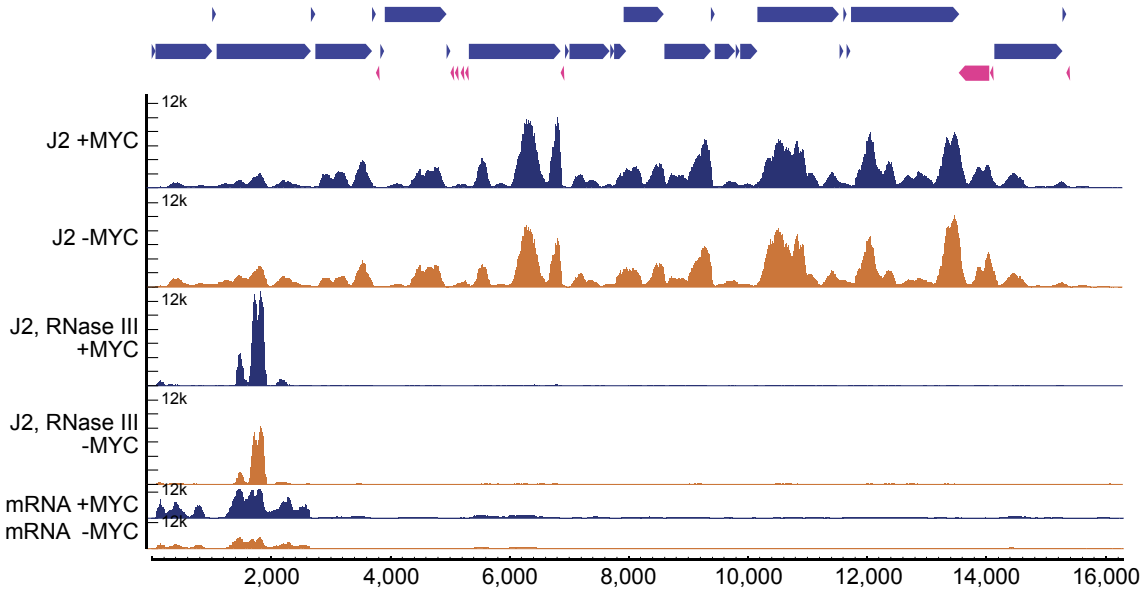

Figure 30: Browser track of mitochondrial genome from spike-in normalized J2-IP followed by sequencing. *MYC transgene was switched of in KPC cells with knockout of endogenous MYC (-MYC) for 48 h.*

Controlling and promoting mitochondrial biogenesis is one of the main functions of MYC biology and MYC strongly regulates TFAM, the major transcription factor in mitochondria (Li *et al.*, 2005). Therefore, the total amount of dsRNA from mitochondria is regulated by MYC. Browser tracks from the nuclear genome showed that most of the nuclear dsRNA originates from repetitive elements ***(Figure 31, Figure 32A)***. Most of the peaks and reads are located in introns of transcribed genes and MYC depletion reduces overall occupancy of reads and peaks in the genome ***(Figure 32B)***. RNase III expression removes the signal completely ***(Figure 31)***. Most of these peaks are found at inverted repeat repetitive

elements. This orientation suggests that reduced RNAPII speed or delay in mRNA processing (e.g., due to defective splicing) allows ssRNA to fold back and form a double-stranded part in the mRNA.

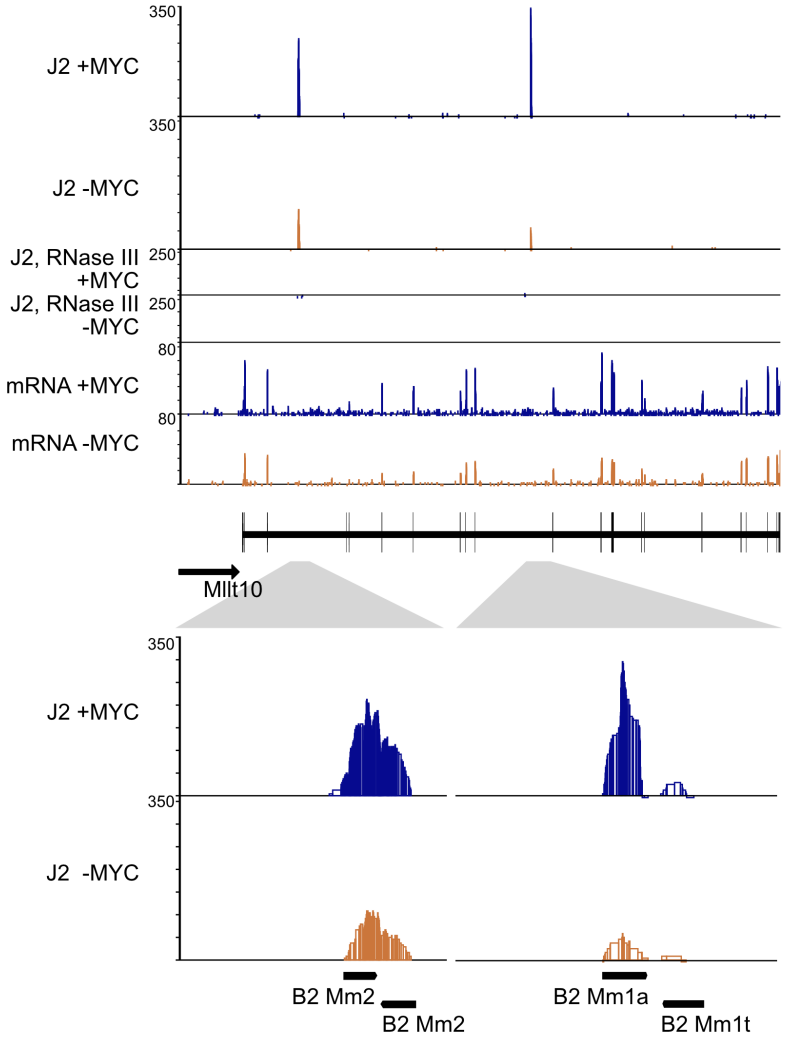

Figure 31: Exemplary browser track of dsRNA peaks in the intron of the nuclear gene Mllt10. *Browser track shows dsRNA peaks and mRNA of the Mllt10 gene. dsRNA peaks in the introns of Mllt10 are annotated with repetitive elements of the B2 family.*

Interestingly, most peaks are in locations annotated for B1 and B2 SINE elements, which show a high similarity to Alu elements that are found in the human genome ***(Figure 31, 32A)***. SINE elements have a size of 100-200 bases and can therefore form dsRNAs which are capable of activating most of PRRs (Ahmad *et al.*, 2018).

In unperturbed (tumor) cells dsRNA originating from the mitochondrial transcription is kept in the mitochondria and is thereby preventing recognition by the immune system (Dhir *et al.*, 2018). The subsequent analysis therefore focuses on the nuclear source of dsRNA. Most reads for dsRNA could be annotated to the B1 and B2 of SINE elements, but also retroviral elements and LINE elements were found to form dsRNAs at single loci in the cells. These elements are located throughout the whole genome und make up to 10% of the genome (Chinwalla *et al.*, 2002; Deininger, 2011).

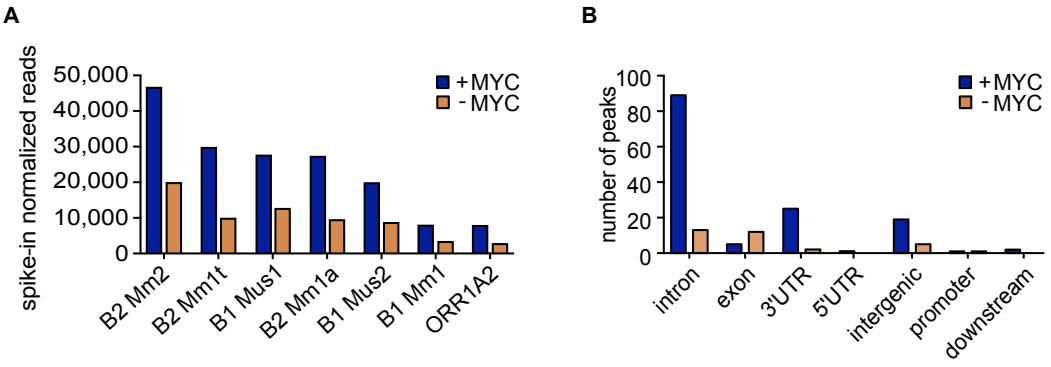

Figure 32: dsRNA derives from inverted repeat repetitive elements. *A: Annotation of reads from sequencing of J2 immunoprecipitates to SINE elements. B: Location of repetitive elements with a dsRNA peak.*

About 60 genes with dsRNA peaks ("host genes") were found and we analyzed the property of these genes using total and nascent RNA sequencing. First, these host genes were only slightly higher expressed compared to the average gene expression in KPC cells ***(Figure 33A)***. Second, these genes were not significantly regulated by the depletion of MYC ***(Figure 33B)***. This observation was also validated using sequencing of nascent RNA ***(Figure 33C)***.

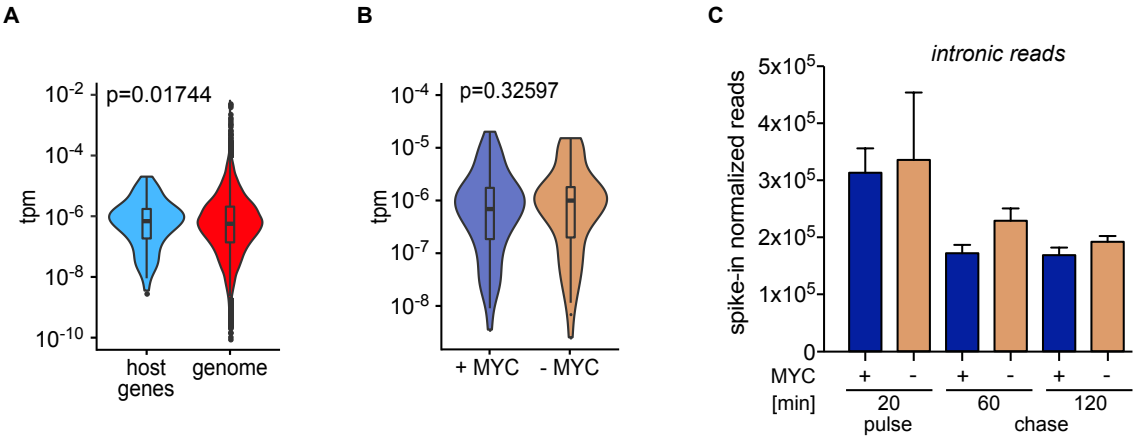

Figure 33: Properties of host genes with dsRNA peaks. *A: Violin plot for transcription of genes with dsRNA peaks ("host genes") and all expresses genes. Transcripts per million kilobases (tpm) are blotted. B: Violin plot of expression of "host genes" with and without deletion of MYC. Transcripts per million kilobases (tpm) are blotted. C: Intronic reads from host genes of dsRNA obtained from labelling of nascent RNA with 4-thiouridine for 20 min and chase for 60 and 120 min in cells with and without depletion of MYC for 48 h. Results are presented as mean ±SEM (n=3).*

Third, host genes of dsRNA peaks have particularly longer introns ***(Figure 34A)*** and a higher AT content ***(Figure 34B)*** compared to the genome. Both properties may be consistent with defective mRNA processing, splicing or editing by ADAR1, an enzyme that is involved in the regulating host dsRNA immunity.

To confirm these findings, a second analysis of dsRNA was performed in human U2OS cells. This analysis validated what was observed in murine PDAC cell lines: The majority of dsRNA originating from the nucleus was found in introns and could be annotated as repetitive elements ***(Figure 35)***. A high

proportion of dsRNA in the human nuclear genome could be annotated to the SINE family of Alu elements, the human equivalent to the family of B1 and B2 SINE elements.

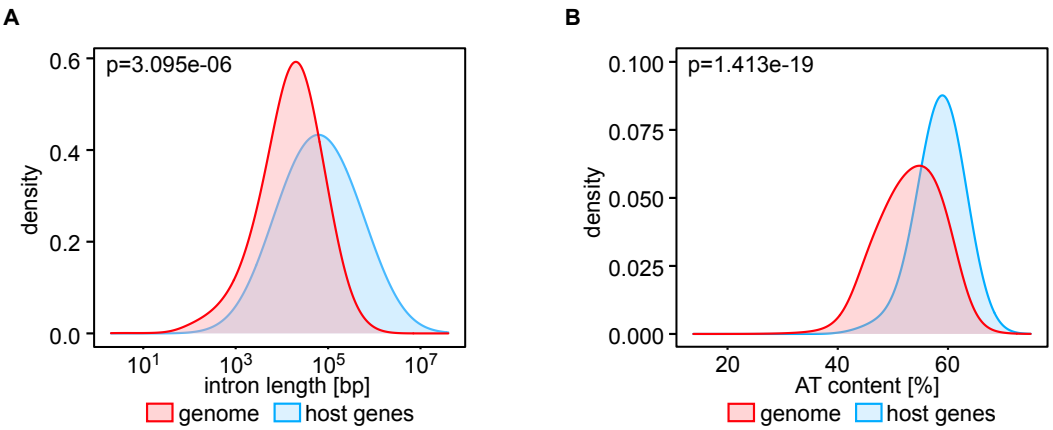

Figure 34: Feature of host genes of dsRNA peaks. *A: Density blot of intron length of genes with dsRNA peaks ("host genes", blue) compared to all murine genes (red). B: Density blot of AT content of "host genes" (blue) compared to all murine genes (red).*

Extensive analysis of dsRNA in KPC cells revealed that cancer cells accumulate dsRNA in a MYC and RNAPII dependent manner and that it originates from mitochondria and inverted repeat repetitive elements, which are located in the introns of transcribed genes. Both species, nuclear and mitochondrial dsRNA, have been described to be highly immunogenic (Ahmad *et al.*, 2018; Dhir *et al.*, 2018).

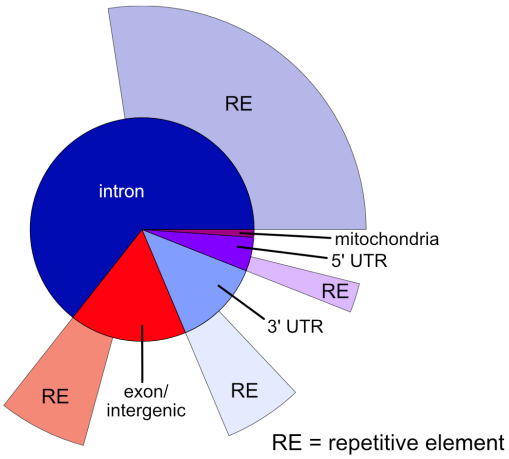

Figure 35: dsRNA in human cancer cells. *Pie diagram showing the distribution of reads from J2 immuno-precipitation from human U2OS cells. RE indicates the proportion of reads derived from repetitive elements.*

First and foremost, dsRNA originates from mtDNA, which is transcribed bidirectionally. This convergent transcription causes synthesis of RNA from both the heavy and the light strand. Importantly, the light strand is readily degraded by the degradosome, preventing critical accumulation of immunogenic dsRNA (Borowski *et al.*, 2013). The steady-state equilibrium between dsRNA formation decay of this RNA ensures that no or little RNA can escape from the mitochondria to activate the immune system.

The second source of dsRNA is repetitive elements. These elements have also previously been implicated in the formation of immunogenic dsRNA (Ahmad *et al.*, 2018; Bowling *et al.*, 2021; Espinet *et al.*, 2021). Repetitive elements, like short and long interspersed elements (SINE and LINE, respectively), cover up to 65% of the genome, depending on the estimation (Criscione *et al.*, 2014). In the human genome one of the most prominent SINE elements are Alu elements, while in the mouse genome B1, B2, ID and B4 elements are prevailing with B2 elements being the best studied group. Alu elements account for up about 11% of the respective genome and have a size of about 300 bp (Chinwalla *et al.*, 2002; Deininger, 2011). The murine paralogue B2 elements have a size of 100-300 bp (Hubley *et al.*, 2015; Jurka *et al.*, 2004). Repetitive elements, and explicitly Alu and B2 elements, are not junk DNA but are fulfilling several functions in cells. For example, Alu elements can be transcribed by RNA polymerase III (Deininger, 2011). Furthermore, RNA derived from human Alu elements and murine B2 elements are self-cleaving ribozymes, act as epigenetic regulator (Hernandez *et al.*, 2020) and contribute in phase separation by maintain the integrity of the nucleolus (Caudron-Herger *et al.*, 2015).

2.3.3 Nuclear dsRNA preferentially binds to TLR3

After characterizing the origin of dsRNA and dependence on MYC, we investigated the engagement of specific PRRs. We performed proximity ligation assays using the J2 antibody and antibodies against the three major PRR that lead to TBK1 activation: RIG-I, MDA5 and TLR3.

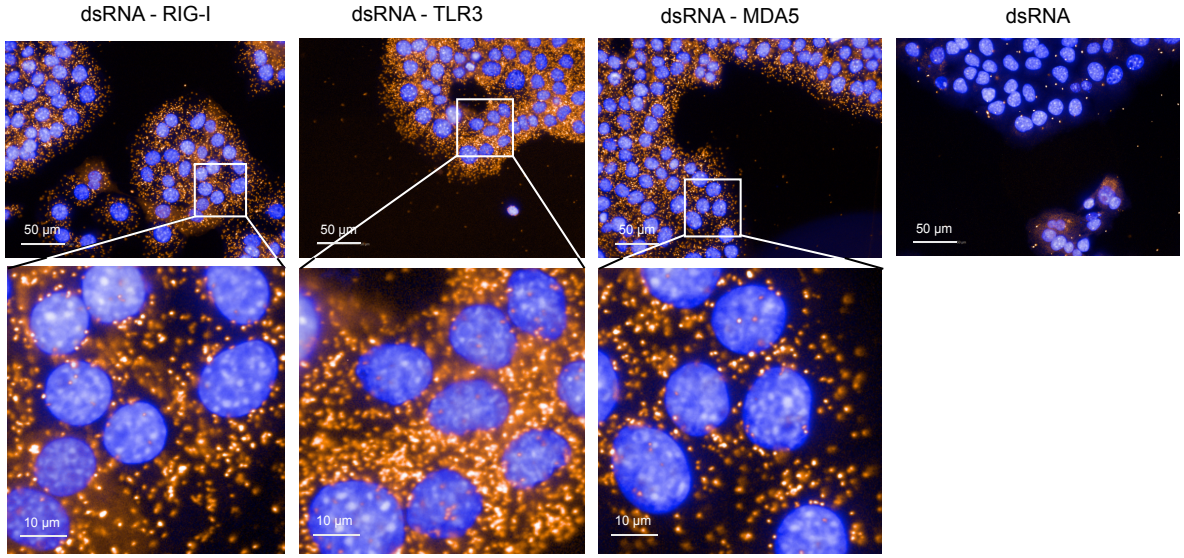

Figure 36: dsRNA is in close proximity to pattern recognition receptors. *In situ proximity ligation assay of dsRNA (J2) and the pattern recognition receptors RIG-I, TLR3 and MDA5 (n=3).*

Proximity between dsRNA and PRR was observed for all three receptors, but PLAs between dsRNA and TLR3 presented the strongest signal ***(Figure 36)***. We investigated the actual binding of dsRNA to these receptors by performing fCLIP (formaldehyde crosslinking and immunoprecipitation of RNA).

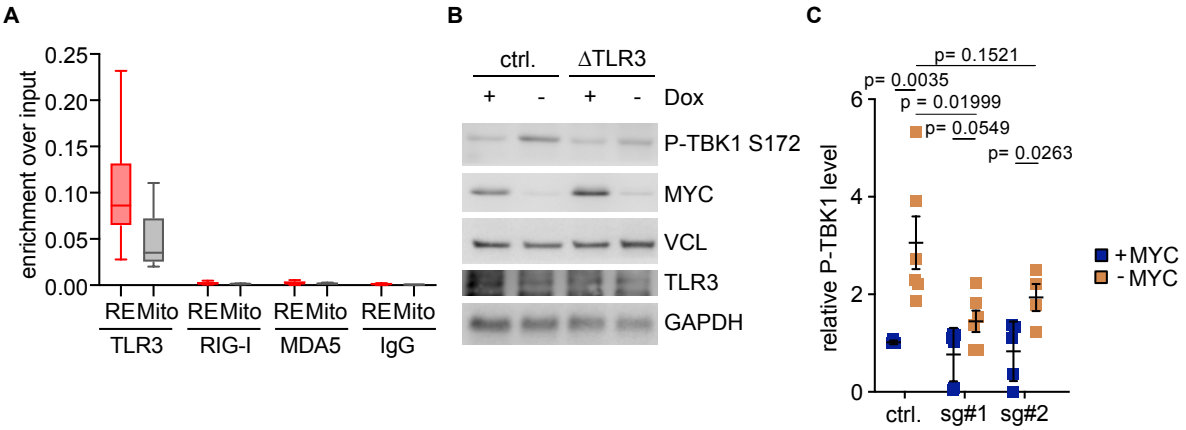

Figure 37: dsRNA predominantly binds to TLR3 in murine PDAC cells. *A: fCLIP showing binding of dsRNA in untreated KPC cells to TLR3, RIG-I, MDA-5 and IgG as control. Box plot groups primers of same origin (nuclear repetitive elements, red or mitochondrial chromosome, grey) ±SD (n=2). B: Immunoblot for P-TBK1, MYC, TLR3, GAPDH and Vinculin of "MYC TET-on" KPC cells. Where indicated TLR3 was deleted using CRISPR/Cas9. To deplete MYC doxycycline was removed for 48 h. C: Quantification of TBK1 phosphorylation (S172) in KPC cells with two different sgRNAs targeting TLR3. Results are presented as individual values ±SEM.*

dsRNA and proteins were crosslinked using paraformaldehyde, immunoprecipitation was performed for the protein of interest and RNA was extracted and converted to cDNA for RQ-PCR. Immunoprecipitation of PRRs provided two important findings: First, TLR3 was the only receptor with a robust and strong

engagement with dsRNA from mitochondria, as well as from the nuclear repetitive elements. Second, in spite of the prevalence of mitochondrial dsRNA, the engagement of TLR3 with nucleus-derived dsRNA was stronger ***(Figure 37A)***.

To link this observation to the activation of TBK1 downstream of TLR3, KPC cells were infected with two sgRNAs targeting *Tlr3*. Knockout of *Tlr3* significantly attenuated the phosphorylation of TBK1 upon depletion of MYC using sgRNA#1. Very similar, albeit not significant phenotype could be observed with sgRNA#2 ***(Figure 37B, C)***. Collectively, these experiments suggest that the activation of TBK1 is dependent on TLR3 signaling upon depletion of MYC.

This observation was verified using an inhibitor which specifically disrupts the complex between double stranded RNA and TLR3 (Cheng *et al.*, 2011). TBK1 autophosphorylation was reduced in a time- and dose-dependent manner while total levels of TBK1 were not affected ***(Figure 38)***.

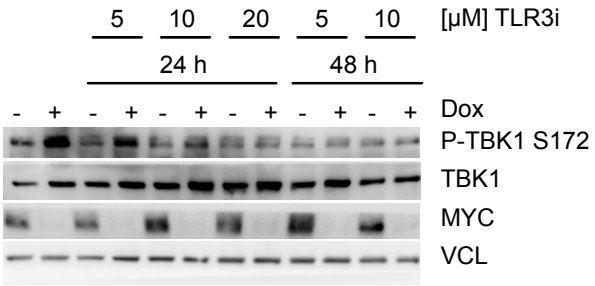

Figure 38: Inhibition of TLR3 reduces activation of TBK1. *KPC cells with inducible shRNA-mediated knockdown of MYC were treated with a TLR3-dsRNA complex inhibitor ("TLR3i") with indicated concentration for the indicated time (n=2).*

To confirm these findings in human PDAC cells, a panel of four cell lines was used to perform fCLIP. All four cell lines showed binding of dsRNA to TLR3 ***(Figure 39A)***. fCLIP experiments with RIG-I and MDA5 showed – as already demonstrated for murine PDAC cells – no substantial binding of SINE-derived double stranded RNA (data not shown). In PaTu 8988T cells, MYC was knocked out by CRISPR/Cas9 and J2-IP and TLR3-fCLIP were performed ***(Figure 39B)***. Depletion of MYC increased the loading of dsRNA onto TLR3 in this human PDAC cell line ***(Figure 39C)***.

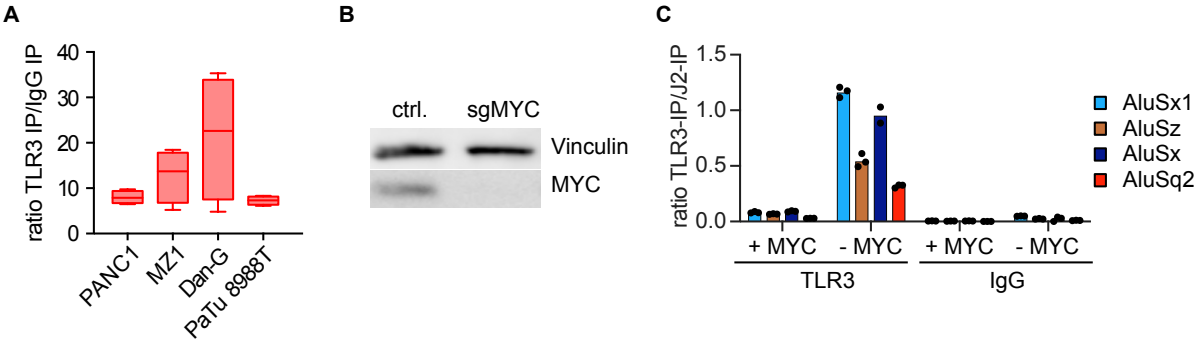

Figure 39: dsRNA engages TLR3 in human PDAC cell lines. *A: fCLIP against TLR3 in human PDAC cell lines. Box plot groups primers of same origin (nuclear repetitive elements) ±SD (n=2). B: Immunoblot of MYC and Vinculin in human PaTu 8988T cells, 7 days after infection with a sgRNA targeting MYC. C: Engagement of human TLR3 with repetitive element derived dsRNA in PaTu 8988T cells. Plot presents ratio of TLR3 loading and J2-immunoprecipitation. Results are presented as single values of technical replicates.*

The definition of TLR3 as the major PRR involved in cytoplasmic dsRNA engagement in murine and human PDAC cells is intriguing. Differently from RIG-I and MDA5 (which are cytoplasm-located and can recognize everything that is exported from the nucleus to the cytoplasm), TLR3 is located on the plasma membrane and in endosomes. Therefore, shuttling of dsRNA and the transport pathway that directs dsRNA from the nucleus to the endosomes should be further investigated.

This result gives rise to the question, why explicitly TLR3 is significantly engaged with dsRNA. However, cells and organisms – and especially cancer cells – evolutionary developed mechanisms and adaption of self-tolerance to host dsRNA to escape from immunogenic response. To tolerate increasing amounts of dsRNA in proliferating or transformed cells, diverse mechanisms evolved in the cell: First, self-dsRNA displays modifications that support the cell in distinguishing self and foreign RNA. RIG-I is monitoring the lack of eukaryotic posttranscriptional modifications on dsRNAs in the cytoplasm. We cannot judge the modification of the 5'-end of dsRNA that originates from repetitive elements. However, two observations make it unlikely that the 5'-UTR has immunogenic alterations: We see that dsRNA is bound by DICER ***(Figure 40)*** and AGO1X has been shown to be implicated in dsRNA degradation, indicating, that the machinery contributes to degradation and turnover of the dsRNA (Ghosh *et al.*, 2020). This provides an explanation why RIG-I is not significantly bound by dsRNA.

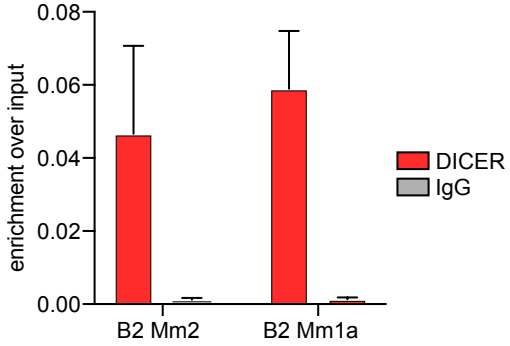

Figure 40: dsRNA derived from repetitive elements is bound by DICER. *Data is presented as mean ±SD (n=3, technical replicates).*

MDA5, a paralog of RIG-I, also monitors dsRNA in the cytoplasm to downstream activate type I IFN signaling via MAVS. However, besides their structural similarities, MDA5 and RIG-I are non-redundant and recognize different dsRNA species. MDA5 is described to predominantly recognize large dsRNAs <1 kb, while RIG-I mainly recognizes short, uncapped dsRNAs. Increasing size of dsRNA (2, 3, and 4 kb) causes increasing activation of MDA5 (del Toro Duany *et al.*, 2015; Kato *et al.*, 2008). This model explains how MDA5 discriminates between endogenous and exogenous dsRNA, as endogenous dsRNA from SINE elements is typically short while many retroviruses have long RNA genomes (Saito and Gale, 2008). B2-element derived dsRNA displays a size of 150-200 bp ***(Figure 29B)*** and is therefore not able to induce activation of MDA5.

Second, there are a number of indicatives that dsRNA is phase separating and/or the cognate PRRs are phase separating in the cytoplasm to prevent an activation of the immune system by self-dsRNA (Cadena *et al.*, 2021; Corbet *et al.*, 2022; Maharana *et al.*, 2022). Viral infections and dsRNA can induce the formation of stress granules to control the immune response (Iadevaia *et al.*, 2021; Zhang *et al.*,

2014b). We hypothesize that similar mechanisms may be involved in shielding dsRNA from PRRs or vice versa in transformed cells.

Third, TLR3, the pattern recognition receptors we showed to be engaged by B2-element derived dsRNA in immunoprecipitation experiments, is located in endosomes or on the plasma membrane to detect DAMPs and PAMPs (Matsumoto *et al.*, 2003). Experiments with synthetic oligonucleotides showed that RNA dimers of 45 bp or larger are sufficient to trigger dimerization of TLR3 and activation of innate immunity (Jelinek *et al.*, 2011; Leonard *et al.*, 2008). TLR3 was already described to bind ERVs causing production of IFNB that further activates the immune system, pointing its capacity to bind endogenous dsRNA (Chiappinelli *et al.*, 2015). Besides RIG-I and MDA5 that evolved with the capability to discriminate between foreign and self-RNA via size or post-transcriptional modifications, TLR3 is activated only by the duplex form of RNA. Therefore, TLR3 is located on the plasma membrane or in endosome where it is first protected from self-RNA but has access to exogenous dsRNA and conditions a transport pathway to load self-dsRNA on TLR3.

2.4 dsRNA is metabolized via a vesicular transport pathway

2.4.1 MYC and MIZ stabilize each other at the promoter of vesicular transport genes

As described in ***section 1.1.5*** MYC forms heterodimers with MIZ1 in order to repress transcription. A link between MIZ1 and autophagy, exosomes, endosomal maturation and lysosomal flux (vesicular transport) was previously suggested by the Eilers laboratory, showing that MIZ1 is essential for autophagy in the development of the brain (Wolf *et al.*, 2013). More recently, MIZ1 has been connected to an immune evasive or suppressive phenotype, similar to what has been previously observed for MYC (Muthalagu *et al.*, 2020; Zhang *et al.*, 2021). Additionally, deletion of the POZ domain of MIZ1, which is crucial for the interaction with MYC, was already shown to be haplo-insufficient for PDAC development (Walz *et al.*, 2014). We hence hypothesize a role of MIZ1 in an autophagy-related vesicular transport pathway that contributes to the immune evasive phenotype of MYC in PDAC.

First, we performed proximity ligation assays between MYC and MIZ1 to validate the interaction between both proteins in human and murine PDAC cells ***(Figure 41A, B)***.

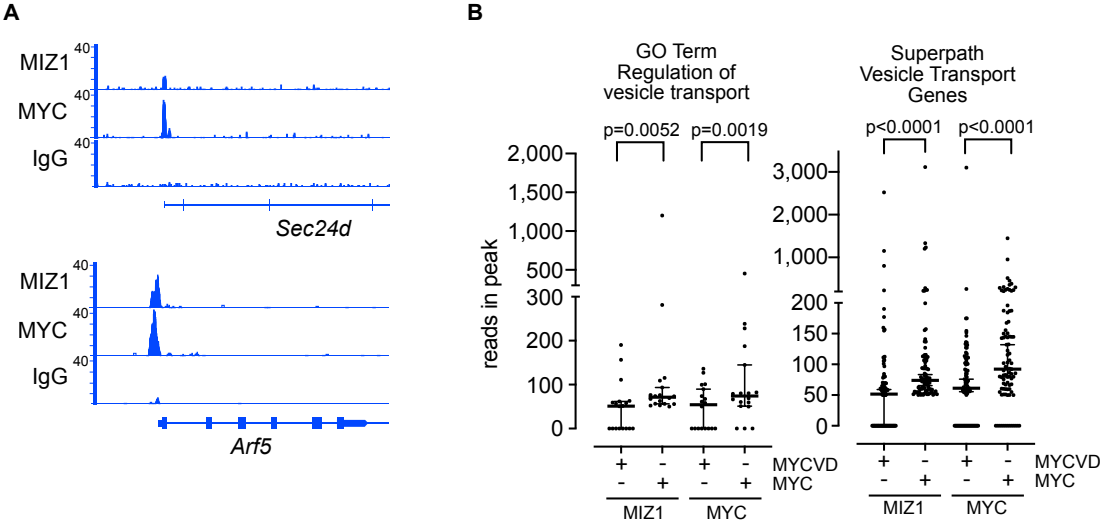

Figure 41: MYC and MIZ1 cooperate in binding to the promoter of repressed genes. *A: In situ proximity ligation assay (PLA) for MYC and MIZ in human PDAC cell lines and KPC cells (murine). B: Quantification of PLA. Results are presented as individual values and mean ±SD (n=3). C: Browser track of ChIP sequencing for MYC, MIZ1 and IgG in murine KPC cells. D: Analysis of MYC, MYCVD and MIZ1 binding to promoter of indicated gene sets. P value was calculated using Wilcoxon matched-pairs signed rank test.*

MYC and MIZ1 chromatin binding behavior in KPC cells were analyzed using published data sets (Wiese *et al.*, 2015). MYC and MIZ1 cooperatively bind to the promoter of genes that are associated with vesicular transport ***(Figure 41A)***. Strikingly, the overexpression of MYC^{V394D} (MYCVD), a MYC point mutant that does not interact with MIZ1, significantly reduced the binding of both MYC and MIZ1 to the promoters of those genes ***(Figure 41B)***.

2.4.2 MYC/MIZ1 cooperate to suppress the transport and loading of dsRNA to TLR3

In order to understand whether heterodimerization of MYC to MIZ1 shapes the global expression profile of KPC cells RNA sequencing was re-analyzed. Depletion of MYC or overexpression of MYCVD induced

an upregulation of hallmark gene sets and GO terms involved in endocytosis and exocytosis as well as autophagy and lysosomal transport ***(Figure 42A)***.

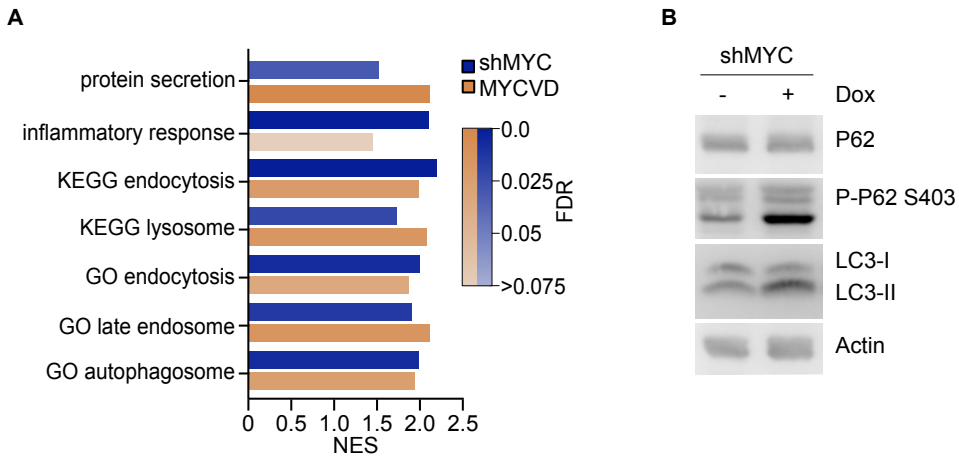

Figure 42: MYC/MIZ1 repress autophagy and lysosomal flux. *A: Gene set enrichment analysis of global RNA expression profile of KPC cells expressing doxycycline-inducible shRNAs to target MYC or ectopic expression of a mutant MYC^{V394D} compared to wildtype MYC for 48 h (n=3). B: Immunoblot of KPC cells after 48 h of depletion of MYC for Actin, LC3, P62 and P-P62 (n=3).*

We confirmed this expression profiles with immunoblot against two markers for autophagy. First, conversion of LC3-I to LC3-II is significantly increased upon depletion of MYC. Second, P62/SQSTM, a direct target of TBK1, is phosphorylated at S403 upon depletion of MYC ***(Figure 42B)***.

MYC and MIZ1 repress the transcription of genes like SEC24D, the RAB family and other genes that are implicated in shuttling, loading and signaling of TLR3 and lysosomal flux (Lee and Barton, 2014; Wandinger-Ness and Zerial, 2014). However, we did not conclusively investigate whether a single MYC/MIZ1 repressed gene is critical to prevent activation of the immune system or whether this cooperation orchestrates the repression of a set of genes that is involved in the regulation of vesicular transport. We can argue that there are at minimum two aspects that favor a model of MYC and MIZ1 repressing not a specific gene but dampening the transcription of a set of genes: First, MYC and MIZ1 stabilize each other at the core promoter of a large vesicular transport gene set. Second, the transcriptional activation of genes after depletion of MYC or overexpression of MYCVD is mild. It is unlikely that the mild upregulation of a specific gene is responsible for the switch from a highly immune-suppressive microenvironment to a T cell infiltrate anti-tumorigenic microenvironment.

This concept is supported by the recent changes in the view on MYC biology that draws back MYC from being a pure transcription factor but more a global “interaction platform” that recruits bystander proteins to facilitate their function and fine-tune the transcriptional program (Baluapuri *et al.*, 2020). Similar observations have been recently made in TNBC, suggesting that MYC globally represses innate immunity as master regulator (Zimmerli *et al.*, 2022). However, better understanding of MYC/MIZ1 dependent regulation of vesicular transport and immunity is needed to answer the question whether interfering with this interaction can be a promising therapeutic approach.

The role of MIZ1 in tumorigenesis and maintenance has already been investigated in mouse models. Deletion of the POZ domain of MIZ1 delays tumor formation in mouse pancreatic cancer models. Both, Muthalagu *et al.* and Walz *et al.* showed that the interaction between MYC and MIZ1 is important to promote immune evasion in pancreatic cancer (Muthalagu *et al.*, 2020; Walz *et al.*, 2014).

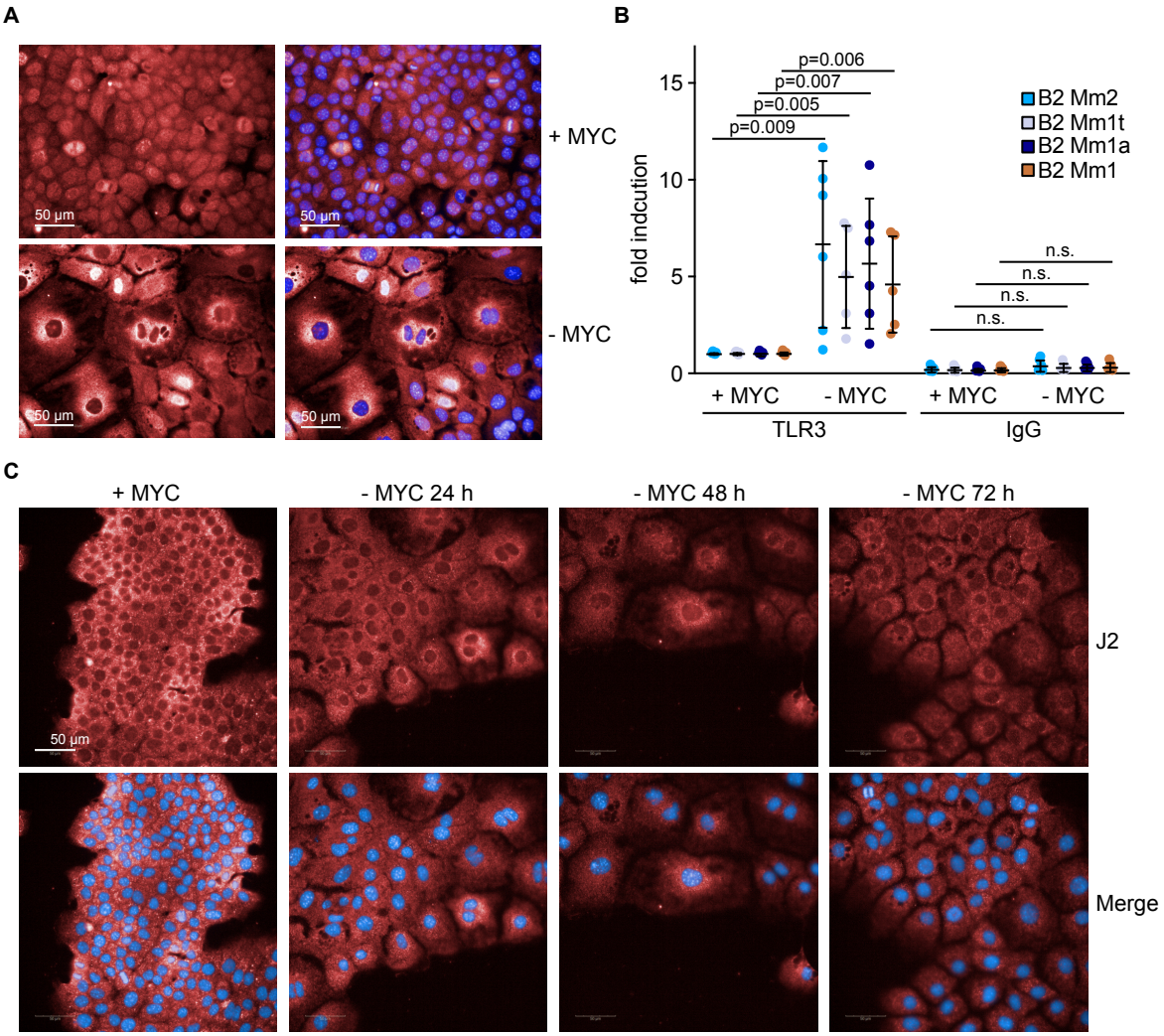

Figure 43: Depletion of MYC increases engagement of TLR3. *A: Immunofluorescence of TLR3 (red) in KPC cells with and without doxycycline induced depletion of MYC. B: fCLIP for TLR3 from KPC cells with and without depletion of MYC was performed (n=6). Results are presented as individual values with mean ±SEM. P values were calculated using two-tailed unpaired t test. C: Immunofluorescence of dsRNA (red) from KPC cells with high levels of MYC and shRNA mediated depletion of MYC for 24 h, 48 h and 72 h.*

With the aim of studying TLR3 dynamics upon dsRNA generation, TLR3 immunofluorescence was performed. After MYC depletion, TLR3 revealed a translocation to the perinuclear region of the cell, indicating the activation and transport of TLR3 (Lee *et al.*, 2006) ***(Figure 43A)***. A fCLIP experiment for TLR3 performed in parallel confirmed that TLR3 activation was concomitant with dsRNA loading on TLR3 ***(Figure 43B)***. The translocation of TLR3 is paralleled by a translocation of the dsRNA in the perinuclear region of the cell. Despite the reduction in total dsRNA staining, the staining in the perinuclear region increased and displayed a very similar phenotype compared to what has been observed in the immunofluorescence of TLR3 ***(Figure 43C)***.

2.4.3 Loading of dsRNA onto TLR3 is independent of canonical autophagy

To better understand which pathway promotes the loading of dsRNA we considered several hypotheses. First, we examined whether canonical autophagy is responsible for the metabolism of dsRNA. We used two different experimental settings in KPC cells to perform fCLIP for TLR3. First, chloroquine (CQ), a compound that prevents autophagic flux, was used (Mauthe *et al.*, 2018). The treatment of KPC cells with chloroquine significantly increased the loading of dsRNA onto TLR3, indicating that canonical autophagy is not needed for dsRNA loading onto TLR3 ***(Figure 44A)***. Second, a cell line with knockout of ATG7, which is incapable in forming autophagosomes, was compared to KPC cells with restored ATG7 function (i.e., ectopic expression of ATG7). ATG7 knockouts and ATG7 restored cells did not show a difference in TLR3 engagement ***(Figure 44B)***. Especially the fCLIP of ATG7$^{-/-}$ cells suggest that canonical autophagy is not responsible for the loading of dsRNA onto TLR3. More likely, a vesicular transport pathway, which can be affected by treatment with chloroquine, promotes the transport and metabolism of dsRNA. The increased loading of dsRNA onto TLR3 after treatment with chloroquine points towards a pathway that includes endosomal maturation and degradation of dsRNA in the lysosomes. Furthermore, the inhibition of autophagy and the blockade of lysosomal flux using chloroquine promoted the phosphorylation of TBK1 and stabilization of LC3-II in murine KPC cells as well as in human PDAC cell lines ***(Figure 44C)***.

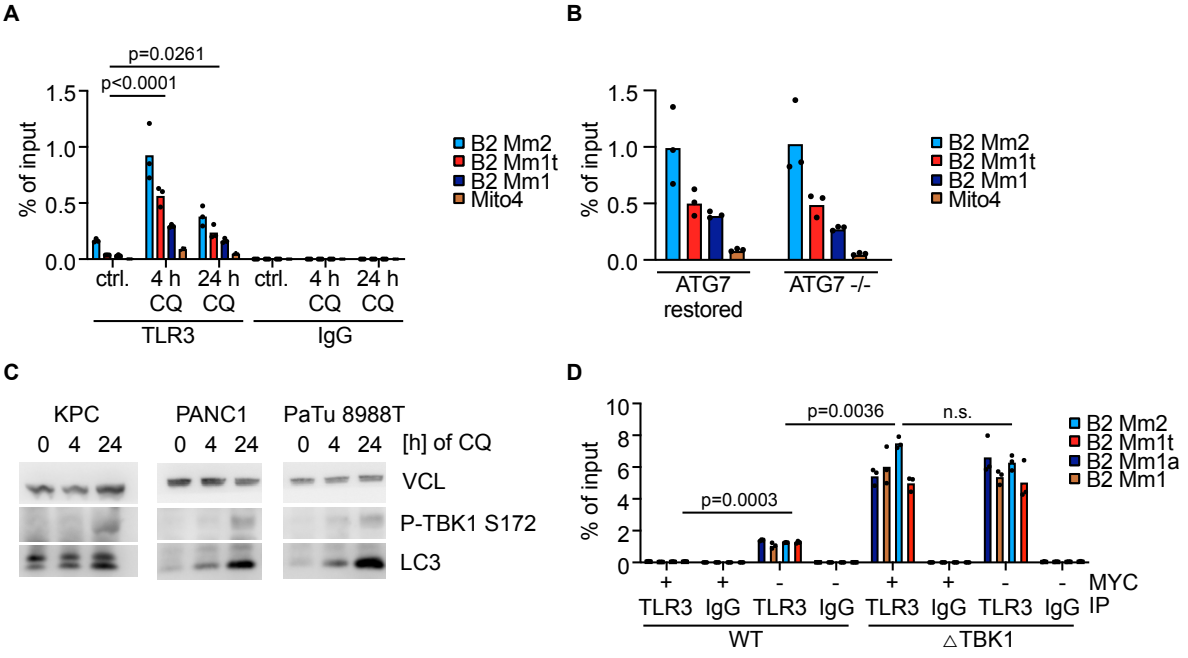

Figure 44: TLR3 engagement is independent of canonical autophagy but dependent on TBK1 mediated dsRNA metabolism. *A: fCLIP from KPC cells treated with chloroquine (10 μM CQ) for 4 or 24 h (n=2). The P value was calculated using ANOVA with Fisher LSD. B: fCLIP from autophagy deficient KPC cells (ATG7$^{-/-}$) and autophagy restored KPC cells followed by RNA extraction and RQ-PCR. C: Immunoblot of murine and human PDAC cell lines for Vinculin, P-TBK1 and LC3 after treatment with 10 μM chloroquine (CQ). D: fCLIP from KPC cells with and without knockout of TBK1. Where indicated, MYC was depleted using doxycycline inducible shRNAs. Results are presented as individual values of technical replicates (n=2). The P value was calculates using ANOVA with Fisher LSD.*

Strikingly, TBK1 deletion induced a strong increase in dsRNA loading onto TLR3. Interestingly, this increase is independent of MYC levels. The accumulation of dsRNA upon TBK1 knockout suggests that TBK1 mediates dsRNA degradation, potentially by promoting the transport of dsRNA-loaded TLR3 to the lysosome ***(Figure 44D)***.

Treatment with chloroquine averted the reduction of dsRNA resulting from MYC depletion in a dose dependent manner. Preventing the degradation of dsRNA in the lysosome using chloroquine prevents the reduction of J2 signal upon MYC depletion (***Figure 45)***.

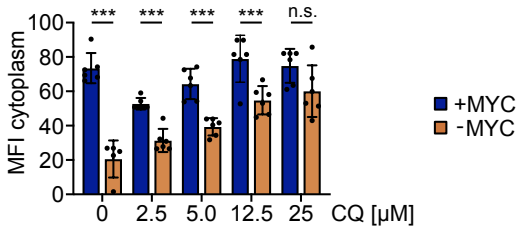

Figure 45: Inhibition of autophagy stabilizes dsRNA. *Quantification of immunofluorescence for dsRNA. Results are presented as individual biological replicates and mean ±SD, 2-tailed t test (n=6).*

2.4.4 PDAC cells release dsRNA containing vesicles

The involvement of an endosomal pathway allows the hypothesis that dsRNA is encapsulated in vesicle which are then released by the cell. To test this, we used α-dsRNA-antibody and precipitated dsRNA from supernatant that was treated with a detergent. This experiment showed that MYC depletion caused an increase of dsRNA in the supernatant, which was more pronounced for dsRNA originating from repetitive elements than from mitochondria ***(Figure 46A)***.

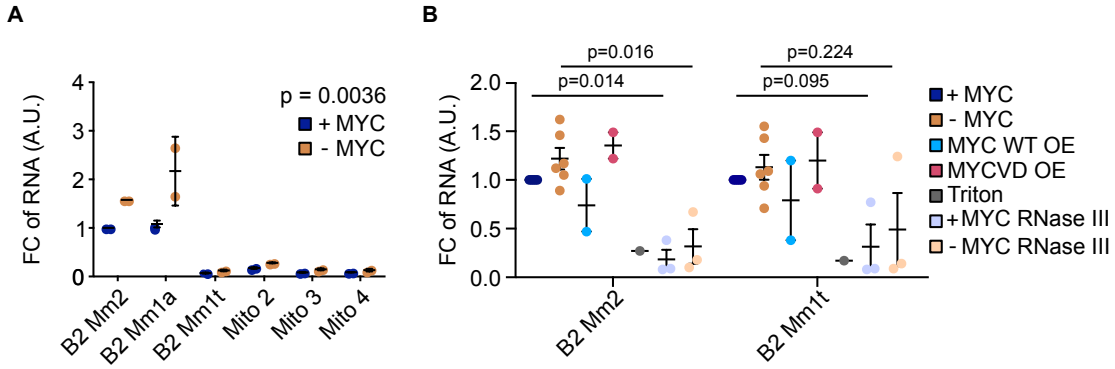

Figure 46: dsRNA is secreted in membrane-containing vesicles*. A: RQ-PCR from J2-immunoprecipitation from supernatant of KPC cells. Cells were treated with doxycycline for 48 h to induce MYC depletion. Results are presented as individual values, mean ±SD (n= 2). The P value was calculated using two-way RM ANOVA. B: RNA content of extracellular vesicles purified with ultracentrifugation from the supernatant of KPC cells determined by RQ-PCR (n=6). Results are presented as mean ±SEM. The P value was calculated using two-tailed, unpaired t test.*

To confirm this, extracellular vesicles were collected and analyzed for their dsRNA content. In detail, supernatant of KPC cells was filtered and ultracentrifugation was performed. This experiment confirmed the J2-immunoprecipitation and corroborated the involvement of MIZ1 by comparing the overexpression of MYC WT and MYCVD ***(Figure 46B)***. While overexpression of wildtype MYC reduced the dsRNA vesicle content in supernatant, overexpression of MYCVD strongly increased its amount. Importantly, this experiment also proves that the detected dsRNA is packed in vesicles, as pretreatment with the non-ionic detergent Triton-X 100 (i.e., preventing sedimentation of these vesicles) abrogated the dsRNA detection. In line with this, RNase III also reduced the signal, verifying the double-stranded structure of the precipitated RNA ***(Figure 46B)***.

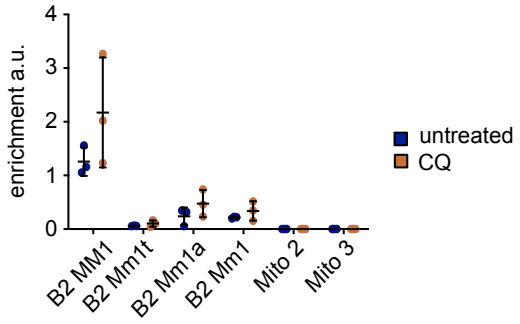

Figure 47: Chloroquine does not change the release of extracellular vesicles. *RNA content of extracellular vesicles purified with ultracentrifugation from the supernatant of KPC cells determined by RQ-PCR (n=6).Cells were treated with 10 µM chloroquine for 24 h. Results are presented as mean ±SD (n=3).*

CQ treatment has been shown to promote exosome formation (Ortega *et al.*, 2019). In KPC cells treatment with CQ did not promote the release of extracellular vesicles ***(Figure 47)***.
Concluding this part, we uncovered that the trafficking of dsRNA is a complex and multi-layered vesicular transport pathway:

(1) dsRNA is released from nuclei to the cytoplasm, where it is bound only to a minimal extent by the cytoplasmic pattern recognition receptors MDA5 and RIG-I. This scarce engagement can be explained by two models: First, dsRNA can largely escape the cytoplasm through the release of shedding microvesicles or uptake via macro- or microautophagy or RNautophagy via SIDT2 to mediate decay (Aizawa *et al.*, 2016; Frankel *et al.*, 2017; Guo *et al.*, 2014; Hase *et al.*, 2020; Yim and Mizushima, 2020). Second, PRR and dsRNA both can phase separate in stress-granules or P-bodies, preventing that MDA5 or RIG-I can be engaged (Cadena *et al.*, 2021; Maharana *et al.*, 2022). We could reject the hypothesis that dsRNA enters the endo-lysosomal compartment via canonical autophagy using a knockout of ATG7 that is critical for the formation of the phagophore (Collier *et al.*, 2021; Komatsu *et al.*, 2005). This is supported by the observation that chloroquine – a widely used inhibitor for autophagy – is increasing the loading of dsRNA onto TLR3 instead of restricting it (Mauthe *et al.*, 2018).
(2) We confirmed the hypothesis that dsRNA is secreted in membrane-containing extracellular vesicles (EVs) using ultracentrifugation. EVs are carriers of proteins, RNAs, and other biomolecules and play a role in metastasis, cellular stress response and immune-modulation of the tumor micro-environment (Kao and Papoutsakis, 2019; Marar *et al.*, 2021). They arise by multifarious mechanisms: Exosomes are released by multivesicular bodies that originate from the endo-lysosomal compartment. In contrast, shed microvesicles (sMV) are not of endocytic origin but form by budding of the plasma membrane. The budding of the plasma membrane causes sMVs and can incorporate biomolecules from the cytoplasm – including dsRNA – without transport to a distinct subcellular compartment (Tricarico *et al.*, 2017; Xu *et al.*, 2018). It is more likely that we observe sMVs, but not exosomes, since we did not observe an increase in EV formation after CQ treatment.
(3) Treatment with CQ stabilizes dsRNA in the cytoplasm, since increasing the pH level with CQ in the endolysosomal compartment dampens the activity of the hydrolytic enzymes in the lysosome (de Duve, 2005; Fedele and Proud, 2020; Halcrow *et al.*, 2021). We conclude that alkalinization of the vesicular transport pathway prevents degradation and turnover of dsRNA in the lysosome at a late step of the process. In consequence, treatment with CQ increases not only loading of dsRNA onto TLR3 but also downstream activation of TBK1. Interfering with vesicular transport using CQ blocks loading, transport and degradation of dsRNA, pointing out that this pathway plays a key role in TLR3 signaling, TBK1 activation and therefore also immune dependent regression of PDAC tumors.

We observe that MYC depletion increases autophagosomal and lysosomal flux as a result of the interruption of MYC/MIZ1 dependent repression of genes. TBK1 is not only the central hub to mediate

activation of IRF3 and IRF7 in consequence of PRR activation, but it can also activate lysosomal flux (Heo *et al.*, 2018; Honda *et al.*, 2006; Schlütermann *et al.*, 2021). Activation of TBK1 promotes phosphorylation of SQSTM1 at Serine 403 upon depletion of MYC. SQSTM1 has been described to selectively prone dsRNA virus for degradation via autophagy, pointing out that indeed activation of autophagic and lysosomal flux is a key component of the innate immune program (Xu *et al.*, 2021).

We showed that TLR3-induced TBK1 activation plays a pivotal in tumor regression after MYC depletion by promoting lysosomal flux due to phosphorylation of its target proteins like SQSTM1 and probably also RAB proteins that promote endosomal maturation (Heo *et al.*, 2018). We postulate that this provides a feed-forward loop to increase loading of dsRNA to TLR3 and promote immunogenicity. Depletion of MYC promotes loading of dsRNA onto TLR3 by releasing MYC/MIZ1 dependent repression of vesicular transport genes.

2.5 MYC suppresses NFKB-driven MHC class I presentation

2.5.1 NFKB is upregulated in a TBK1 dependent manner upon MYC depletion

We observe that depletion of MYC activates the expression of the NF-κB hallmark gene set. To further investigate the activation of NF-κB signaling upon the depletion of MYC, KPC cells were infected with IKBAM, a non-phosphorylatable mutant of IKBA that was already shown to efficiently dampen canonical NF-κB signaling (Van Antwerp *et al.*, 1996). Immunoblots validated the expression of the transgene ***(Figure 48)***.

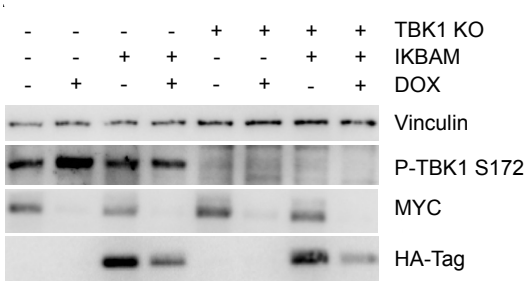

Figure 48: Overexpression of IKBAM. *Immunoblot of KPC cells for Vinculin, MYC, HA-tag (recognizing IKBAM) and P-TBK1. Where indicated doxycycline was added to deplete MYC using shRNAs, TBK1 was deleted using CRISPR/Cas9, a mutant IKBA was ectopically expressed.*

Global expression analysis was performed to dissect the TBK1- and NF-κB-dependent transcriptional changes upon depletion of MYC. Deletion of TBK1 or overexpression of IKBAM significantly attenuated the upregulation of the hallmark gene sets for inflammatory response and TNF-α signaling via NF-κB, but not the GO terms for endosomes, which are upregulated by the overexpression of MYC^{V394D} ***(Figure 49A)***.

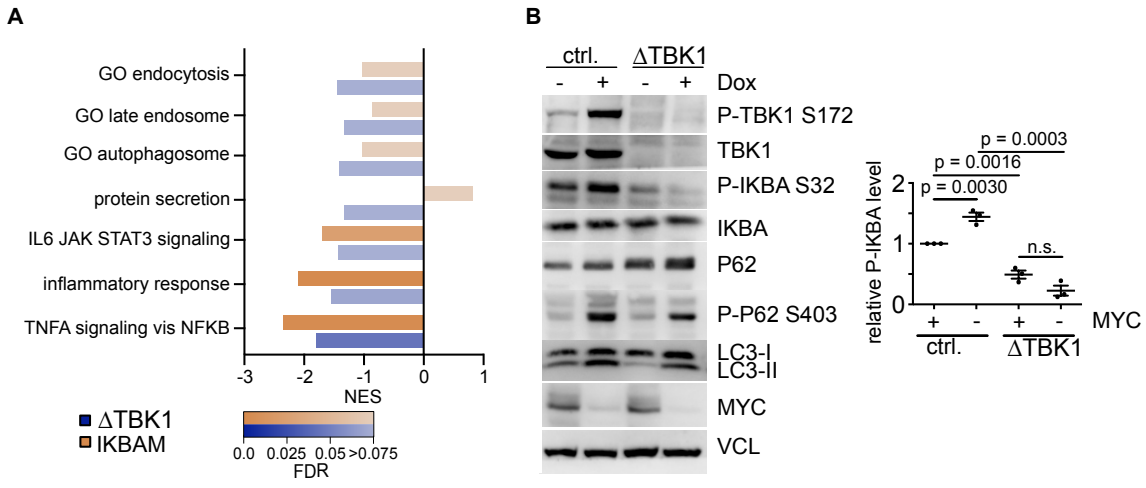

Figure 49: Activation of NFKB signalling is dependent on TBK1. *A: Gene set enrichment analysis of global RNA expression profile of KPC cells expressing doxycycline-inducible shRNAs to target MYC. GSEA was performed by either comparing wildtype TBK1 and deletion of TBK1 or wildtype IKBA and ectopic expression a dominant negative IKBAM in a MYC depleted situation (n=3). B: Immunoblot (left) of KPC cells with shRNA-mediated depletion of MYC and knockout of TBK1 for Vinculin, MYC, LC3, P62, P-62, IKBA, P-IKBA, TBK1 and P-TBK1. Quantification (right) of P-IKBA signal. Data are presented as individual values of biological replicates and mean ±SD (n=3). P values were calculated using one-way ANOVA with post hoc Tukey.*

We confirmed the activation of NF-κB-signaling by immunoblots. The depletion of MYC significantly increased the phosphorylation of Iκ-Bα, which primes Iκ-Bα for degradation by the proteasome and release of the NF-κB-heterodimer to translocate to the nucleus. Deletion of TBK1 completely removed the phosphorylation of Iκ-Bα at S32 ***(Figure 49B)***. Moreover, deletion of TBK1 removed the phosphorylation of P62 on S403 (SQSTM), confirming that the knockout is functional and reduces the activation of canonical targets of TBK1 ***(Figure 49B)***.

Depletion of MYC promotes loading of dsRNA onto TLR3 by releasing MYC/MIZ1-dependent repression of vesicular transport genes. This promotes activation of TBK1 to further increase TLR3 loading and phosphorylation of Iκ-Bα that triggers its proteasome dependent degradation and release of the p50/RELA heterodimer to shuttle to the nucleus. There it activates the transcription of inflammatory cytokines, MHC class I genes, and other proinflammatory genes (Kawai and Akira, 2007). Disturbing the feedforward loop by the deletion of TBK1 therefore dampens the activation of a proinflammatory signature, explaining the essentiality of TBK1 for immune-dependent tumor regression.

Furthermore, a custom "PDAC_NFKB" gene set was designed to study the regulation of NF-κB-signaling. This gene set included genes of the "TNFA signaling via NFKB" hallmark gene set upregulated after depletion of MYC and downregulated upon IKBAM ectopic expression. Depletion of MYC significantly activated the expression of "PDAC_NFKB", while the deletion of TBK1 attenuated the expression of this gene set upon depletion of MYC ***(Figure 50A)***. GO term analysis of this gene set showed that it contains genes that are involved in inflammatory response, chemokine and cytokine regulation as well as MHC class I presentation ***(Figure 50B)***.

A

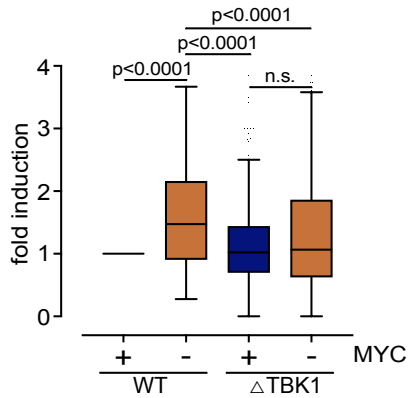

B

gene set	Enrichment	FDR
GO immune response	5.80	1.12e-15
GO immune system process	19.30	6.86e-14
GO inflammatory response	6.95	9.29e-11
GO defense response	4.00	5.88e-7
GO cytokine activity	16.95	8.26e-12
GO chemokine activity	50.47	2.92e-10
GO chemokine receptor binding	50.47	2.92e-10
GO MHC protein binding	18.93	1.35e-2
GO MHC class I protein binding	17.47	1.31e-1
GO CCR chemokine receptor binding	16.22	1.56e-1

Figure 50: TBK1 deletion prevents activation of NF-κB-signaling. *A: Boxplot showing the regulation of genes in the custom designed "PDAC_NFKB" gene set representing NF-κB-signaling. P value was calculated using one-way-ANOVA. B: GO term analysis of genes that are downregulated upon TBK1 deletion or ectopic expression of IKBA. The overlap of genes was used for the GO term analysis.*

Or data show that TBK1 activation induces NF-κB, but not IRF3. However, the literature concerning TBK1 and NF-κB is less unequivocal. TRAF2, TANK and TBK1 probably form a complex to activate

NF-κB (Pomerantz and Baltimore, 1999). However, the lack of functional data implies that the TBK1-dependent phosphorylation of Iκ-Bα is probably via indirect effects. This is underlined by the observation that TBK1 deletion is only affecting a subset of target genes that are affected by overexpressing a dominant negative Iκ-Bα.

NF-κB plays a double-edged role in pancreatic cancer. Its proproliferative and anti-apoptotic capacity is driven by multiple factors, including its target genes BCL-XL or cIAP (Arlt *et al.*, 2012). On the other hand, NF-κB drives the expression of proinflammatory cytokines and MHC class I genes (Jongsma *et al.*, 2019; Liu *et al.*, 2017). Strikingly, NF-κB plays a crucial role in the development of pancreatic cancer driven by KRas and Ink4a mutation in mice (Ling *et al.*, 2012). Moreover, inhibition of NF-κB signaling in KPC cells by overexpression of a mutant Iκ-Bα dampens the growth of culture (data not shown). In contradiction with this, NF-κB can also restrict the growth of MYC-driven hepatocellular cholangiocarcinoma and repress the development of MYC-induced lymphomas (He *et al.*, 2019; Klapproth *et al.*, 2009). PDAC cells show a similar dependence to TLR3 as to NF-κB genes. TLR3 and NF-κB both play a role in pancreatitis that can cause pancreatic cancer via chronic and systemic inflammation (Jakkampudi *et al.*, 2016; Soga *et al.*, 2009; Vaz and Andersson, 2014). Interfering with TLR3 reduces growth of pancreatic cancer cells in culture (Schwartz *et al.*, 2009). This is underlined by the observation that TLR3 expression is a predictor for bad prognosis in pancreatic cancer patients (Nagy *et al.*, 2021) ***(Figure 51A)***.

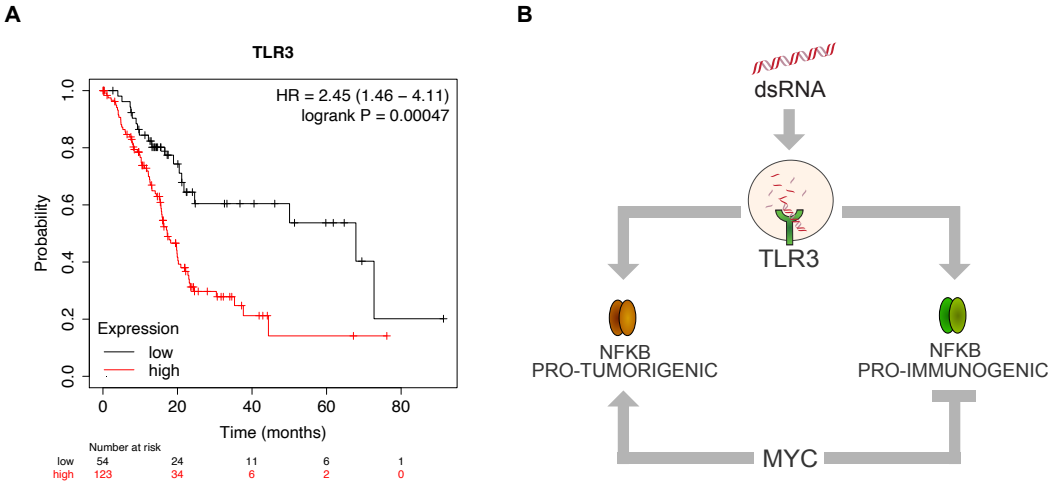

Figure 51: TLR3 and NFKB are a MYC-regulated double-edge sword. *A: High expression of TLR3 (mRNA) correlates with poor prognosis in pancreatic cancer (Lánczky and Győrffy, 2021). B: TLR3 can activate both, pro-tumorigenic and proimmunogenic signaling via NF-κB. MYC controls the expression of these genes via squelching of elongation factors.*

Overexpression of a dominant negative mutant of Iκ-Bα decrease NF-κB target genes in a highly significant manner in KPC cells with oncogenic levels of MYC. Depletion of MYC only upregulates the transcription of a subset of NF-κB target genes, including MHC class I genes.

To summarize: We argue that MYC's immune suppressive function works via two axes. First, oncogenic MYC level, in cooperation with MIZ1, prevent the activation of NF-κB target genes by modulating a highly specific pathway that dampens dsRNA transport, TLR3 loading and activation. Second, MYC acts via its hard-wired function to bind to all core promoters of genes that are transcribed by RNA polymerase II. The activation of NF-κB target genes as a consequence of the depletion of MYC is on the one hand driven by the increased translocation of the NF-κB heterodimer to the nucleus as consequence of TLR3-mediated activation, and on the other hand by restoring SPT5 binding to the promoter of these genes. By not binding to the core promoter of genes that are transcribed by RNAPII it squelches crucial factors from these genes to prevent their efficient transcription (Baluapuri *et al.*, 2019; Baluapuri *et al.*, 2020) ***(Figure 2, Figure 14)***. We argue that MYC specifically shapes the expression profile of NF-κB target genes to facilitate the expression of proproliferative proteins and at the same time, prevents the expression of genes – probably via sequestration of crucial factors from the genes – that would enable the recognition of cancer cells by the immune system ***(Figure 51B)***. This explains why pancreatic cancer cells are dependent on both, the expression of NF-κB target genes and the repression of a subset of NF-κB target genes by MYC.

2.5.2 MYC suppresses presentation of MHC class I

MHC class I presentation of neoantigens is the major mechanism for T cells to specifically recognize cells. Importantly, T cells are the critical species determining *in vivo* tumor regression upon MYC depletion (see ***section 2.2.1***). Therefore, the expression of MHC class I genes in PDAC was further investigated using available RNA sequencing data. MYC depletion induced a strong increase in the expression of all four highly expressed MHC class I genes ***(Figure 52)***.

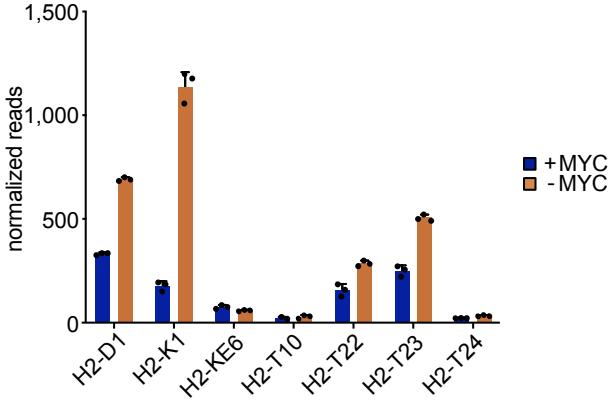

Figure 52: Normalized reads of all genes encoding for MHC class I proteins. *Data shows individual values of different biological replicates and mean ±SD (n=3).*

Analysis of TBK1 knockout cells and cells expressing IKBAM showed that the expression of H2-K1 and H2-D1 was significantly dependent on TBK1 and NF-κB signaling, suggesting that MYC depletion causes a dsRNA-dependent activation of TBK1, leading to downstream activation of NF-κB-signaling and upregulation of MHC class I presentation ***(Figure 53A)***. To confirm this hypothesis, surface expression of H-2Kb and H-2Db of KPC cells was performed using flow cytometry. Consistent to what

was observed at the RNA level, MYC depletion led to an increased presentation of both isotypes, and this upregulation is attenuated in a TBK1-depleted background ***(Figure 53B)***.

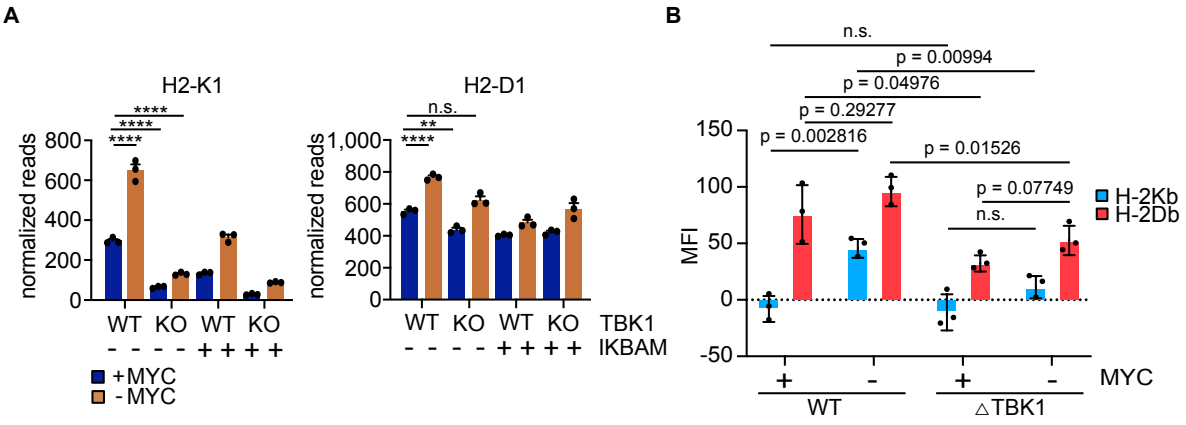

Figure 53: MYC prevents presentation of MHC class I genes. *A: Normalized reads of H2-K1 and H2-D1 in KPC cells after depletion of MYC. Where indicated, TBK1 was deleted or a dominant negative IKBA mutant (IKBAM) overexpressed. Data shows individual values of different biological replicates ±SD (n=3). B: FACS analysis of MHC class I presentation on the surface of KPC cells with doxycycline inducible depletion of MYC and deletion of TBK1. P values were calculated using one-way ANOVA with post hoc Tukey. MFI: Mean fluorescent intensity.*

The observation, that MYC is repressing the transcription of MHC class I genes is probably the oldest described immune suppressive function of the MYC protein family (Bernards *et al.*, 1986; Versteeg *et al.*, 1988). Restoring immunogenic signaling in breast cancer can revert MYC dependent repression of MHC class I presentation machinery and induce regression of tumors. Moreover, they point out that not only MHC class I proteins and B2M are suppressed by the MYC oncogene, but also the whole antigen presenting machinery is restrained by high levels of MYC (Lee *et al.*, 2022a). Overexpression of the MYC protein family is a hallmark of cancer (Gabay *et al.*, 2014; Hanahan and Weinberg, 2011), causing the downregulation of MHC class I and consequently immunological cold tumors with bad prognosis (Dhatchinamoorthy *et al.*, 2021; Garrido *et al.*, 2016; Jongsma *et al.*, 2019).

Repression of MHC class I could be indeed a potential mechanism how MYC facilitates its immune evasive function in mouse pancreatic cancer. This is strengthened by the finding that the absence of T cells prevents regression of tumors after MYC depletion. As part of the adaptive immune system, T cells recognize and clear cells expressing highly specific neoantigens that are presented by MHC class I and clear these cells. Increasing MHC class I presentation has been shown to delay tumor progression in the KPC mouse model (Yamamoto *et al.*, 2020). Mutational burden and therefore neoantigen load are a predictive marker for the response for immunotherapy like α-PD-1 or adoptive T cell therapy (Lauss *et al.*, 2017; McGranahan *et al.*, 2016; Wang *et al.*, 2021). Human PDACs display about 30 neoantigens per tumor that could potentially elicit an immunogenic response (Balachandran *et al.*, 2017). Our study is probably limited by the fact that GEMM display far less (0-11 per tumor) neoantigens (Evans *et al.*, 2016; Rojas and Balachandran, 2021).

2.5.3 MHC class I presentation is not crucial for tumor regression

The presentation of neoantigens is a central mechanism of T cells to recognize and eliminate tumor cells. To determine whether the MYC-dependent downregulation of MHC class I presentation is critical for the immune escape in PDAC tumors, a knockout of β2-microglobulin (B2m) was conducted in murine KPC cells, to proof whether the presentation of MHC class I is critical for the regression of the tumors. Lack of B2M destabilizes the presentation of antigens on the surface of cells (Yamamoto *et al.*, 2020). Wildtype KPC cells (expressing luciferase) were infected with a construct expressing an sgRNA targeting the *B2m* locus as well as expressing Cas9. Single-cell clones were selected and screened for the absence of H-2Kb and H-2Db presentation on the surface. Sanger sequencing of the selected clone (#32) validated the introduced mutation of the gene after the PAM sequence, indicating the knockout of *B2m* in this cell clone ***(Figure 54A)***. The knockout was validated with immunoblotting ***(Figure 54B)***. Flow cytometry showed that knockout of B2m abrogates presentation of MHC class I on the surface ***(Figure 54C, D)***.

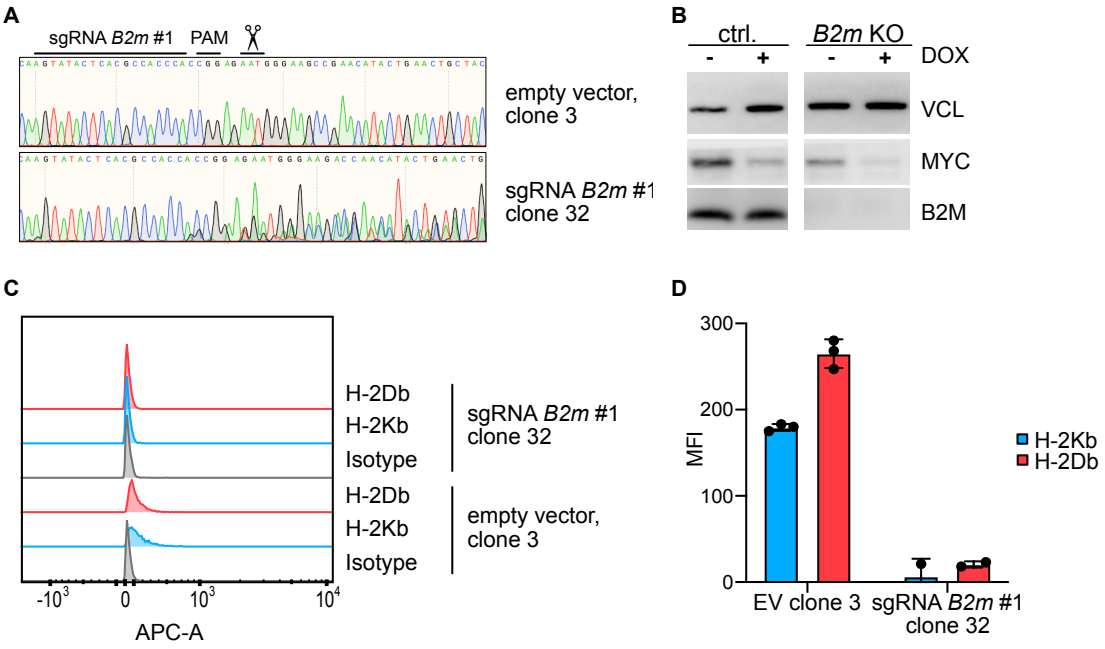

Figure 54: Knockout of B2m. *A: Chromatogram from sanger sequencing of the B2m locus of control cells and knockout cells. B: Immunoblot for B2M in KPC cells with knockout of B2m. C: Profile from flow cytometry comparing the control clone (#3) to the clone with knockout for B2m (#32). Cells were stained for H-2Db and H-2Kb. D: Quantification of staining for H-2Kb and H-2Db in control cells and knockout cells (n=3).*

Immunoblot for B2M confirmed the knockout. We infected both cell clones with two doxycycline inducible shRNAs targeting MYC, which have been previously used for the depletion of MYC. Induction of shRNAs efficiently reduced the levels of MYC protein in both cell lines ***(Figure 54B)***.

We transplanted the *B2m*$^{-/-}$ KPC cell line and the control cell into the pancreata of immunocompetent C57BL/6J mice. Tumors engrafted for 7 days and treatment with doxycycline was started. Tumors in mice that did not receive doxycycline did not show a regression, while mice that received doxycycline tumors showed a regression after 7 days of treatment. Strikingly, tumors regressed independent of the presentation of MHC class I on the surface ***(Figure 55)***.

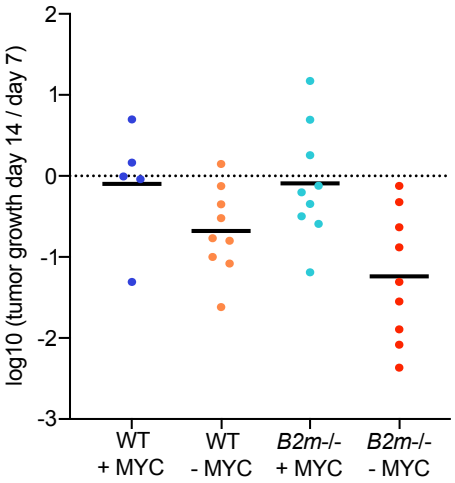

Figure 55: Knockout of B2m in KPC cells does not affect regression of tumors after depletion of MYC. *Tumor size was measured using IVIS. Tumor growth is shown as individual samples and mean (n=5/9/9/9). The mouse experiment was conducted by Anneli Gebhardt-Wolf.*

The observation that KPC tumors still regress in the absence of MHC class I presentation allows two different interpretations. If MYC mediated immune evasion is not dependent on antigen presentation, regression of tumors is not dependent on CD8-positive CTLs. We would therefore argue that CD4-positive T helper cells are the T cell population that is needed for the regression of the tumors. This would also fit our observation that nude mice, that lack both CD4- and CD8-positive T cells, are crucial for the regression of tumors. Besides activating CD8-positive T cells, T helper cells are also capable to activate B cells or NK cells (Garaud *et al.*, 2022; Janeway, 2005). This hypothesis is supported by the fact that $Rag^{-/-}$ and NRG mice display stronger tumor growth compared to nude mice. Early work on the immune evasive capacity of MYC had also shown that CD4-positive T cells are crucial for tumor control (Rakhra *et al.*, 2010). Additionally, it has been shown that B cells and NK cells contribute to tumor cell death *in vivo* after inactivation of MYC in PDAC and lung adenocarcinoma (Kortlever *et al.*, 2017; Sodir *et al.*, 2020).

Alternatively, the knockout of *B2m* could also allow NK cells to attack the KPC cells, since they miss the expression of antigens via MHC class I. NK specifically recognize the absence of antigen-presentation and their activation is dampened by the binding to HLA-E (Kärre, 2002; Kärre *et al.*, 1986; Pereira *et al.*, 2019). In parallel, MYC depletion causes an upregulation of NK-cell-activating ligands like CD155 on the surface (data not shown) (Chester *et al.*, 2015; Raulet and Vance, 2006). Analysis of the TME using flow cytometry or histochemistry is needed to understand whether MYC mediated immune evasion is independent on antigen presentation or whether the knockout of B2m itself allows a NK-cell-dependent tumor regression.

2.6 Translating MYC depletion into therapy

2.6.1 Target MYC translation using cardiac glycosides

In order to restore immune surveillance in pancreatic cancer interfering with MYC and/or its function can be a promising strategy. We therefore aimed to substitute the genetic approach of RNAi mediated depletion with a small molecule that could be transferred into patient trials.

Several publications have shown that the treatment of transformed cells with cardiac glycosides, which target the major subunit of the sodium-potassium pump ATP1A1, interferes with the levels of MYC protein (Steinberger *et al.*, 2019; Wiegering *et al.*, 2015). Consistently, treatment of human colorectal cancer or PDAC cell lines with the cardiac glycoside cymarin led to a significant decrease of MYC protein levels. Murine cancer cell line did not respond to treatment with cardiac glycosides, because murine ATP1A1 is 1,000-fold more resistant to cardiac glycosides than the human isoform ***(Figure 56)***.

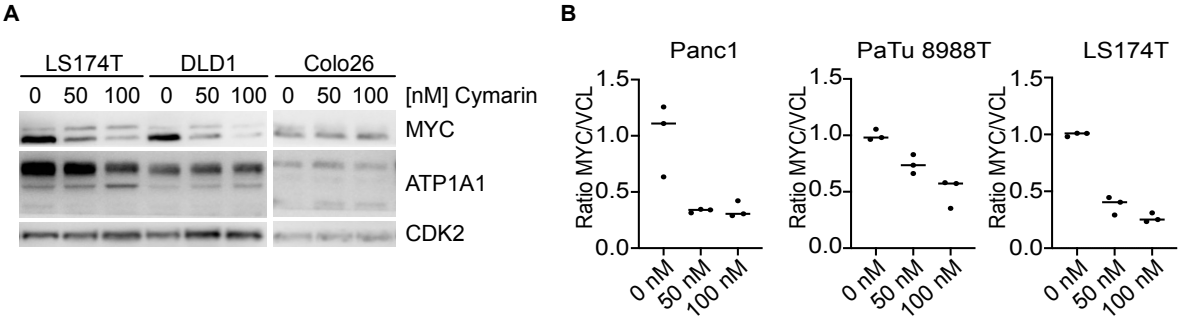

Figure 56: Cardiac glycosides reduce levels of MYC protein in human but not in murine cancer cells. *A: Immunoblot of colorectal cancer cells treated with indicated concentration of cymarin for 24 h. CDK2, ATP1A1 and MYC are blotted. LS174T and DLD1 are derived from human patients. Murine Colo26 cells are derived from an N-nitroso-N-methylurethane-induced colon carcinoma. B: Quantification of MYC levels normalized to Vinculin in human PDAC and colon cancer cell lines treated with indicated concentrations of cymarin for 24 h. Results are presented as values of individual replicates and mean (n=3).*

To further study this aspect, depletion of ATP1A1 was performed to assess whether cymarin acts on target via its canonical binding and inhibition of the sodium-potassium pump. Depletion of ATP1A1 using doxycycline inducible shRNAs causes a robust decrease of ATP1A1 protein levels, accompanied by a mild decrease of MYC protein levels ***(Figure 57A)***. Ectopic expression of human ATP1A1 had no effect on the response of human and murine cells to cymarin, while ectopic expression of the murine isoform of ATP1A1 rendered human cancer cells resistant, confirming that the effect on MYC protein levels is dependent on the inhibition of the sodium-potassium pump ***(Figure 57B)***. Treatment of human cancer cells with cymarin causes a strong decrease in proliferation, while murine cells were not affected ***(Figure 57C)***.

Cardiac glycosides have been previously implicated already as potential drugs to target tumor cells and to affect MYC protein levels (Didiot *et al.*, 2013; Du *et al.*, 2021; Steinberger *et al.*, 2019; Wiegering *et al.*, 2015). Cardiac glycosides are well described to bind to the sodium-potassium pump and inhibit the export of sodium and the import of potassium. Since murine cells are resistant and shRNAs targeting ATP1A1 in human cancer cell reduce MYC protein levels, this indicates that the regulation of MYC protein with cardiac glycoside is not mediated via the IRES of the MYC mRNA, as described by

Wiegering *et al.* and Didiot *et al.*, but by the capacity of cardiac glycosides to inhibit the sodium-potassium pump.

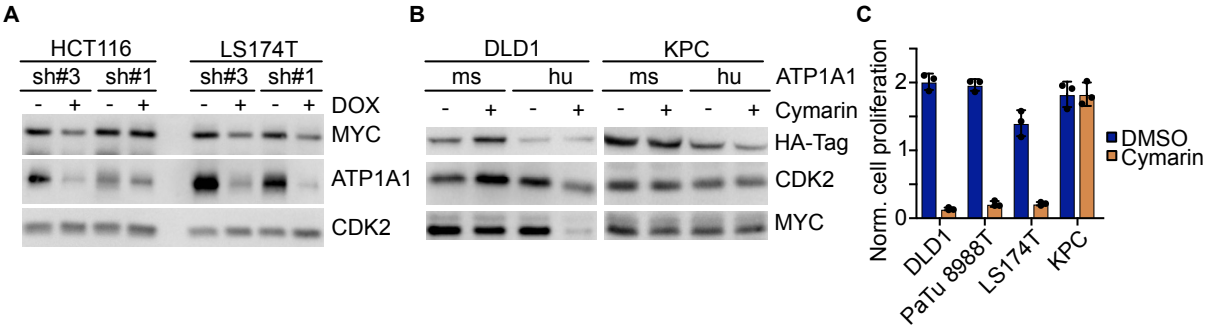

Figure 57: Effects of cardiac glycosides on MYC protein levels are dependent on ATP1A1. *A: Immunoblot of human CRC cell lines with shRNA mediated depletion of ATP1A1 for 48 h of indicated proteins. B: Immunoblot of KPC cells (murine) and DLD1 cells (human) with ectopic expression of either human or mouse HA-tagged ATP1A1. Cells were treated with cymarin for 24 h. C: Cell counts of human and murine cancer cell lines. Cells were treated with 100 nM cymarin for 96 h. Data is shown as individual values of replicates with mean ±SD (n=3).*

2.6.2 Cardiac glycosides regulate MYC translation via the 3'-UTR

We speculated that the fast downregulation of MYC can be due to an impaired translation of its mRNA, as previously described (Dejure *et al.*, 2017). To investigate whether cymarin-induced decrease of MYC protein relies on this phenomenon, we overexpressed a number of different constructs representing parts of the MYC-CDS in human cancer cells.

All constructs express the same coding sequence of MYC with alterations in the untranslated regions (UTR) of the MYC mRNA. MYC immunofluorescence revealed that treatment with cymarin in human DLD1 cells expressing the CDS of MYC is not affecting the levels of MYC proteins ***(Figure 58)***. Similarly, MYC protein translated from the CDS including the 5'-UTR was not downregulated upon cymarin treatment in the immunofluorescence. Only with the addition of the 3'-UTR to the CDS of MYC, the protein levels decreased with cymarin treatment. Thus, the regulation of MYC protein level after treatment with cymarin is dependent on its 3'-UTR ***(Figure 58)***.

Overexpression of the MYC-CDS with four differently truncated 3'-UTR further showed that only with the smallest truncation (Δ2262-2366) cells are still reacting to treatment with cardiac glycosides. Larger deletions made the human tumor cells resistant to treatment with cardiac glycosides. The observed effects are clearer in the normalized immunofluorescence compared to the immunoblot, but the truncated 3'-UTR-CDS-constructs (Δ2127-2366, Δ2025-2366, Δ1997-2366) show a clear resistance for treatment with cardiac glycosides ***(Figure 58, 59)***.

Analysis of MYC protein levels using immunoblotting showed a reduction in the levels of MYC also with only CDS or CDS-5'-UTR while the deletion of the 3'-UTR stabilize the MYC protein levels when treated with cardiac glycosides ***(Figure 58 bottom, 59)***.

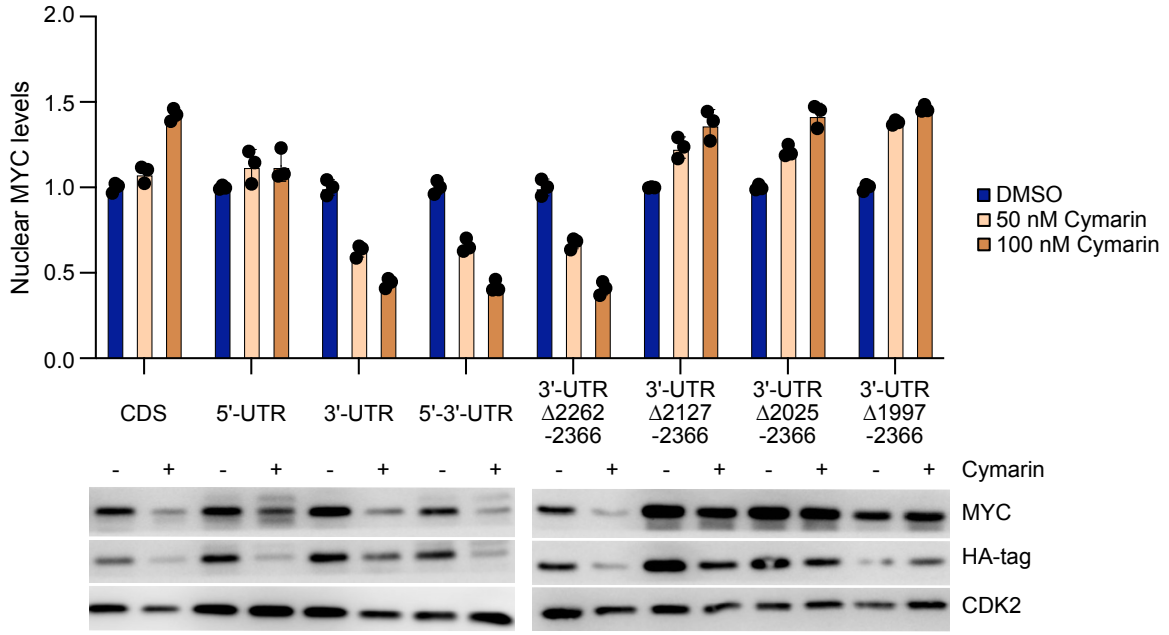

Figure 58: Cardiac glycosides target MYC translation via the 3'-UTR. *Top: Quantification of immunofluorescence of MYC from DLD1 cells with ectopic expression of different constructs of MYC. Cells were treated with indicated concentrations of cymarin for 24 h. Data is shown as individual values of replicates with mean ±SD (n=3). Bottom: Immunoblot of same DLD1 cells expressing the HA-tagged MYC constructs and treated for 24 h with 100 nM cymarin (n=2).*

The observation that only MYC with 3'-UTR Δ2262-2366 still displays a reduction of MYC after treatment with cymarin resembles the effect of glutamine starvation described in Dejure *et al.*, indicating that there are probably parallels between the treatment of tumor cells with cymarin and starvation of glutamine (Dejure *et al.*, 2017).

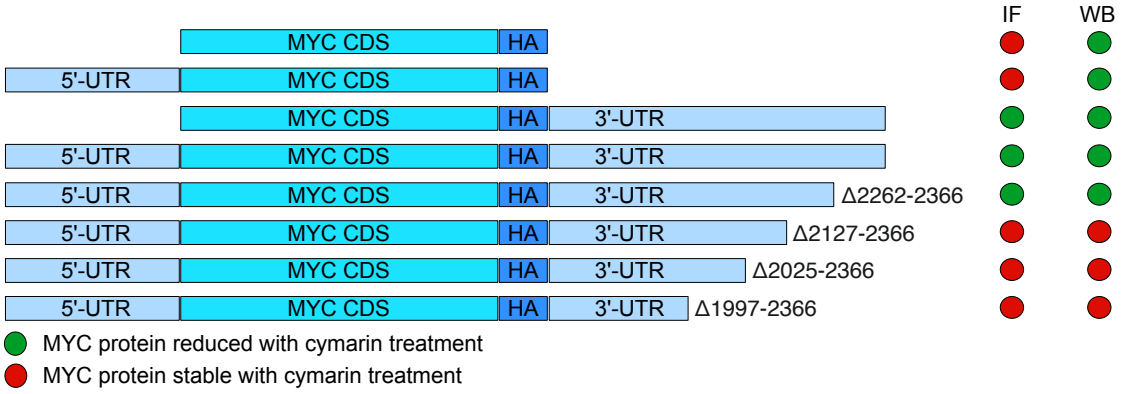

Figure 59: Scheme of transfected MYC constructs in Figure 58. *Colors indicate stability of MYC protein after treatment with cymarin.*

It has been described in Dejure *et al.* that tumor cells monitor the availability of glutamine in their environment and downregulate translation of MYC when there is not enough glutamine retrievable. The pathway that monitors the nutrient status and controls the translation of MYC has so far not been described, but the regulation of translation is mediated via the 3'-UTR of MYC. Truncation of the 3'-UTR of MYC uncouples glutamine levels from MYC translation (Dejure *et al.*, 2017).

2.6.3 Cardiac glycosides change metabolome of transformed cells

Previous studies have shown that the levels of glutamine regulate MYC protein translation via the 3'-UTR of MYC. Mass spectrometry of all water-soluble metabolites in the cell was performed to assess whether inhibition of the sodium-potassium pump using cymarin could change the metabolome of human PDAC cell lines PaTu 8988T and BxPC3.

Addition of cymarin caused a strong reduction in the amount of most amino acids. Additionally, a massive reduction of glutamine was observed in both analysed human cell lines after cymarin treatment ***(Figure 60, top)***. Glutamine serves as building block for nucleotide biogenesis. Consequently, the content of nucleotides and nucleosides in the measured samples was also strongly reduced upon inhibition of the sodium-potassium pump ***(Figure 60, bottom)***.

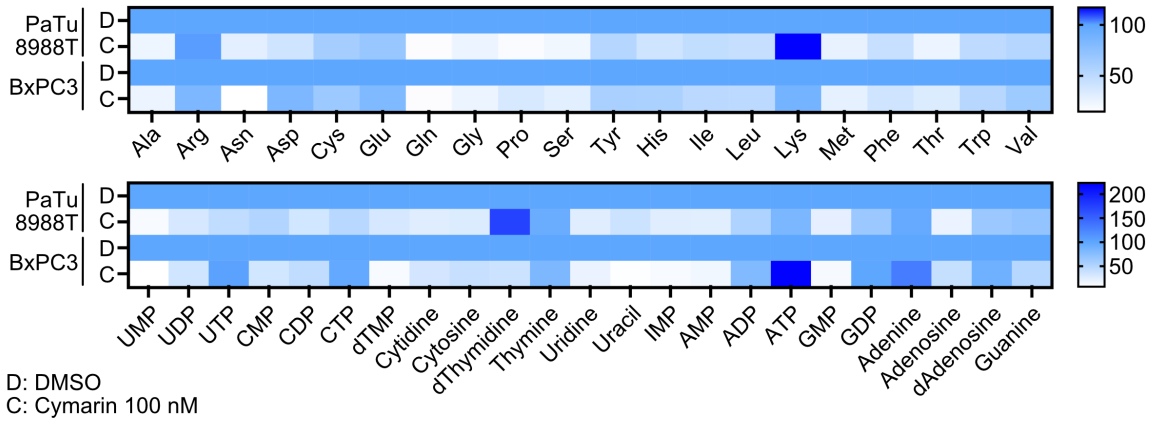

Figure 60: Mass spectrometry analysis from cell pellet of human PDAC cells treated with 100 nM cymarin for 24 h. *Heatmap shows mean of selected metabolites (n=3). Top: Amino acids. Bottom: Nucleotides and Nucleosides.*

Inhibition of the sodium-potassium pump leads to a number of changes in steady-state levels of water-soluble metabolites in the tumor cells. In human PDAC cell lines the content of most amino acids drops dramatically upon inhibition of the sodium-potassium pump. Only basic amino acids did not change after treatment with cymarin. This observation can be explained by the fact that many, but not all, importers for amino acids are making use of the sodium-potassium gradient that is built up by the sodium-potassium pump.

For example, Arg and Lys are imported by CATs (cationic amino acid transporters), a subfamily of the solute carrier family 7 (SLC7). Strikingly, the transport of these two amino acids via CATs is independent of the sodium-gradient, which is also reflected in our measurement ***(Figure 60, top)*** (Closs *et al.*, 2006). In general, neutral and anionic amino acids depend on the sodium gradient, since they are imported by a Na^+-cotransport, while cationic amino acids do not depend on the gradient that is build up by the sodium-potassium pump, since they are imported by amino acid exchange mechanisms or with uniporters like the CAT family (Gauthier-Coles *et al.*, 2021; Poncet and Taylor, 2013).

In consequence to the strong reduction of amino acids in the cell, a massive reduction of nucleosides and nucleotides can be observed. The *de novo* synthesis of purine requires amongst others glutamine, glycine and aspartate (Voet, 2008). The massive reduction of glutamine and glycine impedes the

synthesis of purines. Our laboratory could already show that the starvation of glutamine leads to reduced levels of adenosine. Adenosine promotes the translation of the MYC mRNA dependent on the 3'-UTR. Restoring the levels of adenosine in a glutamine-deprived condition restores the level of MYC protein (Dejure *et al.*, 2017).

In light of Dejure *et al.,* the effects of treatment with cardiac glycosides on MYC protein levels and the metabolic consequences we hypothesize that CG treatment mimics the effects of a glutamine starvation. This is underlined by the fact that the same region in the 3'-UTR of the MYC mRNA is responsible for the downregulation of MYC translation after glutamine starvation or treatment with CGs.
ATP is the only nucleosides or nucleotides that increased after treatment with cardiac glycoside ***(Figure 60, bottom)***. In unperturbed cells the Na^+/K^+ pump is a major consumer of ATP and utilizes up to 50% of the total ATP that is produced by the cells. With the binding of CGs the hydrolysis of ATP is inhibited and accumulates in the cell, leading to increased or stable levels of ATP despite reduced *de novo* synthesis.

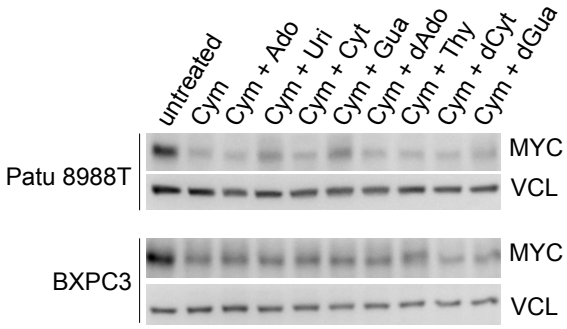

Figure 61: Rescue of MYC decrease after cymarin treatment with nucleoside addition. *Immunoblot for MYC and Vinculin (n=2). Cells were treated for 4 h with 100 nM cymarin and 150 µM of the indicated substrates. Ado: adenosin, Uri: uridine, Cyt: cytidine, Gua: guanosine, dAdo: deoxy-adenosine, Thy: thymidine, dCyt: deoxy-cytidine, dGua: deoxy-guanosine.*

In general, inhibition of the sodium-potassium pump disrupts the gradient that is utilized by many essential transport processes. Therefore, different to glutamine starvation, cells with inhibited sodium-potassium pump cannot restore MYC protein levels by the external supply of nucleosides ***(Figure 61)*** (Kong *et al.*, 2004).

2.6.4 Sensitizing murine PDAC cells for cardiac glycosides

As described, human but not murine cells response to the treatment with cardiac glycosides. To sensitize KPC cells for cardiac glycoside treatment, human ATP1A1 was ectopically expressed in murine KPC cells. In parallel the murine isoform of *Atp1a1* was silenced using sgRNAs. Single cell clones were screened for cymarin sensitivity indicating a successful shift from mouse-to-human ATP1A1.

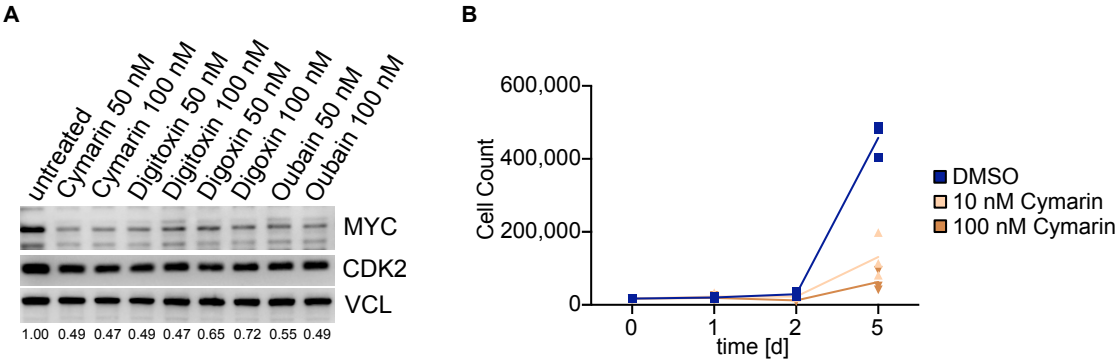

Figure 62: Humanized KPC^{hATP1A1} cells react to cardiac glycosides. *A: Immunoblot of humanized KPC cells after treatment with different cardiac glycosides with the indicated concentration for 24 h. B: Cumulative growth curve of humanized KPC cells after treatment with 10 nM or 100 nM of cymarin. Data is presented as individual values (n=3).*

The obtained KPC clone (KPC^{hATP1A1}) responded to a number of different cardiac glycosides and showed an efficient reduction in MYC protein levels and reduced proliferation in culture ***(Figure 62)***, while parental KPC cells did not respond to the treatment ***(Figure 57C)***.

Mass spectrometry analysis of wildtype KPC cells and KPC^{hATP1A1} cells was performed upon treatment with cymarin. Cymarin-treated KPC^{hATP1A1} cells displayed a rearrangement of the metabolome comparable to the one of human PDAC cells ***(Figure 63)***.

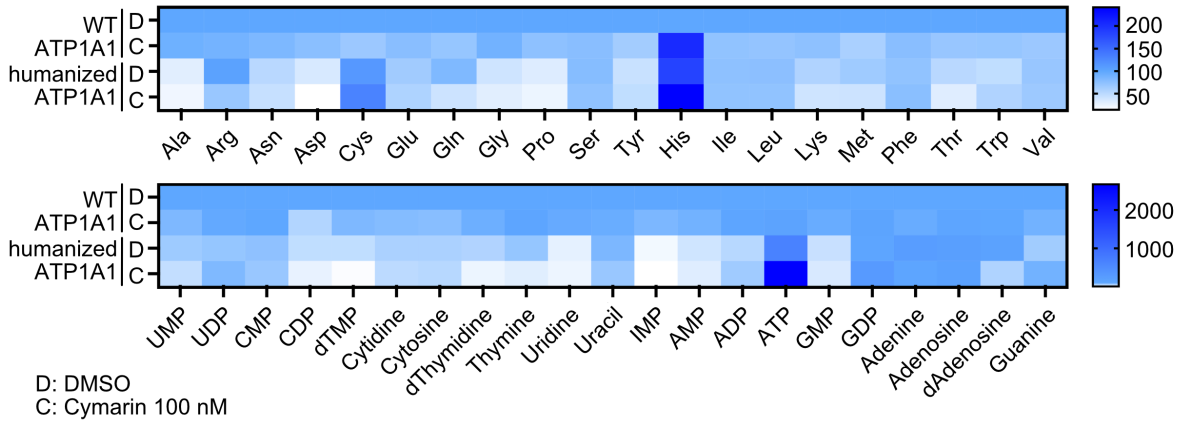

Figure 63: Mass spectrometry analysis from cell pellet of KPC^{hATP1A1} treated with 100 nM cymarin for 24 h. *Heatmap shows selected metabolites (n=3). Top: Amino acids. Bottom: Nucleotides and Nucleosides.*

Amino acids as well as downstream nucleosides are decreased upon cymarin treatment of WT KPC, which overexpress hATP1A1, but have no knockout of endogenous mATP1A1. Overall KPC^{hATP1A1}

displayed already without treatment some changes in growth and in the metabolome compared to wildtype KPC cells ***(Figure 63)***. Still KPC^{hATP1A1} display stronger response to cymarin treatment.

2.6.5 Cardiac glycosides impede glycolysis in transformed cells

To understand whether the decrease in MYC protein levels after cymarin treatment causes similar transcriptional changes as observed after shRNA mediated depletion of MYC, we performed a global mRNA expression analysis of KPC^{hATP1A1}. We observed a strong activation of "TNFA signaling via NFKB" and oxidative phosphorylation, while glycolysis and bile acid metabolism were strongly decreased after inhibition of the sodium-potassium pump ***(Figure 64)***.

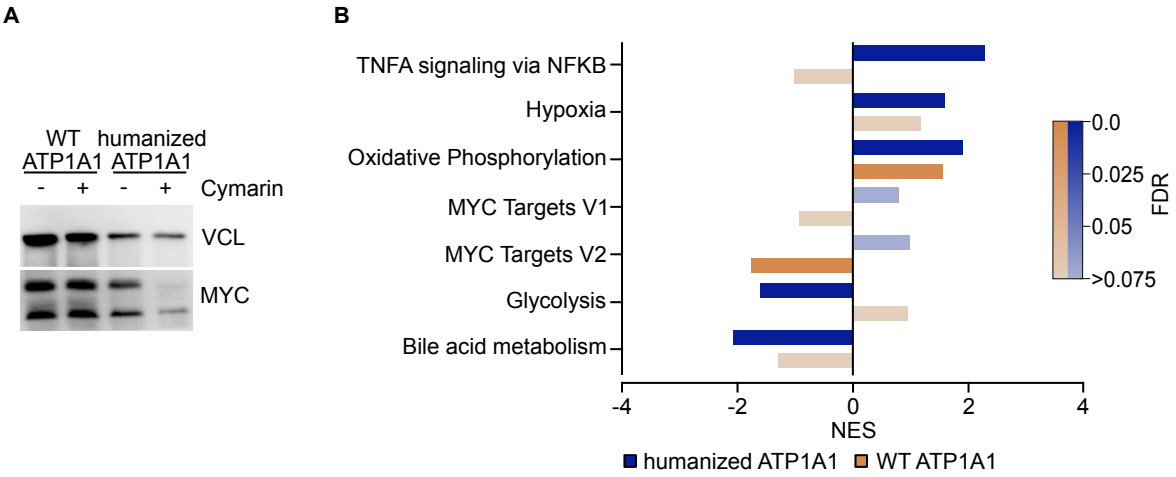

Figure 64: Cardiac glycosides downregulate glycolysis. *A: Immunoblot of KPC^{hATP1A1} cells after treatment with 100 nM of cymarin for 24 h. B: Gene set enrichment analysis of global RNA expression profile of KPC^{hATP1A1} after 24 h of treatment with 100 nM cymarin (n=3).*

To understand the changes in glucose metabolism in human and murine PDAC cells after treatment with cardiac glycoside, we analysed the metabolites of glycolysis and TCA cycle using mass spectrometry. Some intermediates of glycolysis increased upon cymarin treatment, suggesting an accumulation due to defective flux ***(Figure 65A)***. Similarly, humanized KPC cells also showed an increase of glycolysis intermediates after treatment with cymarin ***(Figure 65B)***. Interestingly, intermediates of the TCA only displayed mild changes upon cymarin, suggesting once more a problem in glycolysis ***(Figure 65)***.

Global RNA expression analysis of KPC^{hATP1A1} after treatment with cymarin points to three relevant observations. First, despite strong effects on the MYC protein levels, canonical MYC target genes are not significantly affected in humanized KPC cells after 24 h of treatment with GC. Second, TNF-α signaling via NF-κB, associated with activation of the innate and adaptive immune system, is significantly upregulated. Third and most importantly, treatment with CGs exhibits strong effects on the glucose metabolism of the cell. The hallmark gene set glycolysis is strongly downregulated after treatment with CGs. This was further underlined by the analysis of metabolites of the glycolysis and

TCA-cycle. Intermediates of the glycolysis are accumulating upon treatment with CGs, while the intermediates of the TCA cycle are only mildly affected.

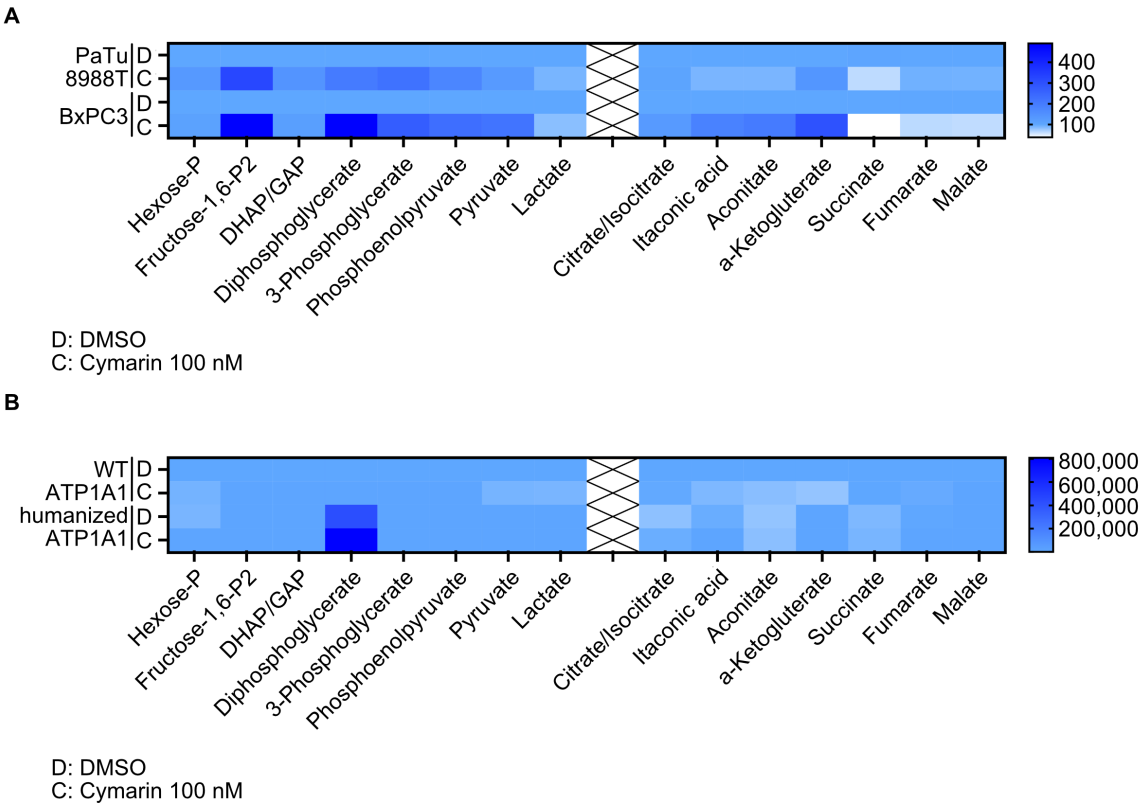

Figure 65: Mass spectrometry analysis from cell pellet of human PDAC cells (A) and KPC^{hATP1A1} (B) treated with 100 nM cymarin for 24 h. *Heatmap shows selected metabolites of the glycolysis (left) and the TCA cycle (right) (n=3).*

The inhibition of the sodium-potassium pump causes a massive excess and accumulation of ATP. High concentrations of ATP cause a general reduction of the glycolytic flux, especially by inhibiting the glycolytic enzymes phosphofructokinase (PFK) and pyruvate kinase (Larsson *et al.*, 2000). ATP acts as an allosteric inhibitor for PFK1, while AMP and ADP act as activators (Müller-Esterl, 2004). Since similarly pyruvate kinase is inhibited, one could first expect accumulation of fructose-6-phosphate and phosphoenolpyruvate instead of fructose-1,6-bisphosphate. Strikingly, it has been already described that the inhibition of the sodium-potassium pump results in the accumulation of fructose-1,6-BP (Sanderson *et al.*, 2020).

So far, we can only speculate why fructose-1,6-BP is increased in CG treated cells: First, the conversion of glyceraldehyde phosphate to diphosphoglycerate by GAPDH (glyceraldehyde phosphate dehydrogenase) requires free NAD+. High levels of ATP block the respiratory chain, consequently NAD+/H cannot be oxidized to create new ATP. This should lead to an accumulation of glyceraldehyde 3-phosphate/dihydroxy-acetone phosphate, because free NAD+ is needed for this step. However, the preceding step, the reaction of the aldolase, is an equilibrium reaction. Enzymes are only accelerating equilibrium reaction by reducing the activation energy but they cannot change the equilibrium of the

reaction. Consequently, if glyceraldehyde 3-phosphate accumulates, also level of FBP are increasing. This explains in part the accumulation of FBP that has been observed in our mass spectrometry as well as in other publications (Sanderson *et al.*, 2020) ***(Figure 66)***.

The second intermediate that is heavily accumulating is diphosphoglycerate. For the dephosphorylation to 3-Phosphoglycerate a free ADP is needed that takes over the phosphate. Cells with inhibited sodium-potassium pump have a strong reduction in consumption of ATP and in parallel the synthesis of nucleotides is reduced. Consequently, the levels of available ADP, which is crucial for this step, are reduced ***(Figure 66)***.

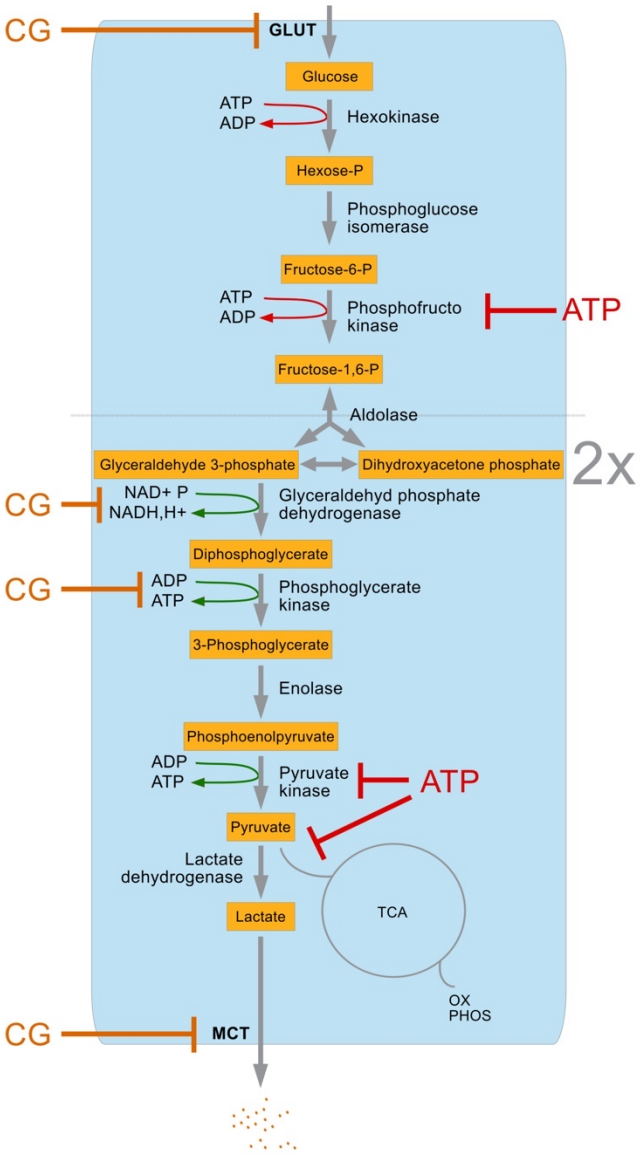

Figure 66: High levels of ATP are inhibiting the glycolysis by downregulating the activity of the phosphofructokinase and the pyruvate kinase. *Where indicated CG block the enzymatic reaction in glycolysis and cause the accumulation of intermediates.*

To better assess the nature of the suspected glycolytic problem, the extracellular acidification ratio (ECAR) of cymarin treated cells was measured using the Seahorse platform. Strikingly, human PDAC cells and KPC^{hATP1A1}, but not wildtype KPC cells displayed a strong reduction in the ECAR ***(Figure 67)***.

We explain this observation with two facts: First, inhibition of the sodium-gradient dependent import of glucose and fructose via GLUT transporters is blocked due to the disrupt gradient (Brown, 2000). Second, we observe that cymarin blocks glycolysis in several steps causing accumulation of several intermediates leading to less lactic acid that can be released to the medium ***(Figure 65, 67)***. Third, monocarboxylate-transporters (MCTs), that are responsible for the transport of lactate out of the cell, are dependent on the sodium gradient (Ganapathy *et al.*, 2008; Vijay and Morris, 2014). This also explains, why we do not observe a clear reduction in lactate in the measurement of the water-soluble metabolites in the cell ***(Figure 65)***.

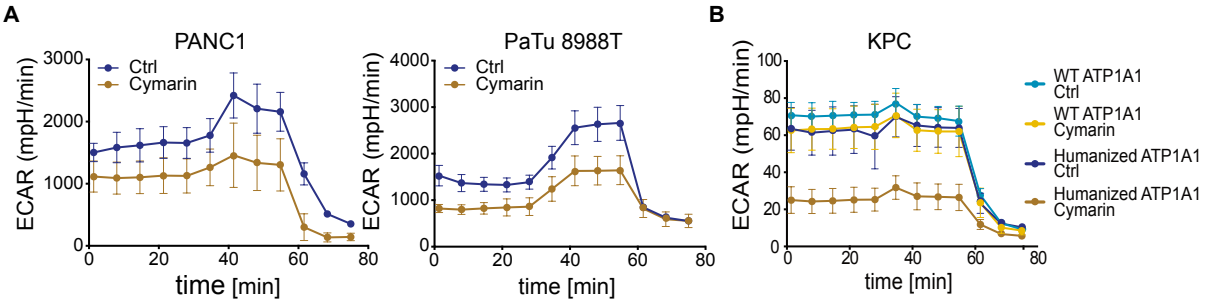

Figure 67: Treatment with cymarin reduces ECAR in PDAC cell lines. *A: Seahorse measurement of human PDAC cell lines treated with 100 nM cymarin for 24 h (n=5). B: Seahorse measurement of wildtype KPC and KPC^{hATP1A1} treated with 100 nM cymarin for 24 h (n=5).*

Biochemical analysis of these cells showed that – differently from shRNA-mediated depletion of MYC – KPC cells do not display an activation of TBK1 and increased presentation of MHC class I upon treatment with cymarin (data not shown). Cardiac glycosides act instead as inhibitors of MYC-driven oncogenic metabolism. They prevent that cancer cells consume all nutrients (glucose, amino acids) in the tumor microenvironment and they prevent the secretion of immune-suppressive lactate. Untransformed cells generate most of their ATP in the presence of oxygen through oxidative phosphorylation. Despite the presence of oxygen, cancer cells gain most of their energy by glycolysis (Koppenol *et al.*, 2011). This process has a much higher capacity than the ATP generation via oxidative phosphorylation, even though during glycolysis only two ATP are generated from one glucose (Liberti and Locasale, 2016).

Three major conclusions can be drawn from the biochemical analyses of the effects of cardiac glycosides onto tumor cells: First, tumor cells downregulate MYC protein levels upon treatment with cardiac glycosides and this is paralleled by changes in the metabolome. These changes show similarity to changes observed upon deprivation of glutamine. We assume that these changes are causal for the translational downregulation of MYC proteins, even though we cannot formally test the hypothesis with supply of external nucleosides, since the corresponding transporter is dependent on the sodium-gradient (***Figure 61)*** (Dejure *et al.*, 2017; Kong *et al.*, 2004). Second, cardiac glycosides stop the glycolytic flux in cells in culture. Third, the secretion of immune-suppressive lactic acid is nearly completely abrogated upon treatment with CGs.

2.6.6 Cardiac glycosides induce regression of tumors

To investigate how this translates into tumor growth *in vivo*, KPC^{hATP1A1} were transplanted into syngeneic, immunocompetent mice. After tumors engrafted for 7 days treatment with intraperitoneal digitoxin (2 mg/kg) every second day was started. Mice were treated for 28 days in total. Mice treated with digitoxin showed complete regression of tumors without relapse in 150 days after start of the experiment ***(Figure 68)***.

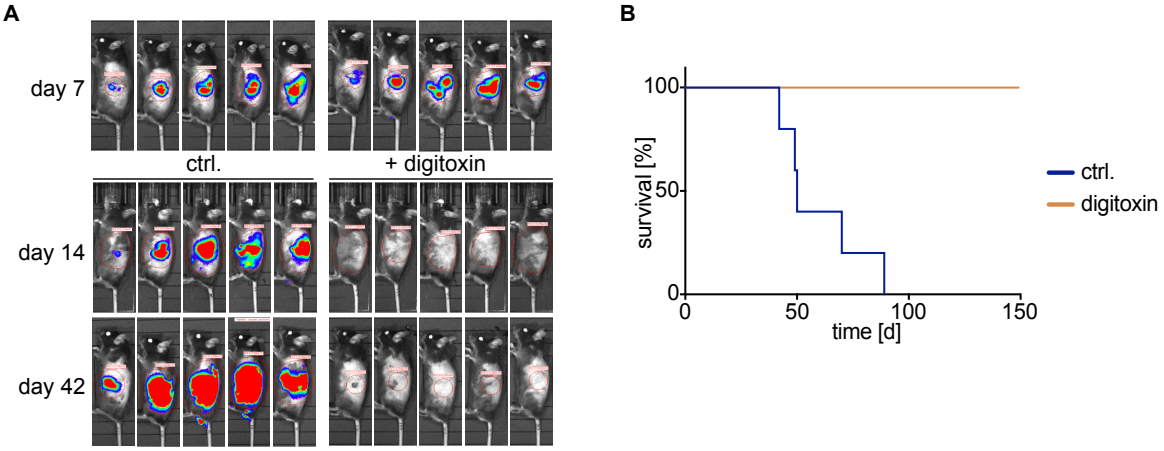

Figure 68: KPC^{hATP1A1} tumors regress upon treatment with digitoxin in C57BL/6J mice. *A: IVIS measurement of day 7, day 14 and day 42 in two cohorts. One cohort was treated with solvent, one cohort was treated with digitoxin (2 mg/kg) (n=5). B: Kaplan-Meier-Plot of mice transplanted with KPC^{hATP1A1}. Were indicated, digitoxin was added. The mouse experiment was conducted by Anneli Gebhardt-Wolf.*

Treatment with 2 mg/kg digitoxin in mice is possible, since murine cells are about 1,000-fold less sensitive than human cells (Dostanic-Larson *et al.*, 2005). Treatment of human cancer cell lines in xenograft mouse modes showed only limited or nearly no benefit (Gan *et al.*, 2020; Svensson *et al.*, 2005). We therefore speculate that the remission of the tumor is dependent on the immune system. Cardiac glycosides have been described to induce *in vivo* immunogenic cell death that causes an immune system dependent regression of tumors in combination with chemotherapeutics (Menger *et al.*, 2012).

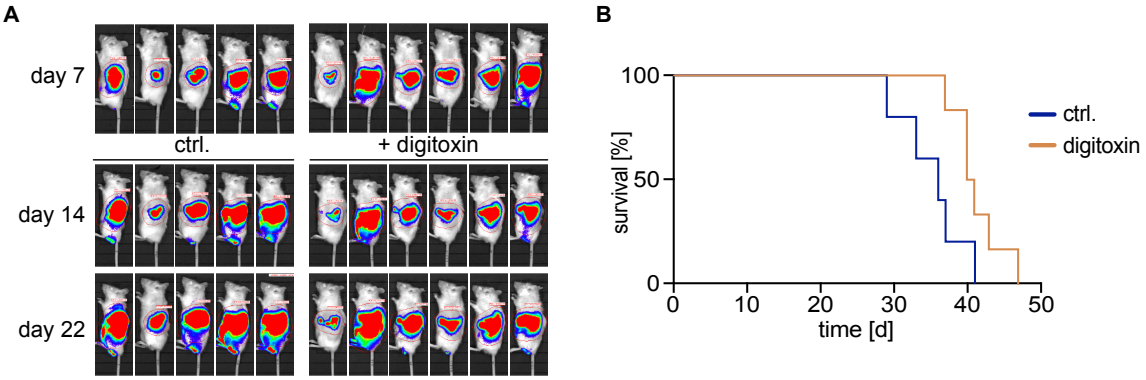

Figure 69: KPC^{hATP1A1} tumors do not regress upon digitoxin treatment in NRG mice. *A: IVIS measurement of day 7 and day 14 in two cohorts. One cohort was treated with solvent, one cohort was treated with digitoxin (2mg/kg) (n=5/6). B: Kaplan-Meier-Plot of NRG mice transplanted with humanized KPC cells. Were indicated, digitoxin was added. The mouse experiment was conducted by Anneli Gebhardt-Wolf.*

We transplanted KPC^{hATP1A1} into the pancreata of immune-compromised NRG mice and used the same treatment regime as in the C57BL/6J mice ***(Figure 69)***. Tumors from KPC^{hATP1A1} cells did not regress upon treatment with digitoxin (2 mg/kg) ***(Figure 69A)*** and despite an increase in overall survival, no mice survived longer than 47 days ***(Figure 69B)***. Tumors kept growing in NRG mice also with treatment of digitoxin ***(Figure 70)***.

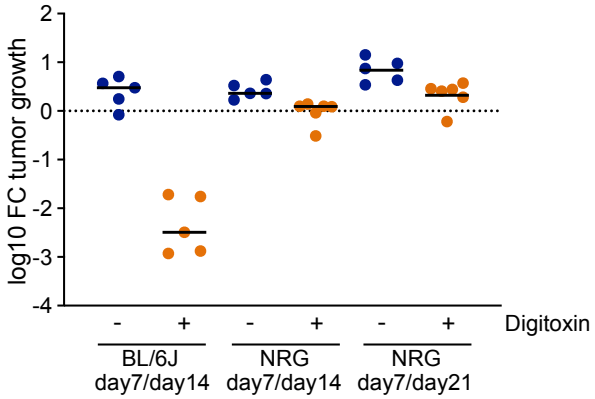

Figure 70: Regression of tumors after treatment with cymarin depends on the immune system. *Tumor growth was measured using IVIS. Tumor growth was calculated compared to day 7. Data is shown as single samples and mean (n=6).*

We compared the regression of KPC tumors in C57BL/6J mice and NRG mice after 7 days of treatment**.** While there was a strong regression of tumors with treatment with digitoxin in immunocompetent mice, tumors from KPC^{hATP1A1} did not regress in NRG mice, but showed only a delayed progression in tumor growth ***(Figure 70)***.

This result from mouse experiments is supported by the observation that patients that receive digitoxin in parallel to anti-cancer treatment display a significant better survival than patients that only received chemotherapeutics (Menger *et al.*, 2012). This implies that indeed there is a therapeutic window to use cardiac glycosides as an anti-cancer therapy in patients.

However, 2 mg/kg digitoxin as a systemic therapy is toxic for human patients (Haux *et al.*, 2001). To utilize cardiac glycosides in human patients we aim in the next step to combine low-dose digitoxin treatment, which would alone not effectively control the tumor, in combination with CAR-T cells, which alone have not shown success in solid tumors (Hou *et al.*, 2021).

2.7 Targeting murine PDAC cells using CAR-T cells

Depletion of MYC causes strong regression of tumors in a syngeneic transplant mouse model. Due to collapse of the shRNA expression over time and rearrangement of the MYC/MAX/MXD network, tumors relapse and mice die within less than 80 days ***(Figure 20)***. To enhance a stronger T cell response directed at the tumor cells, T cells were extracted and engineered with a chimeric antigen receptor targeting an antigen presented on the surface of the tumor cells. For this, a truncated isoform of B7-H3 was cloned into a constitutive lentiviral construct and "KPC shMYC" were infected ***(Figure 71)*** (Birley *et al.*, 2022).

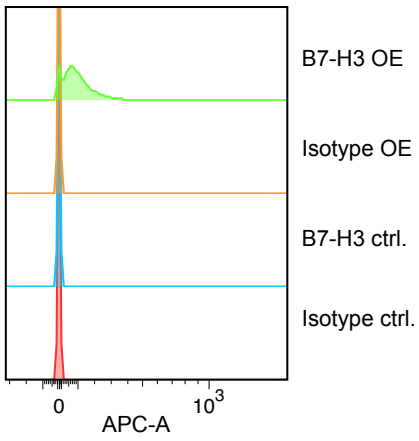

Figure 71: Presentation of B7-H3 at the surface of KPC cells in wildtype KPC and KPC cells with overexpression (OE) of a truncated B7H3.

Co-incubation of untransduced (UT) and CAR-T cells with B7-H3 expressing KPC cells demonstrated that the α-B7-H3-CAR-T cells can efficiently eradicate the tumor cells in culture analyzed by flow cytometry. By staining for B7-H3 (tumor cells) as well as CD3 (T cells) and measuring the APC and FITC signal using flow cytometry we can distinguish between tumor cells and T cells ***(Figure 72)***.

In order to visualize the dynamics and kinetics of CAR-T cells eradicating the tumor cells in culture a time course experiment over 4 days was set up with measurement of the cell confluency every hour. Co-incubation of tumor cells with (CAR-) T cells started at a cell density of about 20%. The fluorescent signal of the tumor cells was used to follow the tumor cells growth and expansion during the co-incubation with (CAR)-T cells.

We observed that CAR-T cells effectively eradicate not only single, scattered cells ***(Figure 72)***, but with higher ratios also cell clusters ***(Figure 73A)***. We compared the elimination of KPC cells with high levels of MYC (NTC) and MYC depletion (shMYC). CAR-T cells controlled the cell layer in all conditions, while un-transduced T cells (UT) did not affect the growth of the cell layer. However, the clearance of tumor cells with depletion of MYC was more efficient and sustainable compared to cells with oncogenic levels of MYC protein, pointing out that either the reduced proliferation of MYC-depleted cells allows CAR-T cells to control the tumor cell layer or the upregulation of a proinflammatory transcription program upon interference with MYC encourages CAR-T cells to effectively attack the tumor cells. Similar results in

culture have been observed with TNBC-organoids where the overexpression of MYC made the organoid resistant for the co-culture with immune cells (Zimmerli *et al.*, 2022).

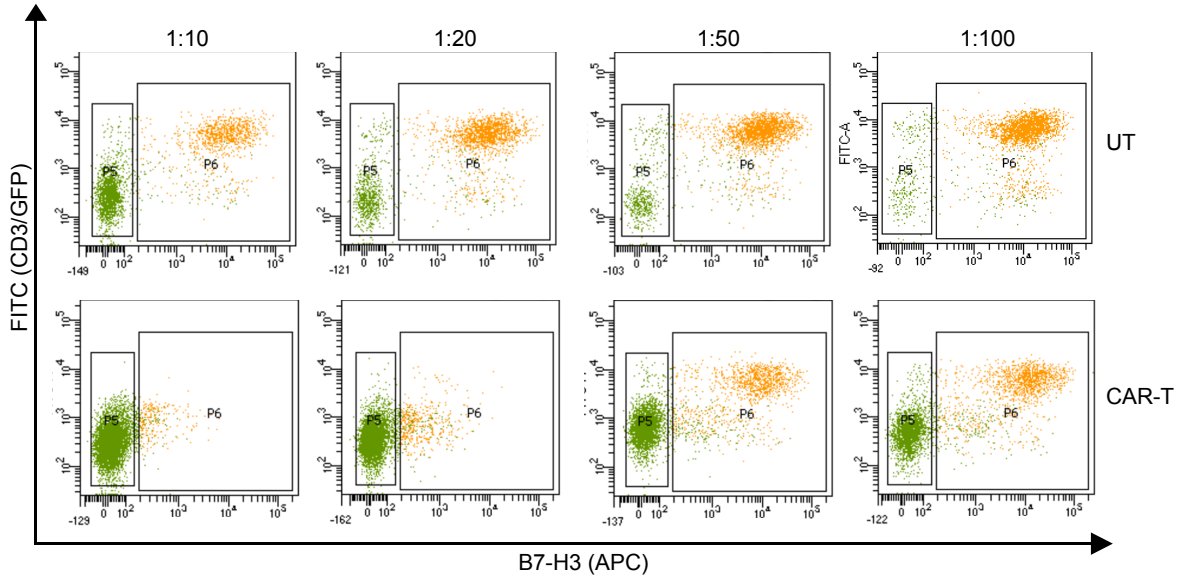

Figure 72: CAR-T cells eradicate KPC cells. *Flow cytometry analysis of co-culture of B7-H3-KPC with T cells (UT) or α-B7-H3-CAR-T cells. T cells were stained with a-CD3 (FITC), KPC cells were stained with α-B7-H3-APC. Ratio indicates T cell/tumor cell ratio.*

We have previously shown that deletion of TBK1 dampens the activation of a proinflammatory program in MYC-depleted cells. We therefore tested whether the depletion of MYC in cells lacking TBK1 (shMYC, ΔTBK1) affects the clearance of tumor cells. We did not observe significant differences in the clearance of tumor cells by CAR-T cells with deletion of TBK1 and wildtype TBK1 at the endpoint of the experiment ***(Figure 73B)***.

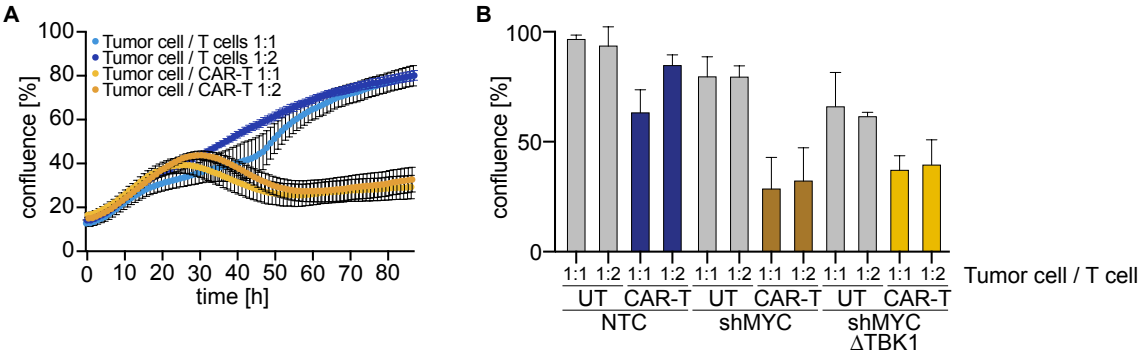

Figure 73: CAR-T cells targeting murine PDAC cells after depletion of MYC. *A: Confluence of tumor cells with depletion of MYC, co-incubated with T cells or CAR-T cells was measured using the Operetta microscope. Results are presented as mean ±SEM (n=5). B: Confluence of tumor cells after 87 h of coincubation of T cells (grey) or CAR-T cells (colored). Results are presented as mean ±SD (n=5).*

We hypothesize that either the induction of a proinflammatory program upon depletion of MYC or the reduced secretion of lactate support CAR-T cells in eradication of the tumor. Despite the success of CAR-T cells in blood disorders, so far CAR-T cells have only shown very limited efficacy in solid tumors (Hou *et al.*, 2021). α-B7-H3 CAR-T cells have been shown to impact the growth of KPC tumors, but

without achieving full remission (Du *et al.*, 2019). Solid tumors, especially with deregulated MYC proteins, display a highly immune-suppressive microenvironment that prevents infiltration with CAR-T cells (Marofi *et al.*, 2021). Targeting this microenvironment provides promising results for CAR-T cells in solid tumors (Srivastava *et al.*, 2021) and we speculate that depletion of MYC mediates changes in the immune-suppressive microenvironment that allows infiltration of tumors and efficient eradication by the co-treatment of MYC depletion and CAR-T cells.

3 Discussion & Perspective

3.1 Model for MYC driven immune evasion in PDAC

Analyzing the immune evasive role of MYC in a mouse model that reflects pathology and mutations of human patients uncovers a new pathway that explains how MYC establishes an immunosuppressive transcription program ***(Figure 11, 42, 49)***. dsRNA originates from repetitive elements of highly transcribed genes ***(Figure 32, 33)***. This dsRNA is accumulating in the cytoplasm ***(Figure 26)*** and released by the cell in extracellular vesicles (probably shed microvesicles) ***(Figure 46)***. dsRNA is taken up in an autocrine or paracrine manner via endocytosis and loaded onto TLR3 ***(Figure 43)***, causing an activation of TBK1 and NF-κB ***(Figure 49B)*** and downstream activation of a proimmunogenic transcription program ***(Figure 49A, 50)***. More sophisticated analyses are needed to confirm whether MHC class I presentation is not critical for the regression of tumors or whether the lack of antigen presentation activates NK cells (Kärre, 2002).

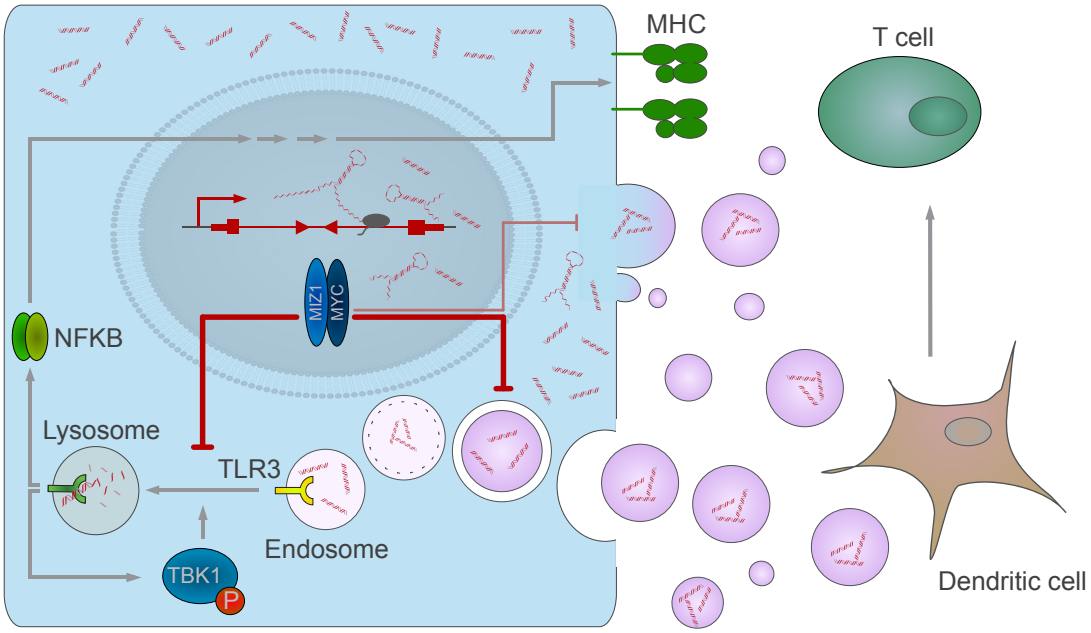

Figure 74: Proposed model for MYC driven immune evasion in pancreatic cancer.

At oncogenic levels MYC binds to MIZ1 in order to suppress this vesicular transport pathway that causes activation of TBK1 and pro-inflammatory NF-κB signaling ***(Figure 41)***, explaining why the deletion of MIZ1 is haplo-insufficient for the development in PDAC in the KPC mouse model (Walz *et al.*, 2014). Additionally, we hypothesize that MYC squelches SPT5 from the core promoter of proimmunogenic genes to establish – independent of the entity – an immunosuppressive program, explaining why the repression of these genes is, independent of the cellular context, closely linked to MYC-driven oncogenic transformation ***(Figure 14)***. These findings are summarized in the proposed model in ***Figure 74***.

3.2 Immune evasion is an imperative for MYC

MYC, MYCN, or MYCL are commonly deregulated in various human cancer entities and mouse modeling showed that interfering with the function of MYC might be a promising therapeutic approach (Sodir *et al.*, 2020; Soucek *et al.*, 2013). For long time MYC was predominantly described as a transforming factor that promotes proliferation and growth of tumor cells via cell-intrinsic mechanisms. However, work in the recent decade sheds light on an important and not negligible function of the MYC family: They are very strong promoters of immune evasion. Mechanistic studies as well as analysis of patients revealed that deregulated level of MYC or MYCN are associated with a poor immune infiltration (Casey *et al.*, 2016; Kortlever *et al.*, 2017; Layer et al., 2017; Sodir *et al.*, 2020).

We propose a model of MYC's oncogenic function in pancreatic cancer that composes of three major aspects: First, our experiments proofed that the major function of MYC *in vivo* is the suppression of the immune response to prevent eradication of tumors. Second, cells can monitor the accumulation of endogenous dsRNA. Similar to the cGAS-STING-pathway, that senses DNA damage in cells, TLR3 sense dsRNA that originate from oncogenic transcription or insufficient splicing. Third, MYC perturbs this pathway at several steps to prevent TLR3 dependent activation of NF-κB signaling and drive immune evasion of tumors.

The accumulation of proimmunogenic DAMPs in the cytoplasm of cancer cells is a new concept that has emerged in the last years, suggesting that this is an Achilles heel of cancer cells (Ahmad *et al.*, 2018; Coquel *et al.*, 2018; Dhir *et al.*, 2018) and consequently cancer cells evolutionary evolved mechanisms to escape clearance by the immune system (Ghosh *et al.*, 2020; Wu *et al.*, 2018). In this study we showed that highly proliferating cells give rise to a significant amount of intron-derived immunogenic dsRNA (and probably also other DAMPs), which explains why the immune suppressive function is a prerequisite for the oncogene MYC. This concerns cancer cells, but probably also transient amplifying cells and proliferating cells. All these cells share the characteristic of high MYC levels and therefore the immune evasion is a categorical imperative for tumor cells and is evolutionary hard-wired into MYC's function.

There is an increasing number of publications showing that DNA damage associated DAMPs signaling (Coquel *et al.*, 2018; Emam *et al.*, 2022), as well as RNA-based DAMPs (Ghosh *et al.*, 2020; Wu *et al.*, 2018) are inducing innate immunogenic programs in the cell and one can utilize these findings for newly emerging therapeutic concepts. We postulated that immunogenic dsRNA is resulting from delayed, co-transcriptional splicing. Even though we could not confirm an induction of the innate immune system, probably due to the toxicity of the spliceosome inhibitor pladienolide B (PlaB), preliminary experiments showed that there is a strong accumulation of B2-element derived dsRNA after treatment with PlaB (data not shown). Inhibition of splicing increases the amount of dsRNA in MYC-deregulated breast

cancer cells and induces an anti-tumor immune response (Bowling *et al.*, 2021). Using the less toxic H3B-8800 that was used by Bowling and colleagues would be probably more promising.
It was shown in our lab that NUAK1 promotes spliceosome activity and its inhibition is synthetic lethal with oncogenic levels of MYC. This also represents a potential small molecule-based therapeutic option in cancer. Due to its effect on splicing, NUAK1 inhibition could also induce immunogenic dsRNA (Cossa *et al.*, 2020; Liu *et al.*, 2012). Moreover, depletion of the exosome in MYCN-driven neuroblastoma or combined inhibition of ATR and AURORA-A have been shown to induce transcription-replication conflicts that are potential sources of R-loops or DNA-associated immunogenic nucleic acids (Papadopoulos *et al.*, 2022; Roeschert *et al.*, 2021). All these concepts point out the same or similar vulnerability: Interfering with transcription and coordination of transcription and replication by targeting MYC functions can induce accumulation of DAMPs that promote a proimmunogenic transcriptional program.

Furthermore, upon stress MYC multimerizes and relocates from its cognate binding sites. This shell-like multimers haven been shown to contain various proteins. Proximity-labeling mass spectrometry (APEX-MS) revealed that YTHDF2 is amongst the best enriched proteins upon induction of the multimers (Solvie *et al.*, 2022). YTHDF2 acts as a reader for m^6A-modification (Shi *et al.*, 2019) and it was described to suppress proinflammatory pathways in stem cells (Mapperley *et al.*, 2020). In eukaryotic cells RIG-I utilize specific modifications of RNAs to distinguish between self- and foreign RNA. m^6A-writers mark circular RNAs as “self”, while foreign circular RNA is bound by RIG-I and subsequently activates anti-viral gene expression (Chen *et al.*, 2019).
Whether depletion of MYC or interfering with the formation of MYC multimers alters the modification of endogenous RNA and thereby increases the immunogenicity of RNA remains to be tested. This would provide a further explanation of how MYC promotes immune evasion and how this is related to the newly discovered feature of MYC to form shell-like structures around stalled replication forks or stalling polymerase as a consequence of interfering with co-transcriptional splicing (Solvie *et al.*, 2022).

3.3 Immune evasion - the major oncogenic function of MYC *in vivo*

MYC is well described as growth-promoting factor in culture and *in vivo* (Dang, 2012). However, our data point out that there is probably a discrepancy between the growth promoting effects *in vivo* and in culture. While MYC is a potent driver of proliferation in culture, the effects in an immune-compromised mouse are much less pronounced ***(Figure 8C, 19A)***. We showed that in culture depletion of MYC causes a reversible arrest in proliferation, while *in vivo* the growth of the tumor is only slightly affected in immune-compromised mice. In immune-competent transplant model we even observe a regression of the tumors. We therefore assume that proliferation effects of MYC play a subordinate role *in vivo*, since depletion of MYC only affected the tumor growth substantially in an immune-competent mouse model. Even though we uncovered further missing pieces in the picture of MYC-driven immune evasion, many questions remain open and further questions are rising, that need to be addressed ***(Figure 75)***:

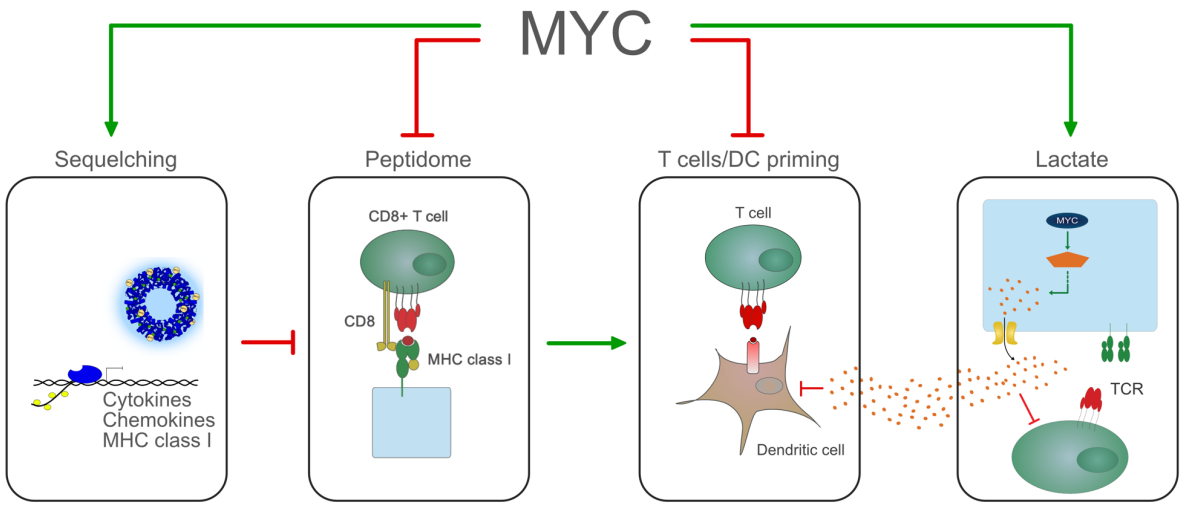

Figure 75: Hypotheses how MYC modulates the tumor microenvironment.

Oncogenic level of MYC repress the expression of proinflammatory T cell cytokines and chemokines or MHC class I genes and thereby effectively prevent the recognition and elimination by the immune system. Many publications that connect MYC biology and immune evasion still describe MYC as a gene-specific regulator that activates and represses distinct genes like MHC class I, PD-L1 or IL23 (Casey *et al.*, 2016; Kortlever *et al.*, 2017; Muthalagu *et al.*, 2020; Versteeg *et al.*, 1988). Considering the recent advances in the MYC field that shift the biology towards a globally binding stress-resilience model, we need to adapt the understanding of its immune evasive property in this context. While expression of specific cytokines or checkpoints is probably dependent on the entity, the mutational burden and the origin of the tumor, it is consensus that MYC suppresses a broad proinflammatory and proimmunogenic program (Muthalagu *et al.*, 2020; Topper *et al.*, 2017; Zimmerli *et al.*, 2022). The results of the KPC$^{B2m-/-}$-transplant *in vivo* make it questionable whether neoantigen presentation and CD8-positive CTLs are crucial for regression. However, the observation, that deletion of TBK1 promotes tumor growth, prevents regression in MYC-depleted tumors and impedes transcription of proimmunogenic NF-κB target genes support the hypothesis that the broad repression of proimmunogenic genes is crucial.

We suggest that this transcriptional program plays a critical role in the activation of T cells and/or the increased visibility of tumor cells for T cells ***(Figure 18B)***. The fact that MYC represses the transcription of MHC class I genes is probably the oldest described immune evasive function of MYC (Bernards *et al.*, 1986; Versteeg *et al.*, 1988). However, the deletion of B2M and consequently the loss of antigen presentation did not impede tumor regression ***(Figure 55)***. Either immune mediated regression after MYC depletion is independent on antigen presentation, CD8-positive T cells and neoantigen load and is mediated by CD4-positive T cells (Nwabugwu *et al.*, 2013; Rakhra *et al.*, 2010), or the knockout of B2M promotes the recognition of the tumor by NK cells (Kärre, 2002). The fact that the increase in MHC class I presentation can induce influx of T cells to control the tumor burden in the same KPC transplant model strengthens the hypothesis that tumor regression upon MYC depletion is independent of MHC class I presentation and CD8-positive T cells (Yamamoto *et al.*, 2020). Nevertheless, more sophisticated analyses of the $KPC^{B2m-/-}$-tumors are needed to draw the right conclusions.

Based on Cibersort analyses ***(Figure 17)*** we observe an influx of dendritic cells after depletion of MYC, implying that cross-presentation and cross-activation of T and B cells by DCs is perturbed by the oncogenic function of MYC. This is supported by the observation that β-catenin stabilization, one of the major activators of MYC transcription, dampens anti-tumor immunity. This can be reversed by the intra-tumoral injection of dendritic cells, indicating that in this model the effect on dendritic cells and not on T cells is dominant (Spranger *et al.*, 2015; Spranger *et al.*, 2017).

We speculate that deregulated levels of MYC prevent the cross-presentation of neoantigens and development of a tumor-reactive TCR-repertoire. The development of the TCRs is a process tightly controlled to ensure the development of an adaptive immune system and to prevent auto-immune response. Neoantigens are cross-presented by dendritic cells to develop the adaptive immune system (Klein *et al.*, 2014). In many cases the repertoire of intra-tumoral TCRs that can recognize neoantigens on tumors is very low (Scheper *et al.*, 2019). It has been shown that the lack of conventional dendritic cells in pancreatic cancer can prevent the formation of cytotoxic T cells and that restoring the function of antigen presenting cells in these tumors reconstitutes the anti-tumor immunity (Hegde *et al.*, 2020). The importance of the cross-presentation is underlined by the finding that knockout of CD103+ DCs impedes tumor control by T cells (Spranger *et al.*, 2017).

The question whether MYC influences the cross-presentation and the development of a tumor-reactive TCR-repertoire in T cells can be addressed with two experiments. First, one can analyze the peptidome that is presented via MHC class I in KPC cells. This would provide information about neoantigens and whether the presentation of neoantigens differs in MYC-deregulated tumor cells and MYC-depleted tumor cells (Purcell *et al.*, 2019). Second, combined with single-cell T cell-receptor sequencing this would provide the information whether depletion of MYC notably changes the immunopeptidome or whether the depletion causes predominantly changes in cross-presentation and priming of T cells (Pauken *et al.*, 2022).

Finally, MYC promotes the Warburg effect and as a consequence, the secretion of lactate to establish an immune-suppressive microenvironment (Dang *et al.*, 2009; Sancho *et al.*, 2015). Cardiac glycosides inhibit oncogenic metabolism, target MYC proteins, block the secretion of lactate and induce immune-dependent regression of tumors. Lactate is well described to be a potent antagonist of cytotoxic T cell activation (de la Cruz-López *et al.*, 2019; Multhoff and Vaupel, 2021; Quinn *et al.*, 2020). It remains to be investigated what the crucial effect of treatment with cardiac glycosides is and whether the treatment with digitoxin prevents exhaustion or downregulation of cytotoxic T cell activity in the tumor microenvironment. Potentially, lactate could not only prime the tumor draining lymph nodes for formation of metastasis, but it could also interfere with the cross-presentation and selection process of DCs and T cells in the lymph node, explaining, why many tumors lack T cells with a tumor-reactive TCR (Riedel *et al.*, 2022; Scheper *et al.*, 2019).

Generally, we can address these questions in two different manners: First, global analysis like spatial transcriptomics, single-cell sequencing or complex flow cytometry analysis of the tumor including its microenvironment would potentially help in seeing and understanding the changes of immune cells and stroma cells after interfering with MYC in an unbiased approach. We would gain information about polarization of macrophages, anergy, and exhaustion of T cells as well as infiltration with regulatory T cells that we lack so far (Lin *et al.*, 2020; Srivastava *et al.*, 2021). Second, we also set up several cellular systems for the orthotope transplant model to address these questions step by step: In $KPC^{hATP1A1}$ cells we can efficiently block the secretion of lactate with cardiac glycoside. The knockout of *B2m* in tumor cells can provide further information about the interaction of immune cells and tumor cells. Blocking NK cells using α-GM1 antibody in our transplant model would give information about the role of NK cells in WT tumors and $KPC^{B2m-/-}$ tumors. Transplanting cells into $CD4^{-/-}$ mice, which do not have T helper cells, would provide information whether this species is critical for regression, probably by activating NK cells and B cells. KPC transplants in $BATF3^{-/-}$ mice that lack dendritic cells, would provide insights into the role of MYC in preventing cross-presentation of tumor-specific antigens (Spranger *et al.*, 2017).
Global analyses like spatial transcriptomics would provide correlative information about MYC-dependent changes in the TME. However, they will not compensate for functional assays that proof causality. Setting up experimental systems with an educated guess to increase the understanding is therefore a worthwhile undertaking.

3.4 Outlook: Understanding and translating

This study underlined and confirmed the finding that one of the most critical oncogenic functions of MYC proteins *in vivo* is to mediate immune evasion in tumors (Casey *et al.*, 2017). This function presumably evolutionary evolved to protect transient amplifying cells from immunogenic activation by DAMPs. However, the key questions of how immune evasion is finally mediated by MYC in tumors, remains open. We speculate that MHC class I repression, impeding of TLR3 loading in cooperation with MIZ1, sequestration of SPT5 and other elongation factors from the promoter of proimmunogenic genes or the secretion of lactate play a role.

We showed that we can target pancreatic cancer cells using cardiac glycosides that induce immune-dependent remission in a highly aggressive transplant model. Cardiac glycosides are well studied drugs with known pharmaco-kinetic that have been used to treat patients with heart failure. Additionally, they have been shown in pre-clinical studies to exert anti-proliferative effects on transformed cells in culture and tumors *in vivo* (Du *et al.*, 2021; Gan *et al.*, 2020; Menger *et al.*, 2012; Shen *et al.*, 2020). There are a number of observations that indicate that there is indeed a therapeutic window to utilize cardiac glycosides as an inhibitor for oncogenic metabolism: First, the expression of ATP1A1, the major subunit of the sodium-potassium pump, is increased in human cancer and predicts for a poor prognosis in pancreatic cancer (Uhlén *et al.*, 2015). Cancer cells are likely to upregulate the sodium-potassium pump to cope with the increased need of tumor cells for metabolites, especially the uptake of amino acids like glutamine (Li *et al.*, 2019b). Menger and colleagues showed in a retrospective analysis of a matched patient cohort that breast cancer patients receiving cardiac glycoside display a significantly better overall survival compared to the control group (Menger *et al.*, 2012).
However, the concentration of 2 mg/kg digitoxion, which was used in this study, is not feasible in human patients. Preliminary experiments showed that reduced dosage of digitoxin only causes limited regression of tumors in immunocompetent mice. The therapeutic window of cardiac glycosides is small and concentration of digitoxin in the serum patients is about 50 to 100-fold lower (Oliver *et al.*, 1968). We therefore aim to combine treatment with lower doses of digitoxin with α-B7-H3-CAR-T cells, which can alone efficiently eradicate tumor cells in culture but show only limited effects in immunocompetent mice (Du *et al.*, 2019). However, our experimental model profits from the fact that only the tumor cells, but not the host cells, are sensitive for the treatment with cardiac glycosides (Dostanic-Larson *et al.*, 2005). To investigate whether there is a therapeutic window that allows treatment of patients with cardiac glycosides we need to test our hypothesis in model systems where host and tumor are both affected by the systemic treatment. It is therefore of interest to establish a GEMM with a humanized ATP1A1, similar to our humanized KPC cells, that allows to monitor the consequences of treatment with cardiac glycosides on the host and especially its immune system. Finally, in a CG-sensitive host we can use the murine allele of ATP1A1 to make (CAR-)T cells resistant against the treatment to ensure that immune cells can efficiently eradicate the tumor without dampening the activity of the immune system.

The immune evasive properties of MYC proteins seem to be the logical consequence of its oncogenic potential. MYC has a strong transforming potential and is crucial for the development and maintenance of tumors. Initially MYC was described as a transcription factor that regulates a specific set of genes to promote oncogenesis. This view shifted when MYC was described as a general and global amplifier of transcription. Work in the recent years again drifts the view on MYC biology from being a pure transcription factor to a protein that controls and promotes many key processes to deal with challenges during oncogenic transformation and tumor maintenance. MYC promotes pause release and elongation (Baluapuri *et al.*, 2019; Herold *et al.*, 2019; Rahl *et al.*, 2010), it coordinates transcription and replication (Büchel *et al.*, 2017; Papadopoulos *et al.*, 2022; Roeschert *et al.*, 2021), it protects stalled replication forks (Solvie *et al.*, 2022), prevents DNA damage and promotes repair at promoters (Das *et al.*, 2022; Endres *et al.*, 2021). All mentioned mechanisms point to the transcription-stress-resilience model ***(section 1.1.4, Figure 1)***. Since MYC orchestrates many hallmarks of tumorigenesis the model is still not reflecting the versatile effects MYC has on various pathways in cells (Gabay *et al.*, 2014). MYC also promotes the Warburg effect and supports tumorigenic growth with a fast supply with energy and secretion of immune-suppressive lactate (Shim *et al.*, 1997). Strikingly, our work shows that the major oncogenic function *in vivo* is the repression of transcription of proimmunogenic transcription to promote immune evasion.

There is the consensus in the MYC-field that oncogenic levels of MYC promote an anti-immunogenic transcriptional program to bypass immune surveillance (Kortlever *et al.*, 2017; Lee *et al.*, 2022b; Muthalagu *et al.*, 2020; Zimmerli *et al.*, 2022). Apart from this, the field is divided whether MYC is a specific regulator of some important genes (Casey *et al.*, 2016; Kortlever *et al.*, 2017), whether MYC and MIZ1 are binding cooperatively to repress transcription of proimmunogenic genes (Muthalagu *et al.*, 2020; Zimmerli *et al.*, 2022), or whether MYC is repressing a broad proimmunogenic gene signature (Krenz *et al.*, 2021; Topper *et al.*, 2017). In order to target the strong immune suppressive capacity of MYC, it is of key interest to precisely understand how MYC mechanistically mediates the suppression of the immune system. First of all, ChIP-Rx data show that MYC is a protein that binds to close to all active promoters of genes with only mild changes in expression. Therefore, claiming that binding and regulation of a single gene are the driving force of the major oncogenic function of MYC is at minimum unlikely. Second, we could show that the interaction of MYC and MIZ1 is important for the suppression of the innate immune signaling in our mouse model by dampening the vesicular transport pathway. So far there is no evidence that MYC and MIZ1 interact at non-oncogenic, physiological levels of MYC, pointing out that this is probably a gain-of-function of oncogenic levels of MYC (Wiese *et al.*, 2013). Despite different models in the field (Muthalagu *et al.*, 2020; Zimmerli *et al.*, 2022), we can agree on the important role of MIZ1 and MYC. It is therefore of great interest to develop either small molecules that disturb the interaction between MYC and MIZ1, or PROTACS that target MIZ1 or the MYC/MIZ1-complex.

Nonetheless, the observation that MYC suppresses specific proimmunogenic genes by binding to their core promoter contradicts the paradigm shift in the MYC field in the recent years. The global binding capacity of MYC to the core promoter of all genes transcribed by RNAPII does not match with the model of specific gene regulation. As argued above, we have several indications that the absence of MYC at the core promoter is causing a sequestration or squelching of elongation factors like SPT5 to prevent processive elongation ***(Figure 2, 14)***. Strikingly, this fits a work in neuroblastoma were MYCN-suppressed genes specifically display a defective elongation, but similarly pause release compared to MYCN activated genes (Herold *et al.*, 2019). Reducing the sequestration of SPT5 by interfering with the multimerization of MYC using HUWE1 inhibitors provides a potential therapy with a small molecule to target this oncogenic function of MYC.

4 Material

4.1 Plasmids and Oligonucleotides

4.1.1 Vectors

Vector	*Source*	*Addgene*	*Clone Collection*
pLXSN IkB alpha M	(Van Antwerp *et al.*, 1996)	Addgene 12330	#2902
pRRL-Hygromycin-IkBam	(Krenz *et al.*, 2021)		#2901
psPAX2	Trono Laboratory	Addgene 12260	#2332
pMD2.G	Trono Laboratory	Addgene 12259	#2333
pInducer21-human MYC			#2594
pInducer21-MYCV394D(human)			#2364
pInducer20-human MYC	Anneli Gebhardt-Wolf		#3213
pInducer20-MYCV394D(human)	Anneli Gebhardt-Wolf		#3214
LT3 GEPIR NTC			#2594
pInducer11 NTC			#2886
pInducer11 shMYC-2 mouse	(Krenz *et al.*, 2021)		#2907
LT3 GEPIR shMYC-3 mouse	(Krenz *et al.*, 2021)		#2905
lentiCRISPR V2	Zhang Laboratory	Addgene 52961	#2686
pLKO-sgRNA-EFS-GFP		Addgene 57822	#2900
lentiCRISPR V2 Puro sgTBK1 #1 mouse	(Krenz *et al.*, 2021)		#3182
lentiCRISPR V2 Puro sgIRF3 #1 mouse	(Krenz *et al.*, 2021)		#3225
lentiCRIPSR V2 Puro sgTLR3 #1 mouse	(Krenz *et al.*, 2021)		#3183
lentiCRIPSR V2 Puro sgTLR3 #2 mouse	(Krenz *et al.*, 2021)		#3184
lentiCRISPR V2 Puro sgMYC #1 (46) intron 1 mouse	(Krenz *et al.*, 2021)		#3215
pLKO-sgRNA-EFS-GFP sgMYC #2 (1002) intron 2 mouse	(Krenz *et al.*, 2021)		#3216
lentiCRISPR V2 Puro sgMYC #2 human	(Krenz *et al.*, 2021)		#3217
lentiCRISPR V2 Blasti	Wolf Laboratory		#3039
lentiCRISPR V2 Blasti sgB2M #1 murine			#3223
eGFP/fluc-FUGW	(Thalheimer *et al.*, 2013)		#2800
pLV[Exp]-Bsd-SV40-murineATP1A1	Wiegering Laboratory		#3218
pLV[Exp]-Bsd-SV40-humanATP1A1	Wiegering Laboratory		#3219
lentiCRISPR V2 Puro sgATP1A1 #2 murine			#3220
LT3 GEPIR shATP1A1 #1 human			#3221
LT3 GEPIR shATP1A1 #3 human			#3222
pInducer 21 Myc WT-HA	(Dejure *et al.*, 2017)		#2594

pInducer 21 5´UTR-Myc-HA	(Dejure *et al.*, 2017)	#2292
pInducer 21 Myc-HA-3´UTR	(Dejure *et al.*, 2017)	#2293
pInducer21 5´ UTR-MYC-HA-3´UTR	(Dejure *et al.*, 2017)	#2838
pInducer 21 MYC-HA-3´UTR (Delta 2262-2366)_Deletion4	(Dejure *et al.*, 2017)	#2841
pInducer 21 MYC-HA-3´UTR (Delta 2127-2366)_Deletion3	(Dejure *et al.*, 2017)	#2842
pInducer 21 MYC-HA-3´UTR (Delta 2025-2366)_Deletion2	(Dejure *et al.*, 2017)	#2843
pInducer 21 MYC-HA-3´UTR (Delta 1997-2366)_Deletion1	(Dejure *et al.*, 2017)	#2844
pRRLSin.cPPT.SFFV-IRES-Hygro.WPRE		#2338
pRRL-Hygro-B7H3trunc		#3205
Anti-B7-H3 CAR-T retroviral construct	(Birley *et al.*, 2022)	#3206

4.1.2 Oligonucleotides

Primer TLR3 knockout #1 fwd: CACCGGTACTGCTCATTCACATCGA	(Labun *et al.*, 2019)
Primer TLR3 knockout #1 rev: AAACTCGATGTGAATGAGCAGTACC	(Labun *et al.*, 2019)
Primer TBK1 knockout #1 fwd: CACCGCGGGAACAACTCAATACCGT	(Labun *et al.*, 2019)
Primer TBK1 knockout #1 rev: AAACACGGTATTGAGTTGTTCCCGC	(Labun *et al.*, 2019)
Primer MYC knockout (135) #1 fwd: CACCGGCTGGGGTAGATCTGAGTCG	(Labun *et al.*, 2019)
Primer MYC knockout (135) #1 rev: CCGACCCCATCTAGACTCAGCCAAA	(Labun *et al.*, 2019)
Primer MYC knockout (1008) #2 fwd: CACCGTATAGCGTCCGGGATTCAGG	(Labun *et al.*, 2019)
Primer MYC knockout (1008) #2 rev: CATATCGCAGGCCCTAAGTCCCAAA	(Labun *et al.*, 2019)
Primer IRF3 knockout #3 fwd: CACCGCGGCTCCGTCCTTGTCCTTG	(Labun *et al.*, 2019)
Primer IRF3 knockout #3 rev: AAACCAAGGACAAGGACGGAGCCGC	(Labun *et al.*, 2019)
Primer murine ATP1A1 knockout #2 fwd: CACCGGTACACGACGATGCCACGTG	(Labun *et al.*, 2019)
Primer murine ATP1A1 knockout #2 rev: AAACCACGTGGCATCGTCGTGTACC	(Labun *et al.*, 2019)
Primer murine B2M knockout #1 fwd: CACCGAGTATACTCACGCCACCCAC	(Labun *et al.*, 2019)
Primer murine B2M knockout #1 rev: AAACGTGGGTGGCGTGAGTATACTC	(Labun *et al.*, 2019)
RQ-PCR Vcl fwd: AGGAGACTTGCGAAGACAGG	
RQ-PCR Vcl fwd: GCCGTCGCCACTTGTTTA	
RQ-PCR H2-K1 fwd: GGAAAAGGAGGGGACTATGC	
RQ-PCR H2-K1 rev: GAGGGTCATGAACCATCACTTTA	
RQ-PCR H2-D1 fwd: GGAAAAGGAGGGGACTATGC	
RQ-PCR H2-D1 rev: GCAGCTGTCTTCACGCTTTA	
RQ-PCR B2_Mm2 fwd: GGGGCTGGAGAGATGGCT	(Hubley *et al.*, 2015; Untergasser et al., 2012)
RQ-PCR B2_Mm2 rev: TGAGTACACTGTAGCTGTCTTCA	(Hubley *et al.*, 2015; Untergasser *et al.*, 2012)
RQ-PCR B2_Mm1t fwd: ATGGCTCAGCGGGTAAGAG	(Hubley *et al.*, 2015; Untergasser *et al.*, 2012)
RQ-PCR B2_Mm1t rev: GAGGGCGTCAGATCTCGTTA	(Hubley *et al.*, 2015; Untergasser *et al.*, 2012)
RQ-PCR B2_Mm1a fwd: AGATGGCTCAGTGGGTAAGAG	(Hubley *et al.*, 2015; Untergasser *et al.*, 2012)
RQ-PCR B2_Mm1a rev: TCAGATCTCGTTACGGATGGT	(Hubley *et al.*, 2015; Untergasser *et al.*, 2012)

RQ-PCR B2_Mm1 fwd: TCCAGAAGAGGGAGTCAGATC	(Hubley *et al.*, 2015; Untergasser *et al.*, 2012)
RQ-PCR B2_Mm1 rev: GGTTAGAGCACCCGACTG	(Hubley *et al.*, 2015; Untergasser *et al.*, 2012)
RQ-PCR Mito2 fwd: TTCTCCGTGCTACCTAAACAC	(Hubley *et al.*, 2015; Untergasser *et al.*, 2012)
RQ-PCR Mito2 rev: AGTACGGGAAGGATTTAAACCA	(Hubley *et al.*, 2015; Untergasser *et al.*, 2012)
RQ-PCR Mito3 fwd: ACAACCCATCCCTCACTCTAC	(Hubley *et al.*, 2015; Untergasser *et al.*, 2012)
RQ-PCR Mito3 rev: GGTAAGAATCCTGTTAGTGGTGG	(Hubley *et al.*, 2015; Untergasser *et al.*, 2012)
RQ-PCR Mito4 fwd: ACCGAGTCGTTCTGCCAATA	(Hubley *et al.*, 2015; Untergasser *et al.*, 2012)
RQ-PCR Mito4 rev: CCCTGGTCGGTTTGATGTTAC	(Hubley *et al.*, 2015; Untergasser *et al.*, 2012)
RQ-PCR AluSx1 fwd: CACTTTGGGAGGCCGAGG	(Hubley *et al.*, 2015; Untergasser *et al.*, 2012)
RQ-PCR AluSx1 rev: GTTCAAGCGATTCTCCTGCC	(Hubley *et al.*, 2015; Untergasser *et al.*, 2012)
RQ-PCR AluSz fwd: CGGATCACTTGAGGTCAGGA	(Hubley *et al.*, 2015; Untergasser *et al.*, 2012)
RQ-PCR AluSz rev: GGTTCAAGCGATTCTCCTGC	(Hubley *et al.*, 2015; Untergasser *et al.*, 2012)
RQ-PCR AluSx fwd: CACTTTGGGAGGCCGAGG	(Hubley *et al.*, 2015; Untergasser *et al.*, 2012)
RQ-PCR AluSx rev: GTTCAAGCGATTCTCCTGCC	(Hubley *et al.*, 2015; Untergasser *et al.*, 2012)
RQ-PCR AluSq2 fwd: TGAGGTCAGGAGTTCGAGAC	(Hubley *et al.*, 2015; Untergasser *et al.*, 2012)
RQ-PCR AluSq2 rev: GTTTCGCTCTTGTCGCCC	(Hubley *et al.*, 2015; Untergasser *et al.*, 2012)
RQ-PCR AluY fwd: GCCTGTAATCCCAGCACTTT	(Hubley *et al.*, 2015; Untergasser *et al.*, 2012)
RQ-PCR AluY rev: GTTCACGCCATTCTCCTGC	(Hubley *et al.*, 2015; Untergasser *et al.*, 2012)
shMYC murine mirE2 TGCTGTTGACAGTGAGCGCAACGTTTATAACAGTTAC AAATAGTGAAGCCACAGATGTATTTGTAACTGTTATAA ACGTTTTGCCTACTGCCTCGGA	(Fellmann *et al.*, 2013)
shMYC murine mirE3 TGCTGTTGACAGTGAGCGAACGAGAACAGTTGAAACA CAATAGTGAAGCCACAGATGTATTGTGTTTCAACTGTT CTCGTCTGCCTACTGCCTCGGA	(Fellmann *et al.*, 2013)
shNTC mirE3 AAGGTATATTGCTGTTGACAGTGAGCGATCTCGCTTG GGCGAGAGTAAGTAGGAAGCCACGATGTACTTACTCT CGCCCAAGCGAGAGTGCCTACTGCCTCGG	
shATP1A1 human mirE3 #1 TGCTGTTGACAGTGAGCGCCCCGGAAAGACTGAAAG AATATAGTGAAGCCACAGATGTATATTCTTTCAGTCTT TCCGGGTTGCCTACTGCCTCGGA	(Fellmann *et al.*, 2013)
shATP1A1 human mirE3 #3 TGCTGTTGACAGTGAGCGCCCAGTTGTCTATTCATAA GAATAGTGAAGCCACAGATGTATTCTTATGAATAGAC AACTGGTTGCCTACTGCCTCGGA	(Fellmann *et al.*, 2013)

mirE_fwd TACAATACTCGAGAAGGTATATTGCTGTTGACAGTGA GCG	
mir3_rev TTAGATGAATTCTAGCCCCTTGAAGTCCGAGGCAGTA GGCA	

4.2 Cell lines, mouse strains and bacteria

4.2.1 Cell lines

Cell line	*Origin*	*Source*	*RRID*
KPC cells (#674)	murine	Sieveke Laboratory	N/A
PKPA 129852 (KPC#10) Pdx1-Cre; KRasG12D/wt; Trp53-/-; Atg5wt/wt; Atg7-/-	murine	Rosenfeldt Laboratory	N/A
PKPA 129852 (KPC#9) Pdx1-Cre; KRasG12D/wt; Trp53-/-; Atg5wt/wt; Atg7-/-, Atg7 re-expressed	murine	Rosenfeldt Laboratory	N/A
DLD1	human	ATCC	RRID: CVCL_0248
LS174T	human	ATCC	RRID: CVCL_1384
Colo26/CT26	murine	ATCC	RRID: CVCL_7256
U2OS	human	ATCC	RRID: CVCL_0042
HEK293TN	human	ATCC	RRID: CVCL_UL49
Phoenix Eco	human	Anderson Laboratory	
PANC1	human	Rosenfeldt Laboratory	RRID: CVCL_0480
MZ1	human	Rosenfeldt Laboratory	RRID: CVCL_1434
Dan-G	human	Rosenfeldt Laboratory	RRID: CVCL_0243
PaTu 8988T	human	Rosenfeldt Laboratory	RRID: CVCL_1847
ASPC1	human	Rosenfeldt Laboratory	RRID: CVCL_0152
IMIM PC1	human	Rosenfeldt Laboratory	RRID: CVCL_4061
PANC 0813	human	Rosenfeldt Laboratory	RRID: CVCL_1638
U2OS W11	human		N/A

Cell lines were routinely tested for mycoplasm. For cultivation of cell lines RPMI-1640 (Thermo Fisher Scientific) or DMEM (Thermo Fisher Scientific) containing 10% FCS and 1% Pen/Strep was used.

4.2.2 Mouse Strains

Strain		*Source*
C57BL/6J (BL/6J)		Charles river
NOD-Rag1^{null} IL2rg^{null}, NOD rag gamma (NRG)	(Pearson *et al.*, 2008)	JAX#007799
BALB/cAnNRj-Foxn1 nu/nu mice (nude)		Janvier LABS
B6.129S7-Rag1tm1Mom/J (Rag1-/-)		JAX#002216

4.2.3 Bacteria

Strain	*Genotyp*
E. coli Stbl3	F^-mcrB mrrhsdS20(r_B^-, m_B^-) recA13 supE44 ara-14 galK2 lacY1 proA2 rpsL20(Str^R) xyl-5 λ^-leumtl-1
E. coli XL1 Blue	recA1 endA1 gyrA96 thi-1 hsdR17 supE44 relA1 lac [F proAB laclqZΔM15 Tn10 (Tetr)]

4.3 Antibodies

Target	*Company*	*RRID*
Rabbit monoclonal anti-MYC (clone Y69)	Abcam	Cat# ab32072 RRID: AB_731658
Rabbit monoclonal anti-TBK1/NAK (D1B4)	Cell signaling	Cat#3504 RRID: AB_2255663
Rabbit monoclonal anti-phospho-TBK1/NAK (Ser172) (D52C2)	Cell signaling	Cat#5483 RRID: AB_10693472
IKBA (L35A5)	Cell signaling	Cat#4814 RRID: AB_390781
P-IKBA (Ser32) (14D4)	Cell signaling	Cat#2859 RRID: AB_561111
TLR3	Abcam	Cat#ab62566 RRID: AB_956368
MDA5	Abcam	Cat#ab79055 RRID: AB_1640683
RIG-I	Abcam	Cat#ab45428 RRID: AB_731876
H3K9me3	Activ Motif	Cat#39062 RRID: AB_2532132
Tubulin	Santa cruz	Cat#sc-12462 RRID: AB_2241125
b-Actin	Sigma-Aldrich	Cat#A5441 RRID: AB_476744
J2	Kerafast	Cat#ES2001
J2	Scicons	Cat#10010200
single-stranded DNA	Millipore	Cat#MAB3868 RRID: AB_570342
GAPDH	Cell signaling	Cat#2118 RRID: AB_561053
Rabbit polyclonal anti-p62/SQSTM1	MBL	Cat#PM045 RRID: AB_1279301
H-2Db Monoclonal Antibody (B22-249.R1)	Invitrogen	Cat#MA5-17992 RRID: AB_2539376
InVivoMAb anti-mouse MHC Class I (H-2Kb)	Bio X Cell	Cat# BE0172 RRID: AB_10949300
MIZ1 10E2	Hybridoma clone	(Wanzel *et al.*, 2005)
IRF3 (D83B9)	Cell Signaling	Cat#4302 RRID: AB_1904036
Rabbit polyclonal anti-phospho-SQSTM1 (Serine 403)	Thermo Fisher Scientific	Cat#PA5-78267 RRID: AB_2736424
Rabbit polyclonal anti-LC3	MBL	Cat#PM036 RRID: AB_2274121
Mouse monoclonal anti-VCL	Sigma-Aldrich	Cat#V9131 RRID: AB_477629

Rabbit polyclonal anti- CDK2	Santa Cruz Biotechnology	Cat#sc-163 RRID: AB_631215
Mouse monoclonal FITC anti-BrdU (clone 3D4)	BioLegend	Cat#364104 RRID: AB_2564481
BrdU (Bu20a)	Cell signaling	Cat#5292 RRID: AB_10548898
CD276 Antibody, anti-human, APC	Miltenyi Biotec	Cat#130-124-242 RRID: AB_2889531
Anti-HA tag antibody – ChIP grade	abcam	Cat#ab9110 RRID: AB_307019
Anti-DICER [13D6]	abcam	Cat#ab14601 RRID: AB_443067
Beta-2 Microglobulin Polyclonal	Thermo Fisher Scientific	Cat#PA5-29580 RRID: AB_2547056
FITC anti-mouse CD3	Biolegend	Cat#BLD-100204 RRID: AB_312661
CD3 Monoclonal Antibody (17A2), Functional Grade, eBioscience™	Invitrogen / Thermo Fisher Scientific	Cat#16-0032-82 RRID: AB_468851
CD28 Monoclonal Antibody (37.51), Functional Grade, eBioscience™	Invitrogen / Thermo Fisher Scientific	Cat#16-0281-82 RRID: AB_468921
APC anti-HIS Tag mouse IgG2a, kappa	Biolegend	Cat#BLD-362605
ATP1A1 monoclonal antibody	Thermo Fisher Scientific	Cat#M7-PB-E9 RRID: AB_258029
beta-2 Microglobulin Polyclonal Antibody	Thermo Fisher Scientific	Cat#PA5-29580 RRID: AB_2547056
ECL-Anti-rabbit IgG Horseradish Peroxidase	GE Healthcare / Fisher Scientific GmbH	Cat#1079-4347 / GEHENA934
ECL-Anti-mouse IgG Horseradish Peroxidase	GE Healthcare / Fisher Scientific GmbH	Cat#1019-6124 / GEHENA931
Goat anti-Rabbit IgG (H+L) Cross-Adsorbed Secondary Antibody, Alexa Fluor 647	Thermo Fisher Scientific	Cat#A-21244 RRID: AB_2535812
Goat anti-Mouse IgG (H+L) Cross-Adsorbed Secondary Antibody, Alexa Fluor 647	Thermo Fisher Scientific	Cat#A-21235 RRID: AB_2535804

4.4 Solutions, chemicals, drugs

Chemical	*Company*	*Ordering Number*
Doxycycline hyclate	Sigma-Aldrich	Cat#D9891-10G
Hydroxychloroquine	Sigma-Aldrich	Cat#C6628-25G
Hematoxylin	Sigma-Aldrich	Cat#GHS332-1L
Triton X-100	Roth	Cat#3051.4
Hoechst 33342	Sigma-Aldrich	Cat#B2261-25MG
Lipofectamine RNAiMAX Transfection Reagent	Thermo Fisher Scientific	Cat#13778-150
Dynabeads Protein A	Thermo Fisher Scientific	Cat#10001D
Dynabeads Protein G	Thermo Fisher Scientific	Cat#10003D
Opti-MEM I	Thermo Fisher Scientific	Cat#31985-047
Propidium iodide	Sigma-Aldrich	Cat#81845
Protease inhibitor cocktail	Sigma-Aldrich	Cat#P8340
Phosphatase inhibitor cocktail 2	Sigma-Aldrich	Cat#P5726
Phosphatase inhibitor cocktail 3	Sigma-Aldrich	Cat#P0044
Proteinase K	Roth	Cat#7528.2
RNase A	Roth	Cat#7156.1
D-Luciferin Firefly, potassium salt	Biosynth Chemistry and Biology	Cat#L-8220
Ursotamin®100mg/mL	Serumwerk Bernburg AG	
Xylavet® 20mg/mL	cp-pharma	
Rimadyl® 50mg/mL	zoetis	
Geltrex basement membrane matrix	Thermo Fisher Scientific	Cat#A1413202
3-0 coated VICRYL suture	Ethicon	
AutoClip Kit	FST	
Doxycycline food	SSNIFF	Cat#A112D70624
16% Paraformaldehyde (Formaldehyde) Aqueous Solution, EM Grade	Science Services GmbH	Cat#E15710
Penicillin-Streptomycin	Sigma-Aldrich	Cat#P4333-100ML
UltraPure BSA (50 mg/mL)	Thermo Fisher Scientific	Cat#AM2616
Polybrene	Sigma-Aldrich	Cat#H9268
N-Ethylmaleinimid	Sigma-Aldrich	Cat#E3876
Puromycin	InvivoGen	Cat#70664-3
Hygromycin B Gold solution	InvivoGen	Cat#ant-hg-05
Agencourt AMPure XP Beads	Beckman Coulter	Cat#A63881
Agencourt RNAClean XP Beads	Beckman Coulter	Cat#A63987
peq GOLD Trifast	peqlab / VWR International	Cat#30-2010
Poly (I:C) LMW	InvivoGen	Cat#tlrl-picw
TLR3/dsRNA Complex Inhiitor	Calbiochem	Cat#614310
5,6-Dichlorobenzimidazole 1-β-D-ribofuranoside	Sigma-Aldrich	Cat#D1916-50MG
THZ1 Hydrochloride	MedChem Express / Hycultec GmbH	Cat#HY-80013-10
Pladienolide B	Santa Cruz	Cat#sc-391691
BI-8626	Hölzel Diagnostika Handels GmbH	Cat# HY-120204-50mg
Ambion™ RNase III	Thermo Fisher Scientific	Cat#AM2290
Rnase T1	Thermo Fisher Scientific	Cat#EN0541
DNase I, RNase-free (supplied with MnCl2) (1U/μL)	Thermo Fisher Scientific	Cat#EN0525

S1 Nuclease	Thermo Fisher Scientific	Cat#EN0321
LDC 0000 67	Selleckchem / Absource Diagnostics GmbH	Cat#S7461
Cymarin	Sigma-Aldrich	Cat#30030-1MG
Digitoxin	Sigma-Aldrich	Cat#D5878-250MG
Oubain Octahydrat	Sigma-Aldrich	Cat#O3125-250MG
Digoxin	Merck	Cat#D6003-100MG
C-178	Abcam	Cat#ab287033
Palbociclib	Selleckchem / Biozol	Cat#SEL-S1579-10MG
TLR3/dsRNA Complex Inhibitor - Calbiochem	Merck	Cat#614310-10MG
M-Z, + 625 mg/kg Doxycycline » RED « [720 ppm doxycycline hyclate] sterilis. 25 kGy Test compound diet, 10 mm + PE, Doxyzyklin Futter für den Tierstall - inkl. aller NK	ssniff Spezialdiäten GmbH	Cat#A112D70624
Murine recombinant IL7	Peprotech	Cat#217-17
Puromycin	InvivoGen	Cat#ant-pr-1
Hygromycin B Gold solution	InvivoGen	Cat#ant-hg-5
G418 (Neomycin)	InvivoGen	Cat#ant-gn-5
Blasticidin S	InvivoGen	Cat#ant-bl-1
Penicillin-Streptomycin Solution	Sigma	Cat#P4333-100ML
DMEM, high glucose, pyruvate	Thermo Fisher Scientific	Cat#41966052
RPMI-1640 Medium with L-Glutamin	Thermo Fisher Scientific	Cat#21875091
IMDM, GlutaMAX™ Supplement	Thermo Fisher Scientific	Cat#31980-048
2.5% Trypsin (10x)	Thermo Fisher Scientific	Cat#15090-046
Phosphatase Inhibitor Cocktail 2	Sigma	Cat#P5726-5ML
Phosphatase Inhibitor Cocktail 2	Sigma	Cat#P0044-5ML
Protease Inhibitor Cocktail	Sigma	Cat#P8340-5ML
PowerUp™ SYBR® Green Master Mix, 10 x 5 ml	Thermo Fisher Scientific	Cat#A25778
M-MLV Reverse Transcriptase	Promega	Cat#M1705
Primer “random”	Sigma	Cat#11034731001
RiboLock RNase Inhibitor	Thermo Fisher Scientific	Cat#11581505
LIVE/DEAD™ Fixable Blue Dead Cell Stain Kit, for UV excitation	Thermo Fisher Scientific	Cat#L23105
His-Tagged hB7-H3 protein	R&D Biosystems	Cat#1949-B3-050

Consumables and disposable plastic were purchased from Eppendorf, Greiner, Nunc Thermo Scientific, VWR and Sarstedt.

4.5 Buffers

Name	*Composition*
Laemmli Buffer (6x)	12% SDS
	60‰ bromphenol blue
	47% glycerol
	60 mM Tris pH 6.8
	9.3% DTT
RIPA lysis buffer	50 mM HEPES pH 7.9
	140 mM NaCl
	1 mM EDTA
	1% Triton X-100
	0.1% SDS
	0.1% sodium deoxycholate
1 x PBS for SA-β-Galactosidase staining	1x PBS
	10 mM MgCl2
	adjusted to pH 5.5 with HCl
Fixing solution for SA-β-Galactosidase staining	2% PFA in 1x PBS
	adjusted to pH 5.5 with HCl
	0.25% Glutaraldehyde
KC-solution 1	100 mM Potassium ferricyanide (III)
KC-solution 1	100 mM Potassium hexocyanoferrate(II)-Trihydrate
40x X-Gal stock solution	0.4 g 5-Brom-4-Chlor-3-indoxyl-β-D-Galactosid
X-Gal staining solution (freshly prepared)	0.25 mL 40x X-Gal
	0.5 mL KC solution 1
	0.5 mL KC solution 2
	8.75 mL of 1x PBS (pH 5.5)
PI staining buffer (BrdU-FACS)	38 mM sodium citrate
	54 μM propidium iodide
	24 μg/μL RNase A
Lysogenic broth (LB) medium	10% (w/v) Bacto tryptone
	0.5% (w/v) yeast extract
	1% (w/v) NaCl
LB-Agar	LB-medium with 1.2 % (w/v) Bacto agar was autoclaved and antibiotics were added
ACK-Buffer	8.024 mg/L NH_4Cl
	1.001 mg/L $KHCO_3$
	3.822 mg/L EDTA $Na_2 \cdot 2H_2O$
NP40-lysis buffer	50 mM Tris-HCl (pH 7.4)
	150 mM NaCl
	1% NP40
	5 mM EDTA

NET-2 buffer	50 mM Tris-Cl pH 7.5
	150 mM NaCl
	1 mM MgCl2
	0.5% NP-40
HSW buffer	50 mM Tris-Cl pH 7.4
	1 M NaCl
	1 mM EDTA
	1% NP-40
	0.5% DOC
fCLIP lysis buffer	20 mM Tris-HCl pH 7.5
	15 mM NaCl
	10 mM EDTA
	0.5% NP-49
	0.1% Triton-X-100
	0.1% DOC
Urea buffer	200 mM Tris HCl pH 7.4
	100 mM NaCl
	20 mM EDTA
	2% SDS
	7 M Urea
ChIP wash buffer I	20 mM Tris/HCl, pH 8.0
	150 mM NaCl
	2 mM EDTA
	0.1% SDS
	1% Triton X-100
ChIP wash buffer II	20 mM Tris/HCl, pH 8.0
	500 mM NaCl
	2 mM EDTA
	0.1% SDS
	1% Triton X-100
ChIP wash buffer III	20 mM Tris/HCl, pH 8.0
	250 mM LiCl
	1 mM EDTA
	1% NP-40
	1% DOX

4.6 Kits

Kit	*Company*	*Ordering Number*
Duolink In Situ PLA Probe Anti-Rabbit PLUS, Affinity purified Donkey anti-Rabbit IgG (H+L)	Sigma-Aldrich	Cat#DUO92002 RRID: AB_2810940
Duolink In Situ PLA Probe Anti-Mouse MINUS, Affinity purified Donkey anti-Mouse IgG (H+L)	Sigma-Aldrich	Cat#DUO92004 RRID: AB_2713942
Duolink In Situ Wash Buffers, Fluorescence	Sigma-Aldrich	Cat#DUO82049
Duolink In Situ Detection Reagents Red	Sigma-Aldrich	Cat#DUO92014
NGS Fragment High Sensitivity Analysis Kit, 1-6,000 bp, 500 samples	Agilent	Cat#DNF-474-0500
Standard Sensitivity RNA Analysis Kit (15nt), 500 samples	Agilent	Cat#DNF-471-0500
RNeasy Mini Kit	Qiagen	Cat#74106
NextSeq 500/550 High Output Kit v2 (75cycles)	Illumina	Cat#FC-404-2005
NEBNext® Poly(A) mRNA Magnetic Isolation Module	NEB	Cat#E7490
NEBNext® Ultra™ RNA Library Prep Kit for Illumina	NEB	Cat#E7530
NEBNest® rRNA Depletion Kit (Human/Mouse/Rat)	NEB	Cat#E6310
NEBNext® Multiplex Oligos for Illumina ® (Dual Index Primers Set 1)	NEB	Cat#E7600S
ABsolute QPCR Mix, SYBR Green, no ROX	Thermo Fisher Scientific	Cat#AB-1158/B
QIAshredder Kit	Qiagen	Cat#79654
Pan T Cell Isolation Kit, mouse	Miltenyi Biotec	Cat#130-095-130
GeneJET Gel Extraction Kit	Thermo Fisher Scientific	Cat#K0692
PureLink Plasmid Maxi	Thermo Fisher Scientific	Cat#K210007
Immobilon Western Substrat	Merck Millipore	Cat#WBKLS0500
Agencourt AmPure XP Beads	Beckman Coulter	Cat#A63881
Rneasy Mini Kit	Qiagen	Cat#74106
QIAshredder	Qiagen	Cat#79656
Seahorse XF Glycolytic Rate Assay Kit	Agilent	Cat#103344-100
Immobilon-P transfer membrane	Millipore	Cat#IPVH00010
Western Blotting Filter Paper, Extra Thick, 20 cm x 20 cm	Life Technologies GmbH	Cat#88620

4.7 Equipment

Equipment	*Company*
Casy® cell counter	Innovatis
BD FACSCanto II	BD Biosciences
LAS-4000 mini	GE healthcare
Infinite® 200 PRO	Tecan
Operetta CLS High-Content Analysis System	Perkin Elmar
StepOnePlus™ Real-Time PCR System	Thermo Fisher Scientific
Seahorse 96XF	Agilent

4.8 Software

Software	*Source*
ApE plasmid editor	by M. Wayne Davis, Version 2.0.51
EndNote X8	Clarative Analytics
FlowJow	Version 8.8.6
LAS-4000 mini 2.1	Fujifilm
Multi Gauge	Fujifilm
Harmony 4.9	Perkin Elmar
ImageStudioLite	LI-COR, Inc.
Microsoft Office 2017	Microsoft
Affinity Desinger	Serif
Prism 8	GraphPad
Agilent Seahorse Analytics	Agilent
FlowJo	BD bioscience

5 Methods

5.1 Cell culture

5.1.1 Culturing cells

HEK293TN, KPC, PANC1, PaTu 8988T and U2OS cells were cultured in DMEM. ASPC1, MZ1, Dan-G, IMIM RC1, Panc0813, LS174T, Colo26, NHO2A and DLD1 were cultured in RPMI-1640. T cells were cultivated in IMDM GlutaMAX Supplement.

Medium was supplemented with 10% fetal calf serum and 1% penicillin-streptomycin. Cells were regularly tested for mycoplasma contamination. All cells were incubated at 37 °C, 95% relative humidity, and 5% CO_2.

5.1.2 Transfection and lentiviral infection

Transfection of KPC cells with Lipofectamin 2000 was performed overnight in Opti-MEM. Cells were selected for 3 days 72 h after transfection. For production of lentivirus, HEK293TN cells were transfected using PEI reagent. 11 μg of lentiviral plasmid with target sequence, 9 μg of packaging plasmid psPAX.2 and 2.5 μg envelope plasmid pMD2.G were used per condition. Supernatant was collected 48 h and 72 h after transfection. Sterile filtered (0.45 μm) supernatant was used for infection. Medium was supplemented with 4 μg/mL polybrene for infection. Cells were selected 48 h after infection with puromycin (2 μg/mL).

5.1.3 Generation of cell lines

KPC cells were lentivirally infected with eGFP-firefly-luciferase and sorted for GFP. Positive cells were infected with pInducer11 shMYC#2, shortly induced with doxycycline and sorted for RFP. Positive cells were additionally infected with LT3 GEPIR shMYC#3 and selected with puromycin for 3 days. A clonal cell line was established by sorting of single cells and determining MYC levels by immunoblot analysis.

For generation of a MYC knockout cell line, KPC cells where first infected with pInducer20 MYC (human) and selected with G-418 for 2 weeks. The cell line was then transfected with lentiCRISPR V2 and PLKO vector expressing one sgRNA targeting intron 1 and one sgRNA targeting intron 2. Cells were selected with puromycin and subsequently single cells were sorted for a strong GFP signal. MYC levels were determined using immunoblot and RQ-PCR.

For generation of a *Tbk1* knockout line, KPC cells were transfected with lentiCRISPR V2 expressing sgRNA targeting TBK1 or empty vector. Cells were selected with puromycin for 3 days and subsequently infected with pInducer11 shMYC#2 and LT3 GEPIR shMYC#3. shRNAs were shortly induced with doxycycline and cells sorted for a strong expression of GFP and RFP. Knockout of *Tlr3* was generated by infection of the MYC knockout cell line with lentiCRISPR V2 sgRNA targeting *Tlr3* and selection with

puromycin for 3 days. For generation of cell lines expressing MYC or MYCVD, the shMYC single-cell clone was infected with pInducer20, expressing a doxycycline inducible human MYC-transgene or human MYCVD-transgene. Cells were selected for 2 weeks using G-418. For generating knockout of *Irf3*, KPC cells with knockout of MYC and doxycycline inducible expression of a MYC transgene were infected with lentiCRIPSR V2 expressing an sgRNA targeting *Irf3*. Cells were selected 48 h post infection.

For the knockout of *B2m*, KPC cells were infected with lentiCRISPR V2 sgRNA targeting *B2m.* Single cell clones were sorted and selected for absence of MHC class I presentation on the surface.

For humanized, digitoxin-sensitive KPC cells, KPC cells expressing luciferase were lentivirally infected with a vector expressing human ATP1A1. Cells were infected with lentiCRISPR V2 sgRNA targeting murine *Atp1a1*. Single cells were sorted and screened for sensitivity with 100 nM cymarin.

5.2 Cumulative growth curve

For the cumulative growth curve 10,000 cells were seeded in triplicates in 6-well-plates. For every condition, a 6-cm-dish was seeded to maintain and re-seed. Cells were trypsinzed with 500 µL trypsin solution. Reaction was stopped using 2 or 1 mL of 10% FCS in PBS. Cells were scattered by pipetting up and down to destroy clusters. 50 µL of suspension were used in 10 mL Casyton to measure the number of cells in CASY cell counter. Triplicates were reseeded from 6-cm-maintaining-plate and incubated for further 72 h. Growth curves over three weeks were conducted with counting once every week. Therefore, 1,000 KPC cells were seeded per well.

5.3 BrdU/PI flow cytometry analysis

For flow cytometry, cells were labelled with 20 µM BrdU (Sigma Aldrich) for 1 h. After collection of cells and washing with ice-cold PBS, cells were fixed in 80% ethanol over night at -20 °C. Cell pellet was washed with PBS and resuspended in 2 M HCl/0.5% Triton X-100 for 30 min at room temperature. HCl was neutralized using $Na_2B_4O_7$. Cells were labelled using anit-BrdU-FITC antibody (BioLegend). Cells were washed with PBS and incubated with RNase A and propidium iodide for 30 min at 37 °C. For cell cycle analysis cells were trypsinized and fixed in 80% ethanol over night at -20 °C. Cell pellet was washed with PBS and incubated with RNase A and propidium iodide for 30 min at 37 °C. Measurement was performed using BD FACSCanto II flow cytometry, BD FACSDIVA software and FlowJo (Version 8.8.6).

5.4 Flow cytometry for surface proteins

For staining of MHC Class I proteins on the surface of the cells, cells were trypsinized and washed twice with PBS. Cells were blocked using 2% FCS in PBS and 1 µg first antibody was added for 30 min at 4 °C per condition. Cells were washed twice using 2% FCS in PBS and secondary antibody was added

in a 1:400 dilution for 30 min at room temperature. Cells were washed twice with 2% FCS in PBS. Measurement was performed using BD FACSCanto II flow cytometry and BD FACSDIVA software.

5.5 Isolation of extracellular vesicles

For purification of extracellular vesicles, KPC cells were incubated in 150 mm culture plates over night to allow attachment of cells. Medium was exchanged and cells were treated for 48 h. Conditioned medium was collected and centrifuged at 1,500 rpm for 10 min at 4 °C and subsequently filtered through a 0.2 μM filter. To destroy extracellular vesicles in respective samples 1% Triton was added and incubated at 4 °C for 10 min. Supernatant was transferred to ultracentrifugation tubes and ultra-centrifuged with a Beckmann SW32Ti rotor at 30,000 rpm for 90 min at 4 °C. Pellet was once washed with cold PBS and centrifuged again at same conditions. Pellet was dissolved in PBS.

5.6 Immunofluorescence staining

Cells were cultivated in 96-well-plates (Greiner, Perkin Elmar) and fixed with 4% PFA for 5 min at room temperature. Cells were permeabilized using 0.2% Triton X-100 for 10 min at room temperature or for 20 min at -20 °C with pure methanol. For BrdU-staining cells were fixed with methanol and permeabilized with 2 M HCl for 4 min. Cells were blocked with 5% BSA in PBS. The plate was incubated over night at 4 °C with primary antibodies in 5% BSA in PBS. After washing with PBS secondary antibody was added in a 1:400 dilution. Hoechst 33343 (Sigma Aldrich) was diluted in PBS and samples were incubated for 10 min. Plate was washed twice with PBS and measured using Operetta High-Content Imaging System with 20x or 40x magnification. Data was analyzed using Harmony High Content Imaging and Analysis Software.

For staining of dsRNA, cells were fixed with 4% PFA and permeabilized with 0.2% Triton X-100. To degrade dsRNA, cells were treated afterwards with 60 U/mL RNase III in respective buffer for 1 h at 37 °C. To degrade ssRNA, cells were treated with 100 U/mL with RNase T1 for 1 h at 37 °C. For the staining of dsRNA clone J2 from Kerafast was used for immunofluorescences.

For staining of ssDNA, first RNA was degraded for 30 min at 37 °C with 0.1 mg/mL RNase A. Second, ssDNA was degraded with S1 Nuclease for 30 min at 37 °C with 40 U/mL.

5.7 Proximity-ligation-assay

Proximity Ligation Assay was performed in 384-well-plates (Perkin Elmar) with Duolink in situ Kit (Sigma Aldrich) according to the manufacturer's protocol. Nuclei were counterstained with Hoechst 33342 (Sigma-Aldrich). Images were takes as described above with Operetta High-Content Imaging System with 40x magnification.

5.8 Immunoblotting

Whole cell lysates were prepared using RIPA buffer containing inhibitors for protease and phosphatases (Sigma-Aldrich). Protein lysates were denaturized with Laemmli buffer. Separation was done on BIS-TRIS-gels and transfer was performed on PVFD membrane (Millipore). Blocking was performed using 5% BSA in TBST. Secondary antibodies were used 1:5000. Membrane was developed with Immobilon Western Substrate.

5.9 SA-β-Galactosidase assay

For SA-β-Galactosidase staining cells were washed with 1x PBS (pH=7.7) and fixed using 2% PFA with 0.25% Glutaraldehyde and incubated for 15 min at room temperature. Cells were washed three times afterwards with 1x PBS (with 10 mM $MgCl_2$, pH=5.5 with 37% HCl). Freshly prepared staining-solution was added and incubated for 24 h at 37 °C (without CO_2). Staining solution was replaced by 1x PBS.

5.10 fCLIP

Cells were fixed with 0.1% formaldehyde for 10 min and subsequently fixation was stopped by addition of 125 mM glycine for 10 min at room temperature. Cells were washed twice with ice-cold PBS and harvested in PBS containing inhibitors against protease and phosphatase. Cell pellet was lysed using fCLIP-Lysis-Buffer and incubated for 10 min on ice. Cells were sonicated for 1 min (10 s pulse, 45 s pausing). RNase T1 (1,000 U) and DNase I (10 U) were added and incubated at 37 °C for 30 min on a rotating wheel. Lysate was centrifuged at 14,000 rpm for 15 min at 4 °C. Supernatant was transferred to a new vial and immobilized antibody was added and incubated at 4 °C for 4 h with rotary agitation. Beads were centrifuged at 800 g for 1 min at 4 °C. Beads were washed 3 times with fCLIP-Lysis-Buffer, 2 times with ChIP Buffer I, 2 times with ChIP Buffer II, 2 times with ChIP Buffer III, 3 times with fCLIP-Lysis-Buffer and finally once with TE-Buffer (1 mL each). For elution beads were resuspended in 300 µL 2x Urea-Buffer and incubated shaking for 2 h at 25 °C. Magnetic beads were removed and 300 µL 10 mg/mL Proteinase K solution were added and incubated for 2 h at 37 °C and subsequently at 65 °C shaking over night for decrosslinking. RNA was extracted by adding 700 µL of Trifast and 200 µL Chloroform, solution was vortexed and subsequently centrifuged. Aqueous phase was transferred to a new vial and RNA was precipitated using 1 mL Isopropanol, 50 µL 3 M sodium acetate and 1 µL Glycoblue. Solution was incubated for 1 h at -20 °C and then centrifuged at 14,000 rpm at 4 °C for 1 h. Pellet was washed twice with 70% ice-cold EtOH and finally air-dried and solved in RNase-free water. cDNA was synthesized using M-MLV Reverse Transcriptase.

5.11 Transcriptomics

5.11.1 RNA extraction for library preparation from cells

For RNA extraction media was removed and cells were harvested with 600 µL RLT Buffer containing 6 µL of β-Mercaptoethanol. Cell extract was shock frosted in liquid nitrogen and stored at –80 °C until

processing. RNA was extracted using the Qiagen Kit RNeasy Mini Kit according protocol. RNA was eluted in 50 µL of nuclease-free water. RNA concentration was determined using Fragment Analyser RNA protocol.

5.11.2 RNA extraction for library preparation from tumor tissue

Tumor tissue was checked under the fluorescent microscope and RFP and GFP-positive tissue was dissected and transferred in 350 µL RLT Buffer with 1% β-Mercaptoethanol. Tissue was crushed using a pestle and subsequently transferred to Qiagen shredder column. Column was centrifuged at 14,000 rpm for 1 min. Flow-through was mixed with 700 µL 70% ethanol and processed according protocol of RNeasy Mini Kit. RNA was eluted in 40 µL of nuclease-free water. RNA concentration and quality were determined using the NanoDrop1000 and the Fragment Analyzer System (Agilent).

5.11.3 PolyA RNA Sequencing

RNA sequencing was performed as previously described using an Illumina NextSeq 500 System (Jaenicke *et al.*, 2016). RNA extraction was done with the RNeasy Kit (Quiagen) with on-column digestion of DNA. Tumor tissue was processed using the QIAshredder Kit as described in **5.11.2**. Messenger RNA was isolated using NEBNext® Poly(A) mRNA Magnetic Isolation module (NEB) and library preparation was done with NEBNext® Ultra RNA Library Prep Kit for Illumina (NEB) or NEBNext® Ultra™ II Directional RNA Library Prep Kit for Illumina (NEB) according to the protocol. Size selection was done using Agencourt AMPure XP Beads (Beckmann Coulter). Quantity and Quality of the sequencing libraries was determined with the Fragment Analyzer System (Agilent).

5.11.4 Sequencing of dsRNA

Cells were trypsinized and counted. $2.4x10^7$ cells were used per biological condition and washed with PBS once. Cell pellet was lysed using 2.5 mL of NP-40 lysis buffer. Lysate was centrifuged for 5 min, at 14,000 rpm for 5 min. Supernatant was transferred to a falcon and diluted 1:4 in NET2-Buffer and supplemented with 10 mM $MgCl_2$. 20 U of DNase I and 1,500 U RNase T1 were added per sample. 50 U RNase III were used in respective conditions. Digestion was done at 37 °C for 30 min. 5 µg of J2 Antibody (Scicons) per condition were coated overnight to 40 µL of Protein G beads in 5 g/L BSA in PBS. 5 µg mixture of mouse and rabbit IgG were used as a control. Labelled Antibodies were added to lysate and incubated on the rotating wheel for 2 h at 4 °C. Beads were washed twice with HSW Buffer and twice with NET2 buffer. RNA was extracted from the beads using 500 µL Trifast. Trifast was separated from the beads and 200 µL chloroform were added. Aqueous phase was mixed with 500 µL Isopropanol and 1 µL Glycoblue and incubated at -20 °C for 20 min. RNA was purified as previous described. RNA pellet was resuspended in 20 µL RNase-free water. Ribosomal RNA was depleted using NEBNext rRNA depletion kit prior library preparation. rRNA depleted samples were processed using NEBNext Ultra RNA Library Prep Kit for Illumina.

5.11.5 Nascent RNA sequencing

Cells were treated for 20 min with 200 μM 4-thiouridine (4sU; Sigma-Aldrich) and then lysed using QIAzol reagent (Qiagen). Samples were spiked with lysates of equal numbers of 4sU-labelled human U2OS cells. Total RNA was extracted from the lysates using the miRNeasy kit (Qiagen) with on-column DNase digestion. Quantity and quality of the RNA was determined on the Fragment Analyzer (Thermo Fisher Scientific). The RNA was biotinylated with EZ-Link Biotin-HPDP (Pierce) in 0.2 mg/ml dimethylformamide and biotin labelling buffer (10 nM Tris-Cl pH 7.4, 1 mM EDTA). After rotating incubation for 2 h at RT, the biotinylated RNA was purified with a chloroform-isoamylalcohol extraction followed by isopropanol precipitation (with 1/10 volume of 5 M NaCl and centrifugation at 20,000 g for 20 min at 4 °C) and washing with 75% ethanol. The pellets were resuspended in water and biotinylated RNA was isolated by binding to Dynabeads MyOne Streptavidin T1 beads (Invitrogen) in Dynabeads washing buffer (2 M NaCl, 10 mM Tris pH 7.5, 1 mM EDTA, 0.1 %v/v Tween 20) for 15 min at RT with rotation. The 4sU-labelled RNA was washed, eluted from the beads, purified with the RNeasy MinElute kit (Qiagen) and quantified using the RiboGreen Assay (Invitrogen). For sequencing library preparation, rRNA was depleted with the NEBNext rRNA Depletion Kit (NEB) and cDNA prepared using the NEBNext Ultra II Directional RNA Library Prep Kit (NEB) following the instructions of the supplier. Quantity and Quality of the sequencing libraries was determined with the Fragment Analyzer System (Agilent).

5.11.6 Bioinformatical analyses and statistics

Bioinformatical analysis was done by Carsten Ade, Apoorva Baluapuri and Florian Röhrig. FASTQ files were generated from Illumina base call files using the bcl2fastq conversion software v1.0.0 or v2.19 and overall sequencing quality was tested using FastQC v0.11.9. Adapter and quality trimming were performed by Trim Galore with default settings.

For double-stranded RNA sequencing, reads were mapped to hg38 for the spike-in reads using Tophat v.2.1.1 (Kim *et al.*, 2013) (Bowtie2 v2.3.4.1) with default parameters but allowing only one reported alignment by adding the "-g 1" parameter. Samples were normalized based on normalization factors to the lowest spike-in sample. Unmapped reads were then subsequently aligned versus reference genomes for murine ribosomal DNA (BK000964.1), murine mitochondrial DNA (chrM of mm10) and the murine reference genome mm10. Peak-calling for dsRNA peaks with MACS2 (Zhang *et al.*, 2008) was performed with the corresponding RNase III (RNase C) treated sample as control using default parameters, but using the background lambda as local lambda by adding –nolambda. Bedgraph files were generated using the 'genomecov' function from BEDtools v2.26.0 (Quinlan and Hall, 2010) and the Integrated Genome Browser (Freese *et al.*, 2016) was used to visualize these density files. Overlap with repeat elements was analyzed by BEDtools 'intersectbed' using a RepeatMasker (rmsk, 2012-02-06) track from UCSC table browser. Classes of repetitive elements were determined using BEDtools intersect. To annotate peaks and for upset plots the R (R Development Core Team, 2020) package 'ChIPseeker' (Yu *et al.*, 2015) was used. To analyze the number of reads within genes, these reads were counted using 'featureCounts' from the 'Rsubread' package (Liao *et al.*, 2019) in R and the bed

files generated by MACS2 as SAF files. Plots were generated using the 'Tidyverse' and 'ggplot2' packages in R.

For mRNA sequencing, reads were mapped to the whole mouse genome mm9 or mm10 with Bowtie2 (v2.3.4.1) (Langmead and Salzberg, 2012). Very weakly and not expressed genes (mean cpm over all replicates <1) were removed and, if required, samples were normalized to the number of mapped reads in the smallest sample of a sample-set. Counting of reads per gene and differential expression analysis were done in R, using the "summaryOverlaps" function of the "GenomicAlignment" tool and the edgeR tool, respectively. For the differential expression of genes, the Benjamini-Höchberg method was used to adjust the p-values for multiple-testing. Gene set enrichment analyses were done using the GSEA software (v4.0.3) (Subramanian *et al.*, 2005) with the "Hallmark", "C2" and "C5" databases (v7.1) from MSigDB (Liberzon *et al.*, 2015). Analyses were performed using default settings and 1000 permutations.

For 4sU sequencing, reads were mapped to the whole mouse genome mm10 and, for identification of the human spike-in, to the whole human genome hg19 with Bowtie2 (v2.3.4.1) (Langmead and Salzberg, 2012). Reads mapping to rRNA, exons and 3'/5'-UTR regions were removed, and then normalized to spike in control. BEDtools intersect function was used to determine the number of reads within the introns of dsRNA host genes.

For showing MYC chromatin binding, ChIP sequencing data from GSE44672 was aligned to mm10 assembly of mouse genome. Equal reads from IgG and MYC ChIP sequencing samples on KPC chromatin were then used to generate average density profiles using NGStools (Shen *et al.*, 2014) for the mentioned gene lists. In order to generate gene list of top 100 regulated and non-regulated genes, RNA sequencing data as described above was utilized as follows. All genes with logCPM values < 1 and p-values (Dox vs EtOH) < 0.05 were discarded, and further sorted for regulation. The top 100 genes from resulting table were labeled as "Top100". Additionally, from the same table, genes with log_2FC values between 0.5 and -0.5 were considered to be not regulated (n=2,782).

5.12 Metabolomics

5.12.1 Mass spectrometry of water-soluble metabolites

To analyze metabolites, cells in culture where trypsinized, washed with 1x PBS, counted and cells pellets of 1 million cells were frozen down. Water soluble metabolites were extracted using Lamivudine in MeOH/H2O (80/20). Mass spectrometry was performed as previously described in (Schmidt *et al.*, 2019). Measurement and analysis were done by Werner Schmitz (Biocenter, University of Würzburg).

5.12.2 Seahorse XF glycolytic rate assay

For seahorse glycolytic rate assay cells were seeded in XFe96 FluxPak. Glycolytic rate assay was performed after manufactures protocol. Port A was loaded with Rotenone (5 μM) and Antimycin A (5 μM). Port B was loaded with 2-deoxy-D-glucose (2-DG, 100 mM).

5.13 *In vivo* methods

5.13.1 Orthotopic PDAC transplant model

C57BL/6J mice were purchased from Charles River and were bred and maintained in the animal facility of the Biocenter, University of Würzburg. All animal procedures were approved by the Regierung von Unterfranken under protocol numbers RUF 55.2-2532-2-148 and RUF 55.2.2-2532.2-1026-15. Mouse experiments were conducted by Anneli Gebhardt-Wolf.

Mice were anaesthetized by an intraperitoneal injection of ketamine (100 mg/kg, Ursotamin, Serumwerk) and xylazine (10 mg/kg, Xylavet, cp-pharma). The spleen and the pancreas were externalized and 50,000 modified KPC cells were injected in 50 µL Matrigel / PBS (2:1) into the pancreatic tail. After the injection, the peritoneum was closed with a 3-0 coated VICRYL suture (Ethicon), and the skin was closed using the AutoClip Kit (FST). Mice were treated with an analgetic (5 mg/kg, Rimadyl, zoetis) for three days. The clips were removed after 7 days. After 6 or 7 days, the luciferase expression was measured with an IVIS camera (150 mg/kg luciferin, Biosynth, in ketamine and xylazine). Doxycycline food (625 mg/kg, SSNIFF) was given after 6 or 7 days. In mice transplanted with MYC CRISPR-KO cells, doxycycline treatment was stopped 6 days after injection. Digitoxin (dissolved in 5% HS15 in saline) was administered intraperitoneal 7 days after transplantation for four weeks every second day in a dose of 2 mg/kg. For long-term survival studies, mice were checked at least daily. Showing symptoms of pain, mice were killed by cervical dislocation.

5.13.2 Generation CAR-T cells

Splenocytes were washed out of spleen using ACK-lysis buffer. Reaction was stopped after 4 min using 1x PBS. T cells were purified from splenocytes using Pan T cell isolation kit (Miltenyi Biotex) according to protocol. Purified T cells were seeded in 12-well plates coated with α-CD3-antibody. T cells were cultivated in IMDM with 10% FCS, 1% P/S, 1 µg/mL α-CD28 antibody, 10 ng/mL recombinant IL7, 1 µL/mL 2-Mercaptoethanol (Gibco) over night.

T cells were infected using retrovirus (Anti-B7-H3 CAR-T) with 10 µg/mL Polybrene and centrifuged for 90 min at 32 °C and 1,500 g. Cells were afterwards incubated for 4 h at 37 °C and medium was exchanged by conditioned medium (containing IL7, α-CD28-antibody and β-Mercaptothanol).

To check transduction efficacy, T cells were stained with B7-H3 recombinant protein and α-His-APC antibody. Viability of T cells was assed using LIVE/DEAD staining (Thermo Fisher Scientific) according protocol.

6 Bibliography

Adhikary, S., Peukert, K., Karsunky, H., Beuger, V., Lutz, W., Elsässer, H.P., Möröy, T., and Eilers, M. (2003). Miz1 is required for early embryonic development during gastrulation. Mol Cell Biol *23*, 7648-7657. 10.1128/mcb.23.21.7648-7657.2003.

Ahmad, S., Mu, X., Yang, F., Greenwald, E., Park, J.W., Jacob, E., Zhang, C.-Z., and Hur, S. (2018). Breaching Self-Tolerance to Alu Duplex RNA Underlies MDA5-Mediated Inflammation. Cell *172*, 797-810.e713. https://doi.org/10.1016/j.cell.2017.12.016.

Aizawa, S., Fujiwara, Y., Contu, V.R., Hase, K., Takahashi, M., Kikuchi, H., Kabuta, C., Wada, K., and Kabuta, T. (2016). Lysosomal putative RNA transporter SIDT2 mediates direct uptake of RNA by lysosomes. Autophagy *12*, 565-578. 10.1080/15548627.2016.1145325.

Akce, M., Zaidi, M.Y., Waller, E.K., El-Rayes, B.F., and Lesinski, G.B. (2018). The Potential of CAR T Cell Therapy in Pancreatic Cancer. Frontiers in immunology *9*, 2166-2166. 10.3389/fimmu.2018.02166.

Alonso-Curbelo, D., Riveiro-Falkenbach, E., Pérez-Guijarro, E., Cifdaloz, M., Karras, P., Osterloh, L., Megías, D., Cañón, E., Calvo, T.G., Olmeda, D., et al. (2014). RAB7 controls melanoma progression by exploiting a lineage-specific wiring of the endolysosomal pathway. Cancer Cell *26*, 61-76. 10.1016/j.ccr.2014.04.030.

Amarante-Mendes, G.P., Adjemian, S., Branco, L.M., Zanetti, L.C., Weinlich, R., and Bortoluci, K.R. (2018). Pattern Recognition Receptors and the Host Cell Death Molecular Machinery. Frontiers in Immunology *9*. 10.3389/fimmu.2018.02379.

Arlt, A., Schäfer, H., and Kalthoff, H. (2012). The 'N-factors' in pancreatic cancer: functional relevance of NF-κB, NFAT and Nrf2 in pancreatic cancer. Oncogenesis *1*, e35-e35. 10.1038/oncsis.2012.35.

Asthana, V., Stern, B.S., Tang, Y., Bugga, P., Li, A., Ferguson, A., Asthana, A., Bao, G., and Drezek, R.A. (2020). Development of a Novel Class of Self-Assembling dsRNA Cancer Therapeutics: A Proof-of-Concept Investigation. Molecular Therapy - Oncolytics *18*, 419-431. 10.1016/j.omto.2020.07.013.

Athanasiadis, A., Rich, A., and Maas, S. (2004). Widespread A-to-I RNA editing of Alu-containing mRNAs in the human transcriptome. PLoS Biol *2*, e391. 10.1371/journal.pbio.0020391.

Bailey, P., Chang, D.K., Nones, K., Johns, A.L., Patch, A.M., Gingras, M.C., Miller, D.K., Christ, A.N., Bruxner, T.J., Quinn, M.C., et al. (2016). Genomic analyses identify molecular subtypes of pancreatic cancer. Nature *531*, 47-52. 10.1038/nature16965.

Balachandran, V.P., Łuksza, M., Zhao, J.N., Makarov, V., Moral, J.A., Remark, R., Herbst, B., Askan, G., Bhanot, U., Senbabaoglu, Y., et al. (2017). Identification of unique neoantigen qualities in long-term survivors of pancreatic cancer. Nature *551*, 512-516. 10.1038/nature24462.

Baluapuri, A., Hofstetter, J., Dudvarski Stankovic, N., Endres, T., Bhandare, P., Vos, S.M., Adhikari, B., Schwarz, J.D., Narain, A., Vogt, M., et al. (2019). MYC Recruits SPT5 to RNA Polymerase II to Promote Processive Transcription Elongation. Mol Cell *74*, 674-687.e611. 10.1016/j.molcel.2019.02.031.

Baluapuri, A., Wolf, E., and Eilers, M. (2020). Target gene-independent functions of MYC oncoproteins. Nat Rev Mol Cell Biol *21*, 255-267. 10.1038/s41580-020-0215-2.

Barriga, F.M., Tsanov, K.M., Ho, Y.-J., Sohail, N., Zhang, A., Baslan, T., Wuest, A.N., Del Priore, I., Meškauskaitė, B., Livshits, G., et al. (2022). MACHETE identifies interferon-encompassing chromosome 9p21.3 deletions as mediators of immune evasion and metastasis. Nature Cancer. 10.1038/s43018-022-00443-5.

Batlle, E., and Massagué, J. (2019). Transforming Growth Factor-β Signaling in Immunity and Cancer. Immunity *50*, 924-940. https://doi.org/10.1016/j.immuni.2019.03.024.

Bernards, R., Dessain, S.K., and Weinberg, R.A. (1986). N-myc amplification causes down-modulation of MHC class I antigen expression in neuroblastoma. Cell *47*, 667-674. 10.1016/0092-8674(86)90509-x.

Bhutia, Y.D., and Ganapathy, V. (2016). Glutamine transporters in mammalian cells and their functions in physiology and cancer. Biochimica et Biophysica Acta (BBA) - Molecular Cell Research *1863*, 2531-2539. https://doi.org/10.1016/j.bbamcr.2015.12.017.

Birley, K., Leboreiro-Babe, C., Rota, E.M., Buschhaus, M., Gavriil, A., Vitali, A., Alonso-Ferrero, M., Hopwood, L., Parienti, L., Ferry, G., et al. (2022). A novel anti-B7-H3 chimeric antigen receptor from a single-chain antibody library for immunotherapy of solid cancers. Mol Ther Oncolytics *26*, 429-443. 10.1016/j.omto.2022.08.008.

Blackwood, E.M., and Eisenman, R.N. (1991). Max: a helix-loop-helix zipper protein that forms a sequence-specific DNA-binding complex with Myc. Science *251*, 1211-1217. 10.1126/science.2006410.

Bold, T.D., and Ernst, J.D. (2012). CD4⁺ T Cell-Dependent IFN-γ Production by CD8⁺ Effector T Cells in Mycobacterium tuberculosis Infection. The Journal of Immunology *189*, 2530. 10.4049/jimmunol.1200994.

Borowski, L.S., Dziembowski, A., Hejnowicz, M.S., Stepien, P.P., and Szczesny, R.J. (2013). Human mitochondrial RNA decay mediated by PNPase-hSuv3 complex takes place in distinct foci. Nucleic acids research *41*, 1223-1240. 10.1093/nar/gks1130.

Bortoluci, K.R., and Medzhitov, R. (2010). Control of infection by pyroptosis and autophagy: role of TLR and NLR. Cell Mol Life Sci *67*, 1643-1651. 10.1007/s00018-010-0335-5.

Böttcher, J.P., Bonavita, E., Chakravarty, P., Blees, H., Cabeza-Cabrerizo, M., Sammicheli, S., Rogers, N.C., Sahai, E., Zelenay, S., and Reis e Sousa, C. (2018). NK Cells Stimulate Recruitment of cDC1 into the Tumor Microenvironment Promoting Cancer Immune Control. Cell *172*, 1022-1037.e1014. 10.1016/j.cell.2018.01.004.

Bowling, E.A., Wang, J.H., Gong, F., Wu, W., Neill, N.J., Kim, I.S., Tyagi, S., Orellana, M., Kurley, S.J., Dominguez-Vidaña, R., et al. (2021). Spliceosome-targeted therapies trigger an antiviral immune response in triple-negative breast cancer. Cell *184*, 384-403.e321. https://doi.org/10.1016/j.cell.2020.12.031.

Brägelmann, J., Böhm, S., Guthrie, M.R., Mollaoglu, G., Oliver, T.G., and Sos, M.L. (2017). Family matters: How MYC family oncogenes impact small cell lung cancer. Cell Cycle *16*, 1489-1498. 10.1080/15384101.2017.1339849.

Brahmer, J.R., Tykodi, S.S., Chow, L.Q., Hwu, W.J., Topalian, S.L., Hwu, P., Drake, C.G., Camacho, L.H., Kauh, J., Odunsi, K., et al. (2012). Safety and activity of anti-PD-L1 antibody in patients with advanced cancer. N Engl J Med *366*, 2455-2465. 10.1056/NEJMoa1200694.

Braud, V.M., Allan, D.S., O'Callaghan, C.A., Söderström, K., D'Andrea, A., Ogg, G.S., Lazetic, S., Young, N.T., Bell, J.I., Phillips, J.H., et al. (1998). HLA-E binds to natural killer cell receptors CD94/NKG2A, B and C. Nature *391*, 795-799. 10.1038/35869.

Brown, G.K. (2000). Glucose transporters: structure, function and consequences of deficiency. J Inherit Metab Dis *23*, 237-246. 10.1023/a:1005632012591.

Broz, M.L., Binnewies, M., Boldajipour, B., Nelson, A.E., Pollack, J.L., Erle, D.J., Barczak, A., Rosenblum, M.D., Daud, A., Barber, D.L., et al. (2014). Dissecting the tumor myeloid compartment reveals rare activating antigen-presenting cells critical for T cell immunity. Cancer Cell *26*, 638-652. 10.1016/j.ccell.2014.09.007.

Brubaker, S.W., Bonham, K.S., Zanoni, I., and Kagan, J.C. (2015). Innate immune pattern recognition: a cell biological perspective. Annu Rev Immunol *33*, 257-290. 10.1146/annurev-immunol-032414-112240.

Büchel, G., Carstensen, A., Mak, K.Y., Roeschert, I., Leen, E., Sumara, O., Hofstetter, J., Herold, S., Kalb, J., Baluapuri, A., et al. (2017). Association with Aurora-A Controls N-MYC-Dependent Promoter Escape and Pause Release of RNA Polymerase II during the Cell Cycle. Cell Rep *21*, 3483-3497. 10.1016/j.celrep.2017.11.090.

Burslem, G.M., and Crews, C.M. (2020). Proteolysis-Targeting Chimeras as Therapeutics and Tools for Biological Discovery. Cell *181*, 102-114. 10.1016/j.cell.2019.11.031.

Cadena, C., Paget, M., Wang, H.-T., Kim, E., Ahmad, S., Zhang, Q., Koo, B., Lyons, S.M., Ivanov, P., Mu, X., and Hur, S. (2021). Stress granules are shock absorbers that prevent excessive innate immune responses to dsRNA. bioRxiv, 2021.2004.2026.441141. 10.1101/2021.04.26.441141.

Carroll, P.A., Freie, B.W., Mathsyaraja, H., and Eisenman, R.N. (2018). The MYC transcription factor network: balancing metabolism, proliferation and oncogenesis. Front Med *12*, 412-425. 10.1007/s11684-018-0650-z.

Casacuberta-Serra, S., and Soucek, L. (2018). Myc and Ras, the Bonnie and Clyde of immune evasion. Translational Cancer Research, S457-S459.

Casey, S.C., Baylot, V., and Felsher, D.W. (2017). MYC: Master Regulator of Immune Privilege. Trends Immunol *38*, 298-305. 10.1016/j.it.2017.01.002.

Casey, S.C., Tong, L., Li, Y., Do, R., Walz, S., Fitzgerald, K.N., Gouw, A.M., Baylot, V., Gutgemann, I., Eilers, M., and Felsher, D.W. (2016). MYC regulates the antitumor immune response through CD47 and PD-L1. Science *352*, 227-231. 10.1126/science.aac9935.

Castro, F., Cardoso, A.P., Gonçalves, R.M., Serre, K., and Oliveira, M.J. (2018). Interferon-Gamma at the Crossroads of Tumor Immune Surveillance or Evasion. Front Immunol *9*, 847. 10.3389/fimmu.2018.00847.

Caudron-Herger, M., Pankert, T., Seiler, J., Németh, A., Voit, R., Grummt, I., and Rippe, K. (2015). Alu element-containing RNAs maintain nucleolar structure and function. The EMBO journal *34*, 2758-2774. 10.15252/embj.201591458.

Chen, Y.G., Chen, R., Ahmad, S., Verma, R., Kasturi, S.P., Amaya, L., Broughton, J.P., Kim, J., Cadena, C., Pulendran, B., et al. (2019). N6-Methyladenosine Modification Controls Circular RNA Immunity. Mol Cell *76*, 96-109.e109. 10.1016/j.molcel.2019.07.016.

Cheng, K., Wang, X., and Yin, H. (2011). Small-molecule inhibitors of the TLR3/dsRNA complex. J Am Chem Soc *133*, 3764-3767. 10.1021/ja111312h.

Chester, C., Fritsch, K., and Kohrt, H.E. (2015). Natural Killer Cell Immunomodulation: Targeting Activating, Inhibitory, and Co-stimulatory Receptor Signaling for Cancer Immunotherapy. Front Immunol *6*, 601. 10.3389/fimmu.2015.00601.

Chiappinelli, Katherine B., Strissel, Pamela L., Desrichard, A., Li, H., Henke, C., Akman, B., Hein, A., Rote, Neal S., Cope, Leslie M., Snyder, A., et al. (2015). Inhibiting DNA Methylation Causes an Interferon Response in Cancer via dsRNA Including Endogenous Retroviruses. Cell *162*, 974-986. 10.1016/j.cell.2015.07.011.

Chinwalla, A.T., Cook, L.L., Delehaunty, K.D., Fewell, G.A., Fulton, L.A., Fulton, R.S., Graves, T.A., Hillier, L.W., Mardis, E.R., McPherson, J.D., et al. (2002). Initial sequencing and comparative analysis of the mouse genome. Nature *420*, 520-562. 10.1038/nature01262.

Chipumuro, E., Marco, E., Christensen, C.L., Kwiatkowski, N., Zhang, T., Hatheway, C.M., Abraham, B.J., Sharma, B., Yeung, C., Altabef, A., et al. (2014). CDK7 inhibition suppresses super-enhancer-linked oncogenic transcription in MYCN-driven cancer. Cell *159*, 1126-1139. 10.1016/j.cell.2014.10.024.

Chitadze, G., Bhat, J., Lettau, M., Janssen, O., and Kabelitz, D. (2013a). Generation of soluble NKG2D ligands: proteolytic cleavage, exosome secretion and functional implications. Scand J Immunol *78*, 120-129. 10.1111/sji.12072.

Chitadze, G., Lettau, M., Bhat, J., Wesch, D., Steinle, A., Fürst, D., Mytilineos, J., Kalthoff, H., Janssen, O., Oberg, H.H., and Kabelitz, D. (2013b). Shedding of endogenous MHC class I-related chain molecules A and B from different human tumor entities: heterogeneous involvement of the "a disintegrin and metalloproteases" 10 and 17. Int J Cancer *133*, 1557-1566. 10.1002/ijc.28174.

Choi, H., Kwon, J., Cho, M.S., Sun, Y., Zheng, X., Wang, J., Bouker, K.B., Casey, J.L., Atkins, M.B., Toretsky, J., and Han, C. (2021). Targeting DDX3X Triggers Antitumor Immunity via a dsRNA-Mediated Tumor-Intrinsic Type I Interferon Response. Cancer Research *81*, 3607-3620. 10.1158/0008-5472.CAN-20-3790.

Closs, E.I., Boissel, J.P., Habermeier, A., and Rotmann, A. (2006). Structure and function of cationic amino acid transporters (CATs). J Membr Biol *213*, 67-77. 10.1007/s00232-006-0875-7.

Collier, J.J., Suomi, F., Oláhová, M., McWilliams, T.G., and Taylor, R.W. (2021). Emerging roles of ATG7 in human health and disease. EMBO Molecular Medicine *13*, e14824. https://doi.org/10.15252/emmm.202114824.

Conacci-Sorrell, M., McFerrin, L., and Eisenman, R.N. (2014). An overview of MYC and its interactome. Cold Spring Harb Perspect Med *4*, a014357. 10.1101/cshperspect.a014357.

Coquel, F., Silva, M.-J., Técher, H., Zadorozhny, K., Sharma, S., Nieminuszczy, J., Mettling, C., Dardillac, E., Barthe, A., Schmitz, A.-L., et al. (2018). SAMHD1 acts at stalled replication forks to prevent interferon induction. Nature *557*, 57-61. 10.1038/s41586-018-0050-1.

Corbet, G.A., Burke, J.M., Bublitz, G.R., and Parker, R. (2022). dsRNA-induced condensation of antiviral proteins promotes PKR activation. bioRxiv, 2022.2001.2014.476399. 10.1101/2022.01.14.476399.

Cornel, A.M., Mimpen, I.L., and Nierkens, S. (2020). MHC Class I Downregulation in Cancer: Underlying Mechanisms and Potential Targets for Cancer Immunotherapy. Cancers *12*, 1760. 10.3390/cancers12071760.

Cossa, G., Roeschert, I., Prinz, F., Baluapuri, A., Silveira Vidal, R., Schulein-Volk, C., Chang, Y.C., Ade, C.P., Mastrobuoni, G., Girard, C., et al. (2020). Localized Inhibition of Protein Phosphatase 1 by NUAK1 Promotes Spliceosome Activity and Reveals a MYC-Sensitive Feedback Control of Transcription. Mol Cell *77*, 1322-1339 e1311. 10.1016/j.molcel.2020.01.008.

Criscione, S.W., Zhang, Y., Thompson, W., Sedivy, J.M., and Neretti, N. (2014). Transcriptional landscape of repetitive elements in normal and cancer human cells. BMC Genomics *15*, 583. 10.1186/1471-2164-15-583.

Csibi, A., Lee, G., Yoon, S.O., Tong, H., Ilter, D., Elia, I., Fendt, S.M., Roberts, T.M., and Blenis, J. (2014). The mTORC1/S6K1 pathway regulates glutamine metabolism through the eIF4B-dependent control of c-Myc translation. Curr Biol *24*, 2274-2280. 10.1016/j.cub.2014.08.007.

Dang, C.V. (2012). MYC on the path to cancer. Cell *149*, 22-35. 10.1016/j.cell.2012.03.003.

Dang, C.V., Le, A., and Gao, P. (2009). MYC-induced cancer cell energy metabolism and therapeutic opportunities. Clin Cancer Res *15*, 6479-6483. 10.1158/1078-0432.Ccr-09-0889.

Das, S.K., Kuzin, V., Cameron, D.P., Sanford, S., Jha, R.K., Nie, Z., Rosello, M.T., Holewinski, R., Andresson, T., Wisniewski, J., et al. (2022). MYC assembles and stimulates topoisomerases 1 and 2 in a "topoisome". Mol Cell *82*, 140-158.e112. 10.1016/j.molcel.2021.11.016.

Dauch, D., Rudalska, R., Cossa, G., Nault, J.C., Kang, T.W., Wuestefeld, T., Hohmeyer, A., Imbeaud, S., Yevsa, T., Hoenicke, L., et al. (2016). A MYC-aurora kinase A protein complex represents an actionable drug target in p53-altered liver cancer. Nat Med *22*, 744-753. 10.1038/nm.4107.

de Duve, C. (2005). The lysosome turns fifty. Nat Cell Biol *7*, 847-849. 10.1038/ncb0905-847.

de Koning, A.P., Gu, W., Castoe, T.A., Batzer, M.A., and Pollock, D.D. (2011). Repetitive elements may comprise over two-thirds of the human genome. PLoS Genet *7*, e1002384. 10.1371/journal.pgen.1002384.

de la Cruz-López, K.G., Castro-Muñoz, L.J., Reyes-Hernández, D.O., García-Carrancá, A., and Manzo-Merino, J. (2019). Lactate in the Regulation of Tumor Microenvironment and Therapeutic Approaches. Frontiers in Oncology *9*. 10.3389/fonc.2019.01143.

de Pretis, S., Kress, T.R., Morelli, M.J., Sabò, A., Locarno, C., Verrecchia, A., Doni, M., Campaner, S., Amati, B., and Pelizzola, M. (2017). Integrative analysis of RNA polymerase II and transcriptional dynamics upon MYC activation. Genome Res *27*, 1658-1664. 10.1101/gr.226035.117.

Decout, A., Katz, J.D., Venkatraman, S., and Ablasser, A. (2021). The cGAS–STING pathway as a therapeutic target in inflammatory diseases. Nature Reviews Immunology *21*, 548-569. 10.1038/s41577-021-00524-z.

Deininger, P. (2011). Alu elements: know the SINEs. Genome Biology *12*, 236. 10.1186/gb-2011-12-12-236.

Dejure, F.R., Royla, N., Herold, S., Kalb, J., Walz, S., Ade, C.P., Mastrobuoni, G., Vanselow, J.T., Schlosser, A., Wolf, E., et al. (2017). The MYC mRNA 3'-UTR couples RNA polymerase II function to glutamine and ribonucleotide levels. EMBO J *36*, 1854-1868. 10.15252/embj.201796662.

del Toro Duany, Y., Wu, B., and Hur, S. (2015). MDA5-filament, dynamics and disease. Curr Opin Virol *12*, 20-25. 10.1016/j.coviro.2015.01.011.

Delaunay, T., Achard, C., Boisgerault, N., Grard, M., Petithomme, T., Chatelain, C., Dutoit, S., Blanquart, C., Royer, P.-J., Minvielle, S., et al. (2020). Frequent Homozygous Deletions of Type I Interferon Genes in Pleural Mesothelioma Confer Sensitivity to Oncolytic Measles Virus. Journal of Thoracic Oncology *15*, 827-842. 10.1016/j.jtho.2019.12.128.

Delgado, M.A., and Deretic, V. (2009). Toll-like receptors in control of immunological autophagy. Cell Death & Differentiation *16*, 976-983. 10.1038/cdd.2009.40.

Dhatchinamoorthy, K., Colbert, J.D., and Rock, K.L. (2021). Cancer Immune Evasion Through Loss of MHC Class I Antigen Presentation. Frontiers in Immunology *12*. 10.3389/fimmu.2021.636568.

Dhir, A., Dhir, S., Borowski, L.S., Jimenez, L., Teitell, M., Rotig, A., Crow, Y.J., Rice, G.I., Duffy, D., Tamby, C., et al. (2018). Mitochondrial double-stranded RNA triggers antiviral signalling in humans. Nature *560*, 238-242. 10.1038/s41586-018-0363-0.

Di, S., Zhou, M., Pan, Z., Sun, R., Chen, M., Jiang, H., Shi, B., Luo, H., and Li, Z. (2019). Combined Adjuvant of Poly I:C Improves Antitumor Effects of CAR-T Cells. Frontiers in Oncology *9*. 10.3389/fonc.2019.00241.

Diao, J., Gu, H., Tang, M., Zhao, J., and Cattral, M.S. (2018). Tumor Dendritic Cells (DCs) Derived from Precursors of Conventional DCs Are Dispensable for Intratumor CTL Responses. J Immunol *201*, 1306-1314. 10.4049/jimmunol.1701514.

Didiot, M.C., Hewett, J., Varin, T., Freuler, F., Selinger, D., Nick, H., Reinhardt, J., Buckler, A., Myer, V., Schuffenhauer, A., et al. (2013). Identification of cardiac glycoside molecules as inhibitors of c-Myc IRES-mediated translation. J Biomol Screen *18*, 407-419. 10.1177/1087057112466698.

Diefenbacher, M.E., Chakraborty, A., Blake, S.M., Mitter, R., Popov, N., Eilers, M., and Behrens, A. (2015). Usp28 counteracts Fbw7 in intestinal homeostasis and cancer. Cancer Res *75*, 1181-1186. 10.1158/0008-5472.CAN-14-1726.

Diefenbacher, M.E., Popov, N., Blake, S.M., Schulein-Volk, C., Nye, E., Spencer-Dene, B., Jaenicke, L.A., Eilers, M., and Behrens, A. (2014). The deubiquitinase USP28 controls intestinal homeostasis and promotes colorectal cancer. J Clin Invest *124*, 3407-3418. 10.1172/JCI73733.

Dostanic-Larson, I., Van Huysse, J.W., Lorenz, J.N., and Lingrel, J.B. (2005). The highly conserved cardiac glycoside binding site of Na,K-ATPase plays a role in blood pressure regulation. Proc Natl Acad Sci U S A *102*, 15845-15850. 10.1073/pnas.0507358102.

Dougan, S.K. (2017). The Pancreatic Cancer Microenvironment. Cancer J *23*, 321-325. 10.1097/ppo.0000000000000288.

Du, H., Hirabayashi, K., Ahn, S., Kren, N.P., Montgomery, S.A., Wang, X., Tiruthani, K., Mirlekar, B., Michaud, D., Greene, K., et al. (2019). Antitumor Responses in the Absence of Toxicity in Solid Tumors by Targeting B7-H3 via Chimeric Antigen Receptor T Cells. Cancer Cell *35*, 221-237.e228. 10.1016/j.ccell.2019.01.002.

Du, J., Jiang, L., Chen, F., Hu, H., and Zhou, M. (2021). Cardiac Glycoside Ouabain Exerts Anticancer Activity via Downregulation of STAT3. Frontiers in Oncology *11*. 10.3389/fonc.2021.684316.

Eilers, M., and Eisenman, R.N. (2008). Myc's broad reach. Genes Dev *22*, 2755-2766. 10.1101/gad.1712408.

Emam, A., Wu, X., Xu, S., Wang, L., Liu, S., and Wang, B. (2022). Stalled replication fork protection limits cGAS–STING and P-body-dependent innate immune signalling. Nature Cell Biology *24*, 1154-1164. 10.1038/s41556-022-00950-8.

Endres, T., Solvie, D., Heidelberger, J.B., Andrioletti, V., Baluapuri, A., Ade, C.P., Muhar, M., Eilers, U., Vos, S.M., Cramer, P., et al. (2021). Ubiquitylation of MYC couples transcription elongation with double-strand break repair at active promoters. Molecular Cell *81*, 830-844.e813. 10.1016/j.molcel.2020.12.035.

Espinet, E., Gu, Z., Imbusch, C.D., Giese, N.A., Büscher, M., Safavi, M., Weisenburger, S., Klein, C., Vogel, V., Falcone, M., et al. (2021). Aggressive PDACs Show Hypomethylation of Repetitive Elements and the Execution of an Intrinsic IFN Program Linked to a Ductal Cell of Origin. Cancer Discovery *11*, 638-659. 10.1158/2159-8290.CD-20-1202.

Evans, R.A., Diamond, M.S., Rech, A.J., Chao, T., Richardson, M.W., Lin, J.H., Bajor, D.L., Byrne, K.T., Stanger, B.Z., Riley, J.L., et al. (2016). Lack of immunoediting in murine pancreatic cancer reversed with neoantigen. JCI Insight *1*. 10.1172/jci.insight.88328.

Fedele, Anthony O., and Proud, Christopher G. (2020). Chloroquine and bafilomycin A mimic lysosomal storage disorders and impair mTORC1 signalling. Bioscience Reports *40*, BSR20200905. 10.1042/BSR20200905.

Fellmann, C., Hoffmann, T., Sridhar, V., Hopfgartner, B., Muhar, M., Roth, M., Lai, D.Y., Barbosa, I.A., Kwon, J.S., Guan, Y., et al. (2013). An optimized microRNA backbone for effective single-copy RNAi. Cell Rep *5*, 1704-1713. 10.1016/j.celrep.2013.11.020.

Felsher, D.W., and Bishop, J.M. (1999). Reversible tumorigenesis by MYC in hematopoietic lineages. Mol Cell *4*, 199-207.

Frankel, L.B., Lubas, M., and Lund, A.H. (2017). Emerging connections between RNA and autophagy. Autophagy *13*, 3-23. 10.1080/15548627.2016.1222992.

Freese, N.H., Norris, D.C., and Loraine, A.E. (2016). Integrated genome browser: visual analytics platform for genomics. Bioinformatics *32*, 2089-2095. 10.1093/bioinformatics/btw069.

Friedlander, S.Y.G., Chu, G.C., Snyder, E.L., Girnius, N., Dibelius, G., Crowley, D., Vasile, E., DePinho, R.A., and Jacks, T. (2009). Context-Dependent Transformation of Adult Pancreatic Cells by Oncogenic K-Ras. Cancer Cell *16*, 379-389. https://doi.org/10.1016/j.ccr.2009.09.027.

Gabay, M., Li, Y., and Felsher, D.W. (2014). MYC activation is a hallmark of cancer initiation and maintenance. Cold Spring Harb Perspect Med *4*. 10.1101/cshperspect.a014241.

Gallant, P., Shiio, Y., Cheng, P.F., Parkhurst, S.M., and Eisenman, R.N. (1996). Myc and Max homologs in Drosophila. Science *274*, 1523-1527. 10.1126/science.274.5292.1523.

Gan, H., Qi, M., Chan, C., Leung, P., Ye, G., Lei, Y., Liu, A., Xue, F., Liu, D., Ye, W., et al. (2020). Digitoxin inhibits HeLa cell growth through the induction of G2/M cell cycle arrest and apoptosis in vitro and in vivo. Int J Oncol *57*, 562-573. 10.3892/ijo.2020.5070.

Ganapathy, V., Thangaraju, M., Gopal, E., Martin, P.M., Itagaki, S., Miyauchi, S., and Prasad, P.D. (2008). Sodium-coupled monocarboxylate transporters in normal tissues and in cancer. Aaps j *10*, 193-199. 10.1208/s12248-008-9022-y.

Garaud, S., Dieu-Nosjean, M.-C., and Willard-Gallo, K. (2022). T follicular helper and B cell crosstalk in tertiary lymphoid structures and cancer immunotherapy. Nature Communications *13*, 2259. 10.1038/s41467-022-29753-z.

Garrido, F., Aptsiauri, N., Doorduijn, E.M., Garcia Lora, A.M., and van Hall, T. (2016). The urgent need to recover MHC class I in cancers for effective immunotherapy. Curr Opin Immunol *39*, 44-51. 10.1016/j.coi.2015.12.007.

Gauthier-Coles, G., Vennitti, J., Zhang, Z., Comb, W.C., Xing, S., Javed, K., Bröer, A., and Bröer, S. (2021). Quantitative modelling of amino acid transport and homeostasis in mammalian cells. Nature Communications *12*, 5282. 10.1038/s41467-021-25563-x.

Gebhardt, A., Frye, M., Herold, S., Benitah, S.A., Braun, K., Samans, B., Watt, F.M., Elsasser, H.P., and Eilers, M. (2006). Myc regulates keratinocyte adhesion and differentiation via complex formation with Miz1. J Cell Biol *172*, 139-149. 10.1083/jcb.200506057.

Ghosh, M., Saha, S., Bettke, J., Nagar, R., Parrales, A., Iwakuma, T., van der Velden, A.W.M., and Martinez, L.A. (2021). Mutant p53 suppresses innate immune signaling to promote tumorigenesis. Cancer Cell *39*, 494-508.e495. 10.1016/j.ccell.2021.01.003.

Ghosh, S., Guimaraes, J.C., Lanzafame, M., Schmidt, A., Syed, A.P., Dimitriades, B., Börsch, A., Ghosh, S., Mittal, N., Montavon, T., et al. (2020). Prevention of dsRNA-induced interferon signaling by AGO1x is linked to breast cancer cell proliferation. Embo j *39*, e103922. 10.15252/embj.2019103922.

Gillen, S., Schuster, T., Meyer Zum Büschenfelde, C., Friess, H., and Kleeff, J. (2010). Preoperative/neoadjuvant therapy in pancreatic cancer: a systematic review and meta-analysis of response and resection percentages. PLoS Med *7*, e1000267. 10.1371/journal.pmed.1000267.

Granados, D.P., Tanguay, P.-L., Hardy, M.-P., Caron, É., de Verteuil, D., Meloche, S., and Perreault, C. (2009). ER stress affects processing of MHC class I-associated peptides. BMC Immunology *10*, 10. 10.1186/1471-2172-10-10.

Grard, M., Chatelain, C., Delaunay, T., Pons-Tostivint, E., Bennouna, J., and Fonteneau, J.-F. (2021). Homozygous Co-Deletion of Type I Interferons and CDKN2A Genes in Thoracic Cancers: Potential Consequences for Therapy. Frontiers in oncology *11*, 695770-695770. 10.3389/fonc.2021.695770.

Gray, J.H., Owen, R.P., and Giacomini, K.M. (2004). The concentrative nucleoside transporter family, SLC28. Pflugers Arch *447*, 728-734. 10.1007/s00424-003-1107-y.

Greasley, P.J., Bonnard, C., and Amati, B. (2000). Myc induces the nucleolin and BN51 genes: possible implications in ribosome biogenesis. Nucleic Acids Res *28*, 446-453. 10.1093/nar/28.2.446.

Guo, H., Chitiprolu, M., Gagnon, D., Meng, L., Perez-Iratxeta, C., Lagace, D., and Gibbings, D. (2014). Autophagy supports genomic stability by degrading retrotransposon RNA. Nature Communications *5*, 5276. 10.1038/ncomms6276.

Haag, S.M., Gulen, M.F., Reymond, L., Gibelin, A., Abrami, L., Decout, A., Heymann, M., van der Goot, F.G., Turcatti, G., Behrendt, R., and Ablasser, A. (2018). Targeting STING with covalent small-molecule inhibitors. Nature *559*, 269-273. 10.1038/s41586-018-0287-8.

Haferkamp, S., Borst, A., Adam, C., Becker, T.M., Motschenbacher, S., Windhovel, S., Hufnagel, A.L., Houben, R., and Meierjohann, S. (2013). Vemurafenib induces senescence features in melanoma cells. J Invest Dermatol *133*, 1601-1609. 10.1038/jid.2013.6.

Halcrow, P.W., Geiger, J.D., and Chen, X. (2021). Overcoming Chemoresistance: Altering pH of Cellular Compartments by Chloroquine and Hydroxychloroquine. Frontiers in Cell and Developmental Biology *9*. 10.3389/fcell.2021.627639.

Hall, W.A., and Goodman, K.A. (2019). Radiation therapy for pancreatic adenocarcinoma, a treatment option that must be considered in the management of a devastating malignancy. Radiat Oncol *14*, 114. 10.1186/s13014-019-1277-1.

Hamperl, S., Bocek, M.J., Saldivar, J.C., Swigut, T., and Cimprich, K.A. (2017). Transcription-Replication Conflict Orientation Modulates R-Loop Levels and Activates Distinct DNA Damage Responses. Cell *170*, 774-786.e719. 10.1016/j.cell.2017.07.043.

Hanahan, D., and Weinberg, Robert A. (2011). Hallmarks of Cancer: The Next Generation. Cell *144*, 646-674. 10.1016/j.cell.2011.02.013.

Hase, K., Contu, V.R., Kabuta, C., Sakai, R., Takahashi, M., Kataoka, N., Hakuno, F., Takahashi, S.I., Fujiwara, Y., Wada, K., and Kabuta, T. (2020). Cytosolic domain of SIDT2 carries an arginine-rich motif that binds to RNA/DNA and is important for the direct transport of nucleic acids into lysosomes. Autophagy *16*, 1974-1988. 10.1080/15548627.2020.1712109.

Haux, J., Klepp, O., Spigset, O., and Tretli, S. (2001). Digitoxin medication and cancer; case control and internal dose-response studies. BMC Cancer *1*, 11. 10.1186/1471-2407-1-11.

He, J., Gerstenlauer, M., Chan, L.K., Leithäuser, F., Yeh, M.M., Wirth, T., and Maier, H.J. (2019). Block of NF-kB signaling accelerates MYC-driven hepatocellular carcinogenesis and modifies the tumor phenotype towards combined hepatocellular cholangiocarcinoma. Cancer Lett *458*, 113-122. 10.1016/j.canlet.2019.05.023.

Hegde, S., Krisnawan, V.E., Herzog, B.H., Zuo, C., Breden, M.A., Knolhoff, B.L., Hogg, G.D., Tang, J.P., Baer, J.M., Mpoy, C., et al. (2020). Dendritic Cell Paucity Leads to Dysfunctional Immune Surveillance in Pancreatic Cancer. Cancer Cell *37*, 289-307.e289. 10.1016/j.ccell.2020.02.008.

Heo, J.M., Ordureau, A., Swarup, S., Paulo, J.A., Shen, K., Sabatini, D.M., and Harper, J.W. (2018). RAB7A phosphorylation by TBK1 promotes mitophagy via the PINK-PARKIN pathway. Sci Adv *4*, eaav0443. 10.1126/sciadv.aav0443.

Hernandez, A.J., Zovoilis, A., Cifuentes-Rojas, C., Han, L., Bujisic, B., and Lee, J.T. (2020). B2 and ALU retrotransposons are self-cleaving ribozymes whose activity is enhanced by EZH2. Proceedings of the National Academy of Sciences *117*, 415-425. doi:10.1073/pnas.1917190117.

Herold, S., Hock, A., Herkert, B., Berns, K., Mullenders, J., Beijersbergen, R., Bernards, R., and Eilers, M. (2008). Miz1 and HectH9 regulate the stability of the checkpoint protein, TopBP1. Embo j *27*, 2851-2861. 10.1038/emboj.2008.200.

Herold, S., Kalb, J., Buchel, G., Ade, C.P., Baluapuri, A., Xu, J., Koster, J., Solvie, D., Carstensen, A., Klotz, C., et al. (2019). Recruitment of BRCA1 limits MYCN-driven accumulation of stalled RNA polymerase. Nature *567*, 545-549. 10.1038/s41586-019-1030-9.

Herold, S., Wanzel, M., Beuger, V., Frohme, C., Beul, D., Hillukkala, T., Syvaoja, J., Saluz, H.P., Haenel, F., and Eilers, M. (2002). Negative regulation of the mammalian UV response by Myc through association with Miz-1. Mol Cell *10*, 509-521.

Hessmann, E., Schneider, G., Ellenrieder, V., and Siveke, J.T. (2016). MYC in pancreatic cancer: novel mechanistic insights and their translation into therapeutic strategies. Oncogene *35*, 1609-1618. 10.1038/onc.2015.216.

Hingorani, S.R., Petricoin, E.F., Maitra, A., Rajapakse, V., King, C., Jacobetz, M.A., Ross, S., Conrads, T.P., Veenstra, T.D., Hitt, B.A., et al. (2003). Preinvasive and invasive ductal pancreatic cancer and its early detection in the mouse. Cancer Cell *4*, 437-450. 10.1016/s1535-6108(03)00309-x.

Hingorani, S.R., Wang, L., Multani, A.S., Combs, C., Deramaudt, T.B., Hruban, R.H., Rustgi, A.K., Chang, S., and Tuveson, D.A. (2005). Trp53R172H and KrasG12D cooperate to promote chromosomal instability and widely metastatic pancreatic ductal adenocarcinoma in mice. Cancer Cell *7*, 469-483. 10.1016/j.ccr.2005.04.023.

Honda, K., Takaoka, A., and Taniguchi, T. (2006). Type I Inteferon Gene Induction by the Interferon Regulatory Factor Family of Transcription Factors. Immunity *25*, 349-360. https://doi.org/10.1016/j.immuni.2006.08.009.

Hoong, B.Y.D., Gan, Y.H., Liu, H., and Chen, E.S. (2020). cGAS-STING pathway in oncogenesis and cancer therapeutics. Oncotarget *11*, 2930-2955. 10.18632/oncotarget.27673.

Hou, A.J., Chen, L.C., and Chen, Y.Y. (2021). Navigating CAR-T cells through the solid-tumour microenvironment. Nature Reviews Drug Discovery *20*, 531-550. 10.1038/s41573-021-00189-2.

Huang, C.H., Lujambio, A., Zuber, J., Tschaharganeh, D.F., Doran, M.G., Evans, M.J., Kitzing, T., Zhu, N., de Stanchina, E., Sawyers, C.L., et al. (2014). CDK9-mediated transcription elongation is required for MYC addiction in hepatocellular carcinoma. Genes Dev *28*, 1800-1814. 10.1101/gad.244368.114.

Hubley, R., Finn, R.D., Clements, J., Eddy, S.R., Jones, T.A., Bao, W., Smit, A.F.A., and Wheeler, T.J. (2015). The Dfam database of repetitive DNA families. Nucleic Acids Research *44*, D81-D89. 10.1093/nar/gkv1272.

Hurlin, P.J., Zhou, Z.Q., Toyo-oka, K., Ota, S., Walker, W.L., Hirotsune, S., and Wynshaw-Boris, A. (2003). Deletion of Mnt leads to disrupted cell cycle control and tumorigenesis. Embo j *22*, 4584-4596. 10.1093/emboj/cdg442.

Iadevaia, V., Burke, J.M., Eke, L., Moller-Levet, C., Parker, R., and Locker, N. (2021). Paracrine granules are cytoplasmic RNP granules distinct from stress granules that assemble in response to viral infection. bioRxiv, 2021.2008.2006.455464. 10.1101/2021.08.06.455464.

Jaenicke, L.A., von Eyss, B., Carstensen, A., Wolf, E., Xu, W., Greifenberg, A.K., Geyer, M., Eilers, M., and Popov, N. (2016). Ubiquitin-Dependent Turnover of MYC Antagonizes MYC/PAF1C Complex Accumulation to Drive Transcriptional Elongation. Mol Cell *61*, 54-67. 10.1016/j.molcel.2015.11.007.

Jakkampudi, A., Jangala, R., Reddy, B.R., Mitnala, S., Nageshwar Reddy, D., and Talukdar, R. (2016). NF-κB in acute pancreatitis: Mechanisms and therapeutic potential. Pancreatology *16*, 477-488. 10.1016/j.pan.2016.05.001.

Janeway, C. (1999). Immunobiology : the immune system in health and disease, 4th Edition (Current Biology Publications ;
Garland Pub.).

Janeway, C. (2005). Immunobiology : the immune system in health and disease, 6th Edition (Garland Science).

Jelinek, I., Leonard, J.N., Price, G.E., Brown, K.N., Meyer-Manlapat, A., Goldsmith, P.K., Wang, Y., Venzon, D., Epstein, S.L., and Segal, D.M. (2011). TLR3-specific double-stranded RNA oligonucleotide adjuvants induce dendritic cell cross-presentation, CTL responses, and antiviral protection. Journal of immunology (Baltimore, Md. : 1950) *186*, 2422-2429. 10.4049/jimmunol.1002845.

Jongsma, M.L.M., Guarda, G., and Spaapen, R.M. (2019). The regulatory network behind MHC class I expression. Molecular Immunology *113*, 16-21. https://doi.org/10.1016/j.molimm.2017.12.005.

Jurka, J., Kohany, O., Pavlicek, A., Kapitonov, V.V., and Jurka, M.V. (2004). Duplication, coclustering, and selection of human Alu retrotransposons. Proceedings of the National Academy of Sciences of the United States of America *101*, 1268-1272. 10.1073/pnas.0308084100.

Kalkat, M., Resetca, D., Lourenco, C., Chan, P.-K., Wei, Y., Shiah, Y.-J., Vitkin, N., Tong, Y., Sunnerhagen, M., Done, S.J., et al. (2018). MYC Protein Interactome Profiling Reveals Functionally Distinct Regions that Cooperate to Drive Tumorigenesis. Molecular Cell *72*, 836-848.e837. https://doi.org/10.1016/j.molcel.2018.09.031.

Kaneko, H., Dridi, S., Tarallo, V., Gelfand, B.D., Fowler, B.J., Cho, W.G., Kleinman, M.E., Ponicsan, S.L., Hauswirth, W.W., Chiodo, V.A., et al. (2011). DICER1 deficit induces Alu RNA toxicity in age-related macular degeneration. Nature *471*, 325-330. 10.1038/nature09830.

Kao, C.-Y., and Papoutsakis, E.T. (2019). Extracellular vesicles: exosomes, microparticles, their parts, and their targets to enable their biomanufacturing and clinical applications. Current Opinion in Biotechnology *60*, 89-98. https://doi.org/10.1016/j.copbio.2019.01.005.

Kärre, K. (2002). NK cells, MHC class I molecules and the missing self. Scand J Immunol *55*, 221-228. 10.1046/j.1365-3083.2002.01053.x.

Kärre, K., Ljunggren, H.G., Piontek, G., and Kiessling, R. (1986). Selective rejection of H-2-deficient lymphoma variants suggests alternative immune defence strategy. Nature *319*, 675-678. 10.1038/319675a0.

Kato, H., Takeuchi, O., Mikamo-Satoh, E., Hirai, R., Kawai, T., Matsushita, K., Hiiragi, A., Dermody, T.S., Fujita, T., and Akira, S. (2008). Length-dependent recognition of double-stranded ribonucleic acids by retinoic acid-inducible gene-I and melanoma differentiation-associated gene 5. J Exp Med *205*, 1601-1610. 10.1084/jem.20080091.

Kawai, T., and Akira, S. (2007). Signaling to NF-kappaB by Toll-like receptors. Trends Mol Med *13*, 460-469. 10.1016/j.molmed.2007.09.002.

Kim, D., Pertea, G., Trapnell, C., Pimentel, H., Kelley, R., and Salzberg, S.L. (2013). TopHat2: accurate alignment of transcriptomes in the presence of insertions, deletions and gene fusions. Genome Biology *14*, R36. 10.1186/gb-2013-14-4-r36.

Klapproth, K., Sander, S., Marinkovic, D., Baumann, B., and Wirth, T. (2009). The IKK2/NF-κB pathway suppresses MYC-induced lymphomagenesis. Blood *114*, 2448-2458. 10.1182/blood-2008-09-181008.

Klein, L., Kyewski, B., Allen, P.M., and Hogquist, K.A. (2014). Positive and negative selection of the T cell repertoire: what thymocytes see (and don't see). Nature reviews. Immunology *14*, 377-391. 10.1038/nri3667.

Kohl, N.E., Kanda, N., Schreck, R.R., Bruns, G., Latt, S.A., Gilbert, F., and Alt, F.W. (1983). Transposition and amplification of oncogene-related sequences in human neuroblastomas. Cell *35*, 359-367. https://doi.org/10.1016/0092-8674(83)90169-1.

Komatsu, M., Waguri, S., Ueno, T., Iwata, J., Murata, S., Tanida, I., Ezaki, J., Mizushima, N., Ohsumi, Y., Uchiyama, Y., et al. (2005a). Impairment of starvation-induced and constitutive autophagy in Atg7-deficient mice. The Journal of cell biology *169*, 425-434. 10.1083/jcb.200412022.

Kong, W., Engel, K., and Wang, J. (2004). Mammalian nucleoside transporters. Curr Drug Metab *5*, 63-84. 10.2174/1389200043489162.

Kopp, J.L., von Figura, G., Mayes, E., Liu, F.F., Dubois, C.L., Morris, J.P.t., Pan, F.C., Akiyama, H., Wright, C.V., Jensen, K., et al. (2012). Identification of Sox9-dependent acinar-to-ductal reprogramming as the principal mechanism for initiation of pancreatic ductal adenocarcinoma. Cancer Cell *22*, 737-750. 10.1016/j.ccr.2012.10.025.

Koppenol, W.H., Bounds, P.L., and Dang, C.V. (2011). Otto Warburg's contributions to current concepts of cancer metabolism. Nat Rev Cancer *11*, 325-337. 10.1038/nrc3038.

Kortlever, R.M., Sodir, N.M., Wilson, C.H., Burkhart, D.L., Pellegrinet, L., Brown Swigart, L., Littlewood, T.D., and Evan, G.I. (2017). Myc Cooperates with Ras by Programming Inflammation and Immune Suppression. Cell *171*, 1301-1315 e1314. 10.1016/j.cell.2017.11.013.

Kosan, C., Saba, I., Godmann, M., Herold, S., Herkert, B., Eilers, M., and Möröy, T. (2010). Transcription factor miz-1 is required to regulate interleukin-7 receptor signaling at early commitment stages of B cell differentiation. Immunity *33*, 917-928. 10.1016/j.immuni.2010.11.028.

Krayev, A.S., Markusheva, T.V., Kramerov, D.A., Ryskov, A.P., Skryabin, K.G., Bayev, A.A., and Georgiev, G.P. (1982). Ubiquitous transposon-like repeats B1 and B2 of the mouse genome: B2 sequencing. Nucleic acids research *10*, 7461-7475. 10.1093/nar/10.23.7461.

Krenz, B., Gebhardt-Wolf, A., Ade, C.P., Gaballa, A., Roehrig, F., Vendelova, E., Baluapuri, A., Eilers, U., Gallant, P., L, D.A., et al. (2021). MYC- and MIZ1-dependent vesicular transport of double-strand RNA controls immune evasion in pancreatic ductal adenocarcinoma. Cancer Res. 10.1158/0008-5472.Can-21-1677.

Kress, T.R., Pellanda, P., Pellegrinet, L., Bianchi, V., Nicoli, P., Doni, M., Recordati, C., Bianchi, S., Rotta, L., Capra, T., et al. (2016). Identification of MYC-Dependent Transcriptional Programs in Oncogene-Addicted Liver Tumors. Cancer Research *76*, 3463. 10.1158/0008-5472.CAN-16-0316.

Kress, T.R., Sabo, A., and Amati, B. (2015). MYC: connecting selective transcriptional control to global RNA production. Nat Rev Cancer *15*, 593-607. 10.1038/nrc3984.

Kretzner, L., Blackwood, E.M., and Eisenman, R.N. (1992). Myc and Max proteins possess distinct transcriptional activities. Nature *359*, 426-429. 10.1038/359426a0.

Kumar, V. (2021). The Trinity of cGAS, TLR9, and ALRs Guardians of the Cellular Galaxy Against Host-Derived Self-DNA. Frontiers in Immunology *11*. 10.3389/fimmu.2020.624597.

Labun, K., Montague, T.G., Krause, M., Torres Cleuren, Y.N., Tjeldnes, H., and Valen, E. (2019). CHOPCHOP v3: expanding the CRISPR web toolbox beyond genome editing. Nucleic acids research *47*, W171-W174. 10.1093/nar/gkz365.

Lan, Y.-L., Wang, X., Lou, J.-C., Xing, J.-S., Yu, Z.-L., Wang, H., Zou, S., Ma, X., and Zhang, B. (2018). Bufalin inhibits glioblastoma growth by promoting proteasomal degradation of the Na+/K+-ATPase α1 subunit. Biomedicine & Pharmacotherapy *103*, 204-215. https://doi.org/10.1016/j.biopha.2018.04.030.

Lánczky, A., and Győrffy, B. (2021). Web-Based Survival Analysis Tool Tailored for Medical Research (KMplot): Development and Implementation. J Med Internet Res *23*, e27633. 10.2196/27633.

Land, H., Parada, L.F., and Weinberg, R.A. (1983). Tumorigenic conversion of primary embryo fibroblasts requires at least two cooperating oncogenes. Nature *304*, 596-602. 10.1038/304596a0.

Langmead, B., and Salzberg, S.L. (2012). Fast gapped-read alignment with Bowtie 2. Nat Methods *9*, 357-359. 10.1038/nmeth.1923.

Larsson, C., Påhlman, I.L., and Gustafsson, L. (2000). The importance of ATP as a regulator of glycolytic flux in Saccharomyces cerevisiae. Yeast *16*, 797-809. 10.1002/1097-0061(20000630)16:9<797::Aid-yea553>3.0.Co;2-5.

Lauss, M., Donia, M., Harbst, K., Andersen, R., Mitra, S., Rosengren, F., Salim, M., Vallon-Christersson, J., Törngren, T., Kvist, A., et al. (2017). Mutational and putative neoantigen load predict clinical benefit of adoptive T cell therapy in melanoma. Nature Communications *8*, 1738. 10.1038/s41467-017-01460-0.

Layer, J.P., Kronmüller, M.T., Quast, T., van den Boorn-Konijnenberg, D., Effern, M., Hinze, D., Althoff, K., Schramm, A., Westermann, F., Peifer, M., et al. (2017). Amplification of N-Myc is associated with a T-cell-poor microenvironment in metastatic neuroblastoma restraining interferon pathway activity and chemokine expression. Oncoimmunology *6*, e1320626. 10.1080/2162402x.2017.1320626.

Leder, A., Pattengale, P.K., Kuo, A., Stewart, T.A., and Leder, P. (1986). Consequences of widespread deregulation of the c-myc gene in transgenic mice: Multiple neoplasms and normal development. Cell *45*, 485-495. https://doi.org/10.1016/0092-8674(86)90280-1.

Lee, B.L., and Barton, G.M. (2014). Trafficking of endosomal Toll-like receptors. Trends in cell biology *24*, 360-369. 10.1016/j.tcb.2013.12.002.

Lee, H.K., Dunzendorfer, S., Soldau, K., and Tobias, P.S. (2006). Double-stranded RNA-mediated TLR3 activation is enhanced by CD14. Immunity *24*, 153-163. 10.1016/j.immuni.2005.12.012.

Lee, J.V., Housley, F., Yau, C., Nakagawa, R., Winkler, J., Anttila, J.M., Munne, P.M., Savelius, M., Houlahan, K.E., Van de Mark, D., et al. (2022a). Combinatorial immunotherapies overcome MYC-driven immune evasion in triple negative breast cancer. Nature Communications *13*, 3671. 10.1038/s41467-022-31238-y.

Lee, K.M., Lin, C.C., Servetto, A., Bae, J., Kandagatla, V., Ye, D., Kim, G., Sudhan, D.R., Mendiratta, S., González Ericsson, P.I., et al. (2022b). Epigenetic Repression of STING by MYC Promotes Immune

Evasion and Resistance to Immune Checkpoint Inhibitors in Triple-Negative Breast Cancer. Cancer Immunol Res *10*, 829-843. 10.1158/2326-6066.Cir-21-0826.

Leonard, J.N., Ghirlando, R., Askins, J., Bell, J.K., Margulies, D.H., Davies, D.R., and Segal, D.M. (2008). The TLR3 signaling complex forms by cooperative receptor dimerization. Proc Natl Acad Sci U S A *105*, 258-263. 10.1073/pnas.0710779105.

Leone, G., Sears, R., Huang, E., Rempel, R., Nuckolls, F., Park, C.H., Giangrande, P., Wu, L., Saavedra, H.I., Field, S.J., et al. (2001). Myc requires distinct E2F activities to induce S phase and apoptosis. Mol Cell *8*, 105-113.

Li, D., and Wu, M. (2021). Pattern recognition receptors in health and diseases. Signal Transduction and Targeted Therapy *6*, 291. 10.1038/s41392-021-00687-0.

Li, F., Wang, Y., Zeller, K.I., Potter, J.J., Wonsey, D.R., O'Donnell, K.A., Kim, J.W., Yustein, J.T., Lee, L.A., and Dang, C.V. (2005). Myc stimulates nuclearly encoded mitochondrial genes and mitochondrial biogenesis. Mol Cell Biol *25*, 6225-6234. 10.1128/MCB.25.14.6225-6234.2005.

Li, J., Qian, W., Qin, T., Xiao, Y., Cheng, L., Cao, J., Chen, X., Ma, Q., and Wu, Z. (2019a). Mouse-Derived Allografts: A Complementary Model to the KPC Mice on Researching Pancreatic Cancer In Vivo. Comput Struct Biotechnol J *17*, 498-506. 10.1016/j.csbj.2019.03.016.

Li, J.T., Wang, Y.P., Yin, M., and Lei, Q.Y. (2019b). Metabolism remodeling in pancreatic ductal adenocarcinoma. Cell Stress *3*, 361-368. 10.15698/cst2019.12.205.

Liao, Y., Smyth, G.K., and Shi, W. (2019). The R package Rsubread is easier, faster, cheaper and better for alignment and quantification of RNA sequencing reads. Nucleic Acids Res *47*, e47. 10.1093/nar/gkz114.

Liberti, M.V., and Locasale, J.W. (2016). The Warburg Effect: How Does it Benefit Cancer Cells? Trends Biochem Sci *41*, 211-218. 10.1016/j.tibs.2015.12.001.

Liberzon, A., Birger, C., Thorvaldsdottir, H., Ghandi, M., Mesirov, J.P., and Tamayo, P. (2015). The Molecular Signatures Database (MSigDB) hallmark gene set collection. Cell Syst *1*, 417-425. 10.1016/j.cels.2015.12.004.

Liddicoat, B.J., Piskol, R., Chalk, A.M., Ramaswami, G., Higuchi, M., Hartner, J.C., Li, J.B., Seeburg, P.H., and Walkley, C.R. (2015). RNA editing by ADAR1 prevents MDA5 sensing of endogenous dsRNA as nonself. Science *349*, 1115-1120. 10.1126/science.aac7049.

Liehr, T. (2021). Repetitive Elements in Humans. International journal of molecular sciences *22*, 2072. 10.3390/ijms22042072.

Lin, C.Y., Lovén, J., Rahl, P.B., Paranal, R.M., Burge, C.B., Bradner, J.E., Lee, T.I., and Young, R.A. (2012). Transcriptional amplification in tumor cells with elevated c-Myc. Cell *151*, 56-67. 10.1016/j.cell.2012.08.026.

Lin, W., Noel, P., Borazanci, E.H., Lee, J., Amini, A., Han, I.W., Heo, J.S., Jameson, G.S., Fraser, C., Steinbach, M., et al. (2020). Single-cell transcriptome analysis of tumor and stromal compartments of pancreatic ductal adenocarcinoma primary tumors and metastatic lesions. Genome Medicine *12*, 80. 10.1186/s13073-020-00776-9.

Lin, Y., Xu, J., and Lan, H. (2019). Tumor-associated macrophages in tumor metastasis: biological roles and clinical therapeutic applications. Journal of Hematology & Oncology *12*, 76. 10.1186/s13045-019-0760-3.

Lin, Y.-L., and Pasero, P. (2017). Transcription-Replication Conflicts: Orientation Matters. Cell *170*, 603-604. 10.1016/j.cell.2017.07.040.

Linder, A., and Hornung, V. (2018). Mitochondrial dsRNA: A New DAMP for MDA5. Developmental Cell *46*, 530-532. https://doi.org/10.1016/j.devcel.2018.08.019.

Ling, J., Kang, Y., Zhao, R., Xia, Q., Lee, D.F., Chang, Z., Li, J., Peng, B., Fleming, J.B., Wang, H., et al. (2012). KrasG12D-induced IKK2/beta/NF-kappaB activation by IL-1alpha and p62 feedforward loops is required for development of pancreatic ductal adenocarcinoma. Cancer Cell *21*, 105-120. 10.1016/j.ccr.2011.12.006.

Liu, G., Rui, W., Zhao, X., and Lin, X. (2021). Enhancing CAR-T cell efficacy in solid tumors by targeting the tumor microenvironment. Cellular & Molecular Immunology *18*, 1085-1095. 10.1038/s41423-021-00655-2.

Liu, L., Ulbrich, J., Müller, J., Wüstefeld, T., Aeberhard, L., Kress, T.R., Muthalagu, N., Rycak, L., Rudalska, R., Moll, R., et al. (2012). Deregulated MYC expression induces dependence upon AMPK-related kinase 5. Nature *483*, 608-612. 10.1038/nature10927.

Liu, T., Zhang, L., Joo, D., and Sun, S.-C. (2017). NF-κB signaling in inflammation. Signal Transduction and Targeted Therapy *2*, 17023. 10.1038/sigtrans.2017.23.

Lorenzin, F., Benary, U., Baluapuri, A., Walz, S., Jung, L.A., von Eyss, B., Kisker, C., Wolf, J., Eilers, M., and Wolf, E. (2016). Different promoter affinities account for specificity in MYC-dependent gene regulation. Elife *5*. 10.7554/eLife.15161.

Lovén, J., Orlando, David A., Sigova, Alla A., Lin, Charles Y., Rahl, Peter B., Burge, Christopher B., Levens, David L., Lee, Tong I., and Young, Richard A. (2012). Revisiting Global Gene Expression Analysis. Cell *151*, 476-482. 10.1016/j.cell.2012.10.012.

Lu, C., Klement, J.D., Ibrahim, M.L., Xiao, W., Redd, P.S., Nayak-Kapoor, A., Zhou, G., and Liu, K. (2019). Type I interferon suppresses tumor growth through activating the STAT3-granzyme B pathway in tumor-infiltrating cytotoxic T lymphocytes. Journal for ImmunoTherapy of Cancer *7*, 157. 10.1186/s40425-019-0635-8.

Macheret, M., and Halazonetis, T.D. (2018). Intragenic origins due to short G1 phases underlie oncogene-induced DNA replication stress. Nature *555*, 112-116. 10.1038/nature25507.

Mackenzie, K.J., Carroll, P., Martin, C.A., Murina, O., Fluteau, A., Simpson, D.J., Olova, N., Sutcliffe, H., Rainger, J.K., Leitch, A., et al. (2017). cGAS surveillance of micronuclei links genome instability to innate immunity. Nature *548*, 461-465. 10.1038/nature23449.

Maharana, S., Kretschmer, S., Hunger, S., Yan, X., Kuster, D., Traikov, S., Zillinger, T., Gentzel, M., Elangovan, S., Dasgupta, P., et al. (2022). SAMHD1 controls innate immunity by regulating condensation of immunogenic self RNA. Molecular Cell *82*, 3712-3728.e3710. 10.1016/j.molcel.2022.08.031.

Malynn, B.A., de Alboran, I.M., O'Hagan, R.C., Bronson, R., Davidson, L., DePinho, R.A., and Alt, F.W. (2000). N-myc can functionally replace c-myc in murine development, cellular growth, and differentiation. Genes Dev *14*, 1390-1399.

Mapperley, C., van de Lagemaat, L.N., Lawson, H., Tavosanis, A., Paris, J., Campos, J., Wotherspoon, D., Durko, J., Sarapuu, A., Choe, J., et al. (2020). The mRNA m6A reader YTHDF2 suppresses proinflammatory pathways and sustains hematopoietic stem cell function. Journal of Experimental Medicine *218*, e20200829. 10.1084/jem.20200829.

Marar, C., Starich, B., and Wirtz, D. (2021). Extracellular vesicles in immunomodulation and tumor progression. Nature Immunology *22*, 560-570. 10.1038/s41590-021-00899-0.

Marofi, F., Motavalli, R., Safonov, V.A., Thangavelu, L., Yumashev, A.V., Alexander, M., Shomali, N., Chartrand, M.S., Pathak, Y., Jarahian, M., et al. (2021). CAR T cells in solid tumors: challenges and opportunities. Stem Cell Research & Therapy *12*, 81. 10.1186/s13287-020-02128-1.

Marshall, J.S., Warrington, R., Watson, W., and Kim, H.L. (2018). An introduction to immunology and immunopathology. Allergy, Asthma & Clinical Immunology *14*, 49. 10.1186/s13223-018-0278-1.

Mathsyaraja, H., Freie, B., Cheng, P.F., Babaeva, E., Catchpole, J.T., Janssens, D., Henikoff, S., and Eisenman, R.N. (2019). Max deletion destabilizes MYC protein and abrogates E*μ*-Myc lymphomagenesis. Genes Dev *33*, 1252-1264. 10.1101/gad.325878.119.

Matsumoto, M., Funami, K., Tanabe, M., Oshiumi, H., Shingai, M., Seto, Y., Yamamoto, A., and Seya, T. (2003). Subcellular Localization of Toll-Like Receptor 3 in Human Dendritic Cells. The Journal of Immunology *171*, 3154. 10.4049/jimmunol.171.6.3154.

Matsumoto, M., Funami, K., Tatematsu, M., Azuma, M., and Seya, T. (2014). Assessment of the Toll-like receptor 3 pathway in endosomal signaling. Methods Enzymol *535*, 149-165. 10.1016/b978-0-12-397925-4.00010-9.

Mauthe, M., Orhon, I., Rocchi, C., Zhou, X., Luhr, M., Hijlkema, K.J., Coppes, R.P., Engedal, N., Mari, M., and Reggiori, F. (2018). Chloroquine inhibits autophagic flux by decreasing autophagosome-lysosome fusion. Autophagy *14*, 1435-1455. 10.1080/15548627.2018.1474314.

McGranahan, N., Furness Andrew, J.S., Rosenthal, R., Ramskov, S., Lyngaa, R., Saini Sunil, K., Jamal-Hanjani, M., Wilson Gareth, A., Birkbak Nicolai, J., Hiley Crispin, T., et al. (2016). Clonal neoantigens elicit T cell immunoreactivity and sensitivity to immune checkpoint blockade. Science *351*, 1463-1469. 10.1126/science.aaf1490.

McMahon, S.B., Van Buskirk, H.A., Dugan, K.A., Copeland, T.D., and Cole, M.D. (1998). The Novel ATM-Related Protein TRRAP Is an Essential Cofactor for the c-Myc and E2F Oncoproteins. Cell *94*, 363-374. https://doi.org/10.1016/S0092-8674(00)81479-8.

Medzhitov, R., and Janeway, C.A., Jr. (1997). Innate immunity: impact on the adaptive immune response. Curr Opin Immunol *9*, 4-9. 10.1016/s0952-7915(97)80152-5.

Medzhitov, R., Preston-Hurlburt, P., and Janeway, C.A. (1997). A human homologue of the Drosophila Toll protein signals activation of adaptive immunity. Nature *388*, 394-397. 10.1038/41131.

Menger, L., Vacchelli, E., Adjemian, S., Martins, I., Ma, Y., Shen, S., Yamazaki, T., Sukkurwala, A.Q., Michaud, M., Mignot, G., et al. (2012). Cardiac Glycosides Exert Anticancer Effects by Inducing Immunogenic Cell Death. Science Translational Medicine *4*, 143ra199-143ra199. doi:10.1126/scitranslmed.3003807.

Merrikh, H. (2017). Spatial and Temporal Control of Evolution through Replication–Transcription Conflicts. Trends in Microbiology *25*, 515-521. 10.1016/j.tim.2017.01.008.

Mertz, J.A., Conery, A.R., Bryant, B.M., Sandy, P., Balasubramanian, S., Mele, D.A., Bergeron, L., and Sims, R.J. (2011). Targeting MYC dependence in cancer by inhibiting BET bromodomains. Proceedings of the National Academy of Sciences *108*, 16669-16674. 10.1073/pnas.1108190108.

Mikulasova, A., Ashby, C.C., Tytarenko, R.G., Bauer, M., Mavrommatis, K., Wardell, C.P., Trotter, M., Deshpande, S., Stephens, O.W., Tian, E., et al. (2017). MYC Rearrangements in Multiple Myeloma Are Complex, Can Involve More Than Five Different Chromosomes, and Correlate with Increased Expression of MYC and a Distinct Downstream Gene Expression Pattern. Blood *130*, 65-65. 10.1182/blood.V130.Suppl_1.65.65.

Mora, J., Alaminos, M., de Torres, C., Illei, P., Qin, J., Cheung, N.K.V., and Gerald, W.L. (2004). Comprehensive analysis of the 9p21 region in neuroblastoma suggests a role for genes mapping to

9p21–23 in the biology of favourable stage 4 tumours. British Journal of Cancer *91*, 1112-1118. 10.1038/sj.bjc.6602094.

Morel, K.L., Sheahan, A.V., Burkhart, D.L., Baca, S.C., Boufaied, N., Liu, Y., Qiu, X., Cañadas, I., Roehle, K., Heckler, M., et al. (2021). EZH2 inhibition activates a dsRNA–STING–interferon stress axis that potentiates response to PD-1 checkpoint blockade in prostate cancer. Nature Cancer *2*, 444-456. 10.1038/s43018-021-00185-w.

Morris, J.P.t., Wang, S.C., and Hebrok, M. (2010). KRAS, Hedgehog, Wnt and the twisted developmental biology of pancreatic ductal adenocarcinoma. Nat Rev Cancer *10*, 683-695. 10.1038/nrc2899.

Mosser, D.M., Hamidzadeh, K., and Goncalves, R. (2021). Macrophages and the maintenance of homeostasis. Cellular & Molecular Immunology *18*, 579-587. 10.1038/s41423-020-00541-3.

Mueller, S., Engleitner, T., Maresch, R., Zukowska, M., Lange, S., Kaltenbacher, T., Konukiewitz, B., Ollinger, R., Zwiebel, M., Strong, A., et al. (2018). Evolutionary routes and KRAS dosage define pancreatic cancer phenotypes. Nature. 10.1038/nature25459.

Mukherjee, S., Hurt, C.N., Bridgewater, J., Falk, S., Cummins, S., Wasan, H., Crosby, T., Jephcott, C., Roy, R., Radhakrishna, G., et al. (2013). Gemcitabine-based or capecitabine-based chemoradiotherapy for locally advanced pancreatic cancer (SCALOP): a multicentre, randomised, phase 2 trial. Lancet Oncol *14*, 317-326. 10.1016/s1470-2045(13)70021-4.

Müller-Esterl, W. (2004). Biochemie : eine Einführung für Mediziner und Naturwissenschaftler (Elsevier, Spektrum, Akad. Verl, München).

Multhoff, G., and Vaupel, P. (2021). Lactate-avid regulatory T cells: metabolic plasticity controls immunosuppression in tumour microenvironment. Signal Transduction and Targeted Therapy *6*, 171. 10.1038/s41392-021-00598-0.

Muthalagu, N., Monteverde, T., Raffo-Iraolagoitia, X., Wiesheu, R., Whyte, D., Hedley, A., Laing, S., Kruspig, B., Upstill-Goddard, R., Shaw, R., et al. (2020). Repression of the Type I Interferon Pathway Underlies MYC- and KRAS-Dependent Evasion of NK and B Cells in Pancreatic Ductal Adenocarcinoma. Cancer Discov *10*, 872-887. 10.1158/2159-8290.Cd-19-0620.

Nagy, Á., Munkácsy, G., and Győrffy, B. (2021). Pancancer survival analysis of cancer hallmark genes. Sci Rep *11*, 6047. 10.1038/s41598-021-84787-5.

Nie, Z., Hu, G., Wei, G., Cui, K., Yamane, A., Resch, W., Wang, R., Green, D.R., Tessarollo, L., Casellas, R., et al. (2012). c-Myc is a universal amplifier of expressed genes in lymphocytes and embryonic stem cells. Cell *151*, 68-79. 10.1016/j.cell.2012.08.033.

Notari, M., Neviani, P., Santhanam, R., Blaser, B.W., Chang, J.-S., Galietta, A., Willis, A.E., Roy, D.C., Caligiuri, M.A., Marcucci, G., and Perrotti, D. (2006). A MAPK/HNRPK pathway controls BCR/ABL oncogenic potential by regulating MYC mRNA translation. Blood *107*, 2507-2516. 10.1182/blood-2005-09-3732.

Nwabugwu, C.I., Rakhra, K., Felsher, D.W., and Paik, D.S. (2013). A tumor-immune mathematical model of CD4+ T helper cell dependent tumor regression by oncogene inactivation. Conf Proc IEEE Eng Med Biol Soc *2013*, 4529-4532. 10.1109/EMBC.2013.6610554.

Oliver, G.C., Jr., Parker, B.M., Brasfield, D.L., and Parker, C.W. (1968). The measurement of digitoxin in human serum by radioimmunoassay. The Journal of Clinical Investigation *47*, 1035-1042. 10.1172/JCI105793.

Ortega, F.G., Roefs, M.T., de Miguel Perez, D., Kooijmans, S.A., de Jong, O.G., Sluijter, J.P., Schiffelers, R.M., and Vader, P. (2019). Interfering with endolysosomal trafficking enhances release of

bioactive exosomes. Nanomedicine: Nanotechnology, Biology and Medicine *20*, 102014. https://doi.org/10.1016/j.nano.2019.102014.

Orth, M., Metzger, P., Gerum, S., Mayerle, J., Schneider, G., Belka, C., Schnurr, M., and Lauber, K. (2019). Pancreatic ductal adenocarcinoma: biological hallmarks, current status, and future perspectives of combined modality treatment approaches. Radiation Oncology *14*, 141. 10.1186/s13014-019-1345-6.

Otto, T., Horn, S., Brockmann, M., Eilers, U., Schüttrumpf, L., Popov, N., Kenney, A.M., Schulte, J.H., Beijersbergen, R., Christiansen, H., et al. (2009). Stabilization of N-Myc is a critical function of Aurora A in human neuroblastoma. Cancer Cell *15*, 67-78. 10.1016/j.ccr.2008.12.005.

Ottolia, M., Torres, N., Bridge, J.H.B., Philipson, K.D., and Goldhaber, J.I. (2013). Na/Ca exchange and contraction of the heart. J Mol Cell Cardiol *61*, 28-33. 10.1016/j.yjmcc.2013.06.001.

Outlioua, A., Pourcelot, M., and Arnoult, D. (2018). The Role of Optineurin in Antiviral Type I Interferon Production. Frontiers in Immunology *9*. 10.3389/fimmu.2018.00853.

Paczulla, A.M., Rothfelder, K., Raffel, S., Konantz, M., Steinbacher, J., Wang, H., Tandler, C., Mbarga, M., Schaefer, T., Falcone, M., et al. (2019). Absence of NKG2D ligands defines leukaemia stem cells and mediates their immune evasion. Nature *572*, 254-259. 10.1038/s41586-019-1410-1.

Papadopoulos, D., Solvie, D., Baluapuri, A., Endres, T., Ha, S.A., Herold, S., Kalb, J., Giansanti, C., Schülein-Völk, C., Ade, C.P., et al. (2022). MYCN recruits the nuclear exosome complex to RNA polymerase II to prevent transcription-replication conflicts. Molecular Cell *82*, 159-176.e112. 10.1016/j.molcel.2021.11.002.

Pauken, K.E., Lagattuta, K.A., Lu, B.Y., Lucca, L.E., Daud, A.I., Hafler, D.A., Kluger, H.M., Raychaudhuri, S., and Sharpe, A.H. (2022). TCR-sequencing in cancer and autoimmunity: barcodes and beyond. Trends in Immunology *43*, 180-194. 10.1016/j.it.2022.01.002.

Pearson, T., Shultz, L.D., Miller, D., King, M., Laning, J., Fodor, W., Cuthbert, A., Burzenski, L., Gott, B., Lyons, B., et al. (2008). Non-obese diabetic-recombination activating gene-1 (NOD-Rag1 null) interleukin (IL)-2 receptor common gamma chain (IL2r gamma null) null mice: a radioresistant model for human lymphohaematopoietic engraftment. Clin Exp Immunol *154*, 270-284. 10.1111/j.1365-2249.2008.03753.x.

Pereira, B.I., Devine, O.P., Vukmanovic-Stejic, M., Chambers, E.S., Subramanian, P., Patel, N., Virasami, A., Sebire, N.J., Kinsler, V., Valdovinos, A., et al. (2019). Senescent cells evade immune clearance via HLA-E-mediated NK and CD8+ T cell inhibition. Nature Communications *10*, 2387. 10.1038/s41467-019-10335-5.

Petryk, N., Kahli, M., d'Aubenton-Carafa, Y., Jaszczyszyn, Y., Shen, Y., Silvain, M., Thermes, C., Chen, C.L., and Hyrien, O. (2016). Replication landscape of the human genome. Nat Commun *7*, 10208. 10.1038/ncomms10208.

Pham, T.N.D., Shields, M.A., Spaulding, C., Principe, D.R., Li, B., Underwood, P.W., Trevino, J.G., Bentrem, D.J., and Munshi, H.G. (2021). Preclinical Models of Pancreatic Ductal Adenocarcinoma and Their Utility in Immunotherapy Studies. Cancers (Basel) *13*. 10.3390/cancers13030440.

Pirahanchi, Y., Jessu, R., and Aeddula, N.R. (2022). Physiology, Sodium Potassium Pump. In StatPearls, (StatPearls Publishing
Copyright © 2022, StatPearls Publishing LLC.).

Pohar, J., Lainšček, D., Ivičak-Kocjan, K., Cajnko, M.-M., Jerala, R., and Benčina, M. (2017). Short single-stranded DNA degradation products augment the activation of Toll-like receptor 9. Nature Communications *8*, 15363. 10.1038/ncomms15363.

Pomerantz, J.L., and Baltimore, D. (1999). NF-kappaB activation by a signaling complex containing TRAF2, TANK and TBK1, a novel IKK-related kinase. The EMBO journal *18*, 6694-6704. 10.1093/emboj/18.23.6694.

Poncet, N., and Taylor, P.M. (2013). The role of amino acid transporters in nutrition. Current Opinion in Clinical Nutrition & Metabolic Care *16*, 57-65. 10.1097/MCO.0b013e32835a885c.

Popay, T.M., Wang, J., Adams, C.M., Howard, G.C., Codreanu, S.G., Sherrod, S.D., McLean, J.A., Thomas, L.R., Lorey, S.L., Machida, Y.J., et al. (2021). MYC regulates ribosome biogenesis and mitochondrial gene expression programs through its interaction with host cell factor-1. Elife *10*. 10.7554/eLife.60191.

Popov, N., Herold, S., Llamazares, M., Schulein, C., and Eilers, M. (2007a). Fbw7 and Usp28 regulate myc protein stability in response to DNA damage. Cell Cycle *6*, 2327-2331. 10.4161/cc.6.19.4804.

Popov, N., Wanzel, M., Madiredjo, M., Zhang, D., Beijersbergen, R., Bernards, R., Moll, R., Elledge, S.J., and Eilers, M. (2007b). The ubiquitin-specific protease USP28 is required for MYC stability. Nature Cell Biology *9*, 765-774. 10.1038/ncb1601.

Purcell, A.W., Ramarathinam, S.H., and Ternette, N. (2019). Mass spectrometry–based identification of MHC-bound peptides for immunopeptidomics. Nature Protocols *14*, 1687-1707. 10.1038/s41596-019-0133-y.

Puri, S., Folias, A.E., and Hebrok, M. (2015). Plasticity and dedifferentiation within the pancreas: development, homeostasis, and disease. Cell Stem Cell *16*, 18-31. 10.1016/j.stem.2014.11.001.

Qu, J., Hou, Z., Han, Q., Zhang, C., Tian, Z., and Zhang, J. (2013). Poly(I:C) exhibits an anti-cancer effect in human gastric adenocarcinoma cells which is dependent on RLRs. Int Immunopharmacol *17*, 814-820. 10.1016/j.intimp.2013.08.013.

Quinlan, A.R., and Hall, I.M. (2010). BEDTools: a flexible suite of utilities for comparing genomic features. Bioinformatics *26*, 841-842. 10.1093/bioinformatics/btq033.

Quinn, W.J., 3rd, Jiao, J., TeSlaa, T., Stadanlick, J., Wang, Z., Wang, L., Akimova, T., Angelin, A., Schäfer, P.M., Cully, M.D., et al. (2020). Lactate Limits T Cell Proliferation via the NAD(H) Redox State. Cell Rep *33*, 108500. 10.1016/j.celrep.2020.108500.

R Development Core Team (2020). R: A language and environment for statistical computing (R Foundation for Statistical Computing).

Rahib, L., Smith, B.D., Aizenberg, R., Rosenzweig, A.B., Fleshman, J.M., and Matrisian, L.M. (2014). Projecting cancer incidence and deaths to 2030: the unexpected burden of thyroid, liver, and pancreas cancers in the United States. Cancer Res *74*, 2913-2921. 10.1158/0008-5472.Can-14-0155.

Rahl, P.B., Lin, C.Y., Seila, A.C., Flynn, R.A., McCuine, S., Burge, C.B., Sharp, P.A., and Young, R.A. (2010). c-Myc Regulates Transcriptional Pause Release. Cell *141*, 432-445. https://doi.org/10.1016/j.cell.2010.03.030.

Rakhra, K., Bachireddy, P., Zabuawala, T., Zeiser, R., Xu, L., Kopelman, A., Fan, A.C., Yang, Q., Braunstein, L., Crosby, E., et al. (2010). CD4(+) T cells contribute to the remodeling of the microenvironment required for sustained tumor regression upon oncogene inactivation. Cancer Cell *18*, 485-498. 10.1016/j.ccr.2010.10.002.

Rangan, A., Fedoroff, O.Y., and Hurley, L.H. (2001). Induction of Duplex to G-quadruplex Transition in the c-myc Promoter Region by a Small Molecule*. Journal of Biological Chemistry *276*, 4640-4646. https://doi.org/10.1074/jbc.M005962200.

Raulet, D.H., Gasser, S., Gowen, B.G., Deng, W., and Jung, H. (2013). Regulation of ligands for the NKG2D activating receptor. Annu Rev Immunol *31*, 413-441. 10.1146/annurev-immunol-032712-095951.

Raulet, D.H., and Vance, R.E. (2006). Self-tolerance of natural killer cells. Nature Reviews Immunology *6*, 520-531. 10.1038/nri1863.

Rehwinkel, J., and Gack, M.U. (2020). RIG-I-like receptors: their regulation and roles in RNA sensing. Nature Reviews Immunology *20*, 537-551. 10.1038/s41577-020-0288-3.

Richards, M.W., Burgess, S.G., Poon, E., Carstensen, A., Eilers, M., Chesler, L., and Bayliss, R. (2016). Structural basis of N-Myc binding by Aurora-A and its destabilization by kinase inhibitors. Proceedings of the National Academy of Sciences *113*, 13726. 10.1073/pnas.1610626113.

Richter, B., Sliter Danielle, A., Herhaus, L., Stolz, A., Wang, C., Beli, P., Zaffagnini, G., Wild, P., Martens, S., Wagner Sebastian, A., et al. (2016). Phosphorylation of OPTN by TBK1 enhances its binding to Ub chains and promotes selective autophagy of damaged mitochondria. Proceedings of the National Academy of Sciences *113*, 4039-4044. 10.1073/pnas.1523926113.

Rickman, D.S., Schulte, J.H., and Eilers, M. (2018). The Expanding World of N-MYC-Driven Tumors. Cancer Discov *8*, 150-163. 10.1158/2159-8290.Cd-17-0273.

Riedel, A., Helal, M., Pedro, L., Swietlik, J.J., Shorthouse, D., Schmitz, W., Haas, L., Young, T., da Costa, A.S.H., Davidson, S., et al. (2022). Tumor-Derived Lactic Acid Modulates Activation and Metabolic Status of Draining Lymph Node Stroma. Cancer Immunology Research *10*, 482-497. 10.1158/2326-6066.CIR-21-0778.

Ritter, J.L., Zhu, Z., Thai, T.C., Mahadevan, N.R., Mertins, P., Knelson, E.H., Piel, B.P., Han, S., Jaffe, J.D., Carr, S.A., et al. (2020). Phosphorylation of RAB7 by TBK1/IKKε Regulates Innate Immune Signaling in Triple-Negative Breast Cancer. Cancer Research *80*, 44-56. 10.1158/0008-5472.CAN-19-1310.

Roeder, F. (2016). Neoadjuvant radiotherapeutic strategies in pancreatic cancer. World J Gastrointest Oncol *8*, 186-197. 10.4251/wjgo.v8.i2.186.

Roeschert, I., Poon, E., Henssen, A.G., Dorado Garcia, H., Gatti, M., Giansanti, C., Jamin, Y., Ade, C.P., Gallant, P., Schülein-Völk, C., et al. (2021). Combined inhibition of Aurora-A and ATR kinases results in regression of MYCN-amplified neuroblastoma. Nature Cancer *2*, 312-326. 10.1038/s43018-020-00171-8.

Rojas, L.A., and Balachandran, V.P. (2021). Scaling the immune incline in PDAC. Nature Reviews Gastroenterology & Hepatology *18*, 453-454. 10.1038/s41575-021-00475-9.

Roussel, M.F., and Robinson, G.W. (2013). Role of MYC in Medulloblastoma. Cold Spring Harb Perspect Med *3*. 10.1101/cshperspect.a014308.

Ruffell, B., Chang-Strachan, D., Chan, V., Rosenbusch, A., Ho, C.M., Pryer, N., Daniel, D., Hwang, E.S., Rugo, H.S., and Coussens, L.M. (2014). Macrophage IL-10 blocks CD8+ T cell-dependent responses to chemotherapy by suppressing IL-12 expression in intratumoral dendritic cells. Cancer Cell *26*, 623-637. 10.1016/j.ccell.2014.09.006.

Saba, I., Kosan, C., Vassen, L., and Möröy, T. (2011). IL-7R-dependent survival and differentiation of early T-lineage progenitors is regulated by the BTB/POZ domain transcription factor Miz-1. Blood *117*, 3370-3381. 10.1182/blood-2010-09-310680.

Saito, T., and Gale, M., Jr. (2008). Differential recognition of double-stranded RNA by RIG-I-like receptors in antiviral immunity. The Journal of experimental medicine *205*, 1523-1527. 10.1084/jem.20081210.

Sakamoto, K.M., Kim, K.B., Kumagai, A., Mercurio, F., Crews, C.M., and Deshaies, R.J. (2001). Protacs: Chimeric molecules that target proteins to the Skp1–Cullin–F box complex for ubiquitination and degradation. Proceedings of the National Academy of Sciences *98*, 8554-8559. 10.1073/pnas.141230798.

Salti, S.M., Hammelev, E.M., Grewal, J.L., Reddy, S.T., Zemple, S.J., Grossman, W.J., Grayson, M.H., and Verbsky, J.W. (2011). Granzyme B regulates antiviral CD8+ T cell responses. J Immunol *187*, 6301-6309. 10.4049/jimmunol.1100891.

Sancho, P., Burgos-Ramos, E., Tavera, A., Bou Kheir, T., Jagust, P., Schoenhals, M., Barneda, D., Sellers, K., Campos-Olivas, R., Graña, O., et al. (2015). MYC/PGC-1α Balance Determines the Metabolic Phenotype and Plasticity of Pancreatic Cancer Stem Cells. Cell Metabolism *22*, 590-605. 10.1016/j.cmet.2015.08.015.

Sanderson, S.M., Xiao, Z., Wisdom, A.J., Bose, S., Liberti, M.V., Reid, M.A., Hocke, E., Gregory, S.G., Kirsch, D.G., and Locasale, J.W. (2020). The Na⁺/K⁺ ATPase Regulates Glycolysis and Modifies Immune Metabolism in Tumors. bioRxiv, 2020.2003.2031.018739. 10.1101/2020.03.31.018739.

Schaub, F.X., Dhankani, V., Berger, A.C., Trivedi, M., Richardson, A.B., Shaw, R., Zhao, W., Zhang, X., Ventura, A., Liu, Y., et al. (2018a). Pan-cancer Alterations of the MYC Oncogene and Its Proximal Network across the Cancer Genome Atlas. Cell Syst *6*, 282-300.e282. 10.1016/j.cels.2018.03.003.

Scheper, W., Kelderman, S., Fanchi, L.F., Linnemann, C., Bendle, G., de Rooij, M.A.J., Hirt, C., Mezzadra, R., Slagter, M., Dijkstra, K., et al. (2019). Low and variable tumor reactivity of the intratumoral TCR repertoire in human cancers. Nat Med *25*, 89-94. 10.1038/s41591-018-0266-5.

Schlitzer, A., McGovern, N., and Ginhoux, F. (2015). Dendritic cells and monocyte-derived cells: Two complementary and integrated functional systems. Semin Cell Dev Biol *41*, 9-22. 10.1016/j.semcdb.2015.03.011.

Schlütermann, D., Berleth, N., Deitersen, J., Wallot-Hieke, N., Friesen, O., Wu, W., Stuhldreier, F., Sun, Y., Berning, L., Friedrich, A., et al. (2021). FIP200 controls the TBK1 activation threshold at SQSTM1/p62-positive condensates. Scientific Reports *11*, 13863. 10.1038/s41598-021-92408-4.

Schmidt, S., Gay, D., Uthe, F.W., Denk, S., Paauwe, M., Matthes, N., Diefenbacher, M.E., Bryson, S., Warrander, F.C., Erhard, F., et al. (2019). A MYC–GCN2–eIF2α negative feedback loop limits protein synthesis to prevent MYC-dependent apoptosis in colorectal cancer. Nature Cell Biology *21*, 1413-1424. 10.1038/s41556-019-0408-0.

Schmitz, R., Ceribelli, M., Pittaluga, S., Wright, G., and Staudt, L.M. (2014). Oncogenic mechanisms in Burkitt lymphoma. Cold Spring Harb Perspect Med *4*. 10.1101/cshperspect.a014282.

Schneider, N.F.Z., Cerella, C., Lee, J.-Y., Mazumder, A., Kim, K.R., de Carvalho, A., Munkert, J., Pádua, R.M., Kreis, W., Kim, K.-W., et al. (2018). Cardiac Glycoside Glucoevatromonoside Induces Cancer Type-Specific Cell Death. Frontiers in Pharmacology *9*. 10.3389/fphar.2018.00070.

Schulein-Volk, C., Wolf, E., Zhu, J., Xu, W., Taranets, L., Hellmann, A., Janicke, L.A., Diefenbacher, M.E., Behrens, A., Eilers, M., and Popov, N. (2014). Dual regulation of Fbw7 function and oncogenic transformation by Usp28. Cell Rep *9*, 1099-1109. 10.1016/j.celrep.2014.09.057.

Schwartz, A., Malgor, R., Dickerson, E., Weeraratna, A., Wortsman, J., Harii, N., Kohn, A., Moon, R., Schwartz, F., Goetz, D., et al. (2009). Phenylmethimazole Decreases Toll-Like Receptor 3 and Noncanonical Wnt5a Expression in Pancreatic Cancer and Melanoma Together with Tumor Cell Growth and Migration. Clinical cancer research : an official journal of the American Association for Cancer Research *15*, 4114-4122. 10.1158/1078-0432.CCR-09-0005.

Sears, R., Leone, G., DeGregori, J., and Nevins, J.R. (1999). Ras Enhances Myc Protein Stability. Molecular Cell *3*, 169-179. https://doi.org/10.1016/S1097-2765(00)80308-1.

Sears, R., Nuckolls, F., Haura, E., Taya, Y., Tamai, K., and Nevins, J.R. (2000). Multiple Ras-dependent phosphorylation pathways regulate Myc protein stability. Genes Dev *14*, 2501-2514. 10.1101/gad.836800.

Seoane, J., Le, H.V., and Massagué, J. (2002). Myc suppression of the p21(Cip1) Cdk inhibitor influences the outcome of the p53 response to DNA damage. Nature *419*, 729-734. 10.1038/nature01119.

Seoane, J., Pouponnot, C., Staller, P., Schader, M., Eilers, M., and Massagué, J. (2001). TGFbeta influences Myc, Miz-1 and Smad to control the CDK inhibitor p15INK4b. Nat Cell Biol *3*, 400-408. 10.1038/35070086.

Shen, J.J., Zhan, Y.C., Li, H.Y., and Wang, Z. (2020). Ouabain impairs cancer metabolism and activates AMPK-Src signaling pathway in human cancer cell lines. Acta Pharmacol Sin *41*, 110-118. 10.1038/s41401-019-0290-0.

Sheykhhasan, M., Manoochehri, H., and Dama, P. (2022). Use of CAR T-cell for acute lymphoblastic leukemia (ALL) treatment: a review study. Cancer Gene Therapy *29*, 1080-1096. 10.1038/s41417-021-00418-1.

Shi, H., Wei, J., and He, C. (2019). Where, When, and How: Context-Dependent Functions of RNA Methylation Writers, Readers, and Erasers. Molecular Cell *74*, 640-650. 10.1016/j.molcel.2019.04.025.

Shim, H., Dolde, C., Lewis, B.C., Wu, C.-S., Dang, G., Jungmann, R.A., Dalla-Favera, R., and Dang, C.V. (1997). c-Myc transactivation of LDH-A: Implications for tumor metabolism and growth. Proceedings of the National Academy of Sciences *94*, 6658-6663. 10.1073/pnas.94.13.6658.

Shivji, M.K.K., Renaudin, X., Williams, Ç.H., and Venkitaraman, A.R. (2018). BRCA2 Regulates Transcription Elongation by RNA Polymerase II to Prevent R-Loop Accumulation. Cell Reports *22*, 1031-1039. 10.1016/j.celrep.2017.12.086.

Shroff, S., Rashid, A., Wang, H., Katz, M.H., Abbruzzese, J.L., Fleming, J.B., and Wang, H. (2014). SOX9: a useful marker for pancreatic ductal lineage of pancreatic neoplasms. Hum Pathol *45*, 456-463. 10.1016/j.humpath.2013.10.008.

Small, M.B., Hay, N., Schwab, M., and Bishop, J.M. (1987). Neoplastic transformation by the human gene N-myc. Mol Cell Biol *7*, 1638-1645. 10.1128/mcb.7.5.1638-1645.1987.

Sodir, N.M., Kortlever, R.M., Barthet, V.J.A., Campos, T., Pellegrinet, L., Kupczak, S., Anastasiou, P., Swigart, L.B., Soucek, L., Arends, M.J., et al. (2020). MYC Instructs and Maintains Pancreatic Adenocarcinoma Phenotype. Cancer Discov. 10.1158/2159-8290.CD-19-0435.

Soga, Y., Komori, H., Miyazaki, T., Arita, N., Terada, M., Kamada, K., Tanaka, Y., Fujino, T., Hiasa, Y., Matsuura, B., et al. (2009). Toll-like receptor 3 signaling induces chronic pancreatitis through the Fas/Fas ligand-mediated cytotoxicity. Tohoku J Exp Med *217*, 175-184. 10.1620/tjem.217.175.

Solvie, D., Baluapuri, A., Uhl, L., Fleischhauer, D., Endres, T., Papadopoulos, D., Aziba, A., Gaballa, A., Mikicic, I., Isaakova, E., et al. (2022). MYC multimers shield stalled replication forks from RNA polymerase. Nature. 10.1038/s41586-022-05469-4.

Soucek, L., Whitfield, J., Martins, C.P., Finch, A.J., Murphy, D.J., Sodir, N.M., Karnezis, A.N., Swigart, L.B., Nasi, S., and Evan, G.I. (2008). Modelling Myc inhibition as a cancer therapy. Nature *455*, 679-683. 10.1038/nature07260.

Soucek, L., Whitfield, J.R., Sodir, N.M., Masso-Valles, D., Serrano, E., Karnezis, A.N., Swigart, L.B., and Evan, G.I. (2013). Inhibition of Myc family proteins eradicates KRas-driven lung cancer in mice. Genes Dev *27*, 504-513. 10.1101/gad.205542.112.

Spranger, S., Bao, R., and Gajewski, T.F. (2015). Melanoma-intrinsic β-catenin signalling prevents anti-tumour immunity. Nature *523*, 231-235. 10.1038/nature14404.

Spranger, S., Dai, D., Horton, B., and Gajewski, T.F. (2017). Tumor-Residing Batf3 Dendritic Cells Are Required for Effector T Cell Trafficking and Adoptive T Cell Therapy. Cancer Cell *31*, 711-723.e714. 10.1016/j.ccell.2017.04.003.

Srivastava, S., Furlan, S.N., Jaeger-Ruckstuhl, C.A., Sarvothama, M., Berger, C., Smythe, K.S., Garrison, S.M., Specht, J.M., Lee, S.M., Amezquita, R.A., et al. (2021). Immunogenic Chemotherapy Enhances Recruitment of CAR-T Cells to Lung Tumors and Improves Antitumor Efficacy when Combined with Checkpoint Blockade. Cancer Cell *39*, 193-208.e110. 10.1016/j.ccell.2020.11.005.

Stead, M.A., Trinh, C.H., Garnett, J.A., Carr, S.B., Baron, A.J., Edwards, T.A., and Wright, S.C. (2007). A Beta-Sheet Interaction Interface Directs the Tetramerisation of the Miz-1 POZ Domain. Journal of Molecular Biology *373*, 820-826. https://doi.org/10.1016/j.jmb.2007.08.026.

Steinberger, J., Robert, F., Hallé, M., Williams, D.E., Cencic, R., Sawhney, N., Pelletier, D., Williams, P., Igarashi, Y., Porco, J.A., et al. (2019). Tracing MYC Expression for Small Molecule Discovery. Cell Chemical Biology *26*, 699-710.e696. https://doi.org/10.1016/j.chembiol.2019.02.007.

Su, Z., Zhang, P., Yu, Y., Lu, H., Liu, Y., Ni, P., Su, X., Wang, D., Liu, Y., Wang, J., et al. (2016). HMGB1 Facilitated Macrophage Reprogramming towards a Proinflammatory M1-like Phenotype in Experimental Autoimmune Myocarditis Development. Scientific Reports *6*, 21884. 10.1038/srep21884.

Subramanian, A., Tamayo, P., Mootha, V.K., Mukherjee, S., Ebert, B.L., Gillette, M.A., Paulovich, A., Pomeroy, S.L., Golub, T.R., Lander, E.S., and Mesirov, J.P. (2005). Gene set enrichment analysis: a knowledge-based approach for interpreting genome-wide expression profiles. Proc Natl Acad Sci U S A *102*, 15545-15550.

Svensson, A., Azarbayjani, F., Bäckman, U., Matsumoto, T., and Christofferson, R. (2005). Digoxin inhibits neuroblastoma tumor growth in mice. Anticancer Res *25*, 207-212.

Swaminathan, S., Hansen, A.S., Heftdal, L.D., Dhanasekaran, R., Deutzmann, A., Fernandez, W.D.M., Liefwalker, D.F., Horton, C., Mosley, A., Liebersbach, M., et al. (2020). MYC functions as a switch for natural killer cell-mediated immune surveillance of lymphoid malignancies. Nat Commun *11*, 2860. 10.1038/s41467-020-16447-7.

Takahashi, K., and Yamanaka, S. (2006). Induction of pluripotent stem cells from mouse embryonic and adult fibroblast cultures by defined factors. Cell *126*, 663-676. 10.1016/j.cell.2006.07.024.

Tesi, A., de Pretis, S., Furlan, M., Filipuzzi, M., Morelli, M.J., Andronache, A., Doni, M., Verrecchia, A., Pelizzola, M., Amati, B., and Sabò, A. (2019). An early Myc-dependent transcriptional program orchestrates cell growth during B-cell activation. EMBO reports *20*, e47987. https://doi.org/10.15252/embr.201947987.

Thalheimer, A., Korb, D., Bönicke, L., Wiegering, A., Mühling, B., Schneider, M., Koch, S., Riedel, S.S., Germer, C.T., Beilhack, A., et al. (2013). Noninvasive visualization of tumor growth in a human colorectal liver metastases xenograft model using bioluminescence in vivo imaging. J Surg Res *185*, 143-151. 10.1016/j.jss.2013.03.024.

Thomas, L.R., Foshage, A.M., Weissmiller, A.M., Popay, T.M., Grieb, B.C., Qualls, S.J., Ng, V., Carboneau, B., Lorey, S., Eischen, C.M., and Tansey, W.P. (2016). Interaction of MYC with host cell factor-1 is mediated by the evolutionarily conserved Myc box IV motif. Oncogene *35*, 3613-3618. 10.1038/onc.2015.416.

Thomas, L.R., Wang, Q., Grieb, B.C., Phan, J., Foshage, A.M., Sun, Q., Olejniczak, E.T., Clark, T., Dey, S., Lorey, S., et al. (2015). Interaction with WDR5 promotes target gene recognition and tumorigenesis by MYC. Mol Cell *58*, 440-452. 10.1016/j.molcel.2015.02.028.

Topper, M.J., Vaz, M., Chiappinelli, K.B., DeStefano Shields, C.E., Niknafs, N., Yen, R.C., Wenzel, A., Hicks, J., Ballew, M., Stone, M., et al. (2017). Epigenetic Therapy Ties MYC Depletion to Reversing Immune Evasion and Treating Lung Cancer. Cell *171*, 1284-1300 e1221. 10.1016/j.cell.2017.10.022.

Tricarico, C., Clancy, J., and D'Souza-Schorey, C. (2017). Biology and biogenesis of shed microvesicles. Small GTPases *8*, 220-232. 10.1080/21541248.2016.1215283.

Uhlén, M., Fagerberg, L., Hallström, B.M., Lindskog, C., Oksvold, P., Mardinoglu, A., Sivertsson, Å., Kampf, C., Sjöstedt, E., Asplund, A., et al. (2015). Tissue-based map of the human proteome. Science *347*, 1260419. 10.1126/science.1260419.

Untergasser, A., Cutcutache, I., Koressaar, T., Ye, J., Faircloth, B.C., Remm, M., and Rozen, S.G. (2012). Primer3--new capabilities and interfaces. Nucleic acids research *40*, e115-e115. 10.1093/nar/gks596.

Van Antwerp, D.J., Martin, S.J., Kafri, T., Green, D.R., and Verma, I.M. (1996). Suppression of TNF-alpha-induced apoptosis by NF-kappaB. Science *274*, 787-789.

van Riggelen, J., Müller, J., Otto, T., Beuger, V., Yetil, A., Choi, P.S., Kosan, C., Möröy, T., Felsher, D.W., and Eilers, M. (2010). The interaction between Myc and Miz1 is required to antagonize TGFbeta-dependent autocrine signaling during lymphoma formation and maintenance. Genes Dev *24*, 1281-1294. 10.1101/gad.585710.

Vaseva, A.V., Blake, D.R., Gilbert, T.S.K., Ng, S., Hostetter, G., Azam, S.H., Ozkan-Dagliyan, I., Gautam, P., Bryant, K.L., Pearce, K.H., et al. (2018). KRAS Suppression-Induced Degradation of MYC Is Antagonized by a MEK5-ERK5 Compensatory Mechanism. Cancer Cell *34*, 807-822 e807. 10.1016/j.ccell.2018.10.001.

Vaz, J., and Andersson, R. (2014). Intervention on toll-like receptors in pancreatic cancer. World J Gastroenterol *20*, 5808-5817. 10.3748/wjg.v20.i19.5808.

Versteeg, R., Noordermeer, I.A., Kruese-Wolters, M., Ruiter, D.J., and Schrier, P.I. (1988). c-myc down-regulates class HLA expression in human melanomas. EMBO J. *7*, 1023-1029.

Viel, S., Marçais, A., Guimaraes, F.S., Loftus, R., Rabilloud, J., Grau, M., Degouve, S., Djebali, S., Sanlaville, A., Charrier, E., et al. (2016). TGF-β inhibits the activation and functions of NK cells by repressing the mTOR pathway. Sci Signal *9*, ra19. 10.1126/scisignal.aad1884.

Vijay, N., and Morris, M.E. (2014). Role of monocarboxylate transporters in drug delivery to the brain. Curr Pharm Des *20*, 1487-1498. 10.2174/13816128113199990462.

Voet, D.V., Judith; Pratt, Charlotte. (2008). Fundamentals of the biochemistry : life at the molecular level.

Waikel, R.L., Kawachi, Y., Waikel, P.A., Wang, X.J., and Roop, D.R. (2001). Deregulated expression of c-Myc depletes epidermal stem cells. Nat Genet *28*, 165-168. 10.1038/88889.

Wall, M., Poortinga, G., Hannan, K.M., Pearson, R.B., Hannan, R.D., and McArthur, G.A. (2008). Translational control of c-MYC by rapamycin promotes terminal myeloid differentiation. Blood *112*, 2305-2317. 10.1182/blood-2007-09-111856.

Walz, S., Lorenzin, F., Morton, J., Wiese, K.E., von Eyss, B., Herold, S., Rycak, L., Dumay-Odelot, H., Karim, S., Bartkuhn, M., et al. (2014). Activation and repression by oncogenic MYC shape tumour-specific gene expression profiles. Nature *511*, 483-487. 10.1038/nature13473.

Wandinger-Ness, A., and Zerial, M. (2014). Rab proteins and the compartmentalization of the endosomal system. Cold Spring Harbor perspectives in biology *6*, a022616-a022616. 10.1101/cshperspect.a022616.

Wang, P., Chen, Y., and Wang, C. (2021). Beyond Tumor Mutation Burden: Tumor Neoantigen Burden as a Biomarker for Immunotherapy and Other Types of Therapy. Frontiers in oncology *11*, 672677-672677. 10.3389/fonc.2021.672677.

Wanzel, M., Kleine-Kohlbrecher, D., Herold, S., Hock, A., Berns, K., Park, J., Hemmings, B., and Eilers, M. (2005). Akt and 14-3-3η regulate Miz1 to control cell-cycle arrest after DNA damage. Nature Cell Biology *7*, 30-41. 10.1038/ncb1202.

Weinreb, J.T., Ghazale, N., Pradhan, K., Gupta, V., Potts, K.S., Tricomi, B., Daniels, N.J., Padgett, R.A., De Oliveira, S., Verma, A., and Bowman, T.V. (2021). Excessive R-loops trigger an inflammatory cascade leading to increased HSPC production. Dev Cell *56*, 627-640.e625. 10.1016/j.devcel.2021.02.006.

Welcker, M., Orian, A., Jin, J., Grim, J.E., Harper, J.W., Eisenman, R.N., and Clurman, B.E. (2004). The Fbw7 tumor suppressor regulates glycogen synthase kinase 3 phosphorylation-dependent c-Myc protein degradation. Proc Natl Acad Sci U S A *101*, 9085-9090. 10.1073/pnas.0402770101.

West, A.P., and Shadel, G.S. (2017). Mitochondrial DNA in innate immune responses and inflammatory pathology. Nature Reviews Immunology *17*, 363-375. 10.1038/nri.2017.21.

Westphalen, C.B., and Olive, K.P. (2012). Genetically engineered mouse models of pancreatic cancer. Cancer journal (Sudbury, Mass.) *18*, 502-510. 10.1097/PPO.0b013e31827ab4c4.

Wherry, E.J. (2011). T cell exhaustion. Nature Immunology *12*, 492-499. 10.1038/ni.2035.

Wiegering, A., Uthe, F.W., Jamieson, T., Ruoss, Y., Hüttenrauch, M., Küspert, M., Pfann, C., Nixon, C., Herold, S., Walz, S., et al. (2015). Targeting Translation Initiation Bypasses Signaling Crosstalk Mechanisms That Maintain High MYC Levels in Colorectal Cancer. Cancer discovery *5*, 768-781. 10.1158/2159-8290.CD-14-1040.

Wiese, K.E., Haikala, H.M., von Eyss, B., Wolf, E., Esnault, C., Rosenwald, A., Treisman, R., Klefström, J., and Eilers, M. (2015). Repression of SRF target genes is critical for Myc-dependent apoptosis of epithelial cells. Embo j *34*, 1554-1571. 10.15252/embj.201490467.

Wiese, K.E., Walz, S., von Eyss, B., Wolf, E., Athineos, D., Sansom, O., and Eilers, M. (2013). The role of MIZ-1 in MYC-dependent tumorigenesis. Cold Spring Harb Perspect Med *3*, a014290. 10.1101/cshperspect.a014290.

Wolf, C., Rapp, A., Berndt, N., Staroske, W., Schuster, M., Dobrick-Mattheuer, M., Kretschmer, S., König, N., Kurth, T., Wieczorek, D., et al. (2016). RPA and Rad51 constitute a cell intrinsic mechanism to protect the cytosol from self DNA. Nature Communications *7*, 11752. 10.1038/ncomms11752.

Wolf, E., and Eilers, M. (2020). Targeting MYC Proteins for Tumor Therapy. Annual Review of Cancer Biology *4*, 61-75. 10.1146/annurev-cancerbio-030518-055826.

Wolf, E., Gebhardt, A., Kawauchi, D., Walz, S., von Eyss, B., Wagner, N., Renninger, C., Krohne, G., Asan, E., Roussel, M.F., and Eilers, M. (2013). Miz1 is required to maintain autophagic flux. Nat Commun *4*, 2535. 10.1038/ncomms3535.

Wu, S.-Y., Xiao, Y., Wei, J.-L., Xu, X.-E., Jin, X., Hu, X., Li, D.-Q., Jiang, Y.-Z., and Shao, Z.-M. (2021). MYC suppresses STING-dependent innate immunity by transcriptionally upregulating DNMT1 in triple-negative breast cancer. Journal for ImmunoTherapy of Cancer *9*, e002528. 10.1136/jitc-2021-002528.

Wu, Y., Zhao, W., Liu, Y., Tan, X., Li, X., Zou, Q., Xiao, Z., Xu, H., Wang, Y., and Yang, X. (2018). Function of HNRNPC in breast cancer cells by controlling the dsRNA-induced interferon response. The EMBO journal *37*, e99017. 10.15252/embj.201899017.

Xu, C., Li, T., Lei, J., Zhang, Y., Zhou, J., and Hu, B. (2021). The Autophagy Cargo Receptor SQSTM1 Inhibits Infectious Bursal Disease Virus Infection through Selective Autophagic Degradation of Double-Stranded Viral RNA. Viruses *13*. 10.3390/v13122494.

Xu, R., Rai, A., Chen, M., Suwakulsiri, W., Greening, D.W., and Simpson, R.J. (2018). Extracellular vesicles in cancer — implications for future improvements in cancer care. Nature Reviews Clinical Oncology *15*, 617-638. 10.1038/s41571-018-0036-9.

Yamamoto, K., Venida, A., Yano, J., Biancur, D.E., Kakiuchi, M., Gupta, S., Sohn, A.S.W., Mukhopadhyay, S., Lin, E.Y., Parker, S.J., et al. (2020). Autophagy promotes immune evasion of pancreatic cancer by degrading MHC-I. Nature *581*, 100-105. 10.1038/s41586-020-2229-5.

Yancopoulos, G.D., Nisen, P.D., Tesfaye, A., Kohl, N.E., Goldfarb, M.P., and Alt, F.W. (1985). N-myc can cooperate with ras to transform normal cells in culture. Proc Natl Acad Sci U S A *82*, 5455-5459. 10.1073/pnas.82.16.5455.

Yang, Y.G., Lindahl, T., and Barnes, D.E. (2007). Trex1 exonuclease degrades ssDNA to prevent chronic checkpoint activation and autoimmune disease. Cell *131*, 873-886. 10.1016/j.cell.2007.10.017.

Yim, W.W.-Y., and Mizushima, N. (2020). Lysosome biology in autophagy. Cell Discovery *6*, 6. 10.1038/s41421-020-0141-7.

Yin, X., Giap, C., Lazo, J.S., and Prochownik, E.V. (2003). Low molecular weight inhibitors of Myc-Max interaction and function. Oncogene *22*, 6151-6159. 10.1038/sj.onc.1206641.

Yu, G., Wang, L.G., and He, Q.Y. (2015). ChIPseeker: an R/Bioconductor package for ChIP peak annotation, comparison and visualization. Bioinformatics *31*, 2382-2383. 10.1093/bioinformatics/btv145.

Zhang, N., Ichikawa, W., Faiola, F., Lo, S.Y., Liu, X., and Martinez, E. (2014a). MYC interacts with the human STAGA coactivator complex via multivalent contacts with the GCN5 and TRRAP subunits. Biochim Biophys Acta *1839*, 395-405. 10.1016/j.bbagrm.2014.03.017.

Zhang, P., Li, Y., Xia, J., He, J., Pu, J., Xie, J., Wu, S., Feng, L., Huang, X., and Zhang, P. (2014b). IPS-1 plays an essential role in dsRNA-induced stress granule formation by interacting with PKR and promoting its activation. Journal of Cell Science *127*, 2471-2482. 10.1242/jcs.139626.

Zhang, W., Zhangyuan, G., Wang, F., Jin, K., Shen, H., Zhang, L., Yuan, X., Wang, J., Zhang, H., Yu, W., et al. (2021). The zinc finger protein Miz1 suppresses liver tumorigenesis by restricting hepatocyte-driven macrophage activation and inflammation. Immunity *54*, 1168-1185.e1168. 10.1016/j.immuni.2021.04.027.

Zhang, Y., Liu, T., Meyer, C.A., Eeckhoute, J., Johnson, D.S., Bernstein, B.E., Nusbaum, C., Myers, R.M., Brown, M., Li, W., and Liu, X.S. (2008). Model-based Analysis of ChIP-Seq (MACS). Genome Biology *9*, R137. 10.1186/gb-2008-9-9-r137.

Zimmerli, D., Brambillasca, C.S., Talens, F., Bhin, J., Linstra, R., Romanens, L., Bhattacharya, A., Joosten, S.E.P., Da Silva, A.M., Padrao, N., et al. (2022). MYC promotes immune-suppression in triple-negative breast cancer via inhibition of interferon signaling. Nature Communications *13*, 6579. 10.1038/s41467-022-34000-6.

Zimmerman, K.A., Yancopoulos, G.D., Collum, R.G., Smith, R.K., Kohl, N.E., Denis, K.A., Nau, M.M., Witte, O.N., Toran-Allerand, D., Gee, C.E., et al. (1986). Differential expression of myc family genes during murine development. Nature *319*, 780-783. 10.1038/319780a0.

7 Appendix

Abbreviations

Prefixes

p	pico
n	nano
µ	micro
m	milli
k	kilo

Units

°C	degree Celsius
A	ampere
Da	dalton
g	gram
h	hour
m	meter
min	minute
M	mol/L
L	liter
s	second
v/v	volume per volume
w/v	weight per volume

ADM	acinar-to-ductal metaplasia
Arg	arginine
BCR	B cell receptor
bp	base pair
CAC	centroacinar cell
CAR	chimeric antigen receptor
CAT	cationic amino acid transporter
CDK	Cycline dependent kinase
cDNA	complementary DNA
CDS	coding sequence
CG	cardiac glycoside
ChIP-Rx	quantitative chromatin immunoprecipitation with reference exogenous genome
CQ	chloroquine
ctrl	control
DAMP	damage associated molecular pattern
DC	dendritic cells

DHAP	dihydroxycetone phosphate
DNA	desoxy-ribonucleic acid
DOX	doxycycline
ds	double-stranded
ECAR	extracellular acidification rate
ER	estrogen receptor
EV	empty vector
EV	extracellular vesicle
FACS	Fluorescence activates cell sorting
FBP	fructose-1,6-bisphosphate
fCLIP	formaldehyde crosslinking and immunoprecipitation of RNA
FDR	false discovery rate
GAP	glyceraldehyde 3 phosphate
GEMM	genetic engineered mouse model
GO	gene ontology
GSEA	gene set enrichment analysis
HCC	hepatocellular carcinoma
IFN	interferon
IgG	immunoglobulin
IR	inverted repeat
IRES	internal ribosome entry site
IRF	interferon-regulatory factors
IVIS	*in vivo* imaging
kb	kilobase
KO	knock out
LINE	long interspersed nuclear element
Lys	lysine
MB	MYC box
MCT	monocarboxylate-transporter
MFI	mean fluorescent intensity
MHC	major histocompatibility complex
mRNA	messenger RNA
MS	mass spectrometry
mtDNA	mitochondrial DNA
mtRNA	mitochondrial RNA
MXD	MAX dimerization protein
n	number of biological replicates
N/A	not available

NES	normalized enrichment score
NK cells	natural killer cells
NTC	non-targeting control
OE	overexpression
PAM	protospacer adjacent motif
PAMP	pathogen associated molecular pattern
PanIN	pancreatic intra-epithelial neoplasia
PDAC	pancreatic ductal adenocarcinoma
PFK	phosphofructokinase
PI	propidium iodid
PROTAC	proteolysis-targeting chimeras
PRR	pattern recognition receptor
RE	repetitive element
RNA	ribonucleic acid
RNAi	RNA interference
RNAPII	RNA polymerase II
RQ-PCR	Real-time quantitative polymerase chain reaction
SD	standard deviation
SEM	standard error of mean
sgRNA	single guide RNA
shRNA	short hairpin RNA
SINE	short interspersed nuclear element
SLC	solute carrier family
sMV	shed microvesicles
ss	single-stranded
TAM	tumor associated macrophages
TCA	tricarboxylic acid
TCR	T cell receptor
TLR	Toll-like receptor
TME	tumor microenvironment
TNBC	triple-negative breast cancer
tpm	transcripts per million kilobases
UT	untransduced
UTR	untranslated region
WT	wild type

Table of figures

Acknowledgement

I am glad and thankful for having the chance to investigate and explore a very small part of the MYC universe in the last five years. Specifically, I want to thank Prof. Dr. Martin Eilers for allowing me to fall down the rabbit hole of immunology (and metabolism). Thank you not only for your guidance and supervision, but especially for sharing your passion and excitement every time someone of us revealed a small secret of the universe.

I want to acknowledge Prof. Dr. Georg Gasteiger and Prof. Dr. Dean Felsher for being the members of my thesis committee, their valuable comments and suggestions.

I want to thank Anneli and Carsten for being motivating and helpful advisors, critics and fellows throughout my whole time in the department. I also want to thank Abdallah, Florian, Lukas and Sarah for your support in developing the concept and the project.

I want to thank Uschi and Christina for measuring a tremendous amount of plates with the Operetta and always having time for a chat. I want to thank Werner Schmitz for measuring the metabolites and Angela Riedel for the support with the seahorse platform. I want to thank Carsten, Peter, Florian and Apoorva for their support with all bioinformatic challenges I had to face.

My gratitude goes to Giacomo, Steffi and Gabriele for carefully proof-reading and reviewing this thesis. I am thankful for profiting the last years from your experience, knowledge and advices.

I want to thank the people that make the institute not only a place of exciting science, but also a place where you always find someone for a discussion on the floor, a quick advice, or a friend for a glass of wine or for a whole evening and several bottles. Sometimes you deserve a bottle of wine, sometimes you really need it. I can finish my PhD with a calm conscience since every one of you now knows GGs.

Finally, I want to thank my family, my wife and my friends. You have always been my rock in the surf. It is not always easy with me, but you made it also easy for me with you.

Publication

B. Krenz*, A. Gebhardt-Wolf*, C. P. Ade, A. Gaballa, F. Roehrig, E. Vendelova, A. Baluapuri, U. Eilers, P. Gallant, L. D'Artista, A. Wiegering, G. Gasteiger, M. T. Rosenfeldt, S. Bauer, L. Zender, E. Wolf, M. Eilers (2021): MYC- and MIZ1-Dependent Vesicular Transport of Double-Strand RNA Controls Immune Evasion in Pancreatic Ductal Adenocarcinoma.
Cancer Research, DOI: 10.1158/0008-5472.CAN-21-1677

*authors contributed equally

Affidavit

I hereby confirm that my thesis entitled: “The immune-evasive potential of MYC in pancreatic ductal adenocarcinoma” is the result of my own work. I did not receive any help or support from commercial consultants. All sources and/or materials are listed and specified in the thesis.

Furthermore, I confirm that this thesis has not yet been submitted as part of another examination process neither in identical nor in similar form.

Place, Date Bastian Krenz

Eidesstattliche Erklärung

Hiermit erkläre ich an Eides statt, die Dissertation: „Das immunevasive Potential von MYC im Pankreaskarzinom” eigenständig, d. h. selbstständig und ohne Hilfe eines kommerziellen Promotionsberaters, angefertigt und keine anderen als die von mir angegebenen Quellen und Hilfsmittel verwendet zu haben.

Ich erkläre außerdem, dass die Dissertation weder in gleicher noch in ähnlicher Form bereits in einem anderen Prüfungsverfahren vorgelegt wurde.

Ort, Datum Bastian Krenz

Curriculum vitae

BASTIAN KRENZ